



---

UNIVERSITÀ  
DEGLI STUDI  
DI BRESCIA

DOTTORATO DI RICERCA IN SCIENZE BIOMEDICHE E  
MEDICINA TRASLAZIONALE

---

Settore Scientifico Disciplinare: BIO/17

CICLO XXXVI

NOVEL APPROACHES FOR THE TREATMENT OF  
UVEAL MELANOMA

DOTTORANDA:  
ALESSANDRA LODA

SUPERVISORI:  
PROF. FRANCESCO SEMERARO  
DOTT.SSA SARA REZZOLA

# TABLE OF CONTENTS

<b>ABBREVIATIONS AND ACRONYMS</b> .....	<b>3</b>
<b>SUMMARY</b> .....	<b>5</b>
<b>RIASSUNTO</b> .....	<b>7</b>
<b>INTRODUCTION</b> .....	<b>9</b>
<b>1. UVEAL MELANOMA</b> .....	<b>9</b>
1.1 ANATOMY OF THE EYE AND TUMOR LOCALIZATION .....	9
1.2 RISK FACTORS AND CLINICAL FEATURES .....	9
1.3 GENETIC FEATURES AND TUMOR CLASSIFICATION.....	10
1.4 THERAPEUTIC STRATEGIES FOR PRIMARY AND METASTATIC UVEAL MELANOMA .....	11
<b>2. CANCER STEM-LIKE CELLS</b> .....	<b>13</b>
2.1 CANCER STEM-LIKE CELLS IN UVEAL MELANOMA.....	15
2.1.1 TARGETING CANCER STEM-LIKE CELLS AS A THERAPEUTIC STRATEGY IN UVEAL MELANOMA	16
<b>3. THE FIBROBLAST GROWTH FACTOR (FGF)/ FIBROBLAST GROWTH FACTOR RECEPTOR (FGFR)</b>	
<b>FAMILY</b> .....	<b>18</b>
3.1 THE FGF/FGFR SYSTEM IN CANCER PROGRESSION.....	18
3.1.1 THE FGF/FGFR SYSTEM IN UVEAL MELANOMA .....	18
3.2 TARGETING THE FGF/FGFR SYSTEM FOR CANCER THERAPY.....	20
3.2.1 THE NOVEL SMALL MOLECULE NSC12 AS A PAN FGF-TRAP IN UVEAL MELANOMA.....	20
3.3 THE FGF/FGFR SYSTEM IN STEMNESS REGULATION .....	21
<b>Exploring the FGF/FGFR System in Ocular Tumors: New Insights and Perspectives</b> .....	<b>23</b>
<b>The Autocrine FGF/FGFR System in both Skin and Uveal Melanoma: FGF Trapping as a Possible Therapeutic Approach</b> .....	<b>39</b>
<b>RESULTS</b> .....	<b>57</b>
<b>FGF-Trapping Hampers Cancer Stem-Like Cells in Uveal Melanoma</b> .....	<b>59</b>
<b>An Orthotopic Model of Uveal Melanoma in Zebrafish Embryo: A Novel Platform for Drug Evaluation</b> .....	<b>73</b>
<b>Uveal Melanoma Cells Impair the Anti-tumor Activity of Natural Killer Lymphocytes</b> .....	<b>89</b>
<b>DISCUSSION</b> .....	<b>99</b>
<b>BIBLIOGRAPHY</b> .....	<b>101</b>
<b>ADDENDUM</b> .....	<b>109</b>

**Angiogenesis-Inflammation Cross Talk in Diabetic Retinopathy: Novel Insights from the Chick Embryo Chorioallantoic Membrane/Human Vitreous Platform ..... 111**

**VEGF-Independent Activation of Müller Cells by the Vitreous from Proliferative Diabetic Retinopathy Patients..... 127**

**Diabetic Retinopathy: Soluble and Imaging Ocular Biomarkers..... 145**

## ABBREVIATIONS AND ACRONYMS

ABC	ATP-Binding Cassette
ALDH	Aldehyde Dehydrogenase
ANG-1	Angiopoietin 1
BAP1	BRCA1 Associated Protein 1
BMP	Bone Morphogenic Protein
CDK9	Cyclin-dependent kinase 9
CM	Conditioned Medium
CSC	Cancer Stem-like Cell
CTLA-4	Cytotoxic T-Lymphocyte Antigen 4
CXCR4	CXC Chemokine Receptor 4
dNK	Decidual Natural Killer
EIF1AX	Eukaryotic Translation Initiation Factor 1A, X-Chromosomal
EMT	Epithelial-Mesenchymal Transition
epCAM	Epithelial Cell Adhesion Molecule
EZH2	Enhancer of Zeste 2 Polycomb Repressive Complex 2 Subunit
FBS	Fetal Bovine Serum
FGF	Fibroblast Growth Factor
FGFR	Fibroblast Growth Factor Receptor
FRS2	Fibroblast Growth Factor Receptor Substrate 2
GNA11	G Protein Subunit Alpha 11
GNAQ	G Protein Subunit Alpha Q
HDAC	Histone deacetylases
hESCs	Human Embryonic Stem Cells
Hh	Hedgehog
ImmTAC	Immune Mobilizing Monoclonal T-cell Receptors Against Cancer
JAK-STAT	Janus Kinase/Signal Transducers and Activators of Transcription
KIR	Killer-cell Immunoglobulin-like Receptor
KLF4	Kruppel-like factor 4
MAPK	Mitogen-Activated Protein Kinase
MTOR	Mechanistic Target of Rapamycin
NF-kB	Nuclear Factor Kappa-Light-Chain-Enhancer of Activated B Cells

NK	Natural Killer
NOD-SCID	Nonobese Diabetic/Severe Combined Immunodeficiency
NOTCH	Neurogenic Locus Notch Homolog
OCT4	Octamer-Binding Transcription Factor 4
p16INK4a	Cyclin-Dependent Kinase Inhibitor 2A
PAX6	Paired Box 6
PBMC	Peripheral Blood Mononuclear Cell
PD-1	Programmed Cell Death Protein 1
PI3K	Phosphatidylinositol 3-Kinase
PIGF	Placental Growth Factor
PRAME	Preferentially Expressed Antigen of Melanoma
RASSF1A	Ras Association Domain-Containing Protein 1
ROS	Reactive Oxygen Species
SF3B1	Splicing Factor 3B Subunit 1
SNAIL	Zinc Finger Protein SNAI1
SOX2	Sex Determining Region Y-Box 2
STAT3	Signal Transducer and Activator of Transcription 3
TCGA	The Cancer Genome Atlas
TGF $\beta$	Transforming Growth Factor $\beta$
TME	Tumor Microenvironment
TTT	Transpupillary Thermotherapy
UM	Uveal Melanoma
VEGF	Vascular Endothelial Growth Factor
YAP1	Yes-Associated Protein 1

## SUMMARY

Uveal melanoma (UM) is a very aggressive tumor, and it represents the most common primary intraocular malignancy in the adult population. While primary tumors are successfully treated in 90% of cases, almost 50% of patients ultimately develops metastasis, with a median survival after diagnosis spanning from 6 to 12 months. Therefore, effective pharmacological therapies are eagerly required. In this frame, during my PhD I have focused on gaining a better understanding on the mechanisms sustaining tumor progression in the attempt to identify novel therapeutic strategies. In this thesis, I have illustrated our results on alternative approaches aimed at hampering both tumor cells as well as the stromal component.

The Fibroblast Growth Factor (FGF)/FGF Receptor (FGFR) system exerts a very important role in UM. Indeed, both clinical and experimental evidence demonstrates the presence of an autocrine FGF/FGFR activation loop, with alterations in the expression of ligands and receptors resulting in a poorer prognosis in patients. In this context, we have previously demonstrated the efficacy of inhibiting the FGF/FGFR system using the pan FGF-trap NSC12 as a strategy to reduce cell proliferation, migration, and survival of UM cell lines. Additionally, FGF-mediated signaling is also involved in the maintenance of Cancer Stem-like Cells (CSCs), a subpopulation of tumor cells responsible for tumorigenesis, metastatic dissemination, therapy resistance, and recurrence. Therefore, eliminating CSCs is a crucial step to achieve a complete tumor eradication. On this premise, we have demonstrated for the first time that the inhibition of the FGF/FGFR system is an effective strategy to hamper the stem-like component due to the enhanced sensitivity of CSCs to FGF-deprivation. In this frame, we have also established an orthotopic model of UM in the zebrafish embryo as a tool for *in vivo* drug screening. By engrafting tumor cells in proximity to the developing choroidal vasculature of the eye, our model closely mimics the microenvironment in which tumors originate. Additionally, we have developed a reliable and accurate method for assessing xenograft tumor growth by exploiting the bioluminescent signal of tumor cells transduced with firefly luciferase.

The advent of immune therapy strategies has failed to improve the clinical management of UM, due to the exploitation of immune escape strategies that are still largely unclear. In this context, Natural Killer (NK) lymphocytes are important regulators of cancer immunosurveillance and their activity is finely controlled by the expression of specific activating and inhibitory receptors that allow them to discriminate and eliminate malignant cells. However, the presence of a pro-tumor and pro-angiogenic subpopulation of decidual-like NK lymphocytes has been recently described in various tumor types. These cells are characterized by the production of pro-angiogenic/pro-inflammatory mediators as well as by an impairment of their cytotoxic functions. On this premise, we have investigated whether decidual-like polarization of NK lymphocytes could be involved in UM, as a process sustaining tumor progression as well as the formation of metastatic lesions. Our data demonstrates that the conditioned media from UM cell can shift NK lymphocytes towards a decidual-like state, characterized by reduced levels of activating receptors and by an impaired cytotoxic activity. These data, together with the evidence that UM cells express the immunosuppressive cytokine TGF $\beta$ , support the hypothesis that soluble factors produced by cancer cells and accumulated within the tumor microenvironment could favor UM immune escape. Our results set the basis for further studies on the role played by UM-derived TGF $\beta$  in reprogramming NK lymphocytes and they hint at TGF $\beta$  as a potential target for the treatment of UM.



---

## RIASSUNTO

Il melanoma uveale (MU) è il principale tumore intraoculare nella popolazione adulta. Nonostante il tumore primario sia trattato con successo nella quasi totalità dei casi, si stima che circa il 50% dei pazienti sviluppi metastasi, con una sopravvivenza media post-diagnosi che si aggira tra i 6 e i 12 mesi. Per questo motivo, è necessario sviluppare nuovi farmaci efficaci che consentano di migliorare la prognosi dei pazienti. Durante il mio dottorato di ricerca, la mia attività scientifica è stata volta allo studio dei meccanismi coinvolti nella progressione del MU, con lo scopo di identificare nuove strategie terapeutiche dirette contro la componente tumorale e stromale.

I fattori di crescita dei fibroblasti (FGF) e i rispettivi recettori tirosinchinasici (FGFR) rivestono un ruolo molto importante nel MU. Dati clinici e sperimentali dimostrano come l'attivazione autocrina del sistema FGF/FGFR sia coinvolto nella crescita e nella progressione tumorale; inoltre, alterati livelli di espressione dei ligandi e/o dei recettori sono associati ad una prognosi peggiore nei pazienti. In questo contesto, il nostro laboratorio ha dimostrato come il *pan* FGF-trap NSC12 sia in grado di inibire l'attivazione del sistema FGF/FGFR nel MU, riducendo così la sopravvivenza, la migrazione e la proliferazione di linee cellulari di MU. Stante il ruolo della famiglia di FGF nel mantenimento della staminalità in condizioni sia fisiologiche che patologiche, parte di questo lavoro di tesi è stato dedicato ad analizzare l'effetto dell'inibizione del sistema FGF/FGFR sulla componente staminale del MU. Le cellule staminali tumorali sono una sottopopolazione di cellule neoplastiche coinvolte nella disseminazione metastatica, nella resistenza alle terapie e nell'insorgenza di recidive. I nostri dati dimostrano per la prima volta come bloccare il sistema FGF/FGFR rappresenti una strategia efficace per colpire le cellule staminali tumorali del MU, come conseguenza della stretta dipendenza della componente staminale nei confronti della cascata di segnale intracellulare attivata da FGF.

Durante il mio dottorato di ricerca ho inoltre partecipato allo sviluppo di un modello ortotopico di MU nell'embrione di zebrafish. In questo modello, le cellule tumorali vengono impiantate in prossimità dei vasi coroidali dell'occhio dell'embrione, permettendo così di riprodurre il microambiente d'origine del tumore. Per valutare la crescita tumorale abbiamo sviluppato un metodo di quantificazione basato sull'analisi del segnale bioluminescente di cellule di MU trasdotte con l'enzima luciferasi, in modo da bypassare i limiti legati alla classica quantificazione di segnali di fluorescenza.

Infine, una parte di questo lavoro di tesi è stata volta ad approfondire i meccanismi di *escape* immunologico messi in atto dal MU per sfuggire al controllo delle cellule dell'immunità. Tra le diverse popolazioni linfocitarie, i linfociti *Natural Killer* (NK) giocano un ruolo fondamentale nell'immunosorveglianza nei confronti delle cellule tumorali. Tuttavia, alterazioni nel microambiente tumorale possono favorire l'inattivazione delle cellule NK, favorendo così l'instaurarsi di condizioni permissive per la crescita tumorale e per la formazione di metastasi. A questo proposito, in alcuni tumori è stata descritta la presenza di una particolare sottopopolazione di linfociti NK "*decidual-like*" caratterizzata da una ridotta attività citotossica e dalla produzione di fattori pro-angiogenici/pro-infiammatori. I nostri dati preliminari dimostrano che il MU esprime elevati livelli del fattore immunosoppressivo TGF $\beta$  e che è in grado "riprogrammare" i linfociti NK verso un fenotipo *decidual-like* pro-tumorale. Questi interessanti risultati pongono le basi per ulteriori studi volti a comprendere i meccanismi di *escape* immunologico del MU e suggeriscono che TGF $\beta$  possa rappresentare un nuovo target terapeutico.





---

# INTRODUCTION

## 1. UVEAL MELANOMA

Uveal melanoma (UM) is the most common primary ocular tumor in the adult population. UM accounts for 5% of all melanomas, with an incidence of approximately 4.6 million cases per year, variable according to age, ethnicity, and latitude [1]. UM is a very aggressive tumor type; indeed, while primary tumors are successfully treated in 90% of cases, almost 50% of patients ultimately develops metastasis *via* hematological dissemination, mainly to the liver (95%), followed by lungs (24%), bones (16%), and skin (11%), with median survival after diagnosis spanning from 6 to 12 months [2].

### 1.1 ANATOMY OF THE EYE AND TUMOR LOCALIZATION

The eye is a highly specialized sensory organ. It allows the collection of external images, which are then transmitted to the brain through the optic nerve [3]. The eyeball consists of three layers of tissue: the sclera, an outer protective layer; the uvea, a middle layer with vascular and nutritive functions; the retina, a light-sensitive inner layer that acts as the neural stratum of the eye [4-6].

UM originates from melanocytes located in the uveal tract. The uvea is a pigmented vascular region, and it includes the iris, the ciliary body, and the choroid (**Figure 1**) [4, 5]. The iris is a contractile diaphragm with a central aperture, the pupil, which regulates the amount of light passing through and reaching the retina [3-6]. The ciliary body is located anterior to the iris and is made up of the ciliary epithelium, the ciliary stroma, and the ciliary muscle [4]. The ciliary body is involved in mediating many ocular functions; for instance, the ciliary epithelium secretes the aqueous humor, while the ciliary muscle is necessary to adjust focus of vision [3, 4, 6]. Finally, the choroid consists mainly of blood vessels and melanocytes, and it carries the essential function of providing nutrients and oxygen to retinal neurons. The choroid is firmly attached on its inner surface to the retinal pigment epithelium, while its outer surface adheres to the sclera [3-6]. Most frequently, UM develops in the choroid (almost 90% of total cases), followed by the ciliary body (6%) and the iris (4%) [7].

### 1.2 RISK FACTORS AND CLINICAL FEATURES

Risk factors for UM include light-colored eyes, fair complexion, ocular melanocytosis, and excessive exposure to natural/artificial ultraviolet and blue lights. Tumors are frequently asymptomatic, and diagnosis typically occurs during routine ophthalmic screening. Still, discoloration of the iris or pupillary distortion may be detected by patients when tumors affect the anterior portion of the eye, thus allowing for earlier diagnosis; in comparison, posterior tumors can remain latent until a disruption of the visual field manifests. Additionally, larger tumors can be associated to complications such as the formation of an exudative retinal detachment [7, 8].

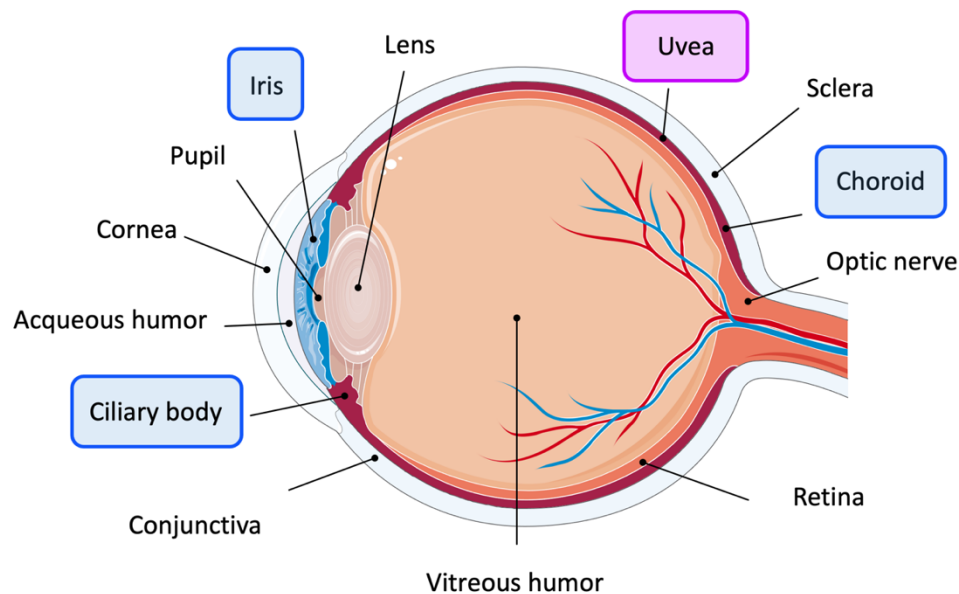


**Figure 1.** Schematic representation of ocular anatomy and UM localization. UM originates from melanocytes located in the uvea (purple), a pigmented vascular layer which provides trophic support to the retina; it consists of the choroid, the iris, and the ciliary body (blue).

### 1.3 GENETIC FEATURES AND TUMOR CLASSIFICATION

UM and cutaneous melanoma display entirely different genetic signatures; indeed, UM lacks alterations in both *BRAF* and *NRAS*. Instead, UM driver, gain-of-function, mutations occur in G-protein subunit Q (*GNAQ*) and *GNA11* genes in a mutually exclusive pattern, leading to the constitutive activation of G-proteins associated to transmembrane receptors and of their respective downstream signaling pathways [9]. Early alterations in UM involve monosomy of chromosome 3, which is often associated to a worse prognosis for patients, as well as gain of 6p and 8q, and loss of chromosome 1p and 8p. Inactivating mutations of the tumor-suppressor gene BRCA-Associated Protein 1 (*BAP1*) are present in over 80% of metastatic UM and are linked to lower disease-free survival rates; additionally, survival is drastically affected by the co-presence of *BAP1* mutations and monosomy 3 [10]. Approximately 15% of UM patients displays mutations in the splicing factor 3B subunit 1 (*SF3B1*) gene, which encodes for a member of the spliceosome; while *SF3B1* mutations are often associated to a good prognosis in UM patients, alterations in the spliceosome component can cause introne retention and aberrant alternative splicing [11]. Epigenetic regulation, especially methylation, plays an important role in UM by affecting tumor suppressor genes, including Cyclin-Dependent Kinase Inhibitor 2A (*p16INK4a*), RAS-Associated Domain Family 1 Isoform A (*RASSF1A*), as well as *BAP1*; of note, *BAP1* methylation might represent a prognostic indicator for the development of metastatic lesions [10, 12]. According to the expression of a specific set of 15 genes, patients affected by UM can be categorized into low-risk (class 1A), intermediate (class 1B), and high-risk (class 2) prognostic groups. Class 1 tumors genetic profile resembles that of normal melanocytes, whereas melanocytic genes are downregulated in class 2 tumors, in favor of genes of primitive neural/ectodermal stem cell lineages, suggesting that class 2 tumors lose their melanocytic identity and revert to a more aggressive, stem-like phenotype [13]; this classification can be furtherly refined by assessing a set of antigens preferentially expressed in melanoma (PRAME), which are linked to an increased risk of metastasis and poorer survival [14].

---

## 1.4 THERAPEUTIC STRATEGIES FOR PRIMARY AND METASTATIC UVEAL MELANOMA

Several therapeutic strategies are employed in the clinical practice to eradicate primary tumors, preserve the globe and vision, and prevent the occurrence of distant metastasis. Brachytherapy is a technique that allows for the direct administration of radiotherapy to the tumor site, through the application of a plaque on the sclera, promoting tumor regression within 2 months of therapy. The most frequently used radioisotopes are ruthenium-106 and iodine-125, according to tumor size [15]. Transpupillary thermotherapy (TTT) targets the tumor with an infrared laser through the pupil, causing hyperthermia up to 4 mm deep. Currently, TTT is mainly administered to reduce tumor size before radiotherapy, and it is best suited for small tumors arising at a distance from the macula and the optic nerve [16]. Photodynamic therapy is a less common procedure in which a photosensitive dye is intravenously injected to induce photochemical toxicity, causing vascular closure and tumor necrosis. Local tumor resection can be a valid treatment for tumors unsuitable for radiotherapy due to location or dimensions, allowing for globe preservation and vision retention. Before the advent of brachytherapy, enucleation, which is the surgical removal of the eye, was the first line treatment for UM. Currently, it is reserved for large tumors that cannot be treated otherwise, while exenteration, which includes the removal of nerves, muscles, and fatty tissue, is applicable in the presence of an extensive extraocular involvement [17]. In any case, systemic examinations should be performed to exclude the presence of metastasis before treatment of the primary tumor; if metastatic loci are detected, local treatment may be deferred in favor of systemic therapy.

Given that the liver is the most common site of metastatic dissemination of UM, liver-directed therapies such as surgical resection, chemoembolization, radioembolization, and percutaneous hepatic infusion of chemotherapeutic drugs are often employed [8]. Nevertheless, systemic management of metastatic disease is extremely complex. Indeed, chemotherapy regimens using dacarbazine, temozolomide, cisplatin, and fotemustine have demonstrated poor response rates and failed to improve survival, both as single agents or in combinational therapies [18]. Therefore, molecular targeted therapies, aimed at blocking specific signaling pathways that regulate the biological behavior of tumor cells, have been tested in UM. In particular, studies have focused on hampering downstream mediators of constitutive activated G $\alpha$ Q and G $\alpha$ 11, including Mitogen-Activated Protein Kinase (MAPK) and Phosphatidylinositol 3-Kinase (PI3K)/AKT/Mechanistic Target of Rapamycin (MTOR) kinase. Despite the promising results of these inhibitors in experimental models *in vitro*, they exerted limited efficacy in clinical trials [19]. Advances in immunotherapy, such as immune checkpoint inhibitors targeting the cytotoxic T-lymphocyte-associated antigen 4 (CTLA-4) and the programmed cell death 1 (PD-1)/PD-1 receptor axis, have significantly improved the treatment of cutaneous melanoma. However, immunotherapy approaches are unsuccessful in UM due to the low mutational burden of tumor cells [20]. Of note, recent studies by single cell RNA-sequencing on primary and metastatic samples have underlined the possibility of active immune surveillance in low-risk tumors. Indeed, mutations of SF3B1 and of the eukaryotic translation initiation factor 1A X-linked (EIF1AX) could result in the generation of tumor neoantigens, favoring immune response. By contrast, genomic aberrations in high-risk tumors could be responsible for the creation of an immunosuppressive tumor microenvironment (TME) which promotes immune escape and sustains metastasis formation [21]. Nevertheless, a new drug has recently been approved for the pharmacological treatment of HLA-A\*02:01-positive unresectable or metastatic UM. Tebentafusp belongs to the immune mobilizing monoclonal T-cell receptors against

cancer (ImmTAC) class of bispecific T-cell engagers, in which an anti-CD3 single-chain antibody fragment is bound to a monoclonal high affinity T-cell receptor directed against a cancer-related antigen. Specifically, tebentafusp recruits CD3+ T lymphocytes and directs them to UM cells presenting a melanoma-associated antigen glycoprotein 100-derived peptide, normally involved in maturation of melanosomes and highly expressed by tumor cells [22]. The safety profile of tebentafusp is positive, with manageable adverse effects, mainly skin reactions, occurring during the first few administrations; therefore, it paves the way for further exploration on the efficacy novel immunotherapy approaches for improving the clinical outcome of high-risk UM patients [23].

## 2. CANCER STEM-LIKE CELLS

Cancer stem-like cells (CSCs) are a small subset of tumor cells characterized by the ability to self-renew and to differentiate into multiple cancer lineages within the tumor mass through symmetric and asymmetric cell division [24]. Additionally, CSCs are responsible for tumor initiation and growth, and they are involved in metastatic dissemination, therapy resistance, and recurrence (**Figure 2**) [25].

The exact process of CSC formation in tumors is still unclear; however, two main hypothesis are currently being discussed: on one side, the idea that CSCs could derive from normal stem cells undergoing mutations or epigenetic changes; on the other, the notion that differentiated cancer cells could activate oncogenic reprogramming, leading to the acquisition of stem-like properties [26]. Nevertheless, a certain degree of plasticity occurs between CSCs and differentiated cancer cells, suggesting that both are capable of phenotypical transitioning in response to environmental stimuli [27]. Moreover, CSCs are strictly dependent on the TME, which is a complex network of various cell types (*i.e.* endothelial and perivascular cells, fibroblasts, and immune cells) that sustain stem cells, while also contributing to their differentiation into stromal lineages [28].

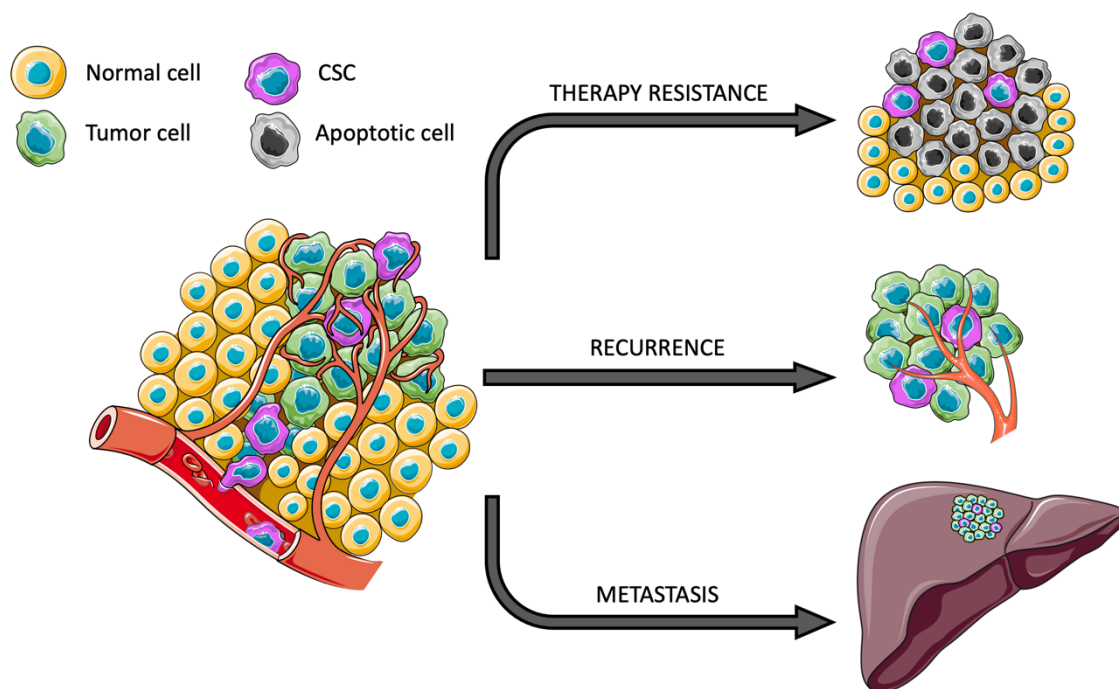


**Figure 2. Cancer stem-like cells (CSCs) in tumors.** CSCs (pink) represent a small subset of total tumor cells (green). Due to their low proliferation rate, the upregulation of anti-apoptotic proteins, and the activation of DNA repair machinery, CSCs can escape therapy-induced apoptosis. Therefore, while conventional therapies eliminate only bulk cells (grey), remaining CSCs could lead to recurrence later on. Additionally, CSCs may acquire a transient epithelial-to-mesenchymal phenotype, which favors metastasis formation.

The first evidence of cancer stem cells dates back to 1997, when Bonnet *et al* demonstrated that a subpopulation of CD34<sup>+</sup>/CD38<sup>-</sup> leukemia cells could initiate the disease when inoculated in severe combined immunodeficient (SCID) mice [29]. Currently, the presence of CSCs has been described in several tumor types, including lung [30], liver [31], breast [32], stomach [33], pancreatic [34], bladder [35], and colon cancer [36], as well as cutaneous and uveal melanoma [37, 38]. Cell surface markers, such as CD24, CD34, CD44, CD90, CD123, CD133, CD166, and the epithelial cell adhesion molecule

(epCAM), are an essential tool to guide the identification of CSCs in both solid and hematological malignancies (**Figure 3**) [39, 40]. Additionally, CSCs may be recognized through the evaluation of distinctive stem-like properties, such as the enhanced expression of enzymes belonging to the aldehyde dehydrogenases (ALDH) superfamily and the ability to grow *in vitro* as three-dimensional spheres [41, 42]. However, markers for CSCs can be extensively variable among tumor types and no universal marker has been identified yet; moreover, markers are often shared by tissue-resident and embryonic stem cells [39].

CSCs are characterized by many distinctive features, including the activation of stemness-associated signaling pathways. Indeed, CSCs upregulate transcription factors and molecules that control self-renewal and pluripotency, such as octamer-binding transcription factor 4 (OCT4), homeobox protein NANOG, Sry-related HMG box 2 (SOX2), c-MYC, nuclear factor kappa B (NF- $\kappa$ B), signal transducer and activator of transcription 3 (STAT3), Kruppel-like factor 4 (KLF4), Hedgehog (Hh), and Notch [43-47]. Additionally, CSCs may acquire a transient epithelial-to-mesenchymal phenotype, which allows them to easily migrate, invade the surrounding tissue, and drive metastasis formation [48], as suggested by the expression of several key regulators of epithelial-to-mesenchymal transition (EMT), such as twist-related protein 1 (TWIST1), zinc-finger protein SNAI1 (Snail), zinc-finger E-box binding homeobox 1 (ZEB1), and ZEB2 [49, 50].

A major challenge in cancer therapy revolves around the onset of chemoresistance and the risk of recurrence. CSCs are crucially involved in these processes since they are able to resist conventional therapies through several mechanisms. First, their low proliferation rate, the upregulation of anti-apoptotic proteins, and the timely activation of DNA repair machinery protects them from therapy-induced cell death [51, 52]. Moreover, CSCs overexpress transporters and enzymes, such as the ATP-binding cassette (ABC) transporters and the ALDH enzyme superfamily, that inactivate and eliminate drugs. Indeed, ABC transporters actively mediate the efflux of various drugs from the cell, while ALDH enzymes are involved in detoxification processes, by lowering levels of intracellular reactive oxygen species (ROS) and reactive aldehydes [53, 54].

Cancer	Markers
Haematological	CD34, CD38, CD19, CD26
Breast	CD44, CD24, CD29, CD133
Colon	CD44, CD24, CD26, CD29, CD133, CD166, Ep-CAM
Brain	CD90, CD133, CD15
Head and neck	CD44, CD271
Skin	CD20, CD271
Liver	CD44, CD90, CD133, CD13, Ep-CAP
Lung	CD44, CD133, CD166
Pancreas	CD44, CD24, CD133
Prostate	CD44, CD24, CD133, CD166, CD151
Oesophagus	CD271, CD44, CD24, CD90
Cervix	CD13, CD29, CD44, CD105
Stomach	CD44, CD133

**Figure 3.** Common cell surface markers for the identification of CSCs in different tumor types [40].

---

To overcome these mechanisms of therapy resistance, several therapeutic strategies are currently being investigated and are briefly reported hereafter:

- 1) Targeting the signaling pathways involved in CSC maintenance, proliferation, and differentiation. Inhibitors directed against Notch, Wnt/ $\beta$ -catenin, and Hh signaling pathways have been developed, showing positive results in clinical trials across different tumor types [55, 56]. Additionally, other potential targets are being investigated, including Transforming Growth Factor  $\beta$  (TGF $\beta$ ), NF- $\kappa$ B, and JAK-STAT [57].
- 2) Designing selective monoclonal antibodies to target CSC membrane antigens. For instance, common surface markers such as CD44, CD47, and CD133 are being assessed as promising targets [58]; however, this approach is hindered by the redundancy of these surface antigens on CSCs and normal stem cells alike [59].
- 3) Striking the TME to hamper the stem-cell niche. Despite the complexity of the TME, direct targeting of stromal cells, such as endothelial cells, tumor-associated fibroblasts, and tumor-associated macrophages, may provide an alternative approach for disrupting the intricate cross-talk of growth factors, cytokines, and chemokines that foster CSCs [60].

Over the years, great improvement in cancer treatment has been achieved. However, eliminating CSCs still represents a critical step to reach complete tumor eradication; therefore, a better understanding of the complex mechanisms regulating CSCs is essential for developing novel approaches and lowering the risk of recurrence.

## 2.1 CANCER STEM-LIKE CELLS IN UVEAL MELANOMA

In the last few years, the existence of CSCs in UM has been validated by experimental studies in which the expression of common markers of stem-like cells was assessed. Indeed, the expression of Nestin, CXCR4, CD44, and c-Kit has been detected in several UM cell lines. Also, the upregulation of Nestin and CD166 has been demonstrated in short-term cultures of primary UM cells compared to normal choroidal melanocytes [61, 62]. Additionally, an enrichment of the CSC subpopulation has been suggested by the high levels of CD166, Nestin, and CD27 found in UM cells resistant to anchorage-dependent cell death [62]. Finally, immunohistochemical analysis of primary tumors revealed a positivity for CD133, Pax6, Musashi, Nestin, SOX2, ABCB5, and CD68, especially at the invading tumor front, thus demonstrating the presence of a stem-like subset [61, 62].

Despite these promising results, the exact identification of the stem-like population in UM is hindered by a lack of reliable surface antigens, which are necessary for cell sorting, isolation, and characterization of the stem-like component. Nevertheless, various strategies have been developed, relying on the evaluation of distinctive properties of stem-like cells, such as sphere-formation capability and ALDH expression. In the sphere-formation assay, CSCs are propagated by allowing them to grow *in vitro* into multicellular three-dimensional spheres, so called melanospheres, through plating in non-adherent conditions in a serum-free medium; sphere-forming capacity is directly related to the number of CSCs in culture [63]. On the other hand, the assessment of enzymatic levels of ALDH by flow cytometric analysis is a reliable strategy to discriminate between CSCs, identified as the ALDH<sup>+</sup> (or ALDH<sup>high</sup>) population, and non-CSCs, which constitute the ALDH<sup>-</sup> (or ALDH<sup>low</sup>) fraction [64]. In this frame, it has been demonstrated that Mel270 and Omm2.5 UM cells, respectively derived from the primary tumor and liver metastasis of the same patient, are able to form melanospheres within 2 weeks of non-adherent culture [38]. Additionally, enhanced sphere-formation ability has been highlighted in primary



---

UM cells derived from poor-prognosis tumors, thus confirming a correlation between stemness and more aggressive tumor types in the clinical setting [62]. Furthermore, the assessment of enzymatic levels of ALDH has been validated as a marker for CSCs in UM, by confirming the presence of an ALDH<sup>+</sup> population of UM cells and illustrating the enhanced tumorigenic capacity *in vivo* of ALDH<sup>+</sup> cells compared to their ALDH<sup>-</sup> counterpart [65].

### 2.1.1 TARGETING CANCER STEM-LIKE CELLS AS A THERAPEUTIC STRATEGY IN UVEAL MELANOMA

Over the years, several strategies for improving the pharmacological treatment of UM have been developed and tested in *in vitro* and *in vivo* experimental models; in this frame, it is of pivotal importance to analyze whether these approaches are effective on the stem-like component in addition to differentiated cancer cells.

Histone deacetylase (HDAC) inhibitors have emerged as promising therapeutic agents in many tumor types, due to their strong selectivity and low toxicity to normal tissues. Currently, four drugs have been approved by the Food and Drug Administration (FDA) and the European Medicine Agency for the treatment of T-cell lymphoma and multiple myeloma, and their efficacy has been assessed also in experimental models of UM, showing promising results [66]. In particular, it has been demonstrated that the novel HDAC inhibitor JSL-1 efficiently targets UM-CSCs *in vitro* and *in vivo*. Indeed, JSL-1 successfully reduces cell proliferation, migration, and invasiveness of UM cells, triggering an apoptotic response; moreover, JSL-1 impairs sphere-formation and serial replating capacity, as well as the percentage of ALDH<sup>+</sup> cells. Finally, JSL-1 significantly reduces tumor growth in a NOD-SCID mouse xenograft model following 2 weeks of administration, confirming a potent anti-tumor activity *in vivo* [67]. Of note, the combined administration of JSL-1 and the chemotherapeutic agent vinblastine exerts a synergistic effect, thus demonstrating the potential improvement of combining HDAC inhibitors with conventional therapies [67].

On the other hand, several promising approaches have emerged recently, involving the direct or indirect inhibition of signaling pathways that contribute to the maintenance of stemness. In this frame, inhibitors of NF- $\kappa$ B and Wnt/ $\beta$ -catenin (*i.e.*, the triterpenoid pristimerin and the salicylanilide niclosamide) impair clonogenic potential and invasiveness of UM cells and reduce cell viability, promoting the production of ROS and triggering apoptosis. Additionally, they affect ALDH<sup>+</sup> and sphere-forming cells, and they downregulate the stemness-associated transcription factors SOX2, Slug, and c-MYC [68, 69]. Of note, niclosamide, which has been approved by FDA and has been safely used in human for over 50 years, displayed a strong anti-tumor effect in *in vivo* UM mice xenografts, with minimal cytotoxicity to normal tissues [69].

Salinomycin, a monocarboxylic polyether with antibiotic activity, has been recognized as a selective CSC inhibitor in breast cancer, colon cancer, renal carcinoma, and leukemia; supposedly, salinomycin exerts its anti-CSC effect by interfering with ABC transporters and inhibiting stemness-associated transcription factors SOX2, Snail, c-MYC, Hedgehog, and Wnt/ $\beta$ -catenin [70-72]. As for UM, it has been demonstrated that salinomycin impairs cell viability, clonogenicity, invasiveness, and migration. Moreover, salinomycin effectively reduces tumor growth of UM xenografts in NOD/SCID mice as well as formation of hepatic metastasis following intrasplenic injection of UM cells. Additionally, salinomycin hampers the ALDH<sup>+</sup> UM stem-like component, lowering the expression of the stemness-related factors

SOX2 and TWIST1. Of note, given that both TWIST1 and SOX2 are correlated to increased risk of metastasis and enhanced mortality in patients, the results obtained with salinomycin represent a significant starting point for further investigation on its clinical application.

Another approach involves targeting of cyclin-dependent kinase 9 (CDK9), which is overexpressed by several UM cell lines, by the selective inhibitor SNS-032. Interestingly, SNS-032 is able to inhibit the activity of the transcription activator Yes-Associated Protein (YAP), which is required for GαQ/11-driven tumorigenesis. Accordingly, SNS-032 significantly reduces cell viability in UM cells, but not in a retinal pigment epithelial cell line; moreover, treatment with SNS-032 inhibits colony formation and activates apoptosis, exerting a synergic effect with the chemotherapeutic drug vinblastine. Furthermore SNS-032 decreases ALDH<sup>+</sup>, sphere-forming CSCs *in vitro* and it reduces UM cell migration and invasiveness, as suggested by the downregulation of metalloproteinases and the impairment of actin polarization and formation of invadopodia. Finally, SNS-032 hinders *in vivo* tumor growth and suppresses liver metastasis formation by targeting the stem-like component, as suggested by the reduced expression of Slug and KLF4, two mediators that are strongly correlated with increased mortality and lower metastasis-free survival in patients [73].

On a similar note, enhancer of zeste homolog 2 (EZH2) is a known regulator of stemness in multiple tumor types and it is associated to a higher risk of metastasis and to a shorter survival in the clinical setting. Immunohistochemical staining on tumor samples and choroidal tissue from donors has detected the overexpression of EZH2 in 88% of tumor cases; moreover, there's a direct correlation between overexpression of EZH2 and more aggressive primary tumors, as well as reduction of overall survival. Indeed, EZH2-transfection in UM cells promotes a more aggressive phenotype by enhancing cell proliferation, clonogenicity, and invasiveness of UM cells, which were instead affected by EZH2 knock-down. Additionally, depletion or inhibition of EZH2 impairs the stem-like component, as well as *in vivo* tumor growth and formation of hepatic metastasis, suggesting the relevance of EZH2 as a potential therapeutic target [65].

A different strategy consists in targeting elements involved in the complex maintenance of the TME. Interestingly, a variety of extracellular proteases contribute to the dynamism of TME, including ADAMTS1, which is correlated to the acquisition of an endothelial-like phenotype in tumor cells, as an alternative mechanism of neovascularization, though the reversion to a stem-like state [74]. Given its high expression in UM patients during the early stages of the disease, the role of ADAMTS1 in UM stemness regulation has been investigated. In particular, the inhibition of ADAMTS1 by CRISPR-CAS9 technology significantly reduces melanosphere-formation capacity and endothelial-like properties of UM cells, and downregulates genes involved in vascular remodeling. Moreover, ADAMTS1 knock-out cells have a weaker tumorigenic potential in *in vivo* mouse xenografts; additionally, the explanted tumors display a significant downregulation of stemness-associated genes such as *NANOG*, *OCT4*, *PROM1*, and *SOX2*, as well as alterations in vascular density, supporting the hypothesis that ADAMTS1 may sustain the development of UM through the induction of stemness [75].

Altogether, these promising results demonstrate both relevance and feasibility of targeting CSCs in UM. Nevertheless, further studies are needed to better elucidate the molecular mechanisms involved in CSCs sustenance in order to widen the spectrum of exploitable strategies in the clinical setting, with the ultimate goal of improving the management of UM and survival expectancy.

### 3. THE FIBROBLAST GROWTH FACTOR (FGF)/ FIBROBLAST GROWTH FACTOR RECEPTOR (FGFR) FAMILY

The fibroblast growth factor (FGF)/FGF receptor system is extremely important for the regulation of several physiological functions, such as cell proliferation, differentiation, tissue homeostasis, embryonal development, and wound healing [76].

The FGF family is extremely diverse. In humans, it comprises 22 ligands, which can be organized based on sequence homology and phylogeny into five paracrine subfamilies and one endocrine subfamily. FGFs exert their biological activities by binding and activating high-affinity tyrosine kinase receptors (*i.e.*, FGFR1, FGFR2, FGFR3, FGFR4), triggering conformational changes and inducing receptor dimerization. The subsequent phosphorylation of intracellular tyrosine residues of FGFRs provides docking sites for signaling molecules. Transduction occurs by FGFR substrate 2 (FRS2) and phospholipase C $\gamma$  (PLC $\gamma$ ), which activate downstream mediators including RAS/RAF-MEK-MAPKs, PI3K/AKT, and STAT. Regulation of FGF/FGFR signaling occurs at different levels, and includes spatial and temporal expression of ligands and receptors, binding specificity, alternate splicing, and interaction with other signaling pathways, such as bone morphogenic protein (BMP) and Wnt signaling [76-78].

#### 3.1 THE FGF/FGFR SYSTEM IN CANCER PROGRESSION

The role of the FGF/FGFR system in cancer progression has been extensively characterized in literature. Briefly, dysregulation of both ligands and receptors occurs frequently, both in the tumor and in the stromal component, and is involved in sustaining tumor growth, invasion, angiogenesis, metastatic dissemination, and resistance to therapies (**Figure 4**) [79]. Aberrant activation of FGF/FGFR-mediated signaling may depend on various mechanisms and it has been described in numerous tumor types, including prostate [79], breast [80], gastric [81], bladder [82], cervical [83], and squamous cell lung cancer [84], as well as lymphoma [85] and multiple myeloma [86]. Common causes of ligand-independent transduction may involve genetic alterations, including activating mutations in the extracellular or in the tyrosine-kinase domain of the receptor, upregulation of FGFRs due to gene amplification, and the formation of fusion proteins with oncogenic activity caused by chromosomal translocations [87]. On the other hand, ligand-dependent activation plays an important role in tumorigenesis. Despite the rarity of mutations involving FGFs, upregulation of gene expression or gene amplification causes increased ligand production, which triggers autocrine or paracrine loops of stimulation in stromal and tumor cells, in order to regulate cell proliferation, migration, and resistance to apoptosis [88, 89]. Indeed, studies point to the aberrant activation of the FGF/FGFR system as a mechanism that actively promotes therapy resistance in cancer cells [90].

##### 3.1.1 THE FGF/FGFR SYSTEM IN UVEAL MELANOMA

Clinical and experimental evidence demonstrates the involvement of the FGF/FGFR system in UM. Indeed, the presence of an autocrine loop of activation sustains proliferation, migration, and survival of UM cells in *in vitro* models; moreover, the overexpression of ligands and/or receptors is linked to a worse prognosis in patients and with enhanced risk of progression to metastatic disease [91].

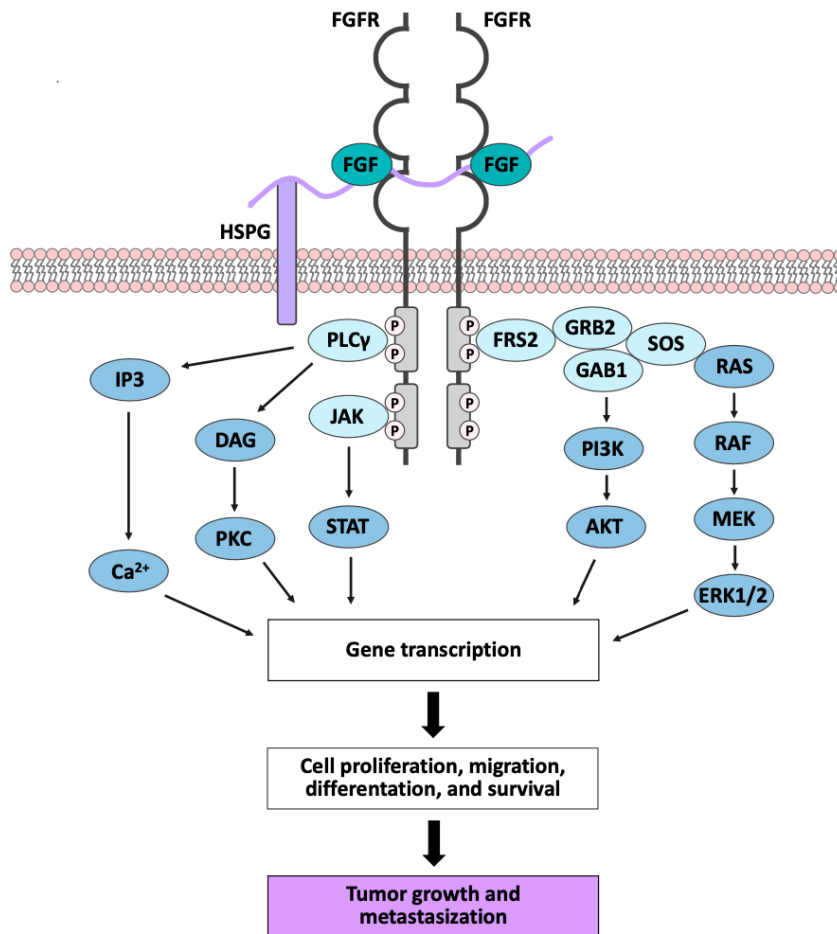


**Figure 4. FGF/FGFR signaling pathways.** The formation of two FGF/FGFR/heparan-sulfate proteoglycan (HSPG) ternary complexes trigger receptor dimerization and trans-phosphorylation of the tyrosine kinase domains. Then, docking of intracellular substrates activates downstream signaling pathways [92].

For more details on the role played by FGF/FGFR system in human cancers and in UM, please consult the following publication at the end of the chapter:

- **Exploring the FGF/FGFR System in Ocular Tumors: New Insights and Perspectives.**  
**A. Loda,** M. Turati, F. Semeraro, S. Rezzola, R. Ronca.  
 Int J Mol Sci. 2022 Mar 30;23(7):3835. doi: 10.3390/ijms23073835. PMID: 35409195; PMCID: PMC8998873.

## 3.2 TARGETING THE FGF/FGFR SYSTEM FOR CANCER THERAPY

The FGF/FGFR system represents an attractive target for the identification of novel pharmacological approaches aimed at improving the treatment of human cancers. Accordingly, several classes of FGF inhibitors have been developed, including tyrosine-kinase inhibitors, monoclonal antibodies, and FGF traps [93]. However, approval for administration of anti-FGF/FGFR drugs in the clinical setting is limited to cholangiocarcinoma, urothelial cancer, and myeloid/lymphoid neoplasms, since the driving role of FGFRs is well characterized in these tumor types [94-96].

### 3.2.1 THE NOVEL SMALL MOLECULE NSC12 AS A PAN FGF-TRAP IN UVEAL MELANOMA

The compound 4,4,4-trifluoro-1-(3-hydroxy-10,13-dimethyl-2,3,4,7,8,9,11,12,14,15,16,17-dodecahydro-1H-cyclopenta(a)phenanthren-17-yl)-3(trifluoromethyl)butane-1,3-diol, hereby referred to as NSC12 (**Figure 5**), is able to bind to all canonical FGFs, preventing FGFR activation and signal transduction [97].

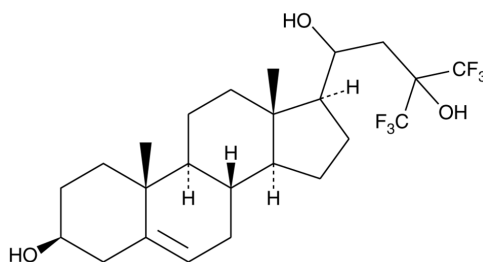


**Figure 5. Chemical structure of NSC12 [97].**

The efficacy of NSC12 as a pan FGF-trap with anti-tumor activity has been demonstrated across several tumor types, including UM [98-102]. Indeed, NSC12 is effective in hampering cell proliferation and migration in both primary and metastatic UM cell lines, triggering the activation of an apoptotic response [103]. For more data about the activity of NSC12 in UM, please refer to the following paper at the end of the chapter:

- **The Autocrine FGF/FGFR System in both Skin and Uveal Melanoma: FGF Trapping as a Possible Therapeutic Approach**

S. Rezzola, R. Ronca, **A. Loda**, Ml. Nawaz, C. Tobia, G. Paganini, F. Maccarinelli, A. Giacomini, F. Semeraro, M. Mor, M. Presta.

Cancers (Basel). 2019 Sep 4;11(9):1305. doi: 10.3390/cancers11091305. PMID: 31487962; PMCID: PMC6770058.

---

### 3.3 THE FGF/FGFR SYSTEM IN STEMNESS REGULATION

The FGF/FGFR system is involved in maintaining pluripotency in physiological conditions. As a matter of fact, the expression of both ligands and receptors has been demonstrated in human embryonic stem cells (hESCs), where they modulate self-renewal and differentiation through the activation of signaling pathways such as MAPK, PI3K/AKT, and JAK/STAT. Indeed, exogenous FGF2 is essential for sustaining self-renewal, and it maintains pluripotency of hESC under feeder-free culture conditions [104, 105]. Additionally, FGF2 maintains pluripotency in human induced pluripotent stem cells (hiPSCs); furthermore, withdraw of FGF2 reduces the expression of stemness-associated transcription factors OCT4, SOX2, and NANOG, promoting cell differentiation [106].

In addition to the role played in physiological settings, the FGF/FGFR system has been associated to the regulation of stem-like properties also in tumor cells and it has been linked to the maintenance of CSCs across various tumor types, such as pancreatic cancer [107, 108], esophageal squamous cell carcinoma [109], head and neck cancer [110, 111], hepatocellular carcinoma [112], and glioblastoma [113]. Accordingly, inhibition of the FGFs/FGFRs or downstream signaling pathways significantly impairs CSCs *in vitro*; moreover, it reduces tumor growth in *in vivo* mouse xenograft models of pancreatic cancer, esophageal squamous cell carcinoma, and glioblastoma [108, 109, 113]. Therefore, pharmacological inhibition of FGF/FGFR axis activation, either alone or in combination with chemotherapeutic drugs, may represent an interesting strategy to strike the stem-like component in human cancers. In this frame, further studies are necessary to gain a more wide-spread understanding on the involvement of the FGF/FGFR system in the sustenance of stem-like cells across various tumor types, including UM.

During my PhD program, my main research activity has been focused on investigating the role of the FGF/FGFR system in the maintenance of CSCs in UM. The results obtained have been published in A. Loda *et al.*, *Cancer Cell Int.*, 2023 and can be found in the next section.



## **Exploring the FGF/FGFR System in Ocular Tumors: New Insights and Perspectives**

**A. Loda**, M. Turati, F. Semeraro, S. Rezzola, R. Ronca.

Int J Mol Sci. 2022 Mar 30;23(7):3835. doi: 10.3390/ijms23073835. PMID: 35409195; PMCID: PMC8998873.







Review

# Exploring the FGF/FGFR System in Ocular Tumors: New Insights and Perspectives

Alessandra Loda <sup>1,†</sup>, Marta Turati <sup>1,†</sup>, Francesco Semeraro <sup>2,‡</sup>, Sara Rezzola <sup>1,‡</sup> and Roberto Ronca <sup>1,\*,‡</sup><sup>1</sup> Department of Molecular and Translational Medicine, School of Medicine, University of Brescia, 25123 Brescia, Italy; a.loda025@unibs.it (A.L.); m.turati004@unibs.it (M.T.); sara.rezzola@unibs.it (S.R.)<sup>2</sup> Eye Clinic, Department of Medical and Surgical Specialties, Radiological Sciences and Public Health, University of Brescia, 25123 Brescia, Italy; francesco.semeraro@unibs.it

\* Correspondence: roberto.ronca@unibs.it; Tel.: +39-030-3717735

† These authors contributed equally to this work.

‡ These authors contributed equally to this work.

**Abstract:** Ocular tumors are a family of rare neoplasms that develop in the eye. Depending on the type of cancer, they mainly originate from cells localized within the retina, the uvea, or the vitreous. Even though current treatments (e.g., radiotherapy, transpupillary thermotherapy, cryotherapy, chemotherapy, local resection, or enucleation) achieve the control of the local tumor in the majority of treated cases, a significant percentage of patients develop metastatic disease. In recent years, new targeting therapies and immuno-therapeutic approaches have been evaluated. Nevertheless, the search for novel targets and players is eagerly required to prevent and control tumor growth and metastasis dissemination. The fibroblast growth factor (FGF)/FGF receptor (FGFR) system consists of a family of proteins involved in a variety of physiological and pathological processes, including cancer. Indeed, tumor and stroma activation of the FGF/FGFR system plays a relevant role in tumor growth, invasion, and resistance, as well as in angiogenesis and dissemination. To date, scattered pieces of literature report that FGFs and FGFRs are expressed by a significant subset of primary eye cancers, where they play relevant and pleiotropic roles. In this review, we provide an up-to-date description of the relevant roles played by the FGF/FGFR system in ocular tumors and speculate on its possible prognostic and therapeutic exploitation.

**Keywords:** ocular tumors; FGF; FGFR; retinoblastoma; uveal melanoma

**Citation:** Loda, A.; Turati, M.; Semeraro, F.; Rezzola, S.; Ronca, R. Exploring the FGF/FGFR System in Ocular Tumors: New Insights and Perspectives. *Int. J. Mol. Sci.* **2022**, *23*, 3835. <https://doi.org/10.3390/ijms23073835>

Academic Editor: Andreas Weigert

Received: 3 March 2022

Accepted: 30 March 2022

Published: 30 March 2022

**Publisher's Note:** MDPI stays neutral with regard to jurisdictional claims in published maps and institutional affiliations.



**Copyright:** © 2022 by the authors. Licensee MDPI, Basel, Switzerland. This article is an open access article distributed under the terms and conditions of the Creative Commons Attribution (CC BY) license (<https://creativecommons.org/licenses/by/4.0/>).

## 1. Introduction

The eye is a highly specialized sensory organ that allows the collection of external images through photoreception, a process by which light energy is detected by specialized neurons in the retina, i.e., the rods and cones. In turn, retinal neurons activate action potentials, which are subsequently transmitted through the optic nerve to the brain, where the information is processed as vision [1].

Structurally, the eye is a slightly asymmetrical globe located in the orbit, a compartment that is closed medially, laterally, and posteriorly (Figure 1). The eyeball is formed by three concentric layers of tissue. The outer protective layer is constituted by the fibrous coat, which includes the transparent cornea and the opaque sclera; it helps to maintain intraocular pressure and provides an attachment site for intraocular muscles. The anterior portion of the eye and the inner surface of the eyelids are covered by the conjunctiva, a protective mucous membrane [1,2]. The middle layer, i.e., the uvea, represents the vascular coat, which exerts nutritive functions to support ocular structures. It comprises the iris, the ciliary body, and the choroid. Finally, the retina constitutes the neural coat, an inner sensory layer which hosts several classes of neuronal cells involved in the visual process [2–4].

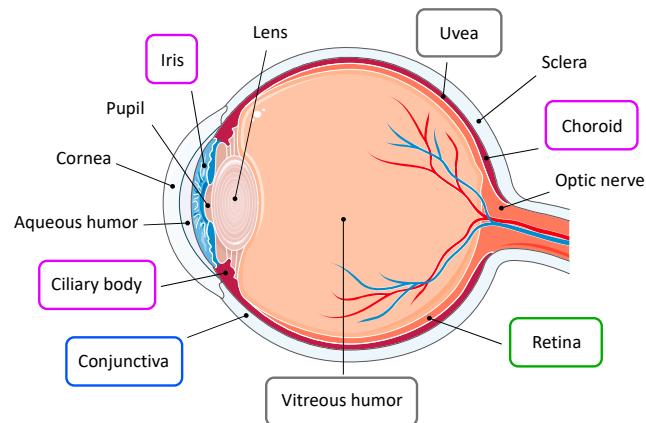


**Figure 1.** Tumors of the eye. Ophthalmic tumors affect specific ocular structures. Retinoblastoma (green) arises in the retina; conjunctival melanoma (blue) involves the conjunctival epithelium; uveal melanoma (purple) develops from any region of the uveal tract; ocular lymphomas (grey) derive from the vitreoretinal tissue or from the uvea.

The globe is divided into two cavities, the anterior and the posterior segments. The anterior segment encompasses the space around the iris and is filled with the aqueous humor, a clear fluid actively secreted by the ciliary processes. The posterior segment is located behind the lens, and it contains the vitreous humor, which is mostly composed of collagen and hyaluronic acid; vitreous humor has a very slow turnover and it helps in maintaining the shape of the eye [1].

## 2. Ocular Cancers

Among the numerous pathologies that may affect the eye and impair vision, ocular cancers are relatively rare, affecting approximately 1/100,000 in the U.S.; their occurrence is variable, according to patients' ethnicity and age [5,6]. Depending on the type of tumor, ophthalmic malignancies might involve distinct ocular structures (Figure 1) [6]. Moreover, the eye may represent the site of metastasis of other primary tumors such as breast and lung cancers, cutaneous melanoma, tumors of the gastrointestinal tract, and kidney cancer [5,7]. In this review, we focus on the most common intraocular cancers, i.e., retinoblastoma, ocular melanomas, and ocular lymphoma, which together represent the majority of ophthalmic neoplasms.

### 2.1. Retinoblastoma

Retinoblastoma is an ophthalmic tumor that predominantly affects children before 4–5 years of age. It represents the most common intraocular malignancy of childhood and, with approximately 9000 new cases diagnosed each year, it accounts for approximately 2% of all childhood cancers worldwide [8]. Retinoblastomas may occur unilaterally or bilaterally. Unilateral tumors develop following the inactivation in a susceptible retinal cell of both wild-type alleles of the *RB1* gene, which codifies for a regulatory transcription factor. On the other hand, all bilateral patients present a germline mutation of *RB1*; therefore, a second hit is sufficient for the development of the benign precursor retinoma, whereas further mutations are necessary for the progression to retinoblastoma [9]. During the initial stages of the disease, retinoblastoma manifests as a circumscribed intraretinal mass. However, tumors can grow in an exophytic pattern towards the subretinal space, causing diffuse retinal detachment. Alternatively, retinoblastoma can extend in an endophytic pattern within the retina and into the vitreous cavity, leading to vitreous seeding and, in severe cases, infiltrating the anterior segment of the eye [5,10]. If untreated, retinoblastoma

is lethal within two years, due to intracranial tumor growth and disease dissemination [11]. Therefore, early diagnosis is essential for its successful clinical management [8].

Currently, chemotherapy combined with focal laser therapy is the preferred method of treatment, while external beam radiation is no longer recommended due to increased risk of secondary malignancies [10]. Enucleation, i.e., the surgical removal of the eye, remains indicated for advanced tumors or in cases of recurrent disease [5]. To date, retinoblastoma has a very high cure rate, with 98% of patients surviving after treatment [10,11]. Nevertheless, metastatic disease occurs in 5% of all retinoblastoma cases and may affect the central nervous system, the bones, and the bone marrow. Despite the successful treatment of the primary tumor, the prognosis for metastatic retinoblastoma remains poor, and few therapeutic options are available [8,10].

## 2.2. Ocular Melanomas

Ocular melanomas are the second most common type of eye tumor, and they represent 10% of all melanomas. They arise from the melanocytes located in different regions of the eye, mainly within the uvea and the conjunctiva, giving rise to uveal or conjunctival melanomas, respectively [12].

Uveal melanoma is the most frequent primary intraocular neoplasm in the adult population, and it accounts for 85% to 95% of all intraocular melanomas [13]. The incidence of uveal melanoma in Europe ranges from 2 to 8 cases per million, and its occurrence increases with age [14]. Tumors may originate from any region of the uveal tract, which is composed of the iris, the ciliary body, and the choroid. Clinical presentation varies according to tumor size and location, with blurred and distorted vision being common symptoms of iris or ciliary body involvement, while choroidal melanomas are associated with vision loss due to retinal detachment [15]. Primary tumors are successfully treated by brachytherapy or phototherapy, whereas enucleation is recommended only for severe cases with extensive intraocular growth [16]. Nevertheless, uveal melanoma is a highly metastatic disease, with a tendency to spread via hematogenous dissemination; the liver represents the most frequent site of metastasis, followed by lungs, bones, skin, and brain [15,17]. Approximately 50% of patients affected by uveal melanoma develop metastasis within 5 years, with median survival ranging from 4 to 15 months due to the lack of effective pharmacological therapies [18]. To date, no standard of care has been approved for treatment of metastatic disease and conventional chemotherapies remain unable to improve the overall survival [14,19,20]. Thus, novel therapeutic approaches are eagerly required. In this context, *in vitro* and *in vivo* experimental models of uveal melanoma may represent a useful tool for the screening of new drug candidates [21]. It is worth mentioning that uveal melanoma lacks the most typical mutations associated with cutaneous melanoma (i.e., *BRAF* and *NRAS*). Instead, activating mutations in *GNAQ* or *GNA11* genes occur in 80–90% of uveal melanoma cases in a mutually exclusive pattern. Both *GNAQ* and *GNA11* genes codify for  $\alpha$ -subunits of G-coupled proteins and have been recognized as uveal melanoma driver mutations [22]. Additionally, mutations of *BAP1* are frequently observed in most metastasizing uveal melanomas. Loss of *BAP1* compromises the maintenance of a differentiated melanocytic phenotype, promoting epithelial-to-mesenchymal transition and metastatic dissemination. In alternative to *BAP1*, metastatic uveal melanomas often present mutations of *SF3B1*, which are associated with a longer disease-free survival [13].

Conjunctival melanoma comprises approximately 5% of all ocular melanomas and it arises from melanocytes located in the basal layer of the conjunctival epithelium, which lines the eyelids and the sclera [12,23]. In rare cases, tumors might grow and extend toward the orbit or into the globe. Moreover, conjunctival melanoma tends to spread via both lymphatic and blood vessels, affecting first the regional lymph nodes in 45% to 60% of patients [12]. Subsequent systemic dissemination may occur in 20% to 30% of patients within 10 years, with metastasis spreading to lungs, brain, bones, liver, skin, and the gastrointestinal tract [12,23]. Currently, the standard treatment for conjunctival melanoma is the surgical resection of the tumor mass, followed by cryotherapy to the tumor margins

after excision. However, effective eradication of conjunctival melanoma is hindered by a high rate of local recurrence. Therefore, adjuvant chemotherapy is often employed through the administration of topical agents [24]. Enucleation or orbital exenteration, which consist in the surgical removal of the globe, muscles, nerves, and fatty tissue adjacent to the eye, may be necessary for patients with advanced tumors, while no standard of care has been defined for metastatic disease [12,24,25].

### 2.3. Ocular Lymphomas

Intraocular lymphomas are a rare type of malignant lymphocytic neoplasm and they include lymphomas derived from the vitreoretinal tissues as well as lymphomas of the uveal tract. Vitreoretinal lymphomas are mainly primary diseases, arising within the central nervous system, while uveal lymphomas generally occur as metastasis of systemic non-Hodgkin lymphomas [26,27]. The exact epidemiology of primary intraocular lymphomas is unclear, as most datasets classify the disease as a subset of primary central nervous system lymphomas [27]. Tumor onset is often subtle, with non-specific symptoms that mimic uveitis and lead to a delayed diagnosis [26]. Moreover, 16% to 34% of patients also manifest central nervous system involvement at presentation. Indeed, the disease progresses to intracranial lymphoma in 42% to 92% of patients, with widespread dissemination occurring in the advanced stages of the disease [27]. Optimal treatment for intraocular lymphoma is not well defined. The primary disease is mainly treated by intravitreal chemotherapy or low-dose localized radiotherapy, whereas high-dose chemotherapy combined with local therapy is recommended for patients with central nervous system involvement [26,28]. Mortality rates are inconsistent due to the rarity of the disease, spanning from 9% to 81% in follow-up periods of 12–35 months [27].

### 2.4. Eye Metastasis

The eye may represent the site of metastasis for several tumors, in particular breast (47%) and lung (21%) cancers, but also of cutaneous melanoma, tumors of the gastrointestinal tract, and kidney cancer [5,7]. Metastasis might arise in any part of the eyeball or the orbit, but 88% of cases affect the posterior uvea due to its extensive vascularization [7,29]. Therapeutic strategies include systemic therapies, local treatment, or a combination of both [29]. Radiotherapy, either with external beam radiation or brachytherapy, is the most common treatment for metastatic disease [30]. However, the average survival expectation following diagnosis of ocular metastasis is approximately 7 months and is essentially linked to the lethality and stage of the primary tumor [7].

## 3. The Fibroblast Growth Factor (FGF)/FGF Receptor (FGFR) System

In mice and humans, the Fibroblast Growth Factor (FGF) family is composed of 22 polypeptides that act as secreted signaling proteins (FGF1–10, FGF16–23) or as receptor-independent intracellular factors (FGF11–14), with the latter being mainly involved in neuronal development and in regulating the electrical excitability of neurons [31,32]. Secreted FGFs are grouped into 6 subfamilies according to phylogenetic analysis and sequence homology. The subfamilies FGF1/2/5, FGF3/4/6, FGF7/10/22, FGF8/17/18, and FGF9/16/20 are known as canonical FGFs and act as local paracrine signaling molecules. The FGF19/21/23 subfamily comprises hormone-like FGFs acting as endocrine factors that control metabolic homeostasis [31,33,34]. Both canonical and hormone-like FGFs mediate their biological functions by activating cell surface tyrosine kinase (TK) receptors (FGFRs), which are encoded by four distinct genes (*FGFR1–4*) in mammals [31,33]. Structurally, FGFRs present an extracellular domain, a transmembrane domain, and a cytoplasmic TK tail, which is responsible for FGF-related signaling. The extracellular domain consists of three immunoglobulin (Ig)-like domains (I–III), with the Ig-like domain II and III being involved in ligand binding and in defining ligand specificity [33,35]. The functional interaction between canonical FGFs and their receptors requires the formation of two

FGF-FGFR-heparan sulfate proteoglycan (HSPG) ternary complexes and their subsequent dimerization (Figure 2) [33,36].

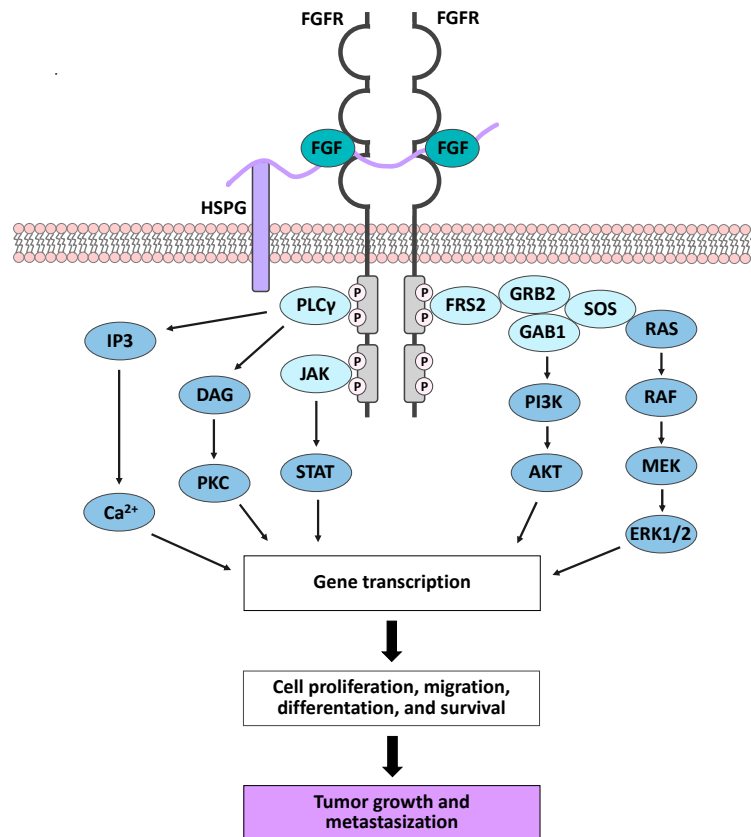


**Figure 2.** Fibroblast Growth Factor (FGF)/FGF receptor (FGFR) signaling pathways. The formation of two FGF-FGFR-heparan sulfate proteoglycan (HSPG) ternary complexes induces receptor dimerization and trans-phosphorylation of the tyrosine kinase (TK) domains. This event leads to the docking of intracellular receptor substrates and consequent activation of downstream signaling pathways. Deregulation of FGF/FGFR-mediated cell activities promotes tumor onset and progression.

Besides their role as coreceptors in FGF/FGFR interaction, HSPGs protect canonical FGFs from extracellular protease-mediated degradation; moreover, they sequester FGF molecules, thus limiting their diffusion through the extracellular matrix and providing a reservoir of the ligands [35,37]. The formation of the FGF-FGFR-HSPG ternary complex triggers conformational changes, leading to trans-phosphorylation of the tyrosine residue within the intracellular TK domain and providing docking sites for intracellular receptor substrates, such as specific adaptor protein FGFR substrate 2 (FRS2) and phospholipase C $\gamma$  (PLC $\gamma$ ). Phosphorylation of FRS2 activates the RAS-MAPK pathway, resulting in proliferation, differentiation, or cell cycle arrest, depending on the different cellular context. Moreover, FRS2 phosphorylation may also activate the anti-apoptotic PI3K-AKT pathway. On the other hand, PLC $\gamma$  leads to protein kinase C (PKC) activation and intracellular Ca<sup>2+</sup> release, promoting cell migration [34,38] (Figure 2).

By mediating such a wide range of cellular activities, the FGF/FGFR system assumes pivotal regulatory roles. Indeed, it is involved from the earliest phases of embryonic development by taking part in mesoderm patterning; moreover, by regulating mesenchymal-epithelial communications, the FGF/FGFR system is essential for organogenesis. Furthermore, FGFs/FGFRs exert homeostatic functions in adults, being involved in tissue repair and remodeling processes [31,34].

Given its ubiquitous and wide-ranging biological functions, the FGF/FGFR system requires tight regulation. Ligand-receptor binding specificity and spatio-temporal expression of FGFs, FGFRs, and HSPGs are necessary to avoid aberrant or unappropriated activation. Furthermore, negative feedback mechanisms occur in response to FGF/FGFR activation, including FGFR internalization and the recruitment of phosphatases and/or negative modulators (e.g., Sprouty proteins) [33,38]. FGFR signaling may also be modulated through the interaction with the non-canonical signaling partners of FGFRs, including extracellular matrix (ECM)-associated proteins, cell adhesion molecules (CAMs), or other transmembrane proteins and serine/threonine kinases [39].

### 3.1. The FGF/FGFR System in Cancer

The FGF/FGFR family has been described to play a relevant role in several pathological conditions, including cancer [33,34,40]. The aberrant activation of the FGF/FGFR system, both in the neoplastic and the stromal compartments, may occur both in a ligand-independent or a ligand-dependent manner, triggering tumor growth, invasion, angiogenesis, metastatic dissemination, and resistance to therapies [41–43]. Activating mutations in the extracellular or TK domains of the receptors are involved in the progression of various tumor types, including bladder and cervical cancers [44], multiple myeloma [45], and prostate cancer [46]. Moreover, chromosomal translocations may generate fusion proteins involving the TK domain of FGFR combined with a transcription factor domain, as, for example, ZNF198 in myeloproliferative syndrome [47] or ETV6 in peripheral T-cell lymphoma [48]. In these cases, the constitutive dimerization and activation of the fusion protein strongly promotes cell proliferation and tumor growth [47,48]. As reported for multiple myeloma, chromosomal translocations may also result in *FGFR* overexpression by bringing *FGFR* genes under the control of a highly active promoter [37,38,40,49]. Additionally, *FGFR* overexpression has been reported for breast [50], gastric [51], and squamous cell lung cancers [52] as a consequence of dysregulated gene transcription and amplification.

Ligand-dependent FGFR signaling activation plays an important role in the pathogenesis of cancer as well. Indeed, FGFs can be produced at high concentrations or “out of context” by cancer cells or by the surrounding stroma, thus causing the hyperactivation of the signaling and sustaining tumor growth through autocrine/paracrine mechanisms. Furthermore, altered gene splicing mechanisms may lead to the production of different splice variants of the receptors, able to bind a wider range of FGFs, resulting in an increased FGF/FGFR activation. Aberrant FGF/FGFR signaling may also result from the impairment of negative feedback mechanisms, including mutations that increase receptor stability or loss of negative feedback regulators [37,49].

Besides their pro-tumor activity exerted on cancer cells, tumor-derived FGFs also mediate tumor/stroma crosstalk, thus playing a relevant role in conditioning the surrounding stromal cells and favoring the onset of a pro-tumor microenvironment [53,54]. It is well documented that FGFs, in particular FGF1 and FGF2, promote tumor-associated angiogenesis and induce the formation of new vessels that provide oxygen and nutrients, and that facilitate cancer cell dissemination [49]. Furthermore, tumor-derived FGFs activate cancer-associated fibroblasts (CAFs), and in turn CAF-produced FGFs sustain cancer progression [55]. FGFs are also involved in the recruitment of tumor-associated macrophages, which exert pro-tumor functions by negatively regulating immune responses to cancer cells. Finally, emerging evidence highlights a possible role of the FGF/FGFR system in the acquisition of resistance to drugs, despite their different molecular structure and mechanisms of action [49,56]. Thus, aberrant activation of FGF/FGFR signaling may have several effects

on tumor biology, including the promotion of cell proliferation and survival, motility and invasiveness, metastatic dissemination, tumor escape from immune control, and resistance to therapy.

Finally, the regulation exerted by non-canonical FGFR interactors plays a relevant role in cancer. Indeed, integrin-regulated FGFR signaling has been directly implicated in tumorigenesis, particularly in angiogenesis, a critical step for metastatic dissemination. FGF1/Integrin- $\alpha$ V $\beta$ 3/FGFR1 crosstalk has been shown to promote both angiogenesis and tumorigenesis, and to enhance epithelial to mesenchymal transition (EMT) in breast cancer cell lines [57,58]. FGFR can also interact with different glycoproteins belonging to the family of CAMs, which are strictly implicated in fostering the migratory properties associated with EMT in cancer. Indeed, neural-CAM (NCAM) has been reported to prevent the binding of FGF to its receptor by acting as a nonconventional ligand of FGFR1, able to mediate an FGF-independent activation [59]. NCAM/FGFR1 complexes cycle rapidly and repeatedly at the cell surface and result in sustained signaling and cell migration. Similarly, L1CAM was described to induce signal transduction through FGFR1 in glioma cells, promoting proliferation and motility [60]. FGFR/cadherins interactions have been reported, leading to different biological effects, either tumorigenic or tumor suppressive, depending on the type of cadherin involved [61]. For instance, the binding of N-cadherin with FGFR1 stabilizes the receptor at the plasma membrane, preventing its internalization and degradation, thus promoting motility, invasion, and metastasis [62]. Galectin-1 and -3 have been described to interact with the extracellular regions of FGFR1, mimicking the ligands in an FGF-independent way and acting as regulators of FGFR1 signaling and trafficking [63]. Indeed, FGFR1/galectin-1 complexes trigger the dimerization of the FGFR, the activation of the downstream signaling, and result in anti-apoptotic and proliferative responses [64]. Conversely, galectin-3 crosslinks FGFR1 on the cell surface and prevents its constitutive internalization.

### 3.2. FGF/FGFR Inhibitors

Due to its crucial role in cancer progression, the FGF/FGFR system represents an attractive target for the development of anti-tumor drugs. In this context, FGFR inhibitors may act either at an extracellular level, by preventing ligand-receptor interaction, or at an intracellular level, by hampering signal transduction. Currently, FGFR inhibitors are classified as: (i) TK inhibitors (TKIs), (ii) monoclonal antibodies (mAbs), and (iii) FGF traps [41,49].

First-generation TKIs are small molecules that inhibit the kinase activity of TK receptors (RTKs) by preventing the binding of ATP to the catalytic site in a non-selective manner. These compounds act on several RTKs, including FGFRs, due to the structural similarity of their TK domains [65]. Although simultaneous inhibition of multiple RTKs may represent a compelling therapeutic strategy, the application of non-selective TKIs in clinical practice is limited by the onset of local and systemic complications, together with the poor efficacy observed in FGFR-dependent tumors. Nevertheless, some of these compounds are currently under investigation in preclinical and clinical trials, whereas other non-selective TKIs have already been approved for the treatment of metastatic thyroid cancer (i.e., lenvatinib) and metastatic colorectal cancer (i.e., regorafenib) [41]. To overcome the off-target effects of first generation TKI drugs, selective FGFR TKIs have been developed and are now under evaluation (e.g., BGJ398 for non-muscle-invasive urothelial carcinoma and AZD4547 for non-small cell lung cancer) or already approved (e.g., pemigatinib for cholangiocarcinoma and JNJ-42756493 for urothelial carcinoma) [66–68] ([www.clinicaltrials.gov](http://www.clinicaltrials.gov), accessed on 17 February 2022).

While most of the compounds described above exert their activity on more than one FGFR, anti-FGFR mAbs have the advantage to target specific receptors or even isoforms. Moreover, they are associated with a reduced toxicity due to the absence of off-target effects. Nevertheless, to date, only two anti-FGFR mAbs have entered clinical trials,



i.e., MGFR1877S for the treatment of advanced solid tumors and FPA144 for gastric cancer [65,66] ([www.clinicaltrials.gov](http://www.clinicaltrials.gov), accessed on 17 February 2022).

Finally, FGF-trap inhibitors may represent a compelling therapeutic strategy for tumors driven by an aberrant ligand-dependent activation of the FGF/FGFR system. These drugs can bind one or more FGFs and, by acting at the extracellular level, they can also affect the tumor microenvironment, hampering the tumor-stroma crosstalk [41,65]. The FGF-trap family comprises several compounds, including FP-1039, a soluble decoy receptor fusion protein, and NSC12, a small molecule that mimics the minimal FGF2-binding sequence of the long Pentraxin-3 [49,69]. Interestingly, this new class of small molecules has displayed a low toxicity profile when evaluated in experimental animal models [69].

#### 4. The FGF/FGFR System in Eye Tumors

Even though the involvement of FGFs/FGFRs has been well documented in most solid and hematological tumors, to date, scattered pieces of literature show that they may also play a relevant role in eye tumors, particularly in uveal melanoma and retinoblastoma.

Clinical and experimental evidence suggests the presence of an FGF/FGFR autocrine activation loop in uveal melanoma. Indeed, data mining performed on the publicly available mRNA profiling dataset of 80 primary human uveal melanoma specimens, present in The Cancer Genome Atlas (TCGA), reports the overexpression of one or more *FGFs* or *FGFRs* in 60% and 21% of cases of uveal melanoma, respectively (Figure 3A). Interestingly, among several *FGFs* and *FGFRs* that were found upregulated, *FGF12* and *FGFR1* were the most represented, reaching 26% and 11% of total cases (Figure 3B). In addition, alterations in *FGFs* and *FGFRs* resulted in a poorer prognosis in terms of reduced overall survival in patients (Figure 3C and [70]). Expression analysis in a set of 9 primary uveal melanomas reported that *FGF1* and *FGF2* were expressed in 77% of samples, with co-expression of *FGF1/FGF2* in 55% of cases. Moreover, primary tumors also expressed all *FGFRs*, with *FGFR1* being the most represented overall, while 33% of tumors expressed both *FGF1/FGF2* ligands and all four receptors [71].

Clinically, high levels of FGF2 were detected in mixed/epithelioid specimens, associated with a poor prognosis, compared to spindle cell type tumor samples [72,73]. Accordingly, primary tumors expressing *FGF2* were associated with an increased metastasis occurrence [72]. In this context, the elevated expression of *FGF2* in uveal melanoma metastases further reinforces the hypothesis that FGFs play a non-redundant role in uveal melanoma progression and invasion. Indeed, it has been recently reported that FGF2, produced by liver stellate cells, can mediate FGFR activation in metastatic uveal melanoma cells; moreover, it is responsible for the resistance to the bromodomain and histone deacetylase inhibitors [74].

From the perspective of therapeutic applications, the blocking of endogenous FGF2 with monoclonal antibodies or antisense nucleotide reduced cell proliferation, clonogenic potential, and cell survival in uveal melanoma cell lines [71]. Indeed, similar results were obtained by targeting *FGFR1* [71]. Accordingly, treatment with the pan FGF-trap NSC12 [69] prevented the activation of *FGFRs* and their downstream signaling mediators *FRS2* and *ERK1/2* in uveal melanoma cells [70]. Moreover, NSC12 treatment induced cell apoptosis through the activation of the pro-apoptotic caspase-3 protein as well as *PARP* cleavage [70]. These events were matched by the degradation of  $\beta$ -catenin, a key mediator of uveal melanoma metastasis [75–77], and resulted in a significant inhibition of cell proliferation and migration [70]. Notably, similar effects were obtained with the selective *FGFR* TK inhibitor BGJ398 [70].

Regarding other ocular neoplasms, scattered evidence obtained on human retinoblastoma cell lines showed the expression of all four *FGFRs*, with cell proliferation in response to stimulation with *FGF1* and *FGF2* [78,79]. In addition, analysis of aqueous humor from retinoblastoma patients revealed higher concentration of FGF2 compared to the control group, thus supporting the hypothesis that FGF may play a role in retinoblastoma progression [80]. Moreover, experimental evidence shows that treatment with exogenous *FGF1*

induces the activation and phosphorylation of FGFR1 in the human retinoblastoma Y-29 cell line, while the selective inhibition of FGFR1 resulted in decreased cell proliferation [79].

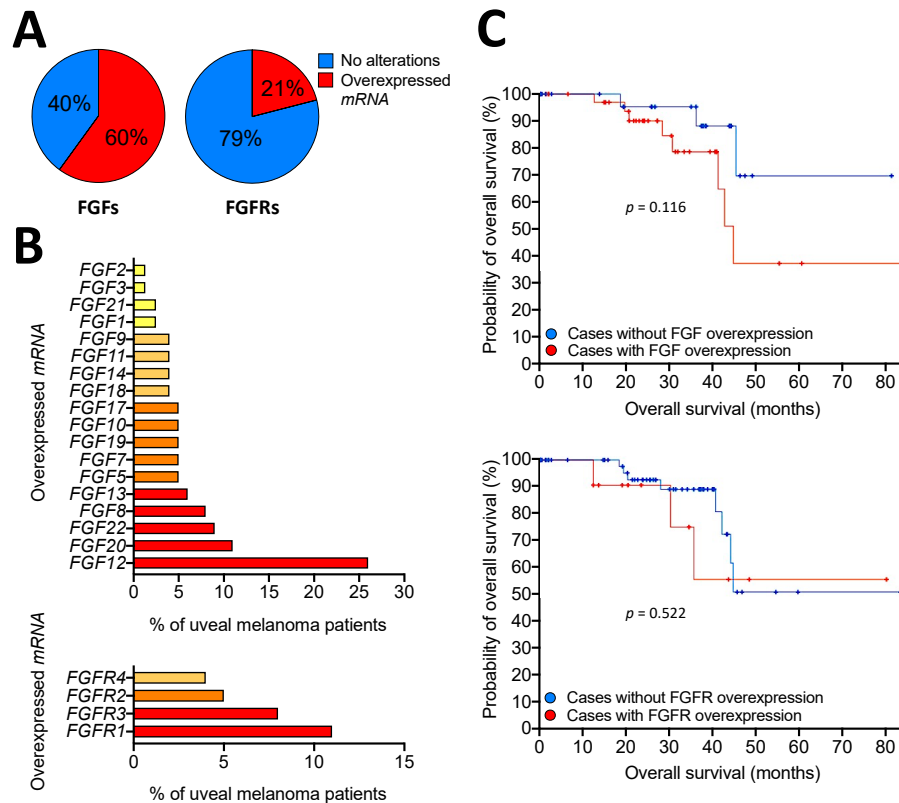


**Figure 3.** Overexpression of FGFs and FGFRs in human primary uveal melanoma. Analysis of The Cancer Genome Atlas (TCGA) dataset performed on 80 primary human uveal melanoma specimens. (A) Pie charts showing the percentage of samples with mRNA overexpression of *FGFs* (left panel) or *FGFRs* (right panel). (B) Percentage of uveal melanoma patients with mRNA overexpression of different members of the FGF (upper panel) or FGFR (lower panel) families. (C) Probability of overall survival of patients with or without FGF (upper panel) or FGFR (lower panel) alterations. Statistical analysis: Logrank Test.

The activation of the angiogenic switch, which requires an imbalance between pro- and anti-angiogenic factors, is essential for tumor progression [81]. In uveal melanoma and retinoblastoma, an increased vascular density has been associated with larger and more invasive tumors as well as with a poorer prognosis in patients [82,83]. In this frame, high levels of Vascular Endothelial Growth Factor (VEGF) have been reported in the ocular fluids of patients affected by both uveal melanoma or retinoblastoma [80,84,85]. Moreover, a significant reduction of tumor growth was observed following treatment with anti-VEGF bevacizumab, in both in vitro and in vivo experimental models, suggesting that anti-angiogenic strategies may be of significance for the clinical management of ocular tumors [86,87]. Given the role of FGF2 as a potent pro-angiogenic mediator, several studies have investigated its involvement in ocular tumor-associated angiogenesis. As mentioned above, high concentrations of FGF2 have been found in the aqueous humor of patients affected by either retinoblastoma or uveal melanoma [80,85]. Moreover, immunohistochem-

istry analysis of uveal melanomas showed that, even though FGF2 is mainly located in the cytoplasm of tumor cells, a positive signal is also detectable in the perivascular area [88]. Accordingly, *in vitro* experiments reported a significant impairment in the proliferation of endothelial cells co-cultured with primary human uveal melanoma cells following the selective inhibition of FGF2 [88], thus pointing to this pathway as a possible target to block neo-angiogenesis in uveal melanoma. Similar results were obtained in a transgenic mouse model of retinoblastoma, where a time-course analysis of FGF2 expression showed a peak of production during the early stages of tumorigenesis, localized in the perivascular area [78]. Accordingly, immunofluorescence analysis of human retinoblastoma tissues showed a positive staining for FGF2 located in both tumor and vascular cells [78]. Finally, Y-29 cells extracts induced proliferation of bovine brain-derived capillary endothelial cells, whereas their pro-angiogenic activity was prevented in the presence of neutralizing anti-FGF2 antibodies [89].

## 5. Concluding Remarks

In the era of personalized medicine and targeted therapies, it is of growing importance to deepen our knowledge on the molecular mechanisms involved in tumor progression; currently, new therapeutic approaches are being constantly investigated and developed. In this context, the FGF/FGFR system represents a paradigm, given its regulatory role in multiple hallmarks of cancer biology, such as proliferation, EMT, angiogenesis, metabolism, and drug resistance. As described in this review, the activity of the FGF/FGFR system has been widely characterized in several tumor types, leading to the introduction of novel therapies, both in clinical trials and in clinical practice [41,90].

Despite their relatively low incidence, eye tumors represent a challenging context for the development of new pharmacological treatments aimed at improving the overall survival of patients as well as their quality of life. In this frame, the FGF/FGFR signaling pathway represents an exploitable therapeutic target, due to its involvement in promoting tumor progression and dissemination, both in uveal melanoma and retinoblastoma. Indeed, experimental data suggest that targeting FGFR deeply affects tumor cells, impairing their capacity to grow, invade, and, eventually, resist first line therapies. Moreover, inhibition of the FGF/FGFR system may also be significant as an anti-angiogenic strategy, taking into consideration the importance of angiogenesis and hematogenous dissemination in ocular tumors, which develop in deeply vascularized area. Despite the lack of direct reports on the pro-angiogenic effect of FGF in ocular tumors, it is reasonable to assume that its mere expression contributes to sustaining neo-vessel formation. Notably, anti-FGF approaches have been widely characterized as anti-angiogenic; furthermore, they can be employed to overcome resistance to conventional anti-VEGF therapies [91,92]. Interestingly, the anti-angiogenic effect exerted by anti-FGFs/FGFRs should be considered from the perspective of an integrate approach, aimed at treating ocular tumors by acting on both the stromal and the parenchymal compartments.

In addition to the direct role of the FGF/FGFR system in ocular tumors, further research is required to investigate the activity of the non-conventional FGFR interactors. For instance, the expression of NCAM has been reported in mixed/epithelioid uveal melanoma cell types, which are associated with an increased metastatic potential [93]. Nevertheless, the involvement of NCAM and other FGFR- activators is largely unexplored in the field of ocular neoplasms.

To date, different therapeutic strategies allow us to block FGFRs with a more or less selective approach; however, their clinical application has been reserved only for those tumors where the driving role of FGFRs is well characterized, such as cholangiocarcinoma and urothelial cancers [66–68]. Notably, a finer modulation of FGFR activation may be achieved through FGF-trap molecules; therefore, their validation would allow better regulation of the crosstalk exerted by different FGFs in the complex tumor microenvironment [38]. FGF/FGFR inhibitors represent an attractive therapeutic perspective for ocular tumors, and especially for the clinical management of uveal melanoma; nevertheless, their legitima-

tion is hampered by the scarcity of literature reporting their involvement in the different phases of tumor growth. Therefore, more studies are needed to expand the knowledge of the FGF/FGFR system into other, less represented, tumors of the eye and to push the currently available FDA-approved anti-FGF/FGFR drugs towards their application in ophthalmic neoplasms.

**Author Contributions:** Conceptualization, S.R. and R.R.; writing—original draft preparation, A.L. and M.T.; writing—review and editing, F.S., S.R. and R.R.; visualization, A.L., M.T. and S.R.; supervision, R.R.; funding acquisition, F.S. and R.R. All authors have read and agreed to the published version of the manuscript.

**Funding:** This work was supported by the Associazione Italiana Ricerca sul Cancro (AIRC) IG grant No. 23151 to R.R., and S.R. was supported by Fondazione Umberto Veronesi and Associazione Garda Vita R. Tosoni fellowships.

**Conflicts of Interest:** The authors declare no conflict of interest.

## References

- Cholkar, K.; Dasari, S.R.; Pal, D.; Mitra, A.K. Eye: Anatomy, physiology and barriers to drug delivery. In *Ocular Transporters and Receptors*; Elsevier: Amsterdam, The Netherlands, 2013; pp. 1–36.
- Malhotra, A.; Minja, F.J.; Crum, A.; Burrowes, D. Ocular anatomy and cross-sectional imaging of the eye. *Semin. Ultrasound CT MR* **2011**, *32*, 2–13. [[CrossRef](#)]
- Masland, R.H. The neuronal organization of the retina. *Neuron* **2012**, *76*, 266–280. [[CrossRef](#)]
- Mafee, M.F.; Karimi, A.; Shah, J.D.; Rapoport, M.; Ansari, S.A. Anatomy and pathology of the eye: Role of mr imaging and ct. *Magn. Reson. Imaging Clin. N. Am.* **2006**, *14*, 249–270. [[CrossRef](#)]
- Williams, B.K.; Di Nicola, M. Ocular oncology—primary and metastatic malignancies. *Med. Clin. N. Am.* **2021**, *105*, 531–550. [[CrossRef](#)]
- Nagarkatti-Gude, N.; Wang, Y.; Ali, M.J.; Honavar, S.G.; Jager, M.J.; Chan, C.C. Genetics of primary intraocular tumors. *Ocul. Immunol. Inflamm.* **2012**, *20*, 244–254. [[CrossRef](#)]
- Cohen, V.M. Ocular metastases. *Eye* **2013**, *27*, 137–141. [[CrossRef](#)]
- Dimaras, H.; Kimani, K.; Dimba, E.A.; Gronsdahl, P.; White, A.; Chan, H.S.; Gallie, B.L. Retinoblastoma. *Lancet* **2012**, *379*, 1436–1446. [[CrossRef](#)]
- Dimaras, H.; Corson, T.W. Retinoblastoma, the visible cns tumor: A review. *J. Neurosci. Res.* **2019**, *97*, 29–44. [[CrossRef](#)]
- Rao, R.; Honavar, S.G. Retinoblastoma. *Indian J. Pediatr.* **2017**, *84*, 937–944. [[CrossRef](#)]
- Pritchard, E.M.; Dyer, M.A.; Guy, R.K. Progress in small molecule therapeutics for the treatment of retinoblastoma. *Mini. Rev. Med. Chem.* **2016**, *16*, 430–454. [[CrossRef](#)]
- Blum, E.S.; Yang, J.; Komatsubara, K.M.; Carvajal, R.D. Clinical management of uveal and conjunctival melanoma. *Oncology* **2016**, *30*, 34–43.
- Smit, K.N.; Jager, M.J.; de Klein, A.; Kiliç, E. Uveal melanoma: Towards a molecular understanding. *Prog. Retin. Eye Res.* **2020**, *75*, 100800. [[CrossRef](#)]
- Krantz, B.A.; Dave, N.; Komatsubara, K.M.; Marr, B.P.; Carvajal, R.D. Uveal melanoma: Epidemiology, etiology, and treatment of primary disease. *Clin. Ophthalmol.* **2017**, *11*, 279–289. [[CrossRef](#)]
- Souto, E.B.; Zielinska, A.; Luis, M.; Carbone, C.; Martins-Gomes, C.; Souto, S.B.; Silva, A.M. Uveal melanoma: Physiopathology and new in situ-specific therapies. *Cancer Chemother. Pharmacol.* **2019**, *84*, 15–32. [[CrossRef](#)]
- Yang, J.; Manson, D.K.; Marr, B.P.; Carvajal, R.D. Treatment of uveal melanoma: Where are we now? *Ther. Adv. Med. Oncol.* **2018**, *10*, 1758834018757175. [[CrossRef](#)]
- Patel, M.; Smyth, E.; Chapman, P.B.; Wolchok, J.D.; Schwartz, G.K.; Abramson, D.H.; Carvajal, R.D. Therapeutic implications of the emerging molecular biology of uveal melanoma. *Clin. Cancer Res.* **2011**, *17*, 2087–2100. [[CrossRef](#)]
- Chattopadhyay, C.; Kim, D.W.; Gombos, D.S.; Oba, J.; Qin, Y.; Williams, M.D.; Esmaeli, B.; Grimm, E.A.; Wargo, J.A.; Woodman, S.E.; et al. Uveal melanoma: From diagnosis to treatment and the science in between. *Cancer* **2016**, *122*, 2299–2312. [[CrossRef](#)]
- Amaro, A.; Gangemi, R.; Piaggio, F.; Angelini, G.; Barisione, G.; Ferrini, S.; Pfeffer, U. The biology of uveal melanoma. *Cancer Metastasis Rev.* **2017**, *36*, 109–140. [[CrossRef](#)]
- Carvajal, R.D.; Schwartz, G.K.; Tezel, T.; Marr, B.; Francis, J.H.; Nathan, P.D. Metastatic disease from uveal melanoma: Treatment options and future prospects. *Br. J. Ophthalmol.* **2017**, *101*, 38–44. [[CrossRef](#)]
- Tobia, C.; Coltrini, D.; Ronca, R.; Loda, A.; Guerra, J.; Scalvini, E.; Semeraro, F.; Rezzola, S. An orthotopic model of uveal melanoma in zebrafish embryo: A novel platform for drug evaluation. *Biomedicines* **2021**, *9*, 1873. [[CrossRef](#)]
- Griewank, K.G.; Murali, R. Pathology and genetics of uveal melanoma. *Pathology* **2013**, *45*, 18–27. [[CrossRef](#)]
- Jovanovic, P.; Mihajlovic, M.; Djordjevic-Jocic, J.; Vlajkovic, S.; Cekic, S.; Stefanovic, V. Ocular melanoma: An overview of the current status. *Int. J. Clin. Exp. Pathol.* **2013**, *6*, 1230–1244.

24. Vora, G.K.; Demirci, H.; Marr, B.; Mruthyunjaya, P. Advances in the management of conjunctival melanoma. *Surv. Ophthalmol.* **2017**, *62*, 26–42. [[CrossRef](#)]
25. Char, D.H. Ocular melanoma. *Surg. Clin. N. Am.* **2003**, *83*, 253–274.vii. [[CrossRef](#)]
26. Kalogeropoulos, D.; Vartholomatos, G.; Mitra, A.; Elaraoud, I.; Ch'ng, S.W.; Zikou, A.; Papoudou-Bai, A.; Moschos, M.M.; Kanavaros, P.; Kalogeropoulos, C. Primary vitreoretinal lymphoma. *Saudi. J. Ophthalmol.* **2019**, *33*, 66–80. [[CrossRef](#)]
27. Sagoo, M.S.; Mehta, H.; Swampillai, A.J.; Cohen, V.M.; Amin, S.Z.; Plowman, P.N.; Lightman, S. Primary intraocular lymphoma. *Surv. Ophthalmol.* **2014**, *59*, 503–516. [[CrossRef](#)]
28. Tang, L.J.; Gu, C.L.; Zhang, P. Intraocular lymphoma. *Int. J. Ophthalmol.* **2017**, *10*, 1301–1307.
29. Qu, Z.; Liu, J.; Zhu, L.; Zhou, Q. A comprehensive understanding of choroidal metastasis from lung cancer. *Oncol. Targets Ther.* **2021**, *14*, 4451–4465. [[CrossRef](#)]
30. Georgalas, I.; Paraskevopoulos, T.; Koutsandrea, C.; Kardara, E.; Malamos, P.; Ladas, D.; Papaconstantinou, D. Ophthalmic metastasis of breast cancer and ocular side effects from breast cancer treatment and management: Mini review. *Biomed. Res. Int.* **2015**, *2015*, 574086. [[CrossRef](#)]
31. Wiedlocha, A.; Haugsten, E.M.; Zakrzewska, M. Roles of the fgf-fgfr signaling system in cancer development and inflammation. *Cells* **2021**, *10*, 2231. [[CrossRef](#)]
32. Itoh, N.; Ornitz, D.M. Fibroblast growth factors: From molecular evolution to roles in development, metabolism and disease. *J. Biochem.* **2011**, *149*, 121–130. [[CrossRef](#)] [[PubMed](#)]
33. Xie, Y.; Su, N.; Yang, J.; Tan, Q.; Huang, S.; Jin, M.; Ni, Z.; Zhang, B.; Zhang, D.; Luo, F.; et al. Fgf/fgfr signaling in health and disease. *Signal Transduct Target Ther.* **2020**, *5*, 181. [[CrossRef](#)] [[PubMed](#)]
34. Ornitz, D.M.; Itoh, N. The fibroblast growth factor signaling pathway. *Wiley Interdiscip Rev. Dev. Biol.* **2015**, *4*, 215–266. [[CrossRef](#)] [[PubMed](#)]
35. Beenken, A.; Mohammadi, M. The fgf family: Biology, pathophysiology and therapy. *Nat. Rev. Drug Discov.* **2009**, *8*, 235–253. [[CrossRef](#)]
36. Plotnikov, A.N.; Schlessinger, J.; Hubbard, S.R.; Mohammadi, M. Structural basis for fgf receptor dimerization and activation. *Cell* **1999**, *98*, 641–650. [[CrossRef](#)]
37. Brooks, A.N.; Kilgour, E.; Smith, P.D. Molecular pathways: Fibroblast growth factor signaling: A new therapeutic opportunity in cancer. *Clin. Cancer Res.* **2012**, *18*, 1855–1862. [[CrossRef](#)]
38. Giacomini, A.; Chiodelli, P.; Matarazzo, S.; Rusnati, M.; Presta, M.; Ronca, R. Blocking the fgf/fgfr system as a “two-compartment” antiangiogenic/antitumor approach in cancer therapy. *Pharmacol. Res.* **2016**, *107*, 172–185. [[CrossRef](#)]
39. Ferguson, H.R.; Smith, M.P.; Francavilla, C. Fibroblast growth factor receptors (fgfrs) and noncanonical partners in cancer signaling. *Cells* **2021**, *10*, 1201. [[CrossRef](#)]
40. Turner, N.; Grose, R. Fibroblast growth factor signalling: From development to cancer. *Nat. Rev. Cancer* **2010**, *10*, 116–129. [[CrossRef](#)]
41. Ghedini, G.C.; Ronca, R.; Presta, M.; Giacomini, A. Future applications of fgf/fgfr inhibitors in cancer. *Expert. Rev. Anticancer Ther.* **2018**, *18*, 861–872. [[CrossRef](#)]
42. Giacomini, A.; Grillo, E.; Rezzola, S.; Ribatti, D.; Rusnati, M.; Ronca, R.; Presta, M. The fgf/fgfr system in the physiopathology of the prostate gland. *Physiol. Rev.* **2021**, *101*, 569–610. [[CrossRef](#)] [[PubMed](#)]
43. Rezzola, S.; Sigmund, E.C.; Halin, C.; Ronca, R. The lymphatic vasculature: An active and dynamic player in cancer progression. *Med. Res. Rev.* **2022**, *42*, 576–614. [[CrossRef](#)] [[PubMed](#)]
44. Cappellen, D.; De Oliveira, C.; Ricol, D.; de Medina, S.; Bourdin, J.; Sastre-Garau, X.; Chopin, D.; Thiery, J.P.; Radvanyi, F. Frequent activating mutations of fgfr3 in human bladder and cervix carcinomas. *Nat. Genet.* **1999**, *23*, 18–20. [[CrossRef](#)] [[PubMed](#)]
45. Chesi, M.; Nardini, E.; Brents, L.A.; Schröck, E.; Ried, T.; Kuehl, W.M.; Bergsagel, P.L. Frequent translocation t(4;14)(p16.3;q32.3) in multiple myeloma is associated with increased expression and activating mutations of fibroblast growth factor receptor 3. *Nat. Genet.* **1997**, *16*, 260–264. [[CrossRef](#)]
46. Hernández, S.; de Muga, S.; Agell, L.; Juanpere, N.; Esgueva, R.; Lorente, J.A.; Mojal, S.; Serrano, S.; Lloreta, J. Fgfr3 mutations in prostate cancer: Association with low-grade tumors. *Mod. Pathol.* **2009**, *22*, 848–856. [[CrossRef](#)]
47. Jackson, C.C.; Medeiros, L.J.; Miranda, R.N. 8p11 myeloproliferative syndrome: A review. *Hum. Pathol.* **2010**, *41*, 461–476. [[CrossRef](#)]
48. Yagasaki, F.; Wakao, D.; Yokoyama, Y.; Uchida, Y.; Murohashi, I.; Kayano, H.; Taniwaki, M.; Matsuda, A.; Bessho, M. Fusion of etv6 to fibroblast growth factor receptor 3 in peripheral t-cell lymphoma with a t(4;12)(p16;p13) chromosomal translocation. *Cancer Res.* **2001**, *61*, 8371–8374.
49. Presta, M.; Chiodelli, P.; Giacomini, A.; Rusnati, M.; Ronca, R. Fibroblast growth factors (fgfs) in cancer: Fgf traps as a new therapeutic approach. *Pharmacol. Ther.* **2017**, *179*, 171–187. [[CrossRef](#)]
50. Courjal, F.; Cuny, M.; Simony-Lafontaine, J.; Louason, G.; Speiser, P.; Zeillinger, R.; Rodriguez, C.; Theillet, C. Mapping of DNA amplifications at 15 chromosomal localizations in 1875 breast tumors: Definition of phenotypic groups. *Cancer Res.* **1997**, *57*, 4360–4367.
51. Kunii, K.; Davis, L.; Gorenstein, J.; Hatch, H.; Yashiro, M.; Di Bacco, A.; Elbi, C.; Lutterbach, B. Fgfr2-amplified gastric cancer cell lines require fgfr2 and erbb3 signaling for growth and survival. *Cancer Res.* **2008**, *68*, 2340–2348. [[CrossRef](#)]

52. Heist, R.S.; Mino-Kenudson, M.; Sequist, L.V.; Tammireddy, S.; Morrissey, L.; Christiani, D.C.; Engelman, J.A.; Iafrate, A.J. Fgfr1 amplification in squamous cell carcinoma of the lung. *J. Thorac. Oncol.* **2012**, *7*, 1775–1780. [[CrossRef](#)] [[PubMed](#)]
53. McMillin, D.W.; Negri, J.M.; Mitsiades, C.S. The role of tumour-stromal interactions in modifying drug response: Challenges and opportunities. *Nat. Rev. Drug Discov.* **2013**, *12*, 217–228. [[CrossRef](#)] [[PubMed](#)]
54. Bosio, D.; Ronca, R.; Salvi, V.; Presta, M.; Sozzani, S. Dendritic cells in inflammatory angiogenesis and lymphangiogenesis. *Curr. Opin. Immunol.* **2018**, *53*, 180–186. [[CrossRef](#)] [[PubMed](#)]
55. Ronca, R.; Van Ginderachter, J.A.; Turtoi, A. Paracrine interactions of cancer-associated fibroblasts, macrophages and endothelial cells: Tumor allies and foes. *Curr. Opin. Oncol.* **2018**, *30*, 45–53. [[CrossRef](#)]
56. Zhou, Y.; Wu, C.; Lu, G.; Hu, Z.; Chen, Q.; Du, X. Fgf/fgfr signaling pathway involved resistance in various cancer types. *J. Cancer* **2020**, *11*, 2000–2007. [[CrossRef](#)]
57. Mori, S.; Tran, V.; Nishikawa, K.; Kaneda, T.; Hamada, Y.; Kawaguchi, N.; Fujita, M.; Saegusa, J.; Takada, Y.K.; Matsuura, N.; et al. A dominant-negative fgf1 mutant (the r50e mutant) suppresses tumorigenesis and angiogenesis. *PLoS ONE* **2013**, *8*, e57927. [[CrossRef](#)]
58. Mori, S.; Kodaira, M.; Ito, A.; Okazaki, M.; Kawaguchi, N.; Hamada, Y.; Takada, Y.; Matsuura, N. Enhanced expression of integrin alphavbeta3 induced by tgfbeta is required for the enhancing effect of fibroblast growth factor 1 (fgf1) in tgfbeta-induced epithelial-mesenchymal transition (emt) in mammary epithelial cells. *PLoS ONE* **2015**, *10*, e0137486. [[CrossRef](#)]
59. Francavilla, C.; Loeffler, S.; Piccini, D.; Kren, A.; Christofori, G.; Cavallaro, U. Neural cell adhesion molecule regulates the cellular response to fibroblast growth factor. *J. Cell Sci.* **2007**, *120*, 4388–4394. [[CrossRef](#)]
60. Mohanan, V.; Temburni, M.K.; Kappes, J.C.; Galileo, D.S. L1cam stimulates glioma cell motility and proliferation through the fibroblast growth factor receptor. *Clin. Exp. Metastasis* **2013**, *30*, 507–520. [[CrossRef](#)]
61. Nguyen, T.; Mege, R.M. N-cadherin and fibroblast growth factor receptors crosstalk in the control of developmental and cancer cell migrations. *Eur. J. Cell Biol.* **2016**, *95*, 415–426. [[CrossRef](#)]
62. Hulit, J.; Suyama, K.; Chung, S.; Keren, R.; Agiostratidou, G.; Shan, W.; Dong, X.; Williams, T.M.; Lisanti, M.P.; Knudsen, K.; et al. N-cadherin signaling potentiates mammary tumor metastasis via enhanced extracellular signal-regulated kinase activation. *Cancer Res.* **2007**, *67*, 3106–3116. [[CrossRef](#)] [[PubMed](#)]
63. Kucinska, M.; Porebska, N.; Lampart, A.; Latko, M.; Knapik, A.; Zakrzewska, M.; Otlewski, J.; Opalinski, L. Differential regulation of fibroblast growth factor receptor 1 trafficking and function by extracellular galectins. *Cell Commun. Signal. CCS* **2019**, *17*, 65. [[CrossRef](#)]
64. Porebska, N.; Latko, M.; Kucinska, M.; Zakrzewska, M.; Otlewski, J.; Opalinski, L. Targeting cellular trafficking of fibroblast growth factor receptors as a strategy for selective cancer treatment. *J. Clin. Med.* **2018**, *8*, 7. [[CrossRef](#)] [[PubMed](#)]
65. Touat, M.; Ileana, E.; Postel-Vinay, S.; André, F.; Soria, J.C. Targeting fgfr signaling in cancer. *Clin. Cancer Res.* **2015**, *21*, 2684–2694. [[CrossRef](#)]
66. Porta, R.; Borea, R.; Coelho, A.; Khan, S.; Araújo, A.; Reclusa, P.; Franchina, T.; Van Der Steen, N.; Van Dam, P.; Ferri, J.; et al. Fgfr a promising druggable target in cancer: Molecular biology and new drugs. *Crit. Rev. Oncol. Hematol.* **2017**, *113*, 256–267. [[CrossRef](#)] [[PubMed](#)]
67. Merz, V.; Zecchetto, C.; Melisi, D. Pemigatinib, a potent inhibitor of fgfrs for the treatment of cholangiocarcinoma. *Future Oncol.* **2021**, *17*, 389–402. [[CrossRef](#)]
68. Weaver, A.; Bossaer, J.B. Fibroblast growth factor receptor (fgfr) inhibitors: A review of a novel therapeutic class. *J. Oncol. Pharm. Pract.* **2021**, *27*, 702–710. [[CrossRef](#)]
69. Ronca, R.; Giacomini, A.; Di Salle, E.; Coltrini, D.; Pagano, K.; Ragona, L.; Matarazzo, S.; Rezzola, S.; Maiolo, D.; Torrella, R.; et al. Long-pentraxin 3 derivative as a small-molecule fgf trap for cancer therapy. *Cancer Cell* **2015**, *28*, 225–239. [[CrossRef](#)]
70. Rezzola, S.; Ronca, R.; Loda, A.; Nawaz, M.I.; Tobia, C.; Paganini, G.; Maccarinelli, F.; Giacomini, A.; Semeraro, F.; Mor, M.; et al. The autocrine fgf/fgfr system in both skin and uveal melanoma: Fgf trapping as a possible therapeutic approach. *Cancers* **2019**, *11*, 1305. [[CrossRef](#)]
71. Lefèvre, G.; Babchia, N.; Calipel, A.; Mouriaux, F.; Faussat, A.M.; Mrzyk, S.; Mascarelli, F. Activation of the fgf2/fgfr1 autocrine loop for cell proliferation and survival in uveal melanoma cells. *Invest. Ophthalmol. Vis. Sci.* **2009**, *50*, 1047–1057. [[CrossRef](#)]
72. Wang, Y.; Bao, X.; Zhang, Z.; Sun, Y.; Zhou, X. Fgf2 promotes metastasis of uveal melanoma cells via store-operated calcium entry. *Oncol. Targets Ther.* **2017**, *10*, 5317–5328. [[CrossRef](#)] [[PubMed](#)]
73. Kaliki, S.; Shields, C.L.; Shields, J.A. Uveal melanoma: Estimating prognosis. *Indian J. Ophthalmol.* **2015**, *63*, 93–102. [[CrossRef](#)] [[PubMed](#)]
74. Chua, V.; Orloff, M.; Teh, J.L.; Sugase, T.; Liao, C.; Purwin, T.J.; Lam, B.Q.; Terai, M.; Ambrosini, G.; Carvajal, R.D.; et al. Stromal fibroblast growth factor 2 reduces the efficacy of bromodomain inhibitors in uveal melanoma. *EMBO Mol. Med.* **2019**, *11*, e9081. [[CrossRef](#)] [[PubMed](#)]
75. Zheng, L.; Pan, J. The anti-malarial drug artesunate blocks wnt/beta-catenin pathway and inhibits growth, migration and invasion of uveal melanoma cells. *Curr. Cancer Drug Targets* **2018**, *18*, 988–998. [[CrossRef](#)]
76. Chang, S.H.; Worley, L.A.; Onken, M.D.; Harbour, J.W. Prognostic biomarkers in uveal melanoma: Evidence for a stem cell-like phenotype associated with metastasis. *Melanoma Res.* **2008**, *18*, 191–200. [[CrossRef](#)]
77. Zuidervaart, W.; Pavey, S.; van Nieuwpoort, F.A.; Packer, L.; Out, C.; Maat, W.; Jager, M.J.; Gruis, N.A.; Hayward, N.K. Expression of wnt5a and its downstream effector beta-catenin in uveal melanoma. *Melanoma Res.* **2007**, *17*, 380–386. [[CrossRef](#)]

78. Cebulla, C.M.; Jockovich, M.E.; Piña, Y.; Boutrid, H.; Alegret, A.; Kulak, A.; Hackam, A.S.; Bhattacharya, S.K.; Feuer, W.J.; Murray, T.G. Basic fibroblast growth factor impact on retinoblastoma progression and survival. *Investig. Ophthalmol. Vis. Sci.* **2008**, *49*, 5215–5221. [[CrossRef](#)]
79. Siffroi-Fernandez, S.; Cinaroglu, A.; Fuhrmann-Panfalone, V.; Normand, G.; Bugra, K.; Sahel, J.; Hicks, D. Acidic fibroblast growth factor (fgf-1) and fgf receptor 1 signaling in human y79 retinoblastoma. *Arch. Ophthalmol.* **2005**, *123*, 368–376. [[CrossRef](#)]
80. Cheng, Y.; Zheng, S.; Pan, C.T.; Yuan, M.; Chang, L.; Yao, Y.; Zhao, M.; Liang, J. Analysis of aqueous humor concentrations of cytokines in retinoblastoma. *PLoS ONE* **2017**, *12*, e0177337. [[CrossRef](#)]
81. Ronca, R.; Benkheil, M.; Mitola, S.; Struyf, S.; Liekens, S. Tumor angiogenesis revisited: Regulators and clinical implications. *Med. Res. Rev.* **2017**, *37*, 1231–1274. [[CrossRef](#)]
82. Mäkitie, T.; Summanen, P.; Tarkkanen, A.; Kivelä, T. Microvascular density in predicting survival of patients with choroidal and ciliary body melanoma. *Investig. Ophthalmol. Vis. Sci.* **1999**, *40*, 2471–2480. [[PubMed](#)]
83. Jockovich, M.E.; Piña, Y.; Alegret, A.; Cebulla, C.; Feuer, W.; Murray, T.G. Heterogeneous tumor vasculature in retinoblastoma: Implications for vessel targeting therapy. *Retina* **2008**, *28*, S81–S86. [[CrossRef](#)] [[PubMed](#)]
84. Boyd, S.R.; Tan, D.; Bunce, C.; Gittos, A.; Neale, M.H.; Hungerford, J.L.; Charnock-Jones, S.; Cree, I.A. Vascular endothelial growth factor is elevated in ocular fluids of eyes harbouring uveal melanoma: Identification of a potential therapeutic window. *Br. J. Ophthalmol.* **2002**, *86*, 448–452. [[CrossRef](#)] [[PubMed](#)]
85. Cheng, Y.; Feng, J.; Zhu, X.; Liang, J. Cytokines concentrations in aqueous humor of eyes with uveal melanoma. *Medicine* **2019**, *98*, e14030. [[CrossRef](#)]
86. Yang, H.; Jager, M.J.; Grossniklaus, H.E. Bevacizumab suppression of establishment of micrometastases in experimental ocular melanoma. *Investig. Ophthalmol. Vis. Sci.* **2010**, *51*, 2835–2842. [[CrossRef](#)]
87. Lee, S.Y.; Kim, D.K.; Cho, J.H.; Koh, J.Y.; Yoon, Y.H. Inhibitory effect of bevacizumab on the angiogenesis and growth of retinoblastoma. *Arch. Ophthalmol.* **2008**, *126*, 953–958. [[CrossRef](#)]
88. Boyd, S.R.; Tan, D.S.; de Souza, L.; Neale, M.H.; Myatt, N.E.; Alexander, R.A.; Robb, M.; Hungerford, J.L.; Cree, I.A. Uveal melanomas express vascular endothelial growth factor and basic fibroblast growth factor and support endothelial cell growth. *Br. J. Ophthalmol.* **2002**, *86*, 440–447. [[CrossRef](#)]
89. Schweigerer, L.; Neufeld, G.; Gospodarowicz, D. Basic fibroblast growth factor is present in cultured human retinoblastoma cells. *Investig. Ophthalmol. Vis. Sci.* **1987**, *28*, 1838–1843.
90. Ronca, R.; Giacomini, A.; Rusnati, M.; Presta, M. The potential of fibroblast growth factor/fibroblast growth factor receptor signaling as a therapeutic target in tumor angiogenesis. *Expert Opin. Ther. Targets* **2015**, *19*, 1361–1377. [[CrossRef](#)]
91. Zahra, F.T.; Sajib, M.S.; Mikelis, C.M. Role of bfgf in acquired resistance upon anti-vegf therapy in cancer. *Cancers* **2021**, *13*, 1422. [[CrossRef](#)]
92. Casanovas, O.; Hicklin, D.J.; Bergers, G.; Hanahan, D. Drug resistance by evasion of antiangiogenic targeting of vegf signaling in late-stage pancreatic islet tumors. *Cancer Cell* **2005**, *8*, 299–309. [[CrossRef](#)] [[PubMed](#)]
93. Mooy, C.M.; Luyten, G.P.; de Jong, P.T.; Jensen, O.A.; Luider, T.M.; van der Ham, F.; Bosman, F.T. Neural cell adhesion molecule distribution in primary and metastatic uveal melanoma. *Hum. Pathol.* **1995**, *26*, 1185–1190. [[CrossRef](#)]

**The Autocrine FGF/FGFR System in both Skin and Uveal Melanoma: FGF Trapping as a Possible Therapeutic Approach**

S. Rezzola, R. Ronca, [A. Loda](#), Ml. Nawaz, C. Tobia, G. Paganini, F. Maccarinelli, A. Giacomini, F. Semeraro, M. Mor, M. Presta.

Cancers (Basel). 2019 Sep 4;11(9):1305. doi: 10.3390/cancers11091305. PMID: 31487962; PMCID: PMC6770058.







Article

# The Autocrine FGF/FGFR System in both Skin and Uveal Melanoma: FGF Trapping as a Possible Therapeutic Approach

Sara Rezzola <sup>1,\*</sup>, Roberto Ronca <sup>1</sup>, Alessandra Loda <sup>1</sup>, Mohd Imtiaz Nawaz <sup>1</sup>, Chiara Tobia <sup>1</sup>, Giuseppe Paganini <sup>1</sup>, Federica Maccarinelli <sup>1</sup>, Arianna Giacomini <sup>1</sup>, Francesco Semeraro <sup>2</sup>, Marco Mor <sup>3</sup> and Marco Presta <sup>1,\*</sup>

<sup>1</sup> Department of Molecular and Translational Medicine, University of Brescia, 25123 Brescia, Italy

<sup>2</sup> Eye Clinic, Department of Medical and Surgical Specialties, Radiological Sciences and Public Health, University of Brescia, 25123 Brescia, Italy

<sup>3</sup> Department of Food and Drug, University of Parma, 43125 Parma, Italy

\* Correspondence: sara.rezzola@unibs.it (S.R.); marco.presta@unibs.it (M.P.)

Received: 2 August 2019; Accepted: 3 September 2019; Published: 4 September 2019



**Abstract:** Fibroblast growth factors (FGFs) play non-redundant autocrine/paracrine functions in various human cancers. The Cancer Genome Atlas (TCGA) data mining indicates that high levels of FGF and/or FGF receptor (FGFR) expression are associated with reduced overall survival, chromosome 3 monosomy and *BAP1* mutation in human uveal melanoma (UM), pointing to the FGF/FGFR system as a target for UM treatment. Here, we investigated the impact of different FGF trapping approaches on the tumorigenic and liver metastatic activity of liver metastasis-derived murine melanoma B16-LS9 cells that, similar to human UM, are characterized by a distinctive hepatic tropism. In vitro and in vivo experiments demonstrated that the overexpression of the natural FGF trap inhibitor long-pentraxin 3 (PTX3) inhibits the oncogenic activity of B16-LS9 cells. In addition, B16-LS9 cells showed a reduced tumor growth and liver metastatic activity when grafted in PTX3-overexpressing transgenic mice. The efficacy of the FGF trapping approach was confirmed by the capacity of the PTX3-derived pan-FGF trap small molecule NSC12 to inhibit B16-LS9 cell growth in vitro, in a zebrafish embryo orthotopic tumor model and in an experimental model of liver metastasis. Possible translational implications for these observations were provided by the capacity of NSC12 to inhibit FGF signaling and cell proliferation in human UM Mel285, Mel270, 92.1, and OMM2.3 cells. In addition, NSC12 caused caspase-3 activation and PARP cleavage followed by apoptotic cell death as well as  $\beta$ -catenin degradation and inhibition of UM cell migration. Together, our findings indicate that FGF trapping may represent a novel therapeutic strategy in UM.

**Keywords:** FGF; FGF receptors; liver metastasis; tumor grafts; uveal melanoma; zebrafish

## 1. Introduction

Uveal melanoma (UM) is the most common primary intraocular malignancy in adults. Its occurrence increases with age and its incidence is more than 20 per million per year [1,2]. Current treatments of primary UM include enucleation, radiotherapy, transpupillary thermotherapy, and local resection, achieving a control of local tumor in up to 97% of treated cases. Anyway, the mortality rate is high because of the frequent occurrence of metastases by hematogenous dissemination: almost 50% of all UM patients develop metastatic disease, mainly in the liver, with a current 5-year mortality ranging from 26% to 32% [1–3]. In the last years, a better understanding of UM biology has provided new indications for the development of efficacious adjuvant therapies and for the treatment of the metastatic

disease [4]. At present, numerous chemotherapy-, targeted therapy-, immunotherapy-, and liver directed therapy-based clinical trials are in progress [4–6]. However, as of today, no specific systemic treatment has been approved, indicating that novel biologically-based therapies are urgently required.

The fibroblast growth factor (FGF)/FGF receptor (FGFR) system plays a pivotal role in different tumor types, leading to autocrine/paracrine stimulation of tumor cell proliferation and angiogenesis [7–9]. The evidence that UM cell cultures express and secrete large quantities of FGFs suggests that an FGF/FGFR autocrine loop of stimulation exists also in these cells [10–12], implying the FGF/FGFR system in UM progression [13] and pointing to this pathway as a possible alternative therapeutic target in UM.

The soluble pattern recognition receptor long pentraxin-3 (PTX3) is a member of the pentraxin family produced locally in response to inflammatory signals [14,15]. Previous observations have shown that PTX3 binds various FGFs, including FGF2, FGF6, FGF8b, FGF10, and FGF17, and inhibits FGF-dependent angiogenic responses [16–18]. Accordingly, transgenic PTX3 overexpression impairs efficaciously the activation and signaling of the FGF/FGFR system in FGF-driven tumors, thus affecting tumor growth and metastasis [16,17,19].

Recently, the PTX3-derived small molecule NSC12 has been identified as the first orally active pan-FGF trap able to inhibit FGFR activation and tumor growth in various FGF-dependent murine and human tumor models [20,21]. Notably, extracellular FGF traps, including NSC12, appear to be devoid of the toxicities associated with tyrosine kinase FGFR inhibitors [21,22], thus representing a potential alternative option to inhibit the FGF/FGFR system in cancer. On this basis, in this work we investigated the impact of a PTX3/NSC12-based, FGF trapping approach in the murine B16-LS9 melanoma model and on human UM cell lines.

## 2. Results

### 2.1. The FGF/FGFR System Is Upregulated in Human Uveal Melanoma

Data mining was performed on The Cancer Genome Atlas (TCGA) UM PanCancer Atlas dataset ([http://www.cbioportal.org/study?id=uvm\\_tcg\\_pan\\_can\\_atlas\\_2018](http://www.cbioportal.org/study?id=uvm_tcg_pan_can_atlas_2018)) to investigate the expression of all the members of the FGFR and FGF families in a UM cohort of 80 patients. We found that FGFRs are overexpressed in 21% of UM cases, these alterations being associated to a poor prognosis when compared to UM cases without FGFR alterations ( $p = 0.023$ , log-rank test; median survival equal to 31 and 52 months for cases with or without FGFR alterations, respectively) (Figure 1A,B). Moreover, overexpression of one or more FGFs was detected in 61% of UM patients (Figure 1C). Again, FGF overexpression appears to be associated to a reduced survival in UM patients, even though the difference between the two groups did not reach the statistical significance (Figure 1D).

In the recent years, analysis of the genetic alterations has identified subsets of UM patients with distinct molecular signatures [23]. Among them, UMs with loss of chromosome 3 are characterized by a poor prognosis when compared to chromosome 3 disomic lesions. On this basis, we performed a preliminary analysis of FGF/FGFR expression in chromosome 3 monosomic and disomic UMs of the cohort of 80 patients present in the TCGA dataset. The results demonstrate that high-risk chromosome 3 monosomic tumors are characterized by a higher expression of FGFR1 and FGFR2, as well as of FGF5, FGF9, FGF10, FGF12, FGF13, and FGF18 (Figure 2).

The tumor suppressor BAP1 plays a key role in UM progression and monosomy of chromosome 3 is highly associated with the loss of nuclear expression of BAP1, frequently related to loss-of-function BAP1 mutations (see [24] and references therein). Accordingly, 13 out of the 40 chromosome 3 monosomic tumors present in the UM TCGA dataset carried a BAP1 mutation, absent in the 40 disomic specimens. Notably, various members of the FGF/FGFR families appear to be upregulated in this subset of BAP1 mutated tumors when compared to BAP1 wild-type UMs (Figure 2).

Together, these data point to a potential role of the FGF/FGFR axis in UM.

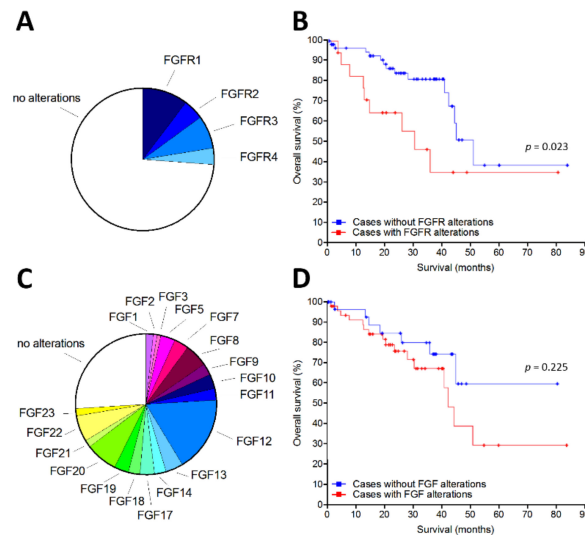


**Figure 1.** Fibroblast growth factor receptor (FGFR) and fibroblast growth factor (FGF) overexpression in human primary uveal melanoma (UM). Analysis of The Cancer Genome Atlas (TCGA) dataset was performed on a cohort of 80 UM patients. (A) Pie chart showing the percentage of samples with mRNA overexpression of the different FGFRs. (B) Overall survival of patients with or without FGFR alterations. (C) Pie chart showing the percentage of samples with mRNA overexpression of different members of the FGF family. Some samples showed the overexpression of more than one FGF family member. (D) Overall survival of patients with or without FGF alterations.

## 2.2. PTX3 Inhibits the Tumorigenic and Metastatic Activity of Murine B16-LS9 Cells

B16-LS9 cells is a murine cell line originated from a B16-F1 liver metastasis and characterized by a unique tropism for the hepatic tissue [25]. Even though of cutaneous origin, this cell line has been utilized as an experimental model to investigate the mechanisms responsible for UM liver tropism [26–28] and drug evaluation for UM treatment [29–31].

As shown in Figure 3A, B16-LS9 cells express FGF2 and its receptors FGFR1 and FGFR3. The autocrine production of FGF2, and possibly of other FGF family members, leads to a basal activation of FGFRs and of the downstream signaling proteins ERK<sub>1,2</sub> and AKT (Figure 3B). Addition of exogenous FGF2 to B16-LS9 cells causes no or only a very modest further increase in FGFR phosphorylation and of the downstream signaling mediators phospho-AKT and phospho-ERK<sub>1,2</sub>, thus confirming the presence of a constitutive autocrine FGF/FGFR loop of activation in these cells under basal cell culture conditions [12].

To assess the capacity of the natural FGF trap PTX3 to suppress the constitutive activation of the FGF/FGFR system, B16-LS9 cells were transfected with a pBABE/Puro vector harboring the full-length human PTX3 (hPTX3) cDNA or with an empty vector. Stable hPTX3\_LS9 and mock\_LS9 cell populations were generated by puromycin selection. After selection, transfectants were assessed for hPTX3 expression and secretion by RT-PCR and Western blotting, respectively (Figure 3C). The production of hPTX3 leads to a significant inhibition of FGFR1, FGFR3, FRS2, and ERK<sub>1,2</sub> activation (Figure 3D) followed by a reduction of the proliferative capacity of hPTX3\_LS9 cells in respect to control non-transfected (WT\_LS9) and mock\_LS9 cells (Figure 3E). Accordingly, hPTX3\_LS9 cells were unable to proliferate in response to exogenous FGF2 stimulation (Figure 3F). In addition, the capacity of hPTX3\_LS9 cells to form colonies when seeded at low cell density and to repair a wounded cell monolayer was significantly reduced in respect to control cells (Figure 3G,H).

To assess the impact of PTX3 overexpression on the tumorigenic activity of B16-LS9 cells, hPTX3\_LS9 and mock\_LS9 cells were injected subcutaneously (s.c.) in syngeneic mice. As shown in Figure 3I, hPTX3\_LS9 grafts show a reduced rate of growth when compared to mock tumors. Next, to assess the capacity of PTX3 to affect the metastatic activity of B16-LS9 cells, WT\_LS9, mock\_LS9 and hPTX3\_LS9 cells were injected into the blood circulation of zebrafish embryos at 48 hours post fertilization (hpf) and the growth of micrometastases in the tail vascular plexus was followed [32]. As shown in Figure 3J, PTX3 overexpression results in a significant reduction of the size of micrometastases evaluated 3 days after cell injection.

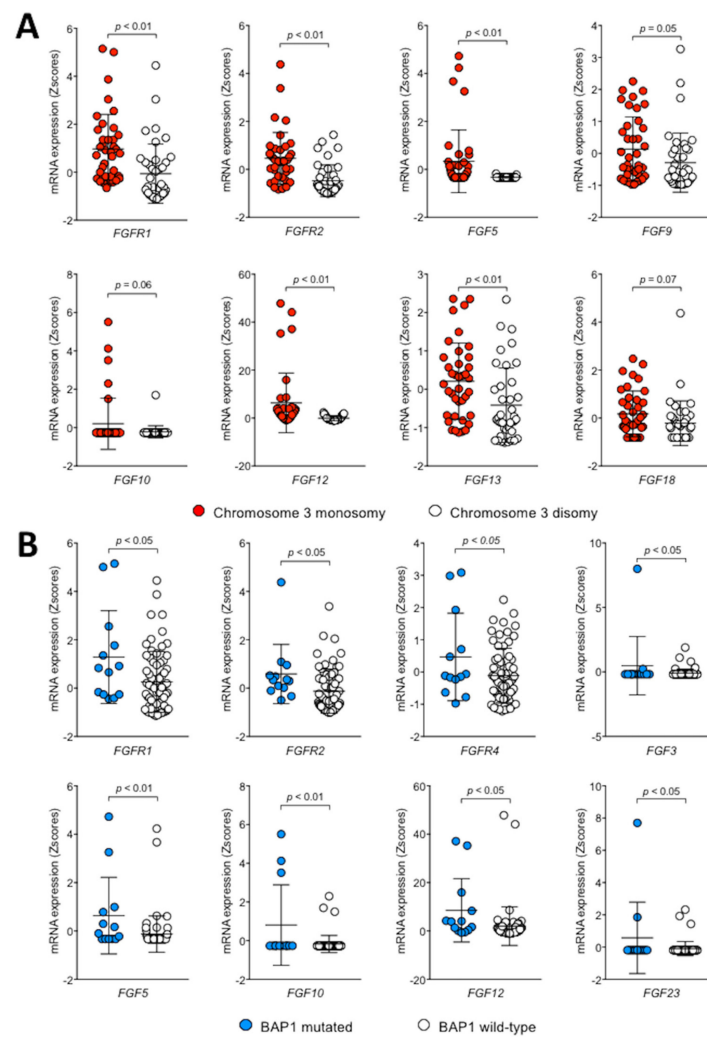


**Figure 2.** Correlation between FGF/FGFR expression and chromosome 3/*BAP1* status in UM. Analysis of the expression of all members of the FGFR and FGF families was performed on the cohort of 80 UM patients present in the UM TCGA dataset. FGF/FGFR genes that showed a significant differential expression between chromosome 3 (monosomic, red symbols; disomic, open symbols) and *BAP1* (mutated, blue symbols; wild-type, open symbols) status.

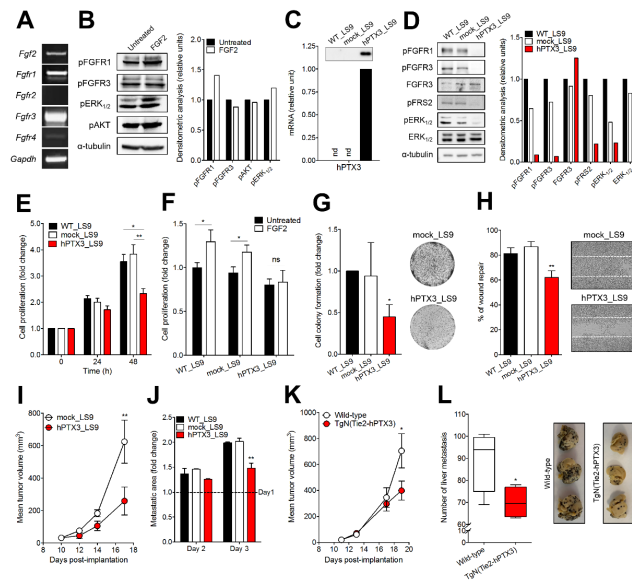


**Figure 3.** Effect of long-pentraxin 3 (PTX3) overexpression on B16-LS9 cells. **(A)** RT-PCR analysis of *Fgf2* and *Fgfr* expression in B16-LS9 cells. **(B)** Western blot analysis of the phosphorylation of FGFR1 and FGFR3 and of the downstream signaling proteins ERK<sub>1/2</sub> and AKT in B16-LS9 cells following 30 min treatment with 30 ng/mL FGF2. **(C)** RT-PCR analysis of human PTX3 (hPTX3) expression in WT\_LS9, mock\_LS9, and hPTX3\_LS9 cells. Inset: Western blot analysis of PTX3 protein levels in the extracts of the same cells. **(D)** Western blot analysis of the phosphorylation of FGFR1, FGFR3, FRS2, and ERK<sub>1/2</sub> proteins in WT\_LS9, mock\_LS9, and hPTX3\_LS9 cell extracts. **(E)** WT\_LS9, mock\_LS9, and hPTX3\_LS9 cells were seeded in 48-well plates at 10<sup>4</sup> cells/well in medium containing 0.4% FBS. After 24 h (T<sub>0</sub>), medium was changed, and cell were counted 24 and 48 h thereafter. Data are the mean ± SEM of three independent experiments in triplicate. **(F)** Cells were seeded as in **(E)**. At T<sub>0</sub>, cells were treated with 30 ng/mL FGF2 and counted 24 h thereafter. Data are the mean ± SEM of three independent experiments in triplicate **(G)** WT\_LS9, mock\_LS9, and hPTX3\_LS9 cells were seeded at 50 cells/cm<sup>2</sup>. After 10 days, cell colonies were stained with crystal violet and quantified by computerized image analysis. Representative images of mock\_LS9 and hPTX3\_LS9 cell colonies are shown on the right. Data are the mean ± SEM of 15 fields for each triplicate sample. **(H)** A mechanical wound was performed in WT\_LS9, mock\_LS9, and hPTX3\_LS9 cell monolayers. After 18 h, cell migration at the leading edge of the wound was quantified by computerized image analysis. Representative images of wounded mock\_LS9 and hPTX3\_LS9 cell monolayers are shown on the right. Data are the mean ± SEM of six microscopic fields. **(I)** Mock\_LS9 and hPTX3\_LS9 cells were injected subcutaneously (s.c.) in syngeneic mice at 50,000 cells/graft and tumor growth was measured with calipers. Data are the mean ± SEM (*n* = 16). **(J)** Red fluorescent WT\_LS9, mock\_LS9, and hPTX3\_LS9 cells were injected into the bloodstream of 48 hours post fertilization (hpf) zebrafish embryos (80–100 cells/embryo). During the next 3 days, the growth of fluorescent metastases in the tail vascular plexus was quantified by fluorescence microscopy followed by computerized image analysis. Data are the mean ± SEM of three independent experiments (*n* = 20) and were normalized to metastasis areas at day 1. **(K)** WT\_LS9 cells were injected s.c. in wild-type and transgenic TgN (Tie2-hPTX3) mice (50,000 cells/graft) and tumor growth was measured with calipers. Data are the mean ± SEM (*n* = 18). **(L)** WT\_LS9 cells were injected into the spleen of wild-type and transgenic TgN (Tie2-hPTX3) mice (20,000 cells/graft). After 14 days, livers were harvested, and metastases were counted. Representative images of harvested livers are shown on the right. Data are the mean ± SEM (*n* = 5). In **(B)** and **(D)**, the right panel shows the densitometric analysis of immunoreactive bands normalized to α-tubulin protein levels. \**p* < 0.05; \*\**p* < 0.01, Student's *t*-test (F,L), one-way (E,H,I) and two-way (I,K) analysis of variance.

These observations prompted us to investigate whether also the systemic/stromal overexpression of PTX3 may exert a significant impact on the tumorigenic and metastatic activity of B16-LS9 cells. To this purpose, WT\_LS9 were grafted in syngeneic transgenic TgN (Tie2-hPTX3) mice in which PTX3 expression is driven by the endothelial specific promoter Tie2. These animals are characterized by high levels of PTX3 protein in the bloodstream and by its accumulation in the stroma of different organs [21]. As shown in Figure 3K, stroma accumulation of PTX3 reduced the growth of B16-LS9 tumors grafted s.c. in transgenic mice when compared to wild-type animals. In addition, a significant difference in liver colonization was observed between wild-type and TgN (Tie2-hPTX3) animals following intrasplenic injection of B16-LS9 cells (Figure 3L). Together, our data indicate that the PTX3 inhibits the tumorigenic and metastatic activity of B16-LS9 cells.

### 2.3. The Pan-FGF Trap NSC12 Inhibits the Tumorigenic and Metastatic Activity of Murine B16-LS9 Cells

PTX3 is a 340 kDa protein composed of eight protomers, with a complex proteinaceous structure that hampers its pharmacological exploitation. To overcome these limitations, NMR data and pharmacophore modeling of PTX3/FGF2 interaction were used in our laboratory to identify the PTX3-derived small molecule NSC12 as the first orally active pan-FGF trap able to inhibit FGFR activation and tumor growth in various FGF-dependent murine and human tumor models [20,21].

As shown in Figure 4A, treatment of B16-LS9 cells with increasing concentrations of NSC12 inhibits FGFR phosphorylation, thus affecting autocrine, FGF-mediated cell proliferation ( $IC_{50} = 2.2 \mu\text{M}$ , Figure 4B). Accordingly, NSC12 treatment hampered the capacity of B16-LS9 cells to form colonies when seeded at low density and to repair a wounded cell monolayer (Figure 4C,D).

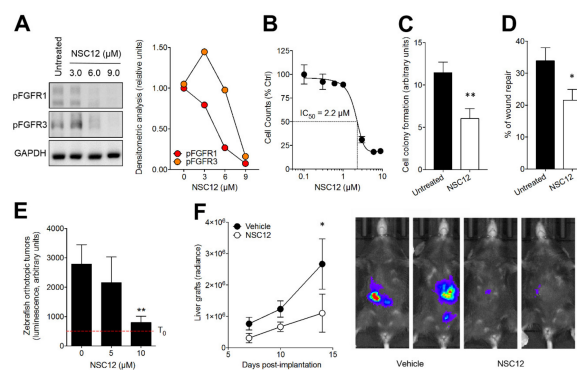


**Figure 4.** Effect of the pan FGF-trap NSC12 on B16-LS9 cells. (A) Western blot analysis of FGFR1 and FGFR3 phosphorylation in B16-LS9 cells treated for 12 h with increasing concentrations of NSC12. The right panel shows the densitometric analysis of immunoreactive bands normalized to GAPDH protein levels. (B) Effect of NSC12 treatment on the proliferation of B16-LS9 cells. Viable cells were counted after 24 h of incubation with increasing concentrations of NSC12. Data are the mean  $\pm$  SEM ( $n = 3$ ). (C) B16-LS9 cells were seeded at 50 cells/cm<sup>2</sup> and treated with 2.5  $\mu\text{M}$  NSC12. After 10 days, cell colonies were stained with crystal violet and quantified by computerized image analysis. Data are the mean  $\pm$  SEM of 15 fields for each triplicate sample. (D) A mechanical wound was performed in a B16-LS9 cell monolayer followed by incubation with 3.0  $\mu\text{M}$  NSC12. After 18 h, cell migration at the leading edge of the wound was quantified by computerized image analysis. Data are the mean  $\pm$  SEM of six microscopic fields. (E) B16-LS9-luc cells were injected into the eye of 48 hpf zebrafish embryos (100 cells/embryo). Then, embryos were incubated with increasing concentrations of NSC12 at T<sub>0</sub>. Tumor growth was evaluated 3 days after grafting by measuring the cell luminescence signal. Data are the mean  $\pm$  SEM ( $n = 20$ ). (F) B16-LS9-luc cells were grafted in the liver of syngeneic mice (50,000 cells/graft). Next, vehicle or NSC12 (7.5 mg/kg) were injected i.p. every other day and tumor growth was imaged with IVIS Lumina III for the following 14 days. Data are the mean  $\pm$  SEM ( $n = 9$ ). Representative images of control and NSC-12 treated mice imaged 14 days after grafting are shown on the right. \* $p < 0.05$ ; \*\* $p < 0.01$ , Student's *t*-test (C,D), one-way (E) and two-way (F) analysis of variance.

To evaluate the effect of NSC12 on the oncogenic potential of B16-LS9 cells, we implemented a novel orthotopic xenograft assay in which luciferase-transfected cells (B16-LS9-luc cells) were injected into the eye of zebrafish embryos at 48 hpf. Then, embryos were transferred in fish water in the absence or in the presence of 5.0 or 10  $\mu$ M NSC12. NSC12 treatment resulted in a significant inhibition of the growth of grafted cells when assessed 3 days after injection (Figure 4E). Accordingly, administration of NSC12 (7.5 mg/kg i.p. every other day) hampered the growth of B16-LS9-luc cells grafted into the liver of wild-type mice (Figure 4F).

#### 2.4. FGF Trapping Inhibits Human FGF/FGFR Signaling and Proliferation in UM Cells

The capacity of the pan-FGF trap NSC12 to inhibit FGF/FGFR signaling in human UM was investigated on three cell lines originating from human primary UM lesions (Mel285, Mel270, and 92.1 cells) and one cell line originating from a human UM metastasis (OMM2.3 cells). The major molecular alterations of these cell lines are summarized in Table 1 (see [33] and references therein).

**Table 1.** Molecular alterations of the human UM cell lines utilized in this study.

	Mel285	92.1	Mel270	OMM2.3
<i>GNAQ</i> (exons 4–5)	WT	Q209L (626 A > T)	Q209P (626 A > C)	Q209P (626 A > C)
<i>GNA11</i> (exons 4–5)	Q209L	WT	WT	WT
<i>BAP1</i>	WT	WT	WT	WT
<i>BAP1</i>	Yes, low	Yes	Yes	Yes
<i>SF3B1</i>	WT	WT	WT	WT
<i>EIF1AX</i>	WT	c.17G/A	WT	WT
Chr3	Disomy 3 Loss 3p26-pter	Disomy 3	Disomy 3 Loss 3p24 Loss 3q21.2-3q24	Disomy 3 Loss 3p24 Loss 3q21.2-3q24
Chr6	Disomy 6p	Gain 6p	Tetrasomy 6p	Tetrasomy 6p
Chr8	Disomy 8p Tetrasomy 8q	Gain 8q	Disomy 8 Extra 8q	Disomy 8 Extra 8q

As observed for B16-LS9 cells, NSC12 treatment inhibits the phosphorylation of the FGF receptors FGFR1 and FGFR3 as well as of their downstream signaling molecules FRS2 and ERK<sub>1,2</sub> in the UM cell lines tested (Figure 5A). This resulted in a significant inhibition of UM cell proliferation/survival with an IC<sub>50</sub> ranging between 6.0 and 8.0  $\mu$ M NSC12 (Figure 5B). Similar results were obtained after treatment with the selective tyrosine kinase FGFR inhibitor BGJ398 [34] (data not shown).

In keeping with the hypothesis that the FGF system may play a pivotal role in UM cell survival [9], NSC12 induced pro-apoptotic caspase-3 activation and PARP cleavage in UM cells (Figure 5C) that were followed by a significant increase of annexin-V<sup>+</sup> apoptotic cells (Figure 5D).

$\beta$ -catenin signaling has been involved in UM cell migration and metastasis [35–37]. Notably, NSC12 treatment caused a significant and rapid decrease of the protein levels of  $\beta$ -catenin in UM cells. (Figure 5E). Accordingly, FGF trapping by NSC12 inhibited cell migration in a Boyden chamber chemotaxis assay and following the mechanical wound of a UM cell monolayer (Figure 5F,G). It must be pointed out that both assays were performed under experimental conditions that did not exert a significant effect on UM cell survival (data not shown).

Together, these findings demonstrate that FGF trapping exerts a significant impact on the autocrine FGF/FGFR axis in human UM cells.



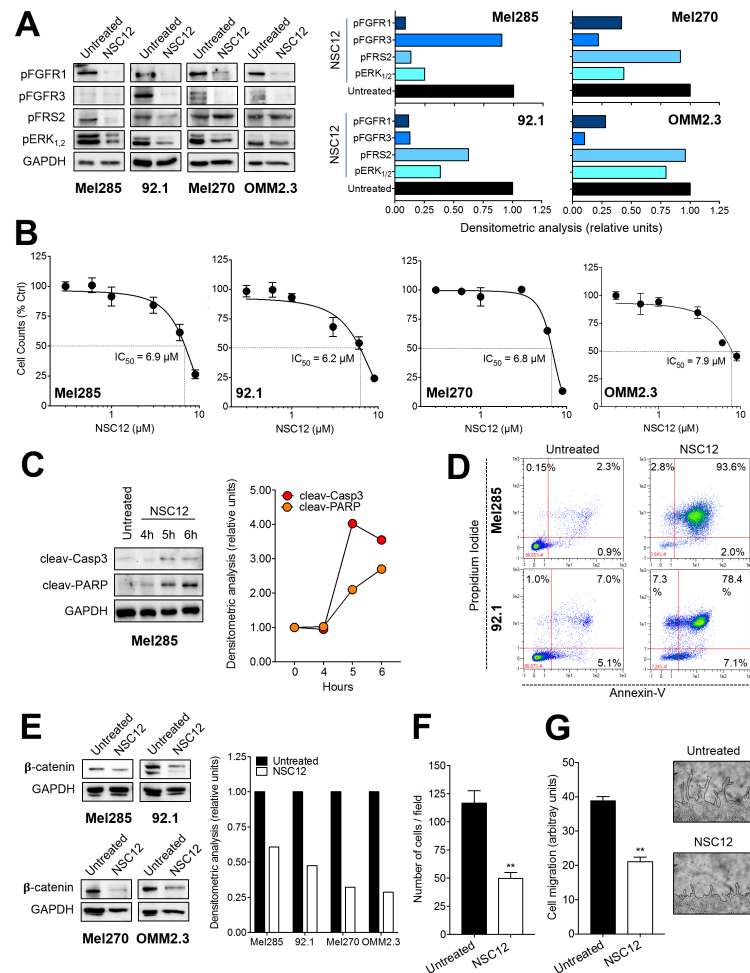


**Figure 5.** Effect of the pan FGF-trap NSC12 on human UM cells. **(A)** Western blot analysis of the phosphorylation of FGFR1 and FGFR3 and of the downstream signaling proteins FRS2 and ERK<sub>1/2</sub> in Mel285, 92.1, Mel270, and OMM2.3 cells after 3 h treatment with 15 μM NSC12. **(B)** Effect of NSC12 treatment on the proliferation of UM cells. Viable cells were counted after 24 h of incubation with increasing concentrations of NSC12. Data are the mean ± SEM ( $n = 3$ ). **(C)** Kinetics of PARP and caspase-3 cleavage following incubation of MEL285 cells with 15 μM NSC12. **(D)** Cytofluorimetric analysis of apoptosis induced in Mel285 cells (upper panels) and 92.1 cells (lower panels) after 12 h treatment with 15 μM NSC12. **(E)** Western blot analysis of the levels of β-catenin in Mel285, 92.1, Mel270, and OMM2.3 cells after 3 h treatment with 15 μM NSC12. **(F)** Boyden chamber chemotaxis assay performed on Mel285 cells treated for 4 h with 6.0 μM NSC12. Data are the mean ± SEM of five fields for each triplicate sample. **(G)** A mechanical wound was performed in a Mel285 cell monolayer followed by 18 h incubation with 6.0 μM NSC12. After 18 h, cell migration at the leading edge of the wound was quantified by computerized image analysis. Representative images of untreated and NSC12-treated cells are shown on the right (black lines highlight the front of cell migration). Data are the mean ± SEM of 6 microscopic fields. In **(A,C,D)** the right panel shows the densitometric analysis of immunoreactive bands normalized to GAPDH protein levels. \*\*  $p < 0.01$ , Student's  $t$  test.

### 3. Discussion

In the present work, we demonstrate that different FGF trapping approaches inhibit the tumorigenic and metastatic activity of hepatotropic murine B16-LS9 cells and hamper the proliferation, survival, and migration of primary and metastatic human UM cell lines.

B16-LS9 cells are a murine cell line originated from a B16-F1 liver metastasis and characterized by a unique tropism for the hepatic tissue that recapitulates the metastatic growth patterns observed in the human disease [25]. Indeed, despite its cutaneous origin, B16-LS9 cells have been selectively developed after serial passages for liver specific metastasis, leading to the only model metastasizing to the liver following intraocular injection in syngeneic animals [38]. Thus, B16-LS9 cells have been utilized as an experimental model to investigate the mechanisms responsible for UM liver tropism [26–28], drug testing for UM therapy [29–31], immunologic and angiogenic aspects of UM and imaging methodologies (see [38] and references therein).

Here, we show that B16-LS9 cells express different FGFRs and the prototypic FGFR ligand FGF2. This leads to the constitutive phosphorylation of FGFR1 and FGFR3, as well as of the downstream signaling proteins FRS2, ERK<sub>1/2</sub>, and AKT. As observed for different FGF-dependent tumor cell types, this activates an autocrine loop of stimulation in B16-LS9 cells, which is inhibited by the overexpression of the natural extracellular FGF trap PTX3 [16,17,21,39]. The capacity of PTX3 to suppress the proliferative and migratory activity of B16-LS9 transfectants highlights the non-redundant role of the autocrine FGF/FGFR system in the tumorigenic activity of these cells [12]. Indeed, PTX3-overexpressing B16-LS9 tumor grafts showed a reduced rate of growth in syngeneic mice and a reduced metastatic activity when injected in the blood stream of zebrafish embryos.

To assess the effect of the systemic delivery and stromal accumulation of PTX3 protein on UM growth, we took advantage of TgN (Tie2-hPTX3) mice, a transgenic mouse line we generated in the C57BL/6 background that expresses PTX3 under the control of the endothelial specific *Tie2/Tek* transcription regulatory sequences [21]. When injected s.c. in TgN (Tie2-hPTX3) mice, B16-LS9 cells showed a reduced rate of growth, thus confirming the oncosuppressive effect exerted by PTX3 on these cells. Notably, the systemic accumulation of PTX3 protein resulted also in a significant inhibition of the capacity of B16-LS9 cells to originate liver metastases when injected into the spleen of the transgenic animals. Even though we cannot rule out the possibility that PTX3 may have multiple impacts on tumor growth, the data support the notion that the anti-tumor effects of PTX3 are related to its inhibitory action on the autocrine/paracrine loops of stimulation triggered by the FGF/FGFR system in FGF-dependent B16-LS9 cells.

Despite its oncosuppressive effects, the complex proteinaceous structure of PTX3 hampers its pharmacological exploitation. For this reason, the scaling down of this macromolecule to PTX3-derived small molecules was attempted to take advantage of its antitumor properties in a translational outlook. This led to the identification of the small molecule NSC12 as the first orally available pan-FGF trap endowed with a potent anti-tumor activity in different FGF-dependent tumor models (reviewed in [7]). On this basis, a series of experiments were performed to assess the effect of NSC12 on B16-LS9 cells. In keeping with its FGF trapping activity, NSC12 inhibits FGFR phosphorylation, proliferation, and migration of B16-LS9 cells. Notably, NSC12 was able to suppress the growth of these cells also when orthotopically implanted in the eye of zebrafish embryos or when injected into the liver of syngeneic mice.

Even though the syngeneic B16-LS9 model shows significant experimental advantages and resemblance to UM behavior concerning its hepatotropic features, significant genetic differences occur between cutaneous and UM [40,41]. This prompted us to assess the impact of the FGF trapping activity of NSC12 on both primary and metastatic human UM cell lines. Notably, NSC12 treatment was able to inhibit FGFR activation and downstream signaling in all the cell lines tested. This was paralleled by the activation of the pro-apoptotic proteins PARP and caspase-3, thus leading to UM cell death.

The  $\beta$ -catenin signaling pathway has been involved in the growth, migratory, and invasive behavior of UM cells [35]. Indeed,  $\beta$ -catenin immunoreactivity is increased in primary UM and

is associated with a shorter patient survival [36], its expression representing a biomarker potentially correlated to metastatic UM [37]. The FGF/FGFR axis has been shown to stabilize  $\beta$ -catenin, leading to its nuclear accumulation and activation of the  $\beta$ -catenin signaling pathway [42,43]. Notably, our data demonstrate that NSC12 induces a decrease of  $\beta$ -catenin levels in UM cells that was paralleled by a significant inhibition of UM cell migration in a Boyden chamber assay or following the mechanical wound of the cell monolayer. Further studies will be required to dissect the impact of  $\beta$ -catenin downregulation induced by FGF inhibitors on the tumorigenic and metastatic behavior of UM cells.

In keeping with our preclinical observations, the analysis of the publicly available mRNA profiling dataset of 80 primary human UM specimens present in TCGA indicates that the upregulation of different members of the FGF or FGFR families are associated with poorer prognosis, chromosome 3 monosomy, and *BAP1* mutation. These data further support the hypothesis that the FGF/FGFR system plays a non-redundant role in UM. Several experimental evidences reinforce this assumption. Similar to NSC12, neutralizing antibodies and an antisense oligonucleotide directed against FGF2 have been shown to reduce cell proliferation and survival in various human UM cell lines [12]. When examined on an array of 32 human UM samples, FGF2 immunoreactivity was detectable in more than 50% of cases, its frequency being higher in mixed/epithelioid samples than in spindle cell type specimens [13]. Notably, immunohistochemical staining revealed an elevated FGF2 expression in UM metastases when compared to primary lesions, further implying FGF2 in UM progression [13]. In addition, the production of FGF2 by UM cells and primary tumors may contribute, together with vascular endothelial growth factor, to the angiogenic activity of UM that, in turn, favors its hematogenous metastatic spread [10,11]. Finally, recent observations have shown that FGF2 produced by hepatic stellate cells confers resistance of metastatic UM cells to bromodomain and extraterminal protein inhibitors and to the histone deacetylase inhibitor vorinostat via FGFR activation [44]. Together with our observations, these data suggest that drugs targeting the FGF/FGFR system might be considered for an adjuvant chemotherapy treatment of metastatic UM.

Thus far, different approaches have been developed to target the FGF/FGFR system [9] and various FGF/FGFR inhibitors are under evaluation in clinical trials on cancer patients affected by different kinds of tumors [8]. In this frame, drugs targeting FGF ligands may represent an interesting alternative to tyrosine kinase FGFR inhibitors. To this respect, the small molecule NSC12 is the first orally active multi-FGF trap. Of note, in keeping with the lack of pathological consequences following constitutive PTX3 overexpression in transgenic mice, the anti-tumor action of NSC12 occurs in the absence of any significant effect on body weight and survival of treated animals [21]. Thus, NSC12 may represent a lead compound for the development of orally active small molecule therapeutics for the treatment of UM in which the ligand-dependent activation of the FGFR pathway is an oncogenic driver. Further experiments aimed to assess the *in vivo* efficacy of this FGF trapping approach in orthotopic and liver metastatic models of human UM are required to confirm this hypothesis.

## 4. Materials and Methods

### 4.1. Reagents

All reagents were of analytical grade. Dulbecco's modified Eagle medium (DMEM), RPMI 1640 medium and fetal bovine serum (FBS) were from GIBCO Life Technologies (Grand Island, NY, USA). Penicillin, streptomycin, Triton-X100, Brij, sodium orthovanadate, protease inhibitor cocktail, and anti- $\alpha$ -tubulin were from Sigma-Aldrich (St. Louis, MO, USA). Bradford reagent was from Bio-Rad Laboratories (Milan, Italy). Trizol, MMLV reverse transcriptase and CellTracker Red CMTPX Dye were from Invitrogen (Carlsbad, CA, USA). PVP-free polycarbonate filters were obtained from Costar (Cambridge, MA, USA). Diff-Quik reagent was obtained from Dade-Behring (Deerfield, IL, USA). ONE-Glo™ Reagent and DNase were from Promega (Milan, Italy). Recombinant FGF2 was purchased from TecnoGen (Caserta, Italy). Anti-FGFR1, anti-ERK<sub>1/2</sub>, anti-phospho-ERK<sub>1/2</sub> (Thr202/Tyr204), anti-phospho-AKT (Ser473), anti-cleaved-PARP,

anti-cleaved-caspase-3, and anti- $\beta$ -catenin were from Cell Signaling Technologies (Danver, MA, USA). Anti-phospho-FGFR1 (Tyr766), anti-phospho-FRS2 (Tyr196), anti-FGFR3, and anti-GAPDH were from Santa Cruz (Santa Cruz, CA, USA). Anti-phospho-FGFR3 (Tyr724) was from ABCAM (Cambridge, UK). Matrigel was from Cultrex BME (Gaithersburg, MD, USA). Floseal hemostatic matrix was from Baxter (Deerfield, IL, USA).

#### 4.2. Cell Cultures

Murine B16-LS9 cells [25] were maintained in DMEM supplemented with 10% FBS, 100 U/mL penicillin, and 100  $\mu$ g/mL streptomycin. B16-LS9 cells were transfected with a pBABE/Puro vector harboring the full-length human PTX3 cDNA or with empty vector as described [19]. Stable hPTX3\_LS9 and mock\_LS9 cell populations were generated by puromycin selection. Luciferase-transfected B16-LS9 cells (B16-LS9-*luc* cells) were generated as described [21]. Human UM cells [45–47] were maintained in RPMI 1640 medium supplemented with 10% (Mel285, 92.1, and OMM2.3 cells) or 20% FBS (Mel270 cells), 100 U/mL penicillin, and 100  $\mu$ g/mL streptomycin.

#### 4.3. Real-Time PCR Analysis

For mRNA expression analysis, cells were processed, and total RNA was extracted using TRIzol Reagent according to manufacturer's instructions. Contaminating DNA was digested using DNase and 2.0  $\mu$ g of total RNA were retro-transcribed with MMLV reverse transcriptase using random hexaprimers in a final 20  $\mu$ L volume. Then, 1/10th of the reaction was analyzed by semi-quantitative RT-PCR using specific primers (Table 2). The PCR products were then electrophoresed on a 1.5% agarose gel and visualized by ethidium bromide staining.

**Table 2.** Oligonucleotide primers used for RT-PCR analysis.

Gene	Forward	Reverse
<i>Fgf2</i>	5'-CCTTCCCACCAGGCCACTTAA-3'	5'-GGTCCGTTTTGGATCCGAGTTT-3'
<i>Fgfr1</i>	5'-GCTGACTCTGGCCTCTACGCT-3'	5'-CAGGATCTGGACATACGGCAA-3'
<i>Fgfr2</i>	5'-CTGCCTGGTGGAGAATGAAT-3'	5'-CGCTGTAAACCTTGCAGACA-3'
<i>Fgfr3</i>	5'-CTGAAGCACGTGGAAGTGAA-3'	5'-CCTCAAAGGTGACATTGTGC-3'
<i>Fgfr4</i>	5'-ACTGTCAAATCCGCTGTCC-3'	5'-AGCGAATGCTACCCAGAGAG-3'
<i>PTX3</i>	5'-CATCTCCTTGGCATTCTGTTTTG-3'	5'-CCCATTCCGAGTGCTCCTGA-3'
<i>Gapdh</i>	5'-GAAGGTCGGTGTGAACGGATT-3'	5'-TGACTGTGCCGTGAATTG-3'

#### 4.4. Western Blot Analysis

For the analysis of FGF signaling, cell samples were homogenized in RIPA buffer containing 1.0% Triton-X100, 0.2% Brij, 1.0 mM sodium orthovanadate, and protease inhibitor cocktail. Protein concentrations were determined using the Bradford protein assay. Western blot analysis was performed using rabbit anti-FGFR1, anti-pFGFR1, anti-FGFR3, anti-pFGFR3, anti-pFRS2, anti-pAKT, anti-ERK<sub>1/2</sub>, anti-pERK<sub>1/2</sub>, anti-cleaved-PARP, anti-cleaved-caspase-3, anti- $\beta$ -catenin antibodies, and normalized with anti- $\alpha$ -tubulin or anti-GAPDH antibodies. Densitometric analysis was performed using the Bio-Rad Image Lab Software 5.2.1. The whole blot showing all the bands with all molecular weight markers on the Western are included in the Supplementary Materials.

#### 4.5. Cell Proliferation Assay

Cells were seeded on 48-well plates at  $1 \times 10^4$  cells/cm<sup>2</sup> (B16-LS9 cells) or at  $1.5 \times 10^4$  cells/cm<sup>2</sup> (Mel285, Mel270, 92.1, and OMM2.3 cells). After 24 h, cells were treated with increasing concentrations of NSC12. After a further 24 or 48 h incubation, cells were trypsinized and viable cell counting was performed with the MACSQuant<sup>®</sup> Analyzer (Miltenyi Biotec) as reported [48].

#### 4.6. Colony Formation Assay

B16-LS9 cells were seeded in 35-mm culture dishes at 50 cells/cm<sup>2</sup>. After 10 days of incubation, cell colonies were stained with crystal violet and quantified by computerized image analysis.

#### 4.7. Chemotaxis Assay

Mel285 cells were seeded at  $1.0 \times 10^6$  cells/mL in the upper compartment of a Boyden chamber containing gelatin-coated PVP-free polycarbonate filters (8 µm pore size). RPMI medium supplemented with 1.0% FBS was placed in the lower compartment in the absence or in the presence of 6.0 µM NSC12. After 4 h of incubation at 37 °C, cells that migrated to the lower side of the filter were stained with Di-Quik reagent. Five random fields were counted for each triplicate sample.

#### 4.8. Wound Healing Assay

Confluent B16-LS9 or Mel285 cells were scraped with a 200 µL tip to obtain a mechanical wound through the cell monolayer. Then, B16-LS9 cells were maintained in DMEM supplemented with 0.4% FBS in the absence or in the presence of 3.0 µM NSC12 whereas Mel285 cells were maintained in RPMI medium supplemented with 1.0% FBS and treated or not with 6.0 µM NSC12. After 18 h, cells at the leading edge of the wound were photographed under an inverted Zeiss Axiovert 200 M photomicroscope and cell migration wound was quantified by computerized image analysis.

#### 4.9. Apoptotic Cell Death Analysis

Mel285 or 92.1 cells were seeded at  $2.5 \times 10^5$  cells/mL in the absence or in the presence of 15 µM NSC12. After 12 h, apoptotic cell death was assessed by cytofluorimetric analysis following Annexin-V/propidium iodide-double staining according to manufacturer's instructions.

#### 4.10. Tumor Graft and Liver Metastasis Assays in Mice

Animal studies were approved by the local animal ethics committee (OPBA, Organismo Preposto al Benessere degli Animali, Università degli Studi di Brescia, Italy) and by the Italian Ministero della Salute (Project: Integrated model for the study and therapy of uveal melanoma; authorization no. 1306/2015-PR). All the procedures and animal care were conformed to institutional guidelines that comply with national and international laws and policies (EEC Council Directive 86/609, OJ L 358, 12 December 1987).

C57BL/6 (Charles River, Calco, Italy) and transgenic TgN (Tie2-hPTX3) mice [21] were maintained under standard housing conditions.

B16-LS9 cells were injected s.c. or into the spleen [28] of wild-type and TgN (Tie2-hPTX3) mice at 50,000 and 20,000 cells/graft, respectively. Subcutaneous tumors were measured with calipers and tumor volume was calculated according to the formula  $V = (D \times d^2)/2$ , where D and d are the major and minor perpendicular tumor diameters, respectively. Liver metastases were counted under a dissecting microscope 14 days after cell injection.

As for liver tumor grafts, 20 µL of a cell suspension containing 50,000 B16-LS9-*luc* cells in Matrigel (1:1, vol/vol) were injected into the liver of wild-type mice. To minimize bleeding and to avoid leakage of tumor cells after needle removal, Floseal hemostatic matrix was applied on the liver surface at the site of injection. NSC12 treatment (7.5 mg/kg) was performed every other day by i.p. injection in a 100 µL final volume. Tumor growth was imaged with IVIS Lumina III during the following 14 days.

#### 4.11. Zebrafish Embryo Assays

The AB zebrafish line was maintained at 28 °C on a 14 h light/10 h dark cycle. After spawning, fertilized eggs were harvested and incubated in fish water at 28 °C. Zebrafish embryos were staged and maintained in 0.003% 1-phenyl-2-thiourea (Sigma) starting from 24 hpf to prevent pigmentation.

For the metastasis assay, B16-F10 cells were stained with the red fluorescent CellTracker Red CMTPX Dye. Then, 80–100 cells/embryo were injected into the blood circulation in the ventral region of the duct of Cuvier of zebrafish embryos at 48 hpf. During the next 3 days, the growth of fluorescent metastases in the tail vascular plexus was quantified by fluorescence microscopy followed by computerized image analysis of the fluorescent tumor area [32].

For the orthotopic UM model, B16-LS9-*luc* cells (100 cells/embryo) were injected into the eye of zebrafish embryos at 48 hpf using a borosilicate needle and an Eppendorf FemtoJet microinjector equipped with an InjectMan N12 manipulator. Then, embryos were transferred in fish water in the absence or in the presence of increasing concentrations of NSC12. Tumor growth was evaluated 3 days after grafting by measuring the cell luminescence signal as it follows: embryos were anesthetized and singularly placed in a well of a white polystyrene 96-well plate; medium was removed and replaced with 50  $\mu$ L of RIPA buffer plus 50  $\mu$ L of ONE-Glo™ Reagent; finally, luminescence was measured using an EnSight multimode plate reader (Perkin Elmer, Waltham, MA, USA).

#### 4.12. Statistical Analysis

Statistical analysis was performed with GraphPad Prism 7 (San Diego, CA, USA) using Student's *t*-test or one-way analysis of variance followed by Bonferroni multiple comparison post-test. Tumor growth data were analyzed by two-way analysis of variance, followed by Bonferroni post-test. Differences were considered significant when *p* values < 0.05.

## 5. Conclusions

We demonstrate that the natural extracellular FGF trap PTX3 inhibits the oncogenic activity of hepatotropic murine melanoma B16-LS9 cells. Translational exploitation of these findings shows that the PTX3-derived pan-FGF trap small molecule NSC12 hampers the tumorigenic and liver metastatic activity of B16-LS9 cells and affects autocrine FGF/FGFR signaling, proliferation, survival, and migration of human UM cells. Together, these findings indicate that FGF trapping may represent a novel therapeutic strategy for the treatment of metastatic UM.

**Supplementary Materials:** The following are available online at <http://www.mdpi.com/2072-6694/11/9/1305/s1>, The whole blot showing all the bands with all molecular weight markers on the Western.

**Author Contributions:** Conceptualization, S.R. and M.P.; methodology, S.R. and C.T.; validation, S.R. and M.P.; investigation, S.R., R.R., A.L., M.I.N., C.T., G.P., F.M., A.G.; resources, M.M.; writing—original draft preparation, S.R. and M.P.; writing—review and editing, S.R., F.S. and M.P.; visualization, S.R.; supervision, M.P.; project administration, M.P.; funding acquisition, M.P. and R.R.

**Funding:** This work was supported by Associazione Italiana Ricerca sul Cancro (AIRC) IG grant no. 18943 to M.P. and AIRC MFAG grant no. 18459 to R.R. S.R. was supported by an AIRC fellowship.

**Acknowledgments:** B16-LS9 cells were kindly provided by L. Morbidelli (University of Siena, Italy). Mel285, Mel270, 92.1 and OMM2.3 cells were obtained from M. Jager (Leiden University, The Netherlands). R. Nascimbeni (University of Brescia, Italy) kindly provided Floseal hemostatic matrix.

**Conflicts of Interest:** The authors declare no conflict of interest.

## References

1. Jovanovic, P.; Mihajlovic, M.; Djordjevic-Jocic, J.; Vlajkovic, S.; Cekic, S.; Stefanovic, V. Ocular melanoma: an overview of the current status. *Int. J. Clin. Exp. Pathol.* **2013**, *6*, 1230–1244. [PubMed]
2. Mahendraraj, K.; Lau, C.S.; Lee, I.; Chamberlain, R.S. Trends in incidence, survival, and management of uveal melanoma: a population-based study of 7,516 patients from the Surveillance, Epidemiology, and End Results database (1973–2012). *Clin. Ophthalmol.* **2016**, *10*, 2113–2119. [CrossRef] [PubMed]
3. Yonekawa, Y.; Kim, I.K. Epidemiology and management of uveal melanoma. *Hematol. Oncol. Clin. North Am.* **2012**, *26*, 1169–1184. [CrossRef] [PubMed]
4. Vivet-Noguer, R.; Tarin, M.; Roman-Roman, S.; Alsafadi, S. Emerging Therapeutic Opportunities Based on Current Knowledge of Uveal Melanoma Biology. *Cancers* **2019**, *11*, 1019. [CrossRef] [PubMed]

5. Mathis, T.; Cassoux, N.; Tardy, M.; Piperno, S.; Gastaud, L.; Dendale, R.; Maschi, C.; Nguyen, A.M.; Meyer, L.; Bonnin, N.; et al. Management of uveal melanomas, guidelines for oncologists. *Bull. Cancer* **2018**, *105*, 967–980. [[CrossRef](#)]
6. Yang, J.; Manson, D.K.; Marr, B.P.; Carvajal, R.D. Treatment of uveal melanoma: where are we now? *Ther. Adv. Med. Oncol.* **2018**, *10*, 1758834018757175. [[CrossRef](#)] [[PubMed](#)]
7. Presta, M.; Chiodelli, P.; Giacomini, A.; Rusnati, M.; Ronca, R. Fibroblast growth factors (FGFs) in cancer: FGF traps as a new therapeutic approach. *Pharmacol. Ther.* **2017**, *179*, 171–187. [[CrossRef](#)]
8. Ghedini, G.C.; Ronca, R.; Presta, M.; Giacomini, A. Future applications of FGF/FGFR inhibitors in cancer. *Expert. Rev. Anticancer Ther.* **2018**, *18*, 861–872. [[CrossRef](#)]
9. Giacomini, A.; Chiodelli, P.; Matarazzo, S.; Rusnati, M.; Presta, M.; Ronca, R. Blocking the FGF/FGFR system as a "two-compartment" antiangiogenic/antitumor approach in cancer therapy. *Pharmacol. Res.* **2016**, *107*, 172–185. [[CrossRef](#)]
10. Boyd, S.R.; Tan, D.S.; de Souza, L.; Neale, M.H.; Myatt, N.E.; Alexander, R.A.; Robb, M.; Hungerford, J.L.; Cree, I.A. Uveal melanomas express vascular endothelial growth factor and basic fibroblast growth factor and support endothelial cell growth. *Br. J. Ophthalmol.* **2002**, *86*, 440–447. [[CrossRef](#)]
11. Notting, I.C.; Missotten, G.S.; Sijmons, B.; Boonman, Z.F.; Keunen, J.E.; van der Pluijm, G. Angiogenic profile of uveal melanoma. *Curr. Eye Res.* **2006**, *31*, 775–785. [[CrossRef](#)] [[PubMed](#)]
12. Lefevre, G.; Babchia, N.; Calipel, A.; Mouriaux, F.; Faussat, A.M.; Mrzyk, S.; Mascarelli, F. Activation of the FGF2/FGFR1 autocrine loop for cell proliferation and survival in uveal melanoma cells. *Invest. Ophthalmol. Vis. Sci.* **2009**, *50*, 1047–1057. [[CrossRef](#)] [[PubMed](#)]
13. Wang, Y.; Bao, X.; Zhang, Z.; Sun, Y.; Zhou, X. FGF2 promotes metastasis of uveal melanoma cells via store-operated calcium entry. *Onco. Targets Ther.* **2017**, *10*, 5317–5328. [[CrossRef](#)] [[PubMed](#)]
14. Garlanda, C.; Bottazzi, B.; Bastone, A.; Mantovani, A. Pentraxins at the crossroads between innate immunity, inflammation, matrix deposition, and female fertility. *Annu. Rev. Immunol.* **2005**, *23*, 337–366. [[CrossRef](#)] [[PubMed](#)]
15. Giacomini, A.; Ghedini, G.C.; Presta, M.; Ronca, R. Long pentraxin 3: A novel multifaceted player in cancer. *Biochim. Biophys. Acta Rev. Cancer* **2018**, *1869*, 53–63. [[CrossRef](#)] [[PubMed](#)]
16. Leali, D.; Alessi, P.; Coltrini, D.; Ronca, R.; Corsini, M.; Nardo, G.; Indraccolo, S.; Presta, M. Long pentraxin-3 inhibits FGF8b-dependent angiogenesis and growth of steroid hormone-regulated tumors. *Mol. Cancer Ther.* **2011**, *10*, 1600–1610. [[CrossRef](#)] [[PubMed](#)]
17. Ronca, R.; Alessi, P.; Coltrini, D.; Di Salle, E.; Giacomini, A.; Leali, D.; Corsini, M.; Belleri, M.; Tobia, C.; Garlanda, C.; et al. Long pentraxin-3 as an epithelial-stromal fibroblast growth factor-targeting inhibitor in prostate cancer. *J. Pathol.* **2013**, *230*, 228–238. [[CrossRef](#)] [[PubMed](#)]
18. Camozzi, M.; Rusnati, M.; Bugatti, A.; Bottazzi, B.; Mantovani, A.; Bastone, A.; Inforzato, A.; Vincenti, S.; Bracci, L.; Mastroianni, D.; et al. Identification of an antiangiogenic FGF2-binding site in the N terminus of the soluble pattern recognition receptor PTX3. *J. Biol. Chem.* **2006**, *281*, 22605–22613. [[CrossRef](#)] [[PubMed](#)]
19. Ronca, R.; Di Salle, E.; Giacomini, A.; Leali, D.; Alessi, P.; Coltrini, D.; Ravelli, C.; Matarazzo, S.; Ribatti, D.; Vermi, W.; et al. Long pentraxin-3 inhibits epithelial-mesenchymal transition in melanoma cells. *Mol. Cancer Ther.* **2013**, *12*, 2760–2771. [[CrossRef](#)]
20. Castelli, R.; Giacomini, A.; Anselmi, M.; Bozza, N.; Vacondio, F.; Rivara, S.; Matarazzo, S.; Presta, M.; Mor, M.; Ronca, R. Synthesis, Structural Elucidation, and Biological Evaluation of NSC12, an Orally Available Fibroblast Growth Factor (FGF) Ligand Trap for the Treatment of FGF-Dependent Lung Tumors. *J. Med. Chem.* **2016**, *59*, 4651–4663. [[CrossRef](#)]
21. Ronca, R.; Giacomini, A.; Di Salle, E.; Coltrini, D.; Pagano, K.; Ragona, L.; Matarazzo, S.; Rezzola, S.; Maiolo, D.; Torrella, R.; et al. Long-Pentraxin 3 Derivative as a Small-Molecule FGF Trap for Cancer Therapy. *Cancer Cell* **2015**, *28*, 225–239. [[CrossRef](#)] [[PubMed](#)]
22. Bono, F.; De Smet, F.; Herbert, C.; De Bock, K.; Georgiadou, M.; Fons, P.; Tjwa, M.; Alcouffe, C.; Ny, A.; Bianciotto, M.; et al. Inhibition of tumor angiogenesis and growth by a small-molecule multi-FGF receptor blocker with allosteric properties. *Cancer Cell* **2013**, *23*, 477–488. [[CrossRef](#)] [[PubMed](#)]
23. Robertson, A.G.; Shih, J.; Yau, C.; Gibb, E.A.; Oba, J.; Mungall, K.L.; Hess, J.M.; Uzunangelov, V.; Walter, V.; Danilova, L.; et al. Integrative Analysis Identifies Four Molecular and Clinical Subsets in Uveal Melanoma. *Cancer Cell* **2017**, *32*, 204–220 e215. [[CrossRef](#)] [[PubMed](#)]

24. Farquhar, N.; Thomson, S.; Coupland, S.E.; Coulson, J.M.; Sacco, J.J.; Krishna, Y.; Heimann, H.; Taktak, A.; Cebulla, C.M.; Abdel-Rahman, M.H.; et al. Patterns of BAP1 protein expression provide insights into prognostic significance and the biology of uveal melanoma. *J. Path. Clin. Res.* **2018**, *4*, 26–38. [[CrossRef](#)] [[PubMed](#)]
25. Diaz, C.E.; Rusciano, D.; Dithmar, S.; Grossniklaus, H.E. B16LS9 melanoma cells spread to the liver from the murine ocular posterior compartment (PC). *Curr. Eye Res.* **1999**, *18*, 125–129. [[CrossRef](#)] [[PubMed](#)]
26. Rusciano, D.; Lorenzoni, P.; Burger, M.M. Regulation of c-met expression in B16 murine melanoma cells by melanocyte stimulating hormone. *J. Cell Sci.* **1999**, *112*, 623–630. [[PubMed](#)]
27. Elia, G.; Ren, Y.; Lorenzoni, P.; Zarnegar, R.; Burger, M.M.; Rusciano, D. Mechanisms regulating c-met overexpression in liver-metastatic B16-LS9 melanoma cells. *J. Cell Biochem.* **2001**, *81*, 477–487. [[CrossRef](#)]
28. Jones, N.M.; Yang, H.; Zhang, Q.; Morales-Tirado, V.M.; Grossniklaus, H.E. Natural killer cells and pigment epithelial-derived factor control the infiltrative and nodular growth of hepatic metastases in an Orthotopic murine model of ocular melanoma. *BMC Cancer* **2019**, *19*, 484. [[CrossRef](#)]
29. Yang, W.; Li, H.; Mayhew, E.; Mellon, J.; Chen, P.W.; Niederkorn, J.Y. NKT cell exacerbation of liver metastases arising from melanomas transplanted into either the eyes or spleens of mice. *Invest. Ophthalmol. Vis. Sci.* **2011**, *52*, 3094–3102. [[CrossRef](#)]
30. Yang, H.; Brackett, C.M.; Morales-Tirado, V.M.; Li, Z.; Zhang, Q.; Wilson, M.W.; Benjamin, C.; Harris, W.; Waller, E.K.; Gudkov, A.V.; et al. The Toll-like receptor 5 agonist entolimod suppresses hepatic metastases in a murine model of ocular melanoma via an NK cell-dependent mechanism. *Oncotarget* **2016**, *7*, 2936–2950. [[CrossRef](#)]
31. Ashur-Fabian, O.; Zloto, O.; Fabian, I.; Tsarfaty, G.; Ellis, M.; Steinberg, D.M.; Hercbergs, A.; Davis, P.J.; Fabian, I.D. Tetrac Delayed the Onset of Ocular Melanoma in an Orthotopic Mouse Model. *Front. Endocrinol.* **2018**, *9*, 775. [[CrossRef](#)] [[PubMed](#)]
32. Tobia, C.; Gariano, G.; De Sena, G.; Presta, M. Zebrafish embryo as a tool to study tumor/endothelial cell cross-talk. *Biochim. Biophys. Acta* **2013**, *1832*, 1371–1377. [[CrossRef](#)] [[PubMed](#)]
33. Jager, M.J.; Magner, J.A.; Ksander, B.R.; Dubovy, S.R. Uveal Melanoma Cell Lines: Where do they come from? (An American Ophthalmological Society Thesis). *Trans. Am. Ophthalmol. Soc.* **2016**, *114*, T5. [[PubMed](#)]
34. Gilbert, J.A. BGJ398 for FGFR-altered advanced cholangiocarcinoma. *Lancet Oncol.* **2018**, *19*, e16. [[CrossRef](#)]
35. Zheng, L.; Pan, J. The Anti-malarial Drug Artesunate Blocks Wnt/beta-catenin Pathway and Inhibits Growth, Migration and Invasion of Uveal Melanoma Cells. *Curr. Cancer Drug Targets* **2018**, *18*, 988–998. [[CrossRef](#)] [[PubMed](#)]
36. Zuidervaart, W.; Pavey, S.; van Nieuwpoort, F.A.; Packer, L.; Out, C.; Maat, W.; Jager, M.J.; Gruis, N.A.; Hayward, N.K. Expression of Wnt5a and its downstream effector beta-catenin in uveal melanoma. *Melanoma Res.* **2007**, *17*, 380–386. [[CrossRef](#)]
37. Chang, S.H.; Worley, L.A.; Onken, M.D.; Harbour, J.W. Prognostic biomarkers in uveal melanoma: evidence for a stem cell-like phenotype associated with metastasis. *Melanoma Res.* **2008**, *18*, 191–200. [[CrossRef](#)] [[PubMed](#)]
38. Stei, M.M.; Loeffler, K.U.; Holz, F.G.; Herwig, M.C. Animal Models of Uveal Melanoma: Methods, Applicability, and Limitations. *Biomed. Res. Int.* **2016**, *2016*, 4521807. [[CrossRef](#)]
39. Rodrigues, P.F.; Matarazzo, S.; Maccarinelli, F.; Foglio, E.; Giacomini, A.; Silva Nunes, J.P.; Presta, M.; Dias, A.A.M.; Ronca, R. Long Pentraxin 3-Mediated Fibroblast Growth Factor Trapping Impairs Fibrosarcoma Growth. *Front. Oncol.* **2018**, *8*, 472. [[CrossRef](#)]
40. Shain, A.H.; Bagger, M.M.; Yu, R.; Chang, D.; Liu, S.; Vemula, S.; Weier, J.F.; Wadt, K.; Heegaard, S.; Bastian, B.C.; et al. The genetic evolution of metastatic uveal melanoma. *Nat. Genet.* **2019**, *51*, 1123–1130. [[CrossRef](#)]
41. Helgadottir, H.; Hoiom, V. The genetics of uveal melanoma: current insights. *Appl. Clin. Genet.* **2016**, *9*, 147–155. [[PubMed](#)]
42. Krejci, P.; Aklia, A.; Kaucka, M.; Sevcikova, E.; Prochazkova, J.; Masek, J.K.; Mikolka, P.; Pospisilova, T.; Spoustova, T.; Weis, M.; et al. Receptor tyrosine kinases activate canonical WNT/beta-catenin signaling via MAP kinase/LRP6 pathway and direct beta-catenin phosphorylation. *PLOS One* **2012**, *7*, e35826. [[CrossRef](#)] [[PubMed](#)]



43. Buchtova, M.; Oralova, V.; Aklian, A.; Masek, J.; Vesela, I.; Ouyang, Z.; Obadalova, T.; Konecna, Z.; Spoustova, T.; Pospisilova, T.; et al. Fibroblast growth factor and canonical WNT/beta-catenin signaling cooperate in suppression of chondrocyte differentiation in experimental models of FGFR signaling in cartilage. *Biochim. Biophys. Acta* **2015**, *1852*, 839–850. [[CrossRef](#)] [[PubMed](#)]
44. Chua, V.; Orloff, M.; Teh, J.L.; Sugase, T.; Liao, C.; Purwin, T.J.; Lam, B.Q.; Terai, M.; Ambrosini, G.; Carvajal, R.D.; et al. Stromal fibroblast growth factor 2 reduces the efficacy of bromodomain inhibitors in uveal melanoma. *EMBO Mol. Med.* **2019**, *11*, e9081. [[CrossRef](#)] [[PubMed](#)]
45. De Waard-Siebinga, I.; Blom, D.J.; Griffioen, M.; Schrier, P.I.; Hoogendoorn, E.; Beverstock, G.; Danen, E.H.; Jager, M.J. Establishment and characterization of an uveal-melanoma cell line. *Int. J. Cancer* **1995**, *62*, 155–161. [[CrossRef](#)]
46. Verbik, D.J.; Murray, T.G.; Tran, J.M.; Ksander, B.R. Melanomas that develop within the eye inhibit lymphocyte proliferation. *Int. J. Cancer* **1997**, *73*, 470–478. [[CrossRef](#)]
47. Chen, P.W.; Murray, T.G.; Uno, T.; Salgaller, M.L.; Reddy, R.; Ksander, B.R. Expression of MAGE genes in ocular melanoma during progression from primary to metastatic disease. *Clin. Exp. Metastasis* **1997**, *15*, 509–518. [[CrossRef](#)]
48. Rezzola, S.; Corsini, M.; Chioldelli, P.; Cancarini, A.; Nawaz, I.M.; Coltrini, D.; Mitola, S.; Ronca, R.; Belleri, M.; Lista, L.; et al. Inflammation and N-formyl peptide receptors mediate the angiogenic activity of human vitreous humour in proliferative diabetic retinopathy. *Diabetologia* **2017**, *60*, 719–728. [[CrossRef](#)]



© 2019 by the authors. Licensee MDPI, Basel, Switzerland. This article is an open access article distributed under the terms and conditions of the Creative Commons Attribution (CC BY) license (<http://creativecommons.org/licenses/by/4.0/>).

---

## RESULTS

During my PhD program, my research activity has been focused on investigating the role of the FGF/FGFR system in the maintenance of CSCs in UM.

The results obtained have been included in the following published paper:

### **FGF-trapping hampers cancer stem-like cells in uveal melanoma**

**A. Loda**, S. Calza, A. Giacomini, C. Ravelli, AM. Krishna Chandran, C. Tobia, G. Tabellini, S. Parolini, F. Semeraro, R. Ronca, S. Rezzola.

Cancer Cell Int. 2023 May 11;23(1):89. doi: 10.1186/s12935-023-02903-z. PMID: 37165394; PMCID: PMC10173517.

Additionally, I was involved in the establishment of a novel orthotopic model of UM in zebrafish, as a tool for drug discovery and screening.

### **An Orthotopic Model of Uveal Melanoma in Zebrafish Embryo: A Novel Platform for Drug Evaluation**

C. Tobia, D. Coltrini, R. Ronca, **A. Loda**, J. Guerra, E. Scalvini, F. Semeraro, S. Rezzola.

Biomedicines. 2021 Dec 10;9(12):1873. doi: 10.3390/biomedicines9121873. PMID: 34944689; PMCID: PMC8698893.

Finally, I've started investigating the mechanisms by which UM impairs the anti-tumor activity of Natural Killer (NK) lymphocytes as a strategy of immune escape. Here, I will show our preliminary results:

### **Uveal Melanoma Cells Impair the Anti-tumor Activity of Natural Killer Lymphocytes**

**A. Loda**, G. Mutti, M. Rossignoli, F. Semeraro, G. Tabellini, S. Parolini, S. Rezzola.

*Unpublished results.*



## **FGF-Trapping Hampers Cancer Stem-Like Cells in Uveal Melanoma**

**A. Loda**, S. Calza, A. Giacomini, C. Ravelli, AM. Krishna Chandran, C. Tobia, G. Tabellini, S. Parolini, F. Semeraro, R. Ronca, S. Rezzola.

Cancer Cell Int. 2023 May 11;23(1):89. doi: 10.1186/s12935-023-02903-z. PMID: 37165394; PMCID: PMC10173517.



## RESEARCH

## Open Access

# FGF-trapping hampers cancer stem-like cells in uveal melanoma



Alessandra Loda<sup>1</sup>, Stefano Calza<sup>1</sup>, Arianna Giacomini<sup>1</sup>, Cosetta Ravelli<sup>1</sup>, Adwaid Manu Krishna Chandran<sup>1</sup>, Chiara Tobia<sup>1</sup>, Giovanna Tabellini<sup>1</sup>, Silvia Parolini<sup>1</sup>, Francesco Semeraro<sup>2</sup>, Roberto Ronca<sup>1\*</sup> and Sara Rezzola<sup>1\*</sup>

## Abstract

**Background** Cancer stem-like cells (CSCs) are a subpopulation of tumor cells responsible for tumor initiation, metastasis, chemoresistance, and relapse. Recently, CSCs have been identified in Uveal Melanoma (UM), which represents the most common primary tumor of the eye. UM is highly resistant to systemic chemotherapy and effective therapies aimed at improving overall survival of patients are eagerly required.

**Methods** Herein, taking advantage from a pan Fibroblast Growth Factor (FGF)-trap molecule, we singled out and analyzed a UM-CSC subset with marked stem-like properties. A hierarchical clustering of gene expression data publicly available on The Cancer Genome Atlas (TCGA) was performed to identify patients' clusters.

**Results** By disrupting the FGF/FGF receptor (FGFR)-mediated signaling, we unmasked an FGF-sensitive UM population characterized by increased expression of numerous stemness-related transcription factors, enhanced aldehyde dehydrogenase (ALDH) activity, and tumor-sphere formation capacity. Moreover, FGF inhibition deeply affected UM-CSC survival *in vivo* in a chorioallantoic membrane (CAM) tumor graft assay, resulting in the reduction of tumor growth. At clinical level, hierarchical clustering of TCGA gene expression data revealed a strong correlation between FGFs/FGFRs and stemness-related genes, allowing the identification of three distinct clusters characterized by different clinical outcomes.

**Conclusions** Our findings support the evidence that the FGF/FGFR axis represents a master regulator of cancer stemness in primary UM tumors and point to anti-FGF treatments as a novel therapeutic strategy to hit the CSC component in UM.

## Highlights

- Overexpression of FGFs/FGFRs correlates with stemness and fate in UM patients
- Blockade of FGFs unmasks an FGF-sensitive UM population with marked stem-like properties
- FGF trapping inhibits the growth of UM by targeting cancer stem cells

**Keywords** Uveal melanoma, Cancer stem-like cells, FGF, FGF inhibitor

\*Correspondence:

Roberto Ronca  
roberto.ronca@unibs.it  
Sara Rezzola  
sara.rezzola@unibs.it

Full list of author information is available at the end of the article



© The Author(s) 2023. **Open Access** This article is licensed under a Creative Commons Attribution 4.0 International License, which permits use, sharing, adaptation, distribution and reproduction in any medium or format, as long as you give appropriate credit to the original author(s) and the source, provide a link to the Creative Commons licence, and indicate if changes were made. The images or other third party material in this article are included in the article's Creative Commons licence, unless indicated otherwise in a credit line to the material. If material is not included in the article's Creative Commons licence and your intended use is not permitted by statutory regulation or exceeds the permitted use, you will need to obtain permission directly from the copyright holder. To view a copy of this licence, visit <http://creativecommons.org/licenses/by/4.0/>. The Creative Commons Public Domain Dedication waiver (<http://creativecommons.org/publicdomain/zero/1.0/>) applies to the data made available in this article, unless otherwise stated in a credit line to the data.

## Background

Uveal melanoma (UM) is the most common primary intraocular malignancy, arising from melanocytes located in the uveal tract of the eye [1]. Incidence of UM in Europe ranges from 2 to 8 per million and its occurrence increases with age [2]. Commonly, primary tumors are successfully treated with brachytherapy and phototherapy, while enucleation remains an appropriate procedure in the presence of large tumors with extensive extraocular growth [3]. However, despite effective control of localized tumors, UM is very aggressive, and it tends to spread via hematological dissemination [4]; more than 50% of patients develop metastasis, most frequently to the liver, with median survival after diagnosis ranging from 3 to 12 months [4, 5]. UM is highly resistant to systemic chemotherapy and no standard of care has been approved for treatment of metastatic disease [2, 6, 7]. Moreover, the low mutational burden of UM, the immunoprivileged site of the eye, as well as the immunosuppressive environment of the liver hamper the efficacy of novel approaches based on immunotherapy [8, 9]. Therefore, effective therapies aimed to improve overall survival of patients are currently lacking [8, 10]. In this context, experimental models of UM represent a useful tool for the identification of new potential drugs [11].

Fibroblast growth factors (FGFs) are involved in several physiological processes such as embryogenesis, angiogenesis, tissue homeostasis, and wound repair, by acting as paracrine, autocrine, or endocrine factors which activate tyrosine-kinase FGF receptors (FGFRs) [12, 13]. The aberrant activation of the FGF/FGFR system is frequently observed in human cancers, affecting cell proliferation, differentiation, migration, and survival [13]. The constitutive activation of the FGF/FGFR system has been described in UM, where the overexpression of the ligands and/or receptors promotes an autologous loop of stimulation which sustains UM progression [14–17]. Recently, we have identified the novel small molecule NSC12 as a pan-FGF-trap able to bind to FGFs and prevent FGFR activation. By disrupting FGF/FGFR-mediated signaling, NSC12 has been shown to hamper tumor growth in several FGF-dependent murine and human cancer models, including UM [18–21]. Indeed, primary and metastatic UM cell lines showed impaired cell migration, proliferation, and survival after treatment with NSC12 [21].

Cancer Stem-like Cells (CSCs) represent a subpopulation of cells responsible for tumor initiation, growth, and metastasis [22–24]. Moreover, CSCs are resistant to both chemotherapy and radiotherapy due to several mechanisms, including their lower proliferation rate, the activation of the DNA repair machinery, and the expression of transporters and enzymes that internalize and inactivate drugs [25, 26]. The presence of CSCs has been reported

in various tumor types, such as cutaneous melanoma, breast, lung, liver, stomach, and bladder cancers [22]. In this context, FGFs reportedly contribute to pluripotency maintenance and self-renewal of stem cells both in normal tissues and in several tumor types [27–31]. Markers of CSCs vary according to the type of cancers, and may include transcriptional factors (e.g. NANOG, OCT4, SOX2), as well as surface proteins such as CD44, CD133, and CD47 [32, 33]. At present, due to their role in promoting tumor heterogeneity, resistance to therapies and recurrence, targeting CSCs with new therapeutic approaches represents a first line challenge to obtain complete tumor eradication [34].

Recently, CSCs have also been identified in UM as a subgroup of cells characterized by increased motility, self-renewal, and chemoresistance [35–37]. Given the absence of reliable surface markers for CSCs in UM [38], current studies assessed their presence by evaluating stem-like properties such as formation of melanospheres and enhanced activity of aldehyde dehydrogenase (ALDH) enzymes [37, 39–42].

In this paper, we demonstrate that sequestration of FGFs by NSC12 hits and unmasks an FGF-sensitive UM population with marked stem-like properties. By targeting the UM-CSC subpopulation, blockade of FGFs results in the inhibition of UM growth both *in vitro* and in the chick embryo chorioallantoic membrane (CAM) *in vivo* model. Moreover, we show that FGF/FGFR expression and stemness are strictly linked in UM patients and are associated with poorer prognosis. Altogether, these findings indicate that the FGF system plays a pivotal role in UM-CSC biology and may be exploited to develop novel anti-CSC strategies for UM.

## Methods

### Reagents

RPMI 1640 medium, fetal bovine serum (FBS), and SYBR Green PCR master mix were from GIBCO Life Technologies (Grand Island, NY, USA). Penicillin, streptomycin, Triton-X100, Brij, sodium orthovanadate, protease inhibitor cocktail, bovine serum albumin (BSA), and 4',6-diamidino-2-phenylindole (DAPI) were from Sigma-Aldrich (St. Louis, MO, USA). Bradford reagent, enhanced chemiluminescence reagent, and iTaq Universal Syber Green Supermix were from Bio-Rad Laboratories (Hercules, CA, USA). TRIZOL Reagent, Moloney murine leukemia virus (MMLV) reverse transcriptase, and MitoSox Red Mitochondrial Superoxide Indicator were from Invitrogen (Carlsbad, CA, USA). 2X XtraRTL Master Mix was from GeneSpin (Milan, Italy). ALDEFLUOR kit was from Stemcell Technologies (Vancouver, Canada). Human Phospho-Kinase Array Kit was from R&D Systems (Minneapolis, Canada).

Anti-phospho-pan-FGFR (Tyr653/Tyr654), anti-Nanog, and anti-phospho-paxillin (Tyr118) antibodies were from Cell Signaling Technology (Beverly, MA, USA). Anti-GAPDH and anti-FGFR1 (C-15) antibodies were from Santa Cruz (Santa Cruz, CA, USA). Chicken anti-rabbit Alexa Fluor 488 and phalloidin-Alexa Fluor 594 antibodies were from Molecular Probes (Eugene, OR, USA). Recombinant FGF2 was purchased from TecnoGen (Caserta, Italy). NSC12 was kindly provided by Dr. M. Mor (University of Parma, Italy).

#### Cell cultures

Human UM cell lines 92.1, Mel285, and Mel270 were obtained from M. Jager (Leiden University, The Netherlands) and cultured in RPMI 1640 medium supplemented with 100 U/mL penicillin, 100 µg/ml streptomycin, and 10% FBS or 20% FBS for 92.1 and Mel285 or Mel270 UM cells, respectively [43–45].

When required, 92.1 and Mel270 cells were seeded at 13,000 cells/cm<sup>2</sup> in complete medium and then starved in RPMI plus 1% FBS. After 24 h, cells were treated with 15 µM NSC12. NSC12<sup>sens</sup> population was identified as the fraction that detached from the substratum after either 2 h or 3 h of treatment for 92.1 and Mel270 cells, respectively, whereas NSC12<sup>res</sup> population remained adherent to the cell culture plastic.

#### Western blot analysis

NSC12<sup>sens</sup> and NSC12<sup>res</sup> cells were harvested, and samples were homogenized in RIPA buffer containing 1% Triton-X100, 0.2% Brij, 1 mM sodium orthovanadate, and protease inhibitor cocktail. Total lysates (50 µg) cells were separated by SDS-PAGE and probed with specific antibodies. Western blot analysis was performed using rabbit anti-pan-phospho-FGFRs, rabbit anti-FGFR1, rabbit anti-Nanog and rabbit anti-phospho-Paxillin antibodies and normalized using mouse anti-GAPDH antibody. Primary antibodies were diluted 1:1000, while secondary antibodies were diluted 1:5000 in blocking solution (TBS 1% Tween 20 supplemented with 1% BSA). Chemiluminescent signal was acquired by ChemiDoc™ Imaging System (Bio-Rad) and quantified by Fiji software [46].

#### Human phospho-protein proteome profiler array

NSC12<sup>sens</sup> and NSC12<sup>res</sup> 92.1 cell lysates were analyzed to assess the phosphorylation levels of several intracellular proteins using the proteome profiler array Human Phospho-Kinase Array Kit (R&D Systems, Minneapolis, Canada). 500 µg of total lysates of NSC12<sup>sens</sup> and NSC12<sup>res</sup> 92.1 cells were incubated with the array according to manufacturer's instructions. Pixel densities were analyzed using the image analysis Fiji software and normalized on reference spots.

#### Immunofluorescence analysis

92.1 and Mel270 cells were seeded 15,000 cells/cm<sup>2</sup> in RPMI 10% or 20% FBS, respectively. After 24 h, cells were treated with 15 µM NSC12 for 1 h, 2 h, or 3 h in RPMI 1% FBS. Then, cells were washed, fixed with 4% paraformaldehyde and permeabilized using PBS 0.2% Triton-X100. Blocking was performed using PBS 0.1% Tween20 supplemented with 1% bovine serum albumin (blocking solution). Primary rabbit anti-phospho-paxillin antibody was diluted 1:100 in blocking solution and cells were incubated for 1 h at room temperature. Then, cells were incubated for 1 more h at room temperature with anti-rabbit secondary antibody (diluted 1:250 in blocking solution) along with phalloidin-Alexa Fluor 594 (diluted 1:150 in blocking solution). Lastly, nuclei were counterstained with DAPI diluted 1:15000 in PBS. Cells were photographed using an Axiovert 200 M epifluorescence microscope equipped with Apotome and a Plan-Apochromat×63/1.4 NA oil objective (Zeiss). Image analysis was performed using Fiji software.

#### Semi-quantitative PCR analysis

Control, NSC12<sup>sens</sup> and NSC12<sup>res</sup> cells were harvested, and total RNA was extracted using Trizol Reagent. Contaminating DNA was eliminated using DNase before performing retrotranscription. For each sample, 2 µg of RNA were retrotranscribed using MMLV reverse transcriptase. cDNA was then amplified using the oligonucleotide primers listed in Additional file 1: Table SI. The PCR products were electrophoresed on a 2.5% agarose gel.

#### Quantitative real-time PCR (qPCR) analysis

NSC12<sup>sens</sup> and NSC12<sup>res</sup> cells were harvested, and total RNA was extracted and retrotranscribed. cDNA was analyzed using the iTaq Universal Syber Green Supermix with the ViiA7 Real-Time PCR System. Samples were analyzed in triplicate using the oligonucleotide primers reported in Additional file 1: Table SII.

#### Cytofluorimetric analysis

Control, NSC12<sup>sens</sup> and NSC12<sup>res</sup> cells were harvested and analyzed by cytofluorimetry. Mitochondrial reactive oxygen species (mtROS) production was determined using the fluorescent probe MitoSox; apoptotic cell death was evaluated by double staining with Annexin-V/Propidium Iodide; ALDH activity was assessed using ALDEFUOR kit. Staining for NANOG was performed with anti-NANOG antibody conjugated with Alexa Fluor 647. Each assay was performed according to the manufacturer's instructions. Cytofluorimetric analyses were performed using the



MACSQuant<sup>®</sup> Analyzer (Miltenyi Biotec, Bergisch Gladbach, Germany).

#### Tumor-sphere assay

92.1, Mel270, and Mel285 cells were pre-treated with increasing doses of NSC12 for 24 h. Then, 3000 viable cells were seeded on low-adhesion plates (Corning) in DMEM/F12 medium supplemented with 100 U/mL penicillin, 100 µg/ml streptomycin, 10 ng/ml FGF2, 20 ng/ml EGF, and B-27 supplement (diluted 1:50). After 7 days, spheres were counted.

#### Chick embryo chorioallantoic membrane (CAM) assay

Fertilized white Leghorn eggs were incubated at 37 °C in a humidified incubator. At 4 days post-incubation, the shells were covered with a transparent adhesive tape and a small window cut with scissors; windows were then resealed with tape. At 7 days post-incubation, 92.1 cell were engrafted on the CAM at a concentration of 100,000 cells/µl in 1:1 Matrigel/PBS (*vol: vol*). NSC12 was added into the cell suspension directly before engraftment (4 pmol/embryo). At 14 days post-incubation tumors were photographed and then explanted. Tumor volume was calculated using the following formula:  $V = (D \times d^2)/2$ , where D and d are the major and minor perpendicular tumor diameters, respectively [47]. RNA was extracted from the grafts and gene expression was analyzed by Real Time PCR.

#### Statistical analyses

Independent groups were compared using one-way analysis of variance followed by pairwise comparisons with Tukey HSD *p*-value adjustment.

Data were clustered using hierarchical clustering with Euclidean distance metric and Ward's agglomerative clustering method [48]. Best number of clusters was determined using the consensus approach provided by the NbClust package [49], *i.e.* as the optimal number of clusters most commonly selected out of 30 different indices. Geneset (FGFs, FGFRs, Stemness) overall expression was computed using single-sample gene set enrichment analysis as provided by gene set variation analysis algorithm [50]. Briefly, the overall expression of a collection of genes (geneset) is computed using a non-parametric model that map from a multiple expression space (gene expression values) to a single cumulative expression value for the gene set. Survival curves relative to patients Disease-Free Survival (DFS) were plotted using Kaplan-Meier estimator and *p*-value computed using a log-rank test.

All tests were two-sided and assumed a 5% significance level. All statistical analyses were performed with GraphPad Prism 9 (San Diego, CA, USA) and R (version 4.0.2).

## Results

### FGF-trapping identifies a subpopulation of UM cells highly dependent on FGF signaling

Previous observations had shown that the pan-FGF trap NSC12 inhibits FGFR activation and its downstream signaling both in primary and metastatic human UM cell lines. Additionally, NSC12 promotes the activation of the pro-apoptotic proteins PARP and caspase-3, thus leading to UM cell death [21]. Here, human 92.1 and Mel270 UM cells were seeded at subconfluent density and allowed to adhere to the tissue culture plastic. Then, cells were treated with NSC12 and their behavior was followed thereafter. As shown in Fig. 1A, during the first few hours of treatment (*i.e.* 2 and 3 h for 92.1 and Mel270 UM cells, respectively) a small percentage of cells ( $\approx$  20% of the total) detached from the tissue culture plastic. Notably, the detachment phenotype was rescued by the addition of a 1:1 molar concentration ratio of FGF2 (Additional file 1: Fig. S1). In addition, treatment with NSC12 induced morphological modifications of the cytoskeleton, with alterations of actin organization and significant dephosphorylation of paxillin at focal adhesions (Fig. 1B–D and Additional file 1: Fig. S2). This approach allowed to identify and isolate a cell population adherent to the substratum and resistant to FGF deprivation (NSC12<sup>res</sup>) and a non-adherent cell population sensitive to the treatment with the anti-FGF drug (NSC12<sup>sens</sup>). Of note, the evaluation of the apoptotic rate of NSC12<sup>res</sup>/NSC12<sup>sens</sup> populations confirmed their viability in both UM cell lines, even though 35% of Mel270\_NSC12<sup>sens</sup> cells showed sign of early apoptosis with positive staining for Annexin-V (Fig. 1E, F).

UM primary tumors express several FGFs and FGFRs [21]. To assess if the higher sensitivity of NSC12<sup>sens</sup> cells to FGF deprivation was due to different FGF/FGFR expression levels, NSC12<sup>res</sup> and NSC12<sup>sens</sup> populations obtained from 92.1 and Mel270 cells were analyzed by semi-quantitative PCR. As shown in Fig. 2A, both NSC12<sup>res</sup> and NSC12<sup>sens</sup> cells express similar levels of FGFs and FGFRs; moreover, treatment with NSC12 triggered a significant inhibition of FGFR phosphorylation in both populations (Fig. 2B).

To get further insights on the impact of FGF blockade in UM, we performed a Phospho-Kinase Antibody Array analysis of NSC12<sup>res</sup>/NSC12<sup>sens</sup> 92.1 cells. As shown in Fig. 2C, NSC12<sup>sens</sup> cells displayed decreased phosphorylation of various intracellular kinases when compared to NSC12<sup>res</sup> cells. NSC12<sup>sens</sup> population showed lower levels of phospho-FAK and a downregulation of p38 signaling pathway with decreased levels of phospho-p38 and its targets phospho-CREB and phospho-HSP27. In addition, when compared to NSC12<sup>res</sup> cells, JNK and ERK MAPK signaling pathways were turned off, as demonstrated by

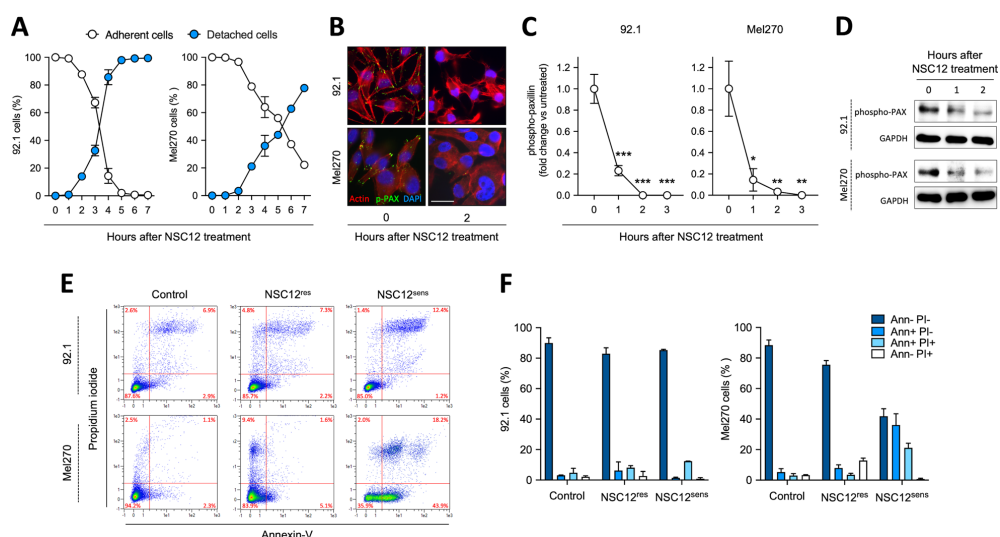


**Fig. 1** Treatment with NSC12 identifies an FGF-dependent subpopulation in UM cells. **A** 92.1 and Mel270 cells were treated with 15 μM NSC12 and its effect on cell adhesion was followed over time. Every hour adherent and non-adherent cells were collected and counted. **B** Immunofluorescence analysis of actin (red fluorescence) and phospho-paxillin (p-PAX, green fluorescence) expression in 92.1 (upper panels) or Mel270 (lower panels) cells treated or not with 15 μM NSC12 for 2 h. Nuclei were counterstained with DAPI (blue fluorescence). Scale bar = 30 μm. **C** Quantification of phospho-paxillin fluorescence signal was normalized to the number of nuclei. Data are the mean ± SEM of 10 fields (n = 70 cells). \**p* < 0.05, \*\**p* < 0.01, \*\*\**p* < 0.001 vs control, ANOVA. **D** Western blot analysis of phospho-PAX in control and NSC12-treated 92.1 (upper panels) and Mel270 (lower panels) cells. Data are representative of two independent experiments that gave similar results (see Additional file 1: Fig. S1). **E** 92.1 and Mel270 cells were treated or not with 15 μM NSC12 for 2 h (92.1) or 3 h (Mel270). Then, control, NSC12<sup>res</sup> and NSC12<sup>sens</sup> cells were harvested, and apoptosis was analyzed by cytofluorimetry. **F** Apoptosis quantification of propidium iodide (PI) and Annexin-V (Ann) positive cells by MACSQuant Software. Data are the mean ± SEM of three independent experiments

reduced phospho-JNK1/2/3, phospho-ERK1/2, phospho-RSK1/2/3, phospho-GSK-3α/β and phospho-p70 S6 kinase levels.

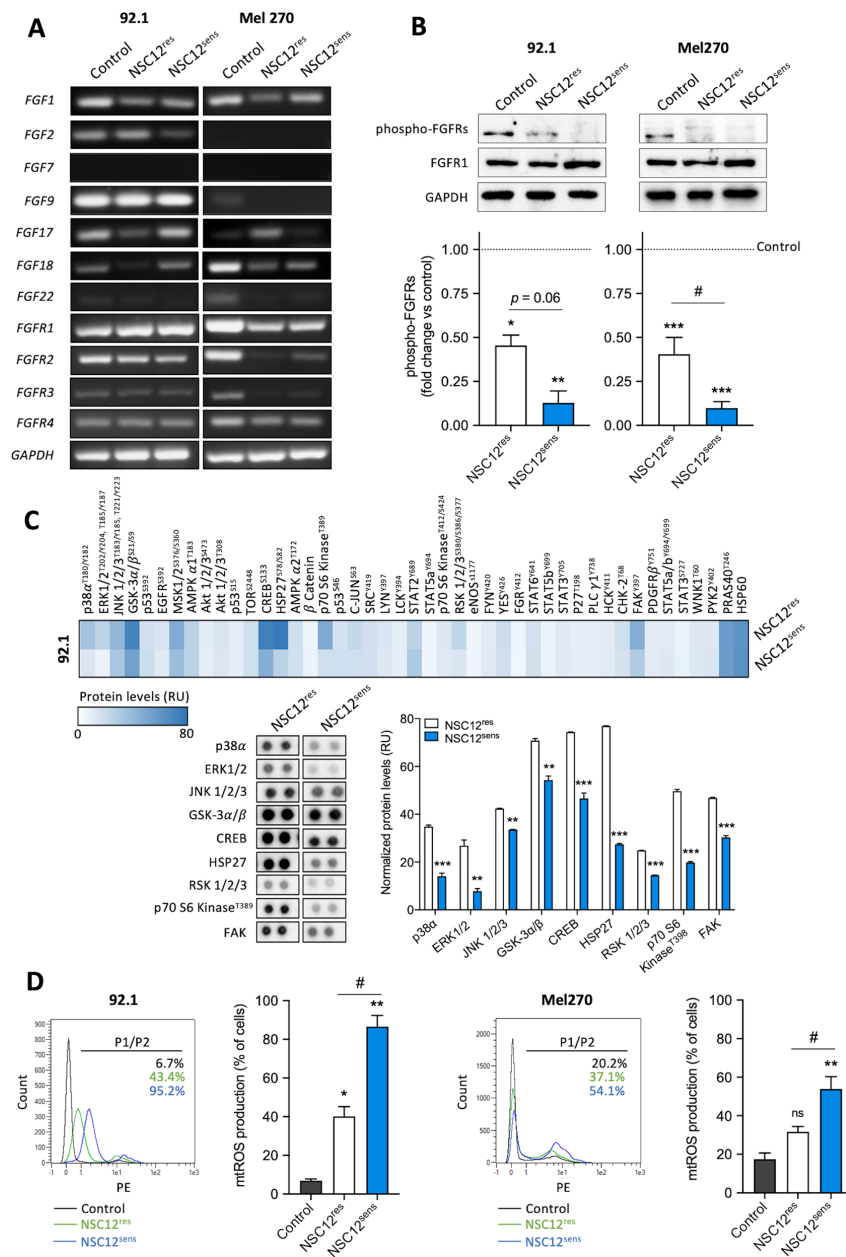
In keeping with previous observations on FGF/FGFR inhibition and intracellular oxidative stress induction [20, 51], NSC12<sup>sens</sup> cells showed an increased production of mtROS compared to untreated and NSC12<sup>res</sup>

cells, revealing a strong mitochondrial oxidative stress response in this cell population following treatment (Fig. 2D).

Together, these data demonstrate that in UM exists a subpopulation of cells that, in response to FGF-trapping, shows an earlier and stronger mitochondrial

(See figure on next page.)

**Fig. 2** Characterization of NSC12<sup>res</sup>/NSC12<sup>sens</sup> UM subpopulations. **A** Semi-quantitative PCR analysis of FGF and FGFR expression in control and NSC12<sup>res</sup>/NSC12<sup>sens</sup> subpopulations of 92.1 (left panels) and Mel270 (right panels) cells. **B** Western blot analysis of phospho-FGFRs and FGFR1 in control and NSC12<sup>res</sup>/NSC12<sup>sens</sup> subpopulations of 92.1 (left panels) and Mel270 (right panels) cells. The lower panels show the densitometric analysis of immunoreactive bands normalized to GAPDH protein levels. Data are the mean ± SEM of three independent experiments. \**p* < 0.05 and \*\**p* < 0.01 vs control; #*p* < 0.05 vs NSC12<sup>res</sup>, ANOVA. **C** Human Phospho-Kinase Antibody Array on 92.1\_NSC12<sup>res</sup> and 92.1\_NSC12<sup>sens</sup> total cell lysates. The heatmap shows the color-coded normalized protein levels of all detected phospho-proteins. The lower panels show the spots of p38α, ERK1/2, JNK1/2/3, GSK-3α/β, CREB, HSP27, RSK 1/2/3, p70 S6 Kinase and FAK and the corresponding densitometric analysis (relative units, RU). Data are the mean ± SEM of two technical replicates in one representative experiment out of three independent measurements that provided similar results. \*\**p* < 0.01 and \*\*\**p* < 0.001 vs NSC12<sup>res</sup>, Student's *t*-test. **D** The production of mtROS was assessed on control and NSC12<sup>res</sup>/NSC12<sup>sens</sup> subpopulations of 92.1 (left panels) and Mel270 (right panels) cells using the fluorescent probe MitoSox by cytofluorimetric analysis. In the plots the black line refers to the gate (P1/P2) setting the positive/negative cell populations. Data are the mean ± SEM of three independent experiments. \**p* < 0.05 and \*\**p* < 0.01 vs control; #*p* < 0.05 vs NSC12<sup>res</sup>, ANOVA



stress response as well as a down-modulation of several pro-survival mediators.

#### NSC12 inhibits UM growth UM growth in vitro and in vivo by targeting the UM-CSC subpopulation

A CSC subpopulation has been identified in UM cell lines based on the ability to form melanospheres and the activity of ALDH enzymes [37, 39–42]. By evaluating these properties, we identified a UM-CSC subpopulation, confirming the presence of CSCs in human 92.1, Mel270, and Mel285 UM cell lines (Additional file 1: Fig. S3). The FGF/FGFR system plays a pivotal role in stem cell maintenance [27–31]; given the presence of distinct subpopulations with different sensitivity to FGF deprivation, we investigated the effect of NSC12-mediated FGF blockade on the UM-CSC subset. As shown in Fig. 3A, B and Additional file 1: Fig. S4, treatment with increasing doses of NSC12 resulted in a significant reduction of the ALDH<sup>br</sup> population in 92.1, Mel270, and Mel285 UM cells. Similar results were obtained after treatment with the FGFR-selective tyrosine-kinase inhibitor BGJ398, thus confirming the FGF/FGFR-restricted specificity of this effect (Additional

file 1: Fig. S5). Interestingly, UM-ALDH<sup>br</sup> cells were resistant to the treatment with standard chemotherapy drug dacarbazine, in accordance with their stem-like traits (Additional file 1: Fig. S6). Additionally, in keeping with ALDH enzymatic activity data, pretreatment with NSC12 resulted in a dose-dependent decrease of the number of melanospheres (Fig. 3C, D), confirming that FGF signaling plays a key role in maintaining stem-like features of UM cells in vitro and that FGF sequestration pauperizes the CSC subpopulation in UM cells.

Based on these results and to further characterize the stem-like features of the NSC12<sup>sens</sup> population, we analyzed the expression levels of a panel of transcription factors known to be involved in stemness maintenance. To this purpose, NSC12<sup>res</sup> and NSC12<sup>sens</sup> cells obtained from 92.1 and Mel270 cells were evaluated by qPCR. As shown in Fig. 4A, when compared to NSC12<sup>res</sup> cells, the NSC12<sup>sens</sup> population expressed higher levels of several markers of stemness, including *SOX2*, *SLUG*, *TWIST*, *OCT4* and *NANOG*. Accordingly, Mel270\_NSC12<sup>sens</sup> cells expressed more Nanog when analyzed by Western blotting (Fig. 4B). In line with these results, cytofluorimetric analysis further confirmed that 92.1\_NSC12<sup>sens</sup>

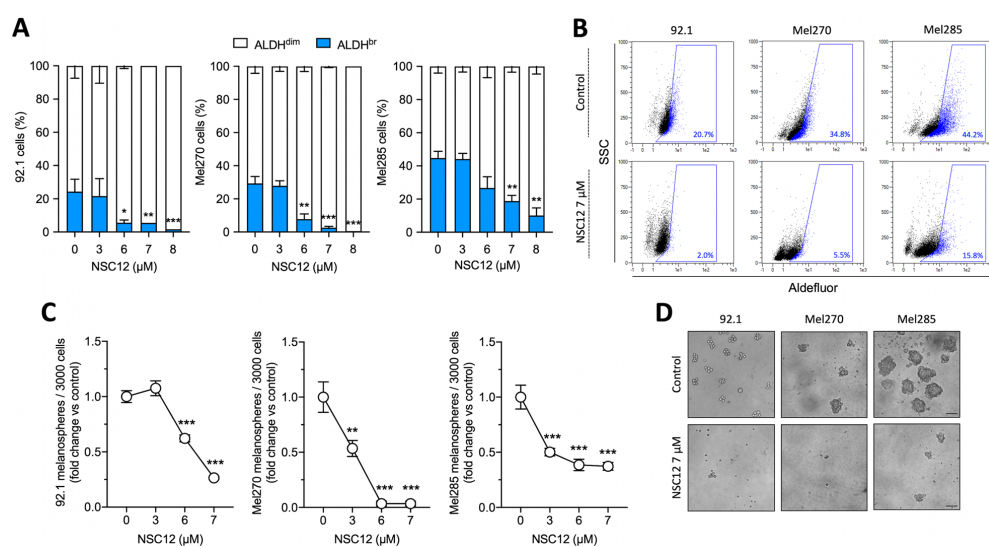


**Fig. 3** Treatment with NSC12 reduces the self-renewal potential of UM cells. **A** 92.1, Mel270 and Mel285 cells were treated with increasing doses of NSC12 for 24 h. Then, ALDH<sup>br</sup> cells were measured by cytofluorimetric analysis. Data are the mean  $\pm$  SEM of three independent experiments. \* $p < 0.05$ , \*\* $p < 0.01$ , \*\*\* $p < 0.001$  vs control, ANOVA. **B** Representative flow cytometry dot plots of control or 7  $\mu$ M NSC12 treated UM cells. The blue gate refers to the positive/negative cell populations as identified in the presence of DEAB inhibitor (see Additional file 1: Fig. S2). **C** 92.1, Mel270 and Mel285 cells were treated with increasing doses of NSC12 for 24 h. Then 3000 viable cells were resuspended in melanospheres culture medium and plated. After 7 days, melanospheres were counted and photographed. Data are the mean  $\pm$  SEM of three independent experiments. \*\* $p < 0.01$ , \*\*\* $p < 0.001$  vs control, ANOVA. **D** Representative images of melanospheres obtained from control or 7  $\mu$ M NSC12 pre-treated UM cells. Scale bar: 100  $\mu$ m

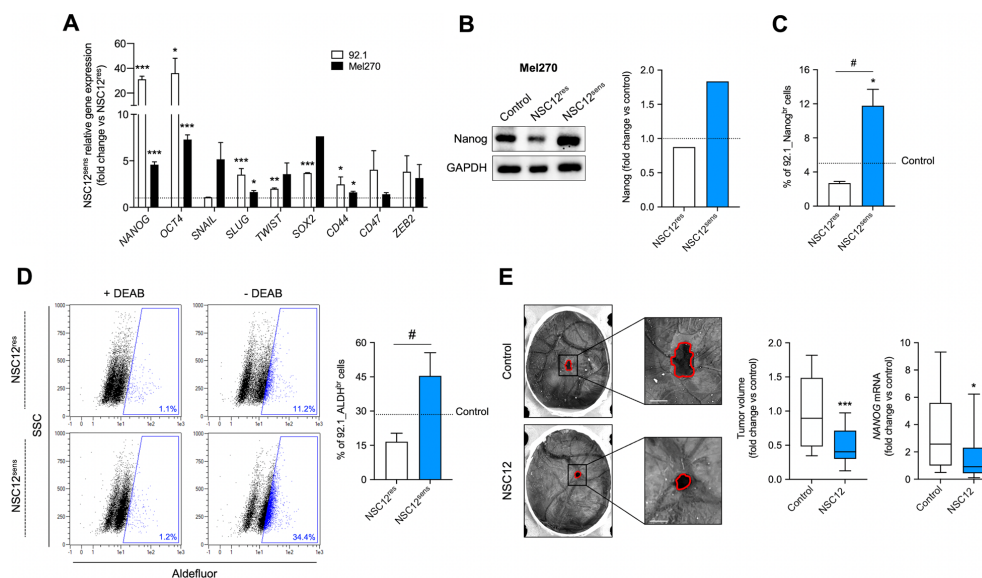


**Fig. 4** NSC12<sup>SENS</sup> cells are characterized by stem-like features. **A** qPCR analysis of *NANOG*, *OCT4*, *SNAIL*, *SLUG*, *TWIST*, *SOX2*, *CD44*, *CD47*, and *ZEB2* expression in NSC12<sup>RES</sup> and NSC12<sup>SENS</sup> subpopulations of 92.1 and Mel270 cells. Data are the mean  $\pm$  SEM of three independent experiments. \* $p < 0.05$ , \*\* $p < 0.01$ , \*\*\* $p < 0.001$  vs NSC12<sup>RES</sup>, Student's *t*-test. **B** Western blot analysis of Nanog in control and NSC12<sup>RES</sup>/NSC12<sup>SENS</sup> Mel270 cells. Right panel: densitometric analysis of immunoreactive bands normalized to GAPDH protein levels. **C** Nanog<sup>br</sup> cells were measured on control and NSC12<sup>RES</sup>/NSC12<sup>SENS</sup> 92.1 cells by cytofluorimetric analysis. Data are the mean  $\pm$  SEM of three independent experiments. \* $p < 0.05$  vs control; # $p < 0.05$  vs NSC12<sup>RES</sup>, ANOVA. **D** ALDH<sup>br</sup> cells were measured on control and NSC12<sup>RES</sup>/NSC12<sup>SENS</sup> 92.1 cells by cytofluorimetric analysis. Representative dot plots are reported in the left panel. Data are the mean  $\pm$  SEM of three independent experiments. \* $p < 0.05$  vs NSC12<sup>RES</sup>, Student's *t*-test. **E** 92.1 cells were engrafted onto the chick embryo CAM at day 7 post-incubation in the absence or in the presence of 4 pmol/embryo NSC12. Tumor growth was assessed after 7 days and qPCR analysis of *NANOG* was performed on the explants (right panels). In box and whisker graphs, boxes extend from the 25th to the 75th percentiles, lines indicate the median values, and whiskers indicate the range of values. Data are the mean  $\pm$  SEM of two independent experiments ( $n = 20$ ). \* $p < 0.05$ , \*\*\* $p < 0.001$  vs control, Student's *t*-test. Representative images of tumors are shown in the left panel. Scale bar: 2 mm

cells were enriched in Nanog<sup>br</sup> cells and were endowed with the highest ALDH enzymatic activity (Fig. 4C, D).

Finally, to evaluate whether NSC12 could affect the CSC population and impair tumor growth of UM cells in vivo, 92.1 cells were engrafted on the chick embryo CAM at day 7 post-incubation and treated with 4 pmol/embryo of NSC12. Tumor growth was assessed 7 days post-implantation and grafts were explanted and analyzed by qPCR. As shown in Fig. 4E, tumor mass was significantly reduced after treatment with NSC12 compared to controls. In addition, tumors treated with NSC12 were characterized by a strong downregulation of *NANOG* expression as evaluated by qPCR, thus confirming the reduction of the CSC component in the NSC12-treated group. Altogether, these data suggest that UM-CSCs strictly depend on FGF signaling and that FGF/FGFR axis inhibition may result in a strong effect on the UM-CSC compartment in vitro and in vivo.

#### Overexpression of FGFs/FGFRs correlates with stemness and fate in UM patients

The analysis of the publicly available mRNA profiling dataset of UM patients, collected in The Cancer Genome Atlas (TCGA), indicates that the upregulation of FGFs and FGFRs is associated with a poorer prognosis as well as with chromosome 3 monosomy and *BAP1* mutation, two distinct molecular signatures that identify specific subsets of UM patients [21]. As already reported for other types of tumors, the high frequency of metastatic spreading, tumor relapse and/or therapy failure in UM have been attributed to the presence of a CSC subpopulation [22–24]. Based on our experimental evidence, we performed data mining on TCGA UM Firehose Legacy dataset ([https://www.cbioportal.org/study/summary?id=uvm\\_tcga](https://www.cbioportal.org/study/summary?id=uvm_tcga)) to investigate the expression of FGF/FGFR family members and of transcription factors associated with stemness (*i.e.* *NANOG*, *OCT4*, *SNAIL*,

*SLUG*, *TWIST*, *SOX2*, *ZEB1*, and *ZEB2*) on a cohort of 80 primary human UM specimens. Hierarchical clustering of the gene expression data identified three distinct molecular clusters, hereinafter referred to as Cluster 1 (n=29), Cluster 2 (n=24) and Cluster 3 (n=27) associated with different levels of *FGFs*, *FGFRs* and stemness genes (Fig. 5A). In detail, Cluster 1 comprised patients characterized by the upregulation of both *FGFs* and *FGFRs* (including the downstream *FGFR*-mediator *FRS2*) and was associated with the highest levels of stemness-related transcription factors. Conversely, Cluster 2 was defined by intermediate levels of *FGFs* and of stemness genes, with low expression of *FGFRs*. Finally, Cluster 3 was characterized by high levels of *FGFRs* and lower expression of both ligands and stemness-associated transcription factors (Fig. 5B). Together, these data point to a tight relationship between activation of the *FGF/FGFR* system and UM stemness in clinical settings. Notably, these three clusters were associated with a distinct

Disease-Free Survival (DFS), with patients belonging to Cluster 1 showing the worst prognosis ( $p=0.0001$  vs Cluster 2 and Cluster 3) (Fig. 5C).

Altogether, these results indicate that *FGF/FGFR* expression and stemness are strictly linked in UM patients and their clustering identifies more aggressive tumors characterized by a poorer prognosis.

## Discussion

A major issue in the management of UM patients is represented by the ability of tumor cells to metastasize to distant organs. This event is the consequence, at least in part, of the presence of a UM-CSC subpopulation, characterized by the ability to initiate tumorigenesis and self-renewal. In the present study, we demonstrate that the UM-CSC subpopulation strongly depends on the *FGF/FGFR* signaling and that *FGF*-trapping represents a strategy to efficiently hamper the growth of UM cells in vitro and in vivo.

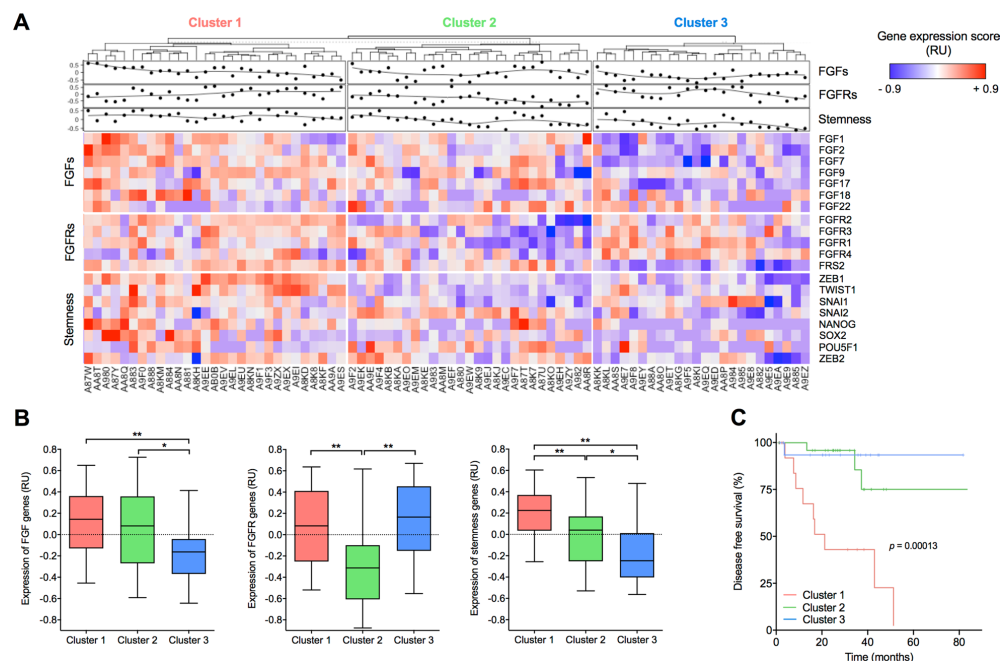


**Fig. 5** Hierarchical cluster analysis of gene expression data on TCGA UM Firehose Legacy Dataset. **A** Heatmap depicting the relative expression of the genes investigated on a cohort of 80 UM samples grouped by hierarchical cluster analysis. Each column represents one UM sample, and each row represents the indicated gene. The expression level of each gene in a single sample is depicted according to the color scale. **B** Fold change of the relative expression of *FGF*, *FGFR* and stemness genes in Cluster 1 (n=29), Cluster 2 (n=24), and Cluster 3 (n=27). In box and whisker graphs, boxes extend from the 25th to the 75th percentiles, lines indicate the median values, and whiskers indicate the range of values. \* $p < 0.05$ , \*\* $p < 0.01$ , ANOVA. **C** Kaplan–Meier curve displaying Disease-Free Survival (DFS) of patients belonging to Cluster 1, Cluster 2, or Cluster 3. Log-rank test  $p$ -value. Relative units, RU

A variety of FGFs and FGFRs are overexpressed by a significant subset of primary eye cancers, particularly in retinoblastoma and UM [17]. However, information about the pleiotropic roles played by FGF/FGFR in ocular tumors is limited. From the clinical point of view, high levels of FGF2 found in UM primary specimens and liver metastasis are associated with an increased invasiveness and a worst prognosis [16]. Accordingly, activation of FGF/FGFR system has been identified as responsible for the resistance to bromodomain and histone deacetylase inhibitors [52]. In this context, blocking FGFs or their receptors resulted in reduced cell proliferation and survival in *in vitro* UM experimental models [14, 21]. Here, we expand these observations by showing that the blockade of FGF/FGFR axis suppresses the activation of a variety of intracellular phospho-kinases, it induces a strong mitochondrial oxidative stress response, and it inhibits tumor growth in the *in vivo* CAM model of tumor graft.

The fact that FGFs play a crucial role for the maintenance of stem cells has been reported both in physiological tissues as well as in a variety of tumor types. Indeed, the FGF/FGFR system is important during embryo development and both ligands and receptors are expressed by human embryonic stem cells, where they regulate proliferation and self-renewal [27, 29, 53, 54]. On the other hand, the FGF/FGFR system has recently been associated with the regulation of stem-like properties in CSCs, the subpopulation of tumor cells responsible for tumor maintenance, metastatic dissemination, chemoresistance, and tumor relapse [22]. For example, the activation of FGF-mediated signaling has been linked to therapy resistance and enrichment in CSCs in an experimental model of hepatocarcinoma [55]. Similarly, it has been reported that the FGF/FGFR system enhanced stemness by increasing stability and nuclear localization of SOX2 in pancreatic cancer [28], promoted the reversion of tumor cells to an undifferentiated, stem-like state in glioblastoma [56], and regulated CSCs through ERK signaling in a model of esophageal squamous cell carcinoma [57]. In this manuscript, we show that UM cells are a heterogeneous population which comprises stem-like cells, and we provide, for the first time, the rationale to select and target this cell population, by exploiting its higher sensitivity to the inhibition of FGF/FGFR system. Indeed, UM cells with a higher sensitivity to the FGF-trap NSC12 display several stem-like properties, such as increased expression of numerous stemness-related transcription factors, enhanced ALDH activity, and tumor-sphere formation capacity. Interestingly, *in vivo* “targeting” of this cell population results in the loss of the CSC subset, as well as in a reduction of tumor growth in the CAM model. These results are propaedeutic and set the basis for further investigation in more complex models. In

addition, the analysis of UM patients’ database revealed that this strong association exists also at clinical level. In fact, the robust correlation between FGFs/FGFRs and stemness-related genes proves that the FGF/FGFR system represents a master regulator of cancer stemness also in primary UM tumors. Notably, the clinical outcome of these patients clearly shows that high expression of both ligands and receptors, as well as stemness-related transcription factors, is prognostic for a worse disease-free survival.

Recent experimental studies have demonstrated that UM-CSC eradication obviates to hepatic metastasization, thus pointing to UM-CSC as a potential therapeutic target [52]. Currently, several FGF/FGFR inhibitors are being evaluated in clinical trials for their efficacy on FGF-dependent tumors; however, their application is limited to tumors where the activity of the FGF/FGFR system is well described as a driver in tumor sustenance.

Based on our results, the clinical use of FGF/FGFR inhibitors, such as NSC12 or other FDA approved FGFRi, might be taken into consideration given their ability to target CSCs, which are known to be intrinsically resistant to conventional chemotherapy. Despite the necessity to perform additional studies, the possibility to exploit FGF/FGFR blockade in combination with other conventional/chemotherapy approaches should be assessed as a strategy to overcome drug resistance and recurrence in UM.

## Conclusions

In this paper, we demonstrated that sequestration of FGFs hits and unmasks a UM population with CSC properties. By targeting the UM-CSC subpopulation, blockade of FGFs inhibits UM growth both *in vitro* and *in vivo*. Moreover, we showed that FGF/FGF receptor expression and stemness are strictly linked in UM patients and are associated with poorer prognosis tumors. Altogether, these findings indicate that the FGF system plays a pivotal role in UM-CSC biology and may be exploited to develop novel anti-CSC strategies for UM.

## Supplementary Information

The online version contains supplementary material available at <https://doi.org/10.1186/s12935-023-02903-z>.

**Additional file 1: Fig S1.** Effect of FGF2 on the detachment phenotype induced by NSC12 on UM cells. 92.1 and Mel270 UM cells were treated with 15  $\mu$ M NSC12 in the absence or in the presence of a 1:1 molar concentration ratio of FGF2. After 3 h, detached cells were collected and counted. **Fig S2.** Effect of NSC12 on paxillin phosphorylation. Densitometric analysis of immunoreactive band shown in Fig. 1D normalized to GAPDH protein levels. Data are the mean  $\pm$  the SEM of two independent experiments. \* $p < 0.01$  vs untreated, ANOVA. **Fig S3.** Formation of melanospheres and ALDH activity of UM cells. A) 3000 viable cells were resuspended in melanospheres culture medium and plated. After 7 days, melanospheres were counted. Data are the mean  $\pm$  SEM of two

independent experiments. B) ALDH<sup>br</sup> population was measured in 92.1, Mel270 and Mel285 cells by cytofluorimetric analysis according to manufacturer's instructions. Data are the mean  $\pm$  SEM of three independent experiments. C) Representative flow cytometry dot plots of Aldefluor + cells. The gate refers to the positive/negative cell populations as identified in the presence of DEAB inhibitor. **Fig S4.** Analysis of ALDH activity. Representative flow cytometry dot plots of Aldefluor+ cells of control or 7  $\mu$ M NSC12 treated 92.1, Mel270 and Mel285 UM cells. The gate refers to the positive/negative cell populations as identified in the presence of DEAB inhibitor, according to manufacturer's instructions. **Fig S5.** Effect of BGJ398 on the ALDH<sup>br</sup> UM subpopulation. 92.1, Mel270 and Mel285 cells were treated with increasing doses of BGJ398 for 24 h. Then, ALDH<sup>br</sup> cells were measured by cytofluorimetric analysis. Data are the mean  $\pm$  SEM of three independent experiments. \* $p < 0.05$  vs control, ANOVA. **Fig S6.** Effect of Dacarbazine on UM cells. A) UM cells were treated with increasing concentrations of Dacarbazine. After 72 h cells were counted. B) Mel285 and 92.1 cells were treated with increasing doses of Dacarbazine for 72 h. Then, ALDH<sup>br</sup> cells were measured by cytofluorimetric analysis. Data are the mean  $\pm$  SEM of two independent experiments. **Table S1.** Oligonucleotide primers used for semi-quantitative PCR analysis. Table S1. Oligonucleotide primers used for qPCR analysis.

#### Acknowledgements

The authors wish to thank M. Presta for his valuable suggestions and helpful discussion.

#### Author contributions

Conceptualization: RR, SR. Methodology: AL, AG, SR. Formal analysis: AL, SC, SR. Investigation: AL, AG, CR, AMKC, CT, SR. Writing—Original draft: AL, RR, SR. Writing—Review and editing: CR, GT, SP, FS. Visualization: AL, SR. Project administration: SR. Funding acquisition: RR, SR. All authors read and approved the final manuscript.

#### Funding

SR was supported by Fondazione Umberto Veronesi and by Fondazione Cariplo (Grant ID. 2021–1563) Grants and by Associazione Garda Vita R. Tosoni fellowship; R.R. was supported by Associazione Italiana per la Ricerca sul Cancro (AIRC IG 2019—ID. 23151); S.C. was supported by Italian Ministry of University (PRIN projects n. 2017854EK9).

#### Availability of data and materials

All data are included in the study and available from the corresponding author on reasonable request.

#### Declarations

##### Ethics approval and consent to participate

Not applicable.

##### Consent for publication

Not applicable.

##### Competing interests

The authors declare that they have no known competing financial interests or personal relationships that could have appeared to influence the work reported in this paper.

##### Author details

<sup>1</sup>Department of Molecular and Translational Medicine, University of Brescia, viale Europa 11, 25123 Brescia, Italy. <sup>2</sup>Eye Clinic, Department of Medical and Surgical Specialties, Radiological Sciences and Public Health, University of Brescia, Brescia, Italy.

Received: 7 October 2022 Accepted: 24 March 2023

Published online: 11 May 2023

#### References

- Smit KN, Jager MJ, de Klein A, Kiliç E. Uveal melanoma: towards a molecular understanding. *Prog Retin Eye Res.* 2020;75:100800.
- Krantz BA, Dave N, Komatsubara KM, Marr BP, Carvajal RD. Uveal melanoma: epidemiology, etiology, and treatment of primary disease. *Clin Ophthalmol.* 2017;11:279–89.
- Yang J, Manson DK, Marr BP, Carvajal RD. Treatment of uveal melanoma: where are we now? *Ther Adv Med Oncol.* 2018;10:1758834018757175.
- Souto EB, Zielinska A, Luis M, Carbone C, Martins-Gomes C, Souto SB, Silva AM. Uveal melanoma: pathophysiology and new in situ-specific therapies. *Cancer Chemother Pharmacol.* 2019;84:15–32.
- Patel M, Smyth E, Chapman PB, Wolchok JD, Schwartz GK, Abramson DH, Carvajal RD. Therapeutic implications of the emerging molecular biology of uveal melanoma. *Clin Cancer Res.* 2011;17:2087–100.
- Amaro A, Gangemi R, Piaggio F, Angelini G, Barisione G, Ferrini S, Pfeffer U. The biology of uveal melanoma. *Cancer Metastasis Rev.* 2017;36:109–40.
- Carvajal RD, Schwartz GK, Tezel T, Marr B, Francis JH, Nathan PD. Metastatic disease from uveal melanoma: treatment options and future prospects. *Br J Ophthalmol.* 2017;101:38–44.
- Komatsubara KM, Carvajal RD. Immunotherapy for the treatment of uveal melanoma: current status and emerging therapies. *Curr Oncol Rep.* 2017;19:45.
- Rossi E, Schinzari G, Zizzari IG, Maiorano BA, Pagliara MM, Sammarco MG, Fiorentino V, Petrone G, Cassano A, Rindi G, Bria E, Blasi MA, Nuti M, Tortora G. Immunological backbone of uveal melanoma: is there a rationale for immunotherapy? *Cancers.* 2019. <https://doi.org/10.3390/cancers11081055>.
- Chattopadhyay C, Kim DW, Gombos DS, Oba J, Qin Y, Williams MD, Esmaili B, Grimm EA, Wargo JA, Woodman SE, Patel SP. Uveal melanoma: from diagnosis to treatment and the science in between. *Cancer.* 2016;122:2299–312.
- Tobia C, Coltrini D, Ronca R, Loda A, Guerra J, Scalvini E, Semeraro F, Rezzola S. An orthotopic model of uveal melanoma in zebrafish embryo: a novel platform for drug evaluation. *Biomedicines.* 2021. <https://doi.org/10.3390/biomedicines9121873>.
- Giacomini A, Chiodelli P, Matarazzo S, Rusnati M, Presta M, Ronca R. Blocking the FGF/FGFR system as a “two-compartment” antiangiogenic/antitumor approach in cancer therapy. *Pharmacol Res.* 2016;107:172–85.
- Presta M, Chiodelli P, Giacomini A, Rusnati M, Ronca R. Fibroblast growth factors (FGFs) in cancer: FGF traps as a new therapeutic approach. *Pharmacol Ther.* 2017;179:171–87.
- Lefèvre G, Babchia N, Galipel A, Mouriaux F, Fausset AM, Mrzyk S, Mascarelli F. Activation of the FGF2/FGFR1 autocrine loop for cell proliferation and survival in uveal melanoma cells. *Invest Ophthalmol Vis Sci.* 2009;50:1047–57.
- Boyd SR, Tan DS, de Souza L, Neale MH, Myatt NE, Alexander RA, Robb M, Hungerford JL, Cree IA. Uveal melanomas express vascular endothelial growth factor and basic fibroblast growth factor and support endothelial cell growth. *Br J Ophthalmol.* 2002;86:440–7.
- Wang Y, Bao X, Zhang Z, Sun Y, Zhou X. FGF2 promotes metastasis of uveal melanoma cells via store-operated calcium entry. *Oncol Targets Ther.* 2017;10:5317–28.
- Loda A, Turati M, Semeraro F, Rezzola S, Ronca R. Exploring the FGF/FGFR system in ocular tumors: new insights and perspectives. *Int J Mol Sci.* 2022. <https://doi.org/10.3390/ijms23073835>.
- Castelli R, Giacomini A, Anselmi M, Bozza N, Vacondio F, Rivara S, Matarazzo S, Presta M, Mor M, Ronca R. Synthesis, structural elucidation, and biological evaluation of NSC12, an orally available fibroblast growth factor (FGF) ligand trap for the treatment of FGF-dependent lung tumors. *J Med Chem.* 2016;59:4651–63.
- Ronca R, Giacomini A, Di Salle E, Coltrini D, Pagano K, Ragona L, Matarazzo S, Rezzola S, Maiolo D, Torrella R, Moroni E, Mazzieri R, Escobar G, Mor M, Colombo G, Presta M. Long-pentraxin 3 derivative as a small-molecule FGF trap for cancer therapy. *Cancer Cell.* 2015;28:225–39.
- Ronca R, Ghedini GC, Maccarinelli F, Sacco A, Locatelli SL, Foglio E, Taranto S, Grillo E, Matarazzo S, Castelli R, Paganini G, Desantis V, Cattaneo A, Mor M, Carlo-Stella C, Belotti A, Roccaro AM, Presta M,



- Giacomini A. FGF trapping inhibits multiple myeloma growth through c-Myc degradation-induced mitochondrial oxidative stress. *Cancer Res.* 2020;80:2340–54.
21. Rezzola S, Ronca R, Loda A, Nawaz MI, Tobia C, Paganini G, Maccarinelli F, Giacomini A, Semeraro F, Mor M, Presta M. The autocrine FGF/FGFR system in both skin and uveal melanoma: FGF trapping as a possible therapeutic approach. *Cancers.* 2019. <https://doi.org/10.3390/cancers11091305>.
  22. Yadav AK, Desai NS. Cancer stem cells: acquisition characteristics, therapeutic implications, targeting strategies and future prospects. *Stem Cell Rev Rep.* 2019;15:331–55.
  23. Talukdar S, Emdad L, Das SK, Sarkar D, Fisher PB. Evolving strategies for therapeutically targeting cancer stem cells. *Adv Cancer Res.* 2016;131:159–91.
  24. Zhao J. Cancer stem cells and chemoresistance: the smartest survives the raid. *Pharmacol Ther.* 2016;160:145–58.
  25. Marquardt S, Solanki M, Spitschak A, Vera J, Pützer BM. Emerging functional markers for cancer stem cell-based therapies: understanding signaling networks for targeting metastasis. *Semin Cancer Biol.* 2018;53:90–109.
  26. Barbato L, Bocchetti M, Di Biase A, Regad T. Cancer stem cells and targeting strategies. *Cells.* 2019. <https://doi.org/10.3390/cells8080926>.
  27. Eom YW, Oh JE, Lee JI, Baik SK, Rhee KJ, Shin HC, Kim YM, Ahn CM, Kong JH, Kim HS, Shim KY. The role of growth factors in maintenance of stemness in bone marrow-derived mesenchymal stem cells. *Biochem Biophys Res Commun.* 2014;445:16–22.
  28. Quan MY, Guo Q, Liu J, Yang R, Bai J, Wang W, Cai Y, Han R, Lv YQ, Ding L, Billadeau DD, Lou Z, Bellusci S, Li X, Zhang JS. An FGFR/AKT/SOX2 signaling axis controls pancreatic cancer stemness. *Front Cell Dev Biol.* 2020;8:287.
  29. Coutu DL, Galipeau J. Roles of FGF signaling in stem cell self-renewal, senescence and aging. *Aging.* 2011;3:920–33.
  30. Fillmore CM, Gupta PB, Rudnick JA, Caballero S, Keller PJ, Lander ES, Kuperwasser C. Estrogen expands breast cancer stem-like cells through paracrine FGF/Tbx3 signaling. *Proc Natl Acad Sci USA.* 2010;107:21737–42.
  31. McDermott SC, Rodriguez-Ramirez C, McDermott SP, Wicha MS, Nör JE. FGFR signaling regulates resistance of head and neck cancer stem cells to cisplatin. *Oncotarget.* 2018;9:25148–65.
  32. Zhao W, Li Y, Zhang X. Stemness-related markers in cancer. *Cancer Transl Med.* 2017;3:87–95.
  33. Walcher L, Kistenmacher AK, Suo H, Kitte R, Dlucecz S, Strauß A, Blandszun AR, Yeysa T, Fricke S, Kossatz-Boehlert U. Cancer stem cells—origins and biomarkers: perspectives for targeted personalized therapies. *Front Immunol.* 2020;11:1280.
  34. Kuşoğlu A, Biray Avcı Ç. Cancer stem cells: a brief review of the current status. *Gene.* 2019;681:80–5.
  35. Kalirai H, Damato BE, Coupland SE. Uveal melanoma cell lines contain stem-like cells that self-renew, produce differentiated progeny, and survive chemotherapy. *Invest Ophthalmol Vis Sci.* 2011;52:8458–66.
  36. Djirackor L, Kalirai H, Coupland SE, Petrovski G. CD166high uveal melanoma cells represent a subpopulation with enhanced migratory capacity. *Invest Ophthalmol Vis Sci.* 2019;60:2696–704.
  37. Zhou J, Liu S, Wang Y, Dai W, Zou H, Wang S, Zhang J, Pan J. Salinomycin effectively eliminates cancer stem-like cells and obviates hepatic metastasis in uveal melanoma. *Mol Cancer.* 2019;18:159.
  38. Chen YN, Li Y, Wei WB. Research progress of cancer stem cells in uveal melanoma. *Onco Targets Ther.* 2020;13:12243–52.
  39. Jin B, Zhang P, Zou H, Ye H, Wang Y, Zhang J, Yang H, Pan J. Verification of EZH2 as a druggable target in metastatic uveal melanoma. *Mol Cancer.* 2020;19:52.
  40. Zhou J, Jin B, Jin Y, Liu Y, Pan J. The antihelminthic drug niclosamide effectively inhibits the malignant phenotypes of uveal melanoma. *Theranostics.* 2017;7:1447–62.
  41. Jin Y, Zhang P, Wang Y, Jin B, Zhou J, Zhang J, Pan J. Neddylation blockade diminishes hepatic metastasis by dampening cancer stem-like cells and angiogenesis in uveal melanoma, clinical cancer research: an official journal of the American association for. *Can Res.* 2018;24:3741–54.
  42. Zhou J, Jin B, Jin Y, Liu Y, Pan J. The antihelminthic drug niclosamide effectively inhibits the malignant phenotypes of uveal melanoma in vitro and in vivo. *Theranostics.* 2017;7:1447–62.
  43. De Waard-Siebinga I, Blom DJ, Griffioen M, Schrier PI, Hoogendoorn E, Beverstock G, Danen EH, Jager MJ. Establishment and characterization of a uveal-melanoma cell line. *Int J Cancer.* 1995;62:155–61.
  44. Verbik DJ, Murray TG, Tran JM, Ksander BR. Melanomas that develop within the eye inhibit lymphocyte proliferation. *Int J Cancer.* 1997;73:470–8.
  45. Chen PW, Murray TG, Uno T, Salgaller ML, Reddy R, Ksander BR. Expression of MAGE genes in ocular melanoma during progression from primary to metastatic disease. *Clin Exp Metastasis.* 1997;15:509–18.
  46. Schindelin J, Arganda-Carreras I, Frise E, Kaynig V, Longair M, Pietzsch T, Preibisch S, Rueden C, Saalfeld S, Schmid B, Tinevez JY, White DJ, Hartenstein V, Eliceiri K, Tomancak P, Cardona A. Fiji: an open-source platform for biological-image analysis. *Nat Methods.* 2012;9:676–82.
  47. Giacomini A, Matarazzo S, Pagano K, Ragona L, Rezzola S, Corsini M, Di Salle E, Presta M, Ronca R. A long pentraxin-3-derived pentapeptide for the therapy of FGF8b-driven steroid hormone-regulated cancers. *Oncotarget.* 2015;6:13790–802.
  48. Murtagh F, Legendre P. Ward's hierarchical agglomerative clustering method: which algorithms implement ward's criterion? *J Classif.* 2014;31:274–95.
  49. Charrad M, Ghazzali N, Boiteau V, Niknafs A. Nbclust: an R package for determining the relevant number of clusters in a data set. *J Stat Softw.* 2014;61:1–36.
  50. Hanzelmann S, Castelo R, Guinney J. GSEA: gene set variation analysis for microarray and RNA-Seq data. *Bmc Bioinform.* 2013. <https://doi.org/10.1186/1471-2105-14-7>.
  51. Giacomini A, Taranto S, Rezzola S, Matarazzo S, Grillo E, Bugatti M, Scotuzzi A, Guerra J, Di Trani M, Presta M, Ronca R. Inhibition of the FGF/FGFR system induces apoptosis in lung cancer cells via c-Myc downregulation and oxidative stress. *Int J Mol Sci.* 2020. <https://doi.org/10.3390/ijms21249376>.
  52. Chua V, Orloff M, Teh JL, Sugase T, Liao C, Purwin TJ, Lam BQ, Terai M, Ambrosini G, Carvajal RD, Schwartz G, Sato T, Aplin AE. Stromal fibroblast growth factor 2 reduces the efficacy of bromodomain inhibitors in uveal melanoma. *EMBO Mol Med.* 2019. <https://doi.org/10.1525/emmm.201809081>.
  53. Xu C, Rosler E, Jiang J, Lebkowski JS, Gold JD, O'Sullivan C, Delavan-Boorsma K, Mok M, Bronstein A, Carpenter MK. Basic fibroblast growth factor supports undifferentiated human embryonic stem cell growth without conditioned medium. *Stem Cells.* 2005;23:315–23.
  54. Levenstein ME, Ludwig TE, Xu RH, Llanas RA, VanDenHeuvel-Kramer K, Manning D, Thomson JA. Basic fibroblast growth factor support of human embryonic stem cell self-renewal. *Stem Cells.* 2006;24:568–74.
  55. Tovar V, Cornella H, Moeini A, Vidal S, Hoshida Y, Sia D, Peix J, Cabellos L, Alsinet C, Torrecilla S, Martinez-Quetglas I, Lozano JJ, Desbois-Mouthon C, Solé M, Domingo-Domenech J, Villanueva A, Llovet JM. Tumour initiating cells and IGF/FGF signalling contribute to sorafenib resistance in hepatocellular carcinoma. *Gut.* 2017;66:530–40.
  56. Fessler E, Borovski T, Medema JP. Endothelial cells induce cancer stem cell features in differentiated glioblastoma cells via bFGF. *Mol Cancer.* 2015;14:157.
  57. Maehara O, Suda G, Natsuzaka M, Ohnishi S, Komatsu Y, Sato F, Nakai M, Sho T, Morikawa K, Ogawa K, Shimazaki T, Kimura M, Asano A, Fujimoto Y, Ohashi S, Kagawa S, Kinugasa H, Naganuma S, Whelan KA, Nakagawa H, Nakagawa K, Takeda H, Sakamoto N. Fibroblast growth factor-2-mediated FGFR/Erk signaling supports maintenance of cancer stem-like cells in esophageal squamous cell carcinoma. *Carcinogenesis.* 2017;38:1073–83.

#### Publisher's Note

Springer Nature remains neutral with regard to jurisdictional claims in published maps and institutional affiliations.

**An Orthotopic Model of Uveal Melanoma in Zebrafish Embryo: A Novel Platform for Drug Evaluation**

C. Tobia, D. Coltrini, R. Ronca, [A. Loda](#), J. Guerra, E. Scalvini, F. Semeraro, S. Rezzola.





Biomedicines. 2021 Dec 10;9(12):1873. doi: 10.3390/biomedicines9121873. PMID: 34944689;

PMCID: PMC8698893.



Article

# An Orthotopic Model of Uveal Melanoma in Zebrafish Embryo: A Novel Platform for Drug Evaluation

Chiara Tobia <sup>1</sup> , Daniela Coltrini <sup>1</sup>, Roberto Ronca <sup>1</sup> , Alessandra Loda <sup>1</sup>, Jessica Guerra <sup>1</sup>, Elisa Scalvini <sup>1</sup>, Francesco Semeraro <sup>2</sup>  and Sara Rezzola <sup>1,\*</sup> 

<sup>1</sup> Department of Molecular and Translational Medicine, University of Brescia, 25123 Brescia, Italy; chiara.tobia@unibs.it (C.T.); daniela.coltrini@unibs.it (D.C.); roberto.ronca@unibs.it (R.R.); a.loda025@unibs.it (A.L.); jessica.guerra@unibs.it (J.G.); scalvini.elisa@yahoo.it (E.S.)

<sup>2</sup> Eye Clinic, Department of Medical and Surgical Specialties, Radiological Sciences and Public Health, University of Brescia, 25123 Brescia, Italy; francesco.semeraro@unibs.it

\* Correspondence: sara.rezzola@unibs.it

**Abstract:** Uveal melanoma is a highly metastatic tumor, representing the most common primary intraocular malignancy in adults. Tumor cell xenografts in zebrafish embryos may provide the opportunity to study in vivo different aspects of the neoplastic disease and its response to therapy. Here, we established an orthotopic model of uveal melanoma in zebrafish by injecting highly metastatic murine B16-BL6 and B16-LS9 melanoma cells, human A375M melanoma cells, and human 92.1 uveal melanoma cells into the eye of zebrafish embryos in the proximity of the developing choroidal vasculature. Immunohistochemical and immunofluorescence analyses showed that melanoma cells proliferate during the first four days after injection and move towards the eye surface. Moreover, bioluminescence analysis of luciferase-expressing human 92.1 uveal melanoma cells allowed the quantitative assessment of the antitumor activity exerted by the canonical chemotherapeutic drugs paclitaxel, panobinostat, and everolimus after their injection into the grafted eye. Altogether, our data demonstrate that the zebrafish embryo eye is a permissive environment for the growth of invasive cutaneous and uveal melanoma cells. In addition, we have established a new luciferase-based in vivo orthotopic model that allows the quantification of human uveal melanoma cells engrafted in the zebrafish embryo eye, and which may represent a suitable tool for the screening of novel drug candidates for uveal melanoma therapy.

**Keywords:** uveal melanoma; zebrafish; orthotopic tumor; xenograft; luciferase



**Citation:** Tobia, C.; Coltrini, D.; Ronca, R.; Loda, A.; Guerra, J.; Scalvini, E.; Semeraro, F.; Rezzola, S. An Orthotopic Model of Uveal Melanoma in Zebrafish Embryo: A Novel Platform for Drug Evaluation. *Biomedicines* **2021**, *9*, 1873. <https://doi.org/10.3390/biomedicines9121873>

Academic Editors: James A. Marrs and Swapnalee Sarmah

Received: 17 September 2021

Accepted: 7 December 2021

Published: 10 December 2021

**Publisher's Note:** MDPI stays neutral with regard to jurisdictional claims in published maps and institutional affiliations.



**Copyright:** © 2021 by the authors. Licensee MDPI, Basel, Switzerland. This article is an open access article distributed under the terms and conditions of the Creative Commons Attribution (CC BY) license (<https://creativecommons.org/licenses/by/4.0/>).

## 1. Introduction

The zebrafish embryo has been successfully employed as a platform for modeling human diseases and for large-scale screening of new drugs [1–4]. Ease of manipulation, relatively low costs of maintenance, and optical transparency, combined with the opportunity to perform high-quality imaging, led to an extensive use of this model in cancer research. In this regard, mammalian tumor cell grafting in zebrafish embryos can be achieved in different anatomical sites, giving opportunity to study various aspects of the disease, such as tumor progression, angiogenesis, cancer cell spreading, and metastasis formation. Tumor cells have been successfully implanted in the perivitelline space, yolk ball, blood stream, pericardial cavity, eye, and brain (see [5–9] and references therein).

One of the major drawbacks of the use of the zebrafish embryo as a model in oncology is the quantification of tumor xenograft growth in the different anatomical sites, generally performed by measuring the fluorescence signal generated by engrafted fluorescent tumor cells [10,11]. This approach has also been used for the study of cancer growth following ocular transplantation of fluorescent tumor cells in zebrafish embryos [7–9]. However, the presence of the lens and the cup-like structure of the eye make difficult the acquisition of high-quality fluorescence images, which may lead to misleading results. This

calls for alternative rapid and reliable quantification methods to be exploited for high throughput analysis.

Uveal melanoma represents the most common primary intraocular malignancy in adults. Classified as a rare neoplasm, its occurrence increases with age and its incidence is over 20 million/year. Despite the results obtained in terms of primary tumor management, the 5-year mortality rate of uveal melanoma patients (ranging from 26 to 32%) has not changed over the years [12–15]. Indeed, almost 50% of uveal melanoma patients develop metastatic disease through haematogenous dissemination [16], leading to an approximately 5–7-month median survival [13,14] which is rarely improved by chemotherapy [17]. At present, no drugs have been approved for the treatment of metastatic uveal melanoma patients and new therapeutic strategies are eagerly required. Nevertheless, despite the urgent need for an *in vivo* platform for the rapid screening of novel drug candidates, an orthotopic uveal melanoma model has not yet been implemented with zebrafish embryos.

Here, we propose a luciferase-based quantification method to demonstrate that transplantation of uveal melanoma cells into the eye of zebrafish embryos represents a useful *in vivo* orthotopic model suitable for the screening of novel drug candidates for uveal melanoma therapy.

## 2. Materials and Methods

### 2.1. Reagents

All reagents were of analytical grade. Dulbecco's modified Eagle medium (DMEM), RPMI 1640 medium, fetal bovine serum (FBS), non-essential amino acid (NEAA), and MEM vitamin solutions were obtained from GIBCO Life Technologies (Grand Island, NY, USA). Penicillin, streptomycin, sodium pyruvate, PTU, tricaine, bovine serum albumin (BSA), diaminobenzidine (DAB), and mouse anti-mouse vimentin antibody (Vim 13.2 clone) were from Sigma-Aldrich (St. Louis, MO, USA). Paclitaxel, panobinostat, and everolimus were from MedChemExpress (Monmouth Junction, NJ, USA). The Annexin-V/propidium iodide double staining kit was from Immunostep Biotec (Salamanca, Spain). The ONE-Glo™ Luciferase Assay System was from Promega (Milan, Italy). Rat anti-mouse Ki-67 antibody (TEC-3) was from Dako (Santa Clara, CA, USA). Rabbit anti-human cleaved caspase 3 (Asp175) was from Cell Signaling (Danvers, MA, USA). Biotinylated anti-mouse IgM, anti-rat, and rabbit antibodies were from Abcam (Cambridge, UK). Biotin Avidin system Vectastain ABC reagent was from Vector Laboratories (Burlingame, CA, USA).

### 2.2. Cell Cultures

Murine melanoma B16-BL6 cells were grown in DMEM plus 10% FBS and 1% penicillin/streptomycin, and were stably transfected with DsRed fluorescent protein, thus generating B16-BL6-DsRed<sup>+</sup> cells [2]. Murine melanoma B16-LS9 cells [18] were kindly provided by Dr. L. Morbidelli (University of Siena, Siena, Italy) and were grown in DMEM plus 10% FBS, 1% penicillin/streptomycin. Luciferase-transfected B16-LS9 cells (B16-LS9-luc<sup>+</sup> cells) were generated as previously described [19]. Human melanoma A375M cells were obtained from Dr. R. Giavazzi (Istituto Ricerche Farmacologiche Mario Negri, Bergamo, Italy) and were grown in DMEM plus 20% FBS, 1% NEAA, 2% MEM vitamin solution, 1% sodium pyruvate, and 1% penicillin/streptomycin. Human uveal melanoma 92.1 cells [20] were obtained from Dr. M. Jager (Leiden University, Leiden, The Netherlands) and were maintained in RPMI 1640 medium plus 10% FBS, 1% penicillin/streptomycin. A375M and 92.1 cells were infected with a lentivirus harboring the RFP/luciferase cDNA, thus generating stable A375M-RFP<sup>+</sup>/luc<sup>+</sup> and 92.1-RFP<sup>+</sup>/luc<sup>+</sup> cells that express both the red fluorescent RFP protein and the bioluminescent firefly luciferase. For eye injection, cells were suspended in PBS (final concentration equal to 100,000 cells/μL).

### 2.3. Cell Proliferation Assay

Cells were seeded on 48-well plates at  $1.0 \times 10^4$  cells/cm<sup>2</sup> or at  $1.5 \times 10^4$  cells/cm<sup>2</sup> for B16-LS9-luc<sup>+</sup> and 92.1-RFP<sup>+</sup>/luc<sup>+</sup> cells, respectively. After 24 h, cells were treated

with increasing concentrations of the different anticancer drugs. After a further 48 h or 72 h incubation, cells were trypsinized and viable cell counting was performed with the MACSQuant<sup>®</sup> Analyzer (Miltenyi Biotec, Bergisch Gladbach, Germany), as reported [21].

#### 2.4. Apoptosis Assay

92.1-RFP<sup>+</sup>/luc<sup>+</sup> cells were seeded on 6-well plates at  $1.0 \times 10^4$  cells/cm<sup>2</sup>. After 24 h, cells were treated with 140 nM paclitaxel, 20 nM panobinostat, and 60 nM everolimus. After 72 h of treatment, apoptotic cell death was assessed by Annexin-V/propidium iodide double staining according to the manufacturer's instructions, and cytofluorimetric analysis was performed using the MACSQuant<sup>®</sup> Analyzer.

#### 2.5. Zebrafish Maintenance and Cell Transplantation

The transgenic tg(*kdrl*:EGFP) zebrafish line was maintained in the facility of the University of Brescia at 28 °C under standard conditions [22], and embryos were staged by h post-fertilization (hpf), as described [23]. To prevent pigmentation, embryo fish water was added with 0.2 mM 1-phenyl-2-thiourea (PTU) starting from 24 hpf. For cell injection and in vivo observation, embryos were anesthetized using 0.16 mg/mL tricaine. For cell engrafting, 48 hpf embryos were microinjected in the eye with tumor cells using a borosilicate needle and an Eppendorf FemtoJet microinjector equipped with an InjectMan NI2 manipulator. A single eye was injected with tumor cells in each zebrafish embryo. When indicated, 2.0 nL of a solution containing the anticancer drug under testing was injected in the same eye. After tumor cell injection, zebrafish embryos were selected under a fluorescence microscope to ensure that tumor cells were located only within the eyeballs and then grown at 33 °C.

#### 2.6. Fluorescence and Light Sheet Microscopy

Live embryos were photographed at 1 h ( $t_0$ , 48 hpf), 1 day ( $t_1$ ) and 4 days ( $t_4$ ) post implantation on agarose-coated dishes using an AxioZoom V16 fluorescence stereomicroscope (Zeiss, Oberkochen, Germany, EU) equipped with a digital AxioCam 506 color camera (Zeiss). The mean area of the tumor was manually measured using FIJI software [24]. Light sheet microscopy experiments were performed using a Light Sheet Z.1 microscope (Zeiss). For this purpose,  $t_0$ ,  $t_1$ , and  $t_4$  embryos were embedded in a low melting agarose cylinder (1% low melting agarose:fish water, 1:1) and immersed in the observation chamber filled with fish water and anesthetic. Maximum intensity projections were obtained using the Zen software (Zeiss) and 3D reconstructions were made after z-stack processing with Arivis software (Zeiss).

To detect apoptotic cells, 48 hpf embryos were microinjected in the eye with 2.0 nL of a solution containing the anticancer drug under testing. After injection, zebrafish embryos were grown at 33 °C for 4 days. At  $t_4$ , live embryos were soaked in fish water containing 2 µg/mL acridine orange and incubated at 28 °C for 20 min. After 8 washes for 5 min each with fish water, embryos were anesthetized and analyzed immediately with a fluorescence stereomicroscope (Zeiss).

#### 2.7. Immunohistochemical Analysis

After tumor cell injection, zebrafish embryos were formalin-fixed, paraffin-embedded, and sections of grafted eyes were analyzed at  $t_0$  and  $t_4$  by hematoxylin and eosin (H&E) or immunohistochemical staining [25]. Briefly, sections were de-waxed, rehydrated, and endogenous peroxidase activity blocked with 0.3% H<sub>2</sub>O<sub>2</sub> in methanol. Antigen retrieval was performed using a thermostatic bath (Labochema, Vilnius, Lithuania), in 10 mM citrate buffer (pH 6.0). Sections were then washed in TBS (pH 7.4) and incubated overnight with a mouse monoclonal (IgM isotype) anti-mouse vimentin antibody (1:200) or with a rat anti-mouse Ki-67 antibody (1:100) or with a rabbit anti-human cleaved caspase 3 (Asp175) (1:100) diluted in TBS plus 1% BSA, 0.1% Triton x-100, and 0.1% Tween, followed by 1 h incubation with biotinylated anti-mouse IgM, anti-rat, or anti-rabbit antibody (1:200),

respectively. Signal was revealed using Biotin Avidin system Vectastain ABC reagent followed by DAB as chromogen and hematoxylin as counterstain. Images were taken using an Axio Imager A2 microscope equipped with a digital AxioCam MRC5 camera (Zeiss).

### 2.8. Luciferase-Based Quantification Method

At different time points after intraocular grafting of luc<sup>+</sup> cells, enucleated eyes or anesthetized embryos were singularly placed in a well of a white polystyrene 96-well plate (Sigma-Aldrich). Embryo medium was removed and replaced with 50 µL of lysis buffer (80 mM Na<sub>2</sub>HPO<sub>4</sub>, 9.3 mM NaH<sub>2</sub>PO<sub>4</sub>, 2% TritonX100, 1.0 mM DTT in MilliQ water) and 50 µL of ONE-Glo™ Reagent. The luminescence was measured using an EnSight® Multimode Plate Reader (PerkinElmer, Milan, Italy) and expressed as relative luminescence units (RLUs).

To generate the calibration curve, a fixed number of B16-LS9-luc<sup>+</sup> cells (ranging from 0 to 1000 cells) was added to non-injected embryos and then the bioluminescence signal quantified as described above.

### 2.9. Statistical Analysis

Statistical analysis was performed with GraphPad Prism 8 (San Diego, CA, USA) using a Student's *t*-test for 2 groups of samples or one-way analysis of variance followed by Tukey's multiple comparison post hoc test for more than 2 groups. Differences were considered significant when *p*-values < 0.05.

## 3. Results and Discussion

### 3.1. Zebrafish Embryo Eye Is a Permissive Environment for the Growth of Engrafted Melanoma Cells

To evaluate whether the zebrafish embryo eye represents a microenvironment suitable for the grafting of melanoma cells, we first assessed the behavior of the well-characterized model of invasive murine melanoma represented by B16-BL6-DsRed<sup>+</sup> cells [2], which were injected into the eye of zebrafish embryos at 48 hpf. At this stage, the embryo eye consists of the retina (mainly composed of neuronal cells that will progressively organize in stratified retinal layers [26]), the hyaloid, and the ciliary vascular systems [27]. On this basis, B16-BL6-DsRed<sup>+</sup> cells were orthotopically injected in the posterior side of the developing eye of tg(*kdrl*:EGFP) embryos (100 cells/embryo) and monitored for the following 4 days by light sheet fluorescence microscopy. One hour after implantation (*t*<sub>0</sub>), maximum intensity projection of the z-stacks and 3D reconstructions confirmed that DsRed<sup>+</sup> cells were present at the bottom of the eye in the proximity of the developing choroidal vasculature (Figure 1A,A'). One day post implantation (*t*<sub>1</sub>), cells relocate towards the eye surface, interacting with the surrounding vasculature (Figure 1B,B'). At 4 days post implantation (*t*<sub>4</sub>), DsRed<sup>+</sup> cells invaded the lens surface and grew without exerting a significant impact on the anatomical architecture of the eye (Figure 1C,C'). To confirm these observations, paraffin sections of tumor cell-grafted eyes were analyzed at *t*<sub>0</sub> and *t*<sub>4</sub> by H&E staining and by Ki-67 and vimentin immunostaining. As shown in Figure 2, implanted B16-BL6-DsRed<sup>+</sup> cells were able to proliferate, as demonstrated by the presence of Ki-67<sup>+</sup> cells, without affecting the physiological development of the retina. Moreover, cells moved towards the eye surface and invaded the lens (Figure 2B). Notably, preliminary observations suggest that the displacement of melanoma cells observed at *t*<sub>4</sub> is in part a consequence of the invasive properties of cancer cells and in part due to the remodeling of the eye that occurs during embryo development, which plays a not negligible role in tumor cell localization within the eye (data not shown).

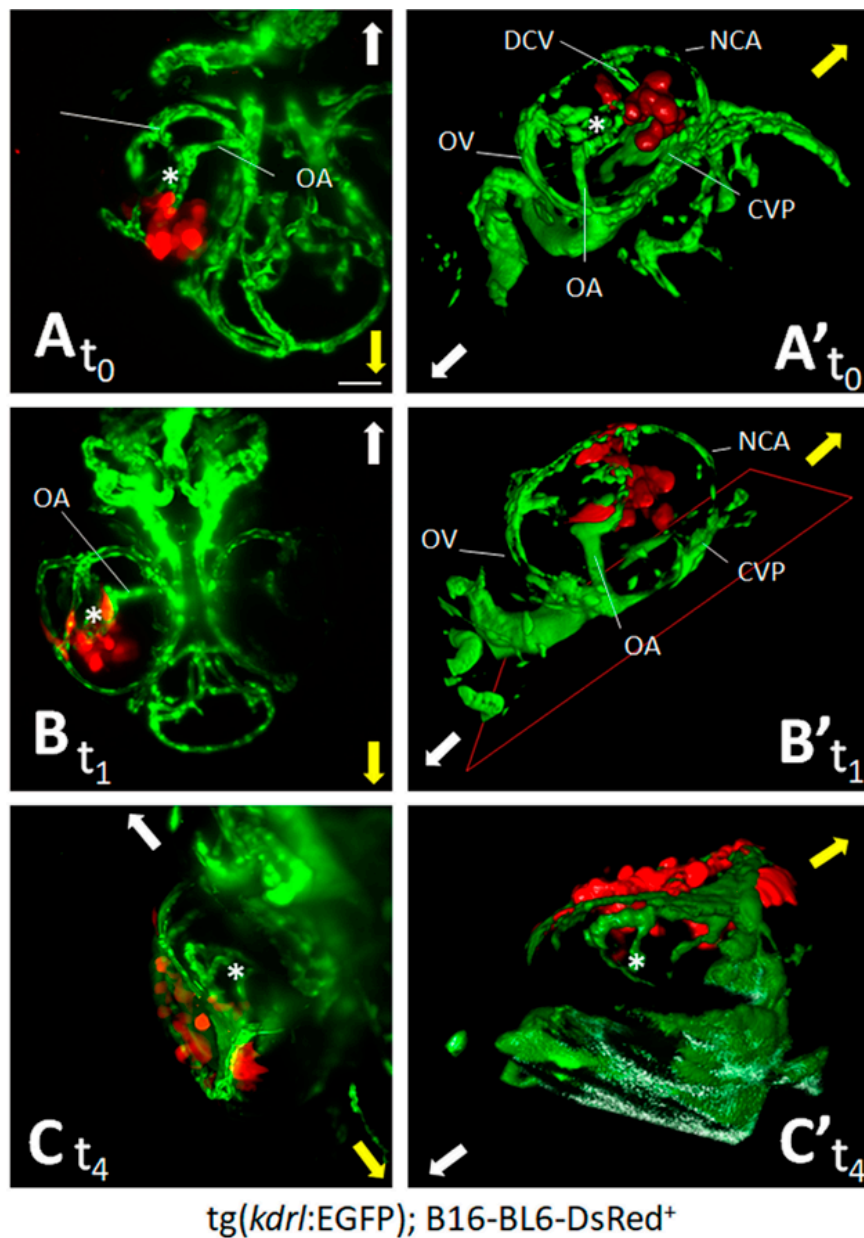


**Figure 1.** Zebrafish embryo eye is a microenvironment suitable for cell grafting. Murine melanoma B16-BL6-DsRed<sup>+</sup> cells (100 cells/embryo) were orthotopically injected in the posterior side of the developing eye of transgenic *tg(kdrl:EGFP)* zebrafish embryos at 48 hpf. Maximum intensity projection of the z-stacks (A–C) and 3D reconstructions (A'–C') of B16-BL6-DsRed<sup>+</sup> cells performed at 1 h (t<sub>0</sub>) (A,A'), 1 day (t<sub>1</sub>) (B,B'), and 4 days (t<sub>4</sub>) (C,C') post implantation. (A,B) ventral view; (C) dorsal view. Asterisk indicates the hyaloid artery. Arrows indicate embryo orientation: white arrow, posterior side; yellow arrow, anterior side. CVP, choroidal vascular plexus; DCV, dorsal ciliary vein; NCA, nasal ciliary artery; OA, optic artery; OV, optic vein. Scale bar: 50  $\mu$ m.



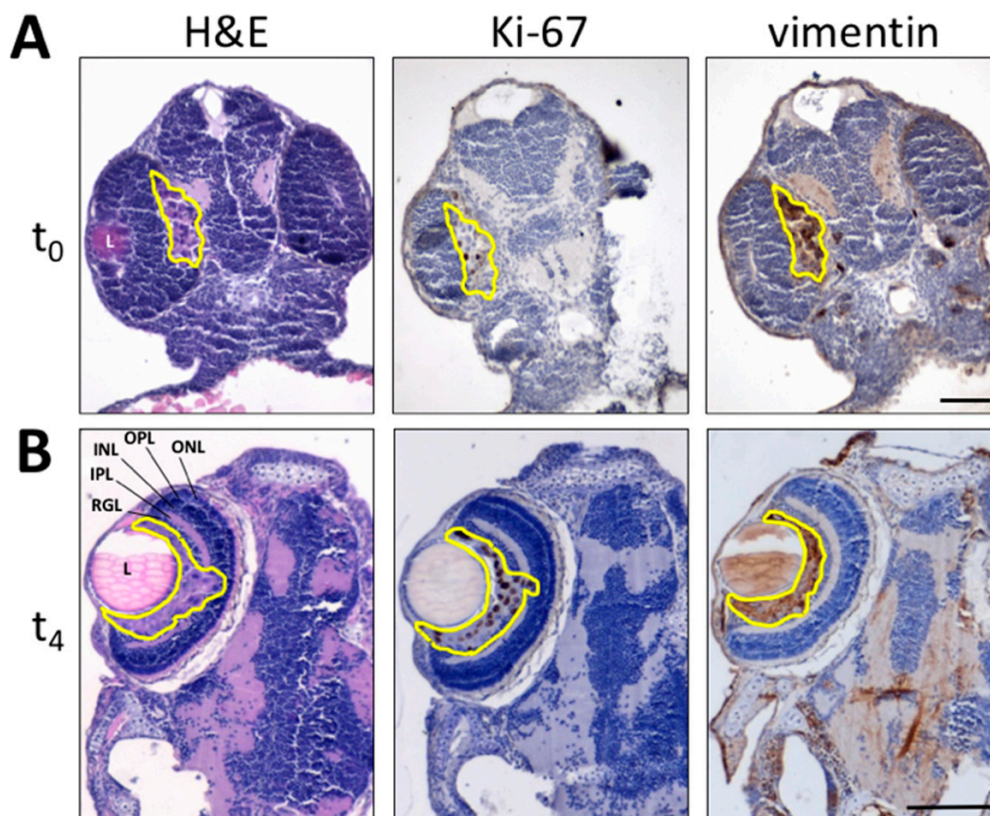


**Figure 2.** Histological analysis of melanoma B16-BL6-DsRed<sup>+</sup> xenografts. Paraffin sections of B16-BL6-DsRed<sup>+</sup> cells grafted into zebrafish embryo eyes obtained at 1 h ( $t_0$ ) (A) or 4 days ( $t_4$ ) post implantation (B) are stained by H&E (left panel) whereas Ki-67 (central panel) and vimentin (right panel) immunoreactivity is shown in brown. Tumor area is highlighted in yellow. L, lens; INL, inner nuclear layer; IPL, inner plexiform layer; ONL, outer nuclear layer; OPL, outer plexiform layer; RGL, retinal ganglion cell layer. Scale bars: 50  $\mu$ m.

### 3.2. Quantification of Melanoma Xenograft Growth in the Zebrafish Embryo Eye

To obtain a reliable and reproducible quantification of melanoma cell growth in zebrafish embryo eyes, we performed a first set of experiments exploiting the fluorescence signal of B16-BL6-DsRed<sup>+</sup> cells. For this purpose, we attempted to measure fluorescent tumor areas in engrafted embryos at  $t_0$ ,  $t_1$ , and  $t_4$  after injection. As anticipated, even though the analysis of digitalized images demonstrated an increase of DsRed<sup>+</sup> tumor areas at  $t_4$  when compared to the other time points (Supplementary Materials, Figure S1), the results suffered significant drawbacks. Indeed, although extended depth of focus of the z-stacks provided a good quality lateral view of the xenografts at  $t_0$  and  $t_1$ , the acquisition of images required to cover the entire thickness of the tumor was difficult at  $t_4$  and was affected by the position of tumor cells that were close to the lens or deeply immersed in the eye.

In addition, the three-dimensional structure of the embryo eye and the presence of the lens, which may generate distorted images, made problematic the choice of the best angle for image acquisition. In this context, the optical accessibility of the zebrafish eye is further limited by the presence of pigmented cells, including neural crest-derived chromatophores

(i.e., melanophores, iridophores, and xanthophores) and the retinal pigment epithelium [28]. Moreover, the blockade of zebrafish pigmentation by the addition of PTU in the fish water [22] has no effect on iridophores and on their nonspecific fluorescence signal [29], which impairs the reproducibility of the quantification technique.

On the other hand, it has been shown that the use of transparent *crystal* zebrafish mutants does not completely avoid refraction of the light due to the presence of the lens and of residual xanthophores present in the mutant eyes [29]. Finally, even though high-quality images may be obtained by confocal microscopy [11], acquisition and analysis procedures are time consuming and not suitable for high-throughput analysis.

To overcome these limitations, we developed an alternative quantification method exploiting the bioluminescence signal generated by tumor cells transduced with firefly luciferase. To this end, we took advantage of a red fluorescent and luciferase expressing human melanoma cell line (A375M-RFP<sup>+</sup>/luc<sup>+</sup>) available in our laboratory. A375M-RFP<sup>+</sup>/luc<sup>+</sup> cells were grafted in the eye of 48 hpf-old zebrafish embryos at 50, 100, and 200 cells/injection. Then, injected and not injected contralateral eyes were enucleated 1 h after grafting. As shown in the Supplementary Materials, Figure S2, analysis of grafted eyes indicates that the bioluminescence signal increases in a cell dose-dependent manner, being distinct from the basal levels measured in the contralateral control eyes. Similar results were obtained by measuring the bioluminescence signal generated by the lysates of the whole embryos engrafted with A375M-RFP<sup>+</sup>/luc<sup>+</sup> cells (data not shown), thus avoiding the technical difficulty and the time-consuming eye enucleation procedure and confirming the reliability of this quantification method.

To assess whether this procedure allowed a quantitative evaluation of the growth of grafted tumors, A375M-RFP<sup>+</sup>/luc<sup>+</sup> cells (100 cells/embryo) were injected in the eye of tg(*kdr*:EGFP) embryos at 48 hpf. Then, injected embryos were analyzed at  $t_0$  and  $t_4$  by light sheet fluorescence microscopy or by evaluation of the bioluminescence of the lysates of the whole animals. As shown in Figure 3A, A375M-RFP<sup>+</sup>/luc<sup>+</sup> cells were clearly visible 1 h after grafting in the embryo eye. At 4 days post implantation, grafted cells were alive and had moved from the injection site toward the lens surface, as already observed for B16-BL6-DsRed<sup>+</sup> cells. In parallel, a significant increase of the A375M-RFP<sup>+</sup>/luc<sup>+</sup> cell-related bioluminescence signal was measured at  $t_4$  when compared to  $t_0$ , thus confirming the capacity of this protocol to monitor the relative growth of tumor grafts (Figure 3B).

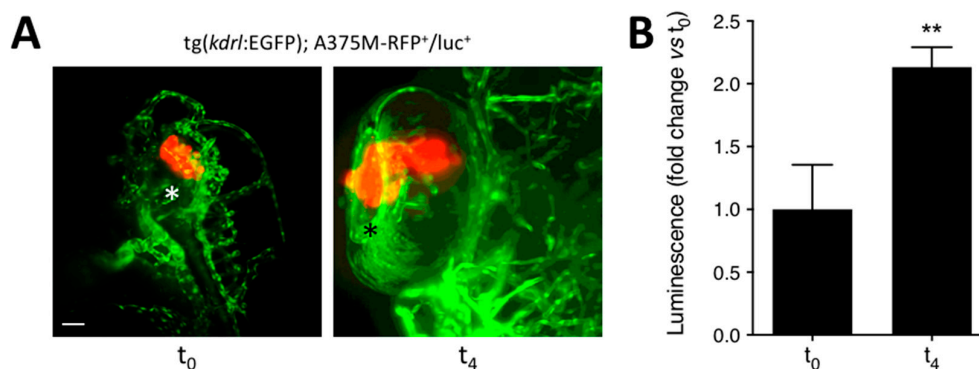


**Figure 3.** Luciferase-based quantification of the growth of human melanoma A375M-RFP<sup>+</sup>/luc<sup>+</sup> xenografts. Human melanoma A375M-RFP<sup>+</sup>/luc<sup>+</sup> cells (100 cells/embryo) were injected into the posterior side of the developing eye of transgenic tg(*kdr*:EGFP) zebrafish embryos at 48 hpf. (A) Maximum intensity projection of the z-stacks of A375M-RFP<sup>+</sup>/luc<sup>+</sup> cells performed at 1 h ( $t_0$ ) and 4 days ( $t_4$ ) post implantation.  $T_0$ , lateral view, anterior to the top;  $t_4$ , dorsal view, anterior to the top. Asterisk indicates the superficial ocular vasculature. Scale bar: 50  $\mu$ m. (B) Evaluation of A375M-RFP<sup>+</sup>/luc<sup>+</sup> bioluminescence signal in the lysates of the whole embryos at  $t_0$  and  $t_4$ . Data are the mean  $\pm$  SEM ( $n = 8$ ). \*\*  $p < 0.01$  vs.  $t_0$ , Student's *t*-test.

### 3.3. Orthotopic Ocular Grafting in the Zebrafish Embryo as a Model for Uveal Melanoma Treatment

Given the promising capacity of luciferase-expressing melanoma cells to grow and to be quantified after grafting in zebrafish eyes, we decided to extend this assay to a well-established murine melanoma model suitable for investigating the mechanisms responsible for uveal melanoma liver tropism [30–32], immunologic and angiogenic aspects [33], and drug response [34–37]. On this basis, B16-LS9-luc<sup>+</sup> cells were injected in the zebrafish embryo eye, grafts were analyzed at  $t_0$  and  $t_4$ , and immunohistochemical analysis of cell grafts showed that tumor cells proliferate, as already observed for B16-BL6 tumors (Figure 4A). In addition, bioluminescence quantification performed at different time points after injection ( $t_0$ ,  $t_1$ ,  $t_2$ ,  $t_3$ , and  $t_4$ ) showed that, after a slight decrease in cell growth at  $t_1$ , B16-LS9-luc<sup>+</sup> cells proliferate rapidly, their cell number increasing up to four times at  $t_3/t_4$  when compared to  $t_0$  (Figure 4B and Supplementary Materials, Figure S3).

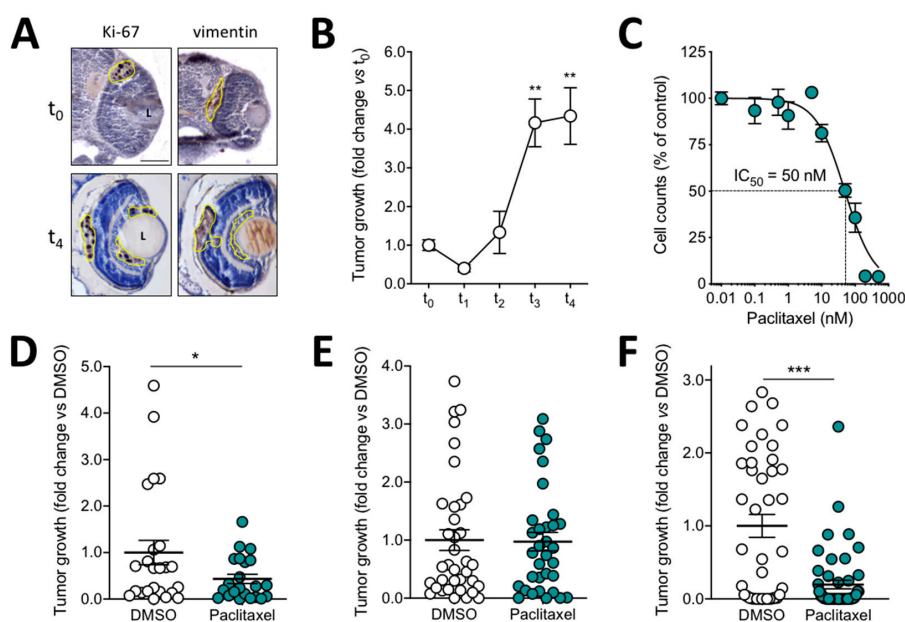


**Figure 4.** Effect of paclitaxel on the growth of murine melanoma B16-LS9-luc<sup>+</sup> xenografts. (A) Immunohistochemical analysis of zebrafish embryo eyes at 1 h ( $t_0$ ) and 4 days ( $t_4$ ) after orthotopic injection of B16-LS9-luc<sup>+</sup> cells. Ki-67 (left panel) and vimentin (right panel) are detected in brown. Tumor area is highlighted in yellow. L, lens. Scale bar: 50  $\mu$ m. (B) B16-LS9-luc<sup>+</sup> bioluminescence signal was evaluated 1 h ( $t_0$ ), 1 day ( $t_1$ ), 2 days ( $t_2$ ), 3 days ( $t_3$ ), and 4 days ( $t_4$ ) post implantation in the lysates of the whole embryos. Data are the mean  $\pm$  SEM of five independent experiments. \*\*  $p < 0.01$  vs.  $t_0$  and  $t_1$ , ANOVA. (C) Effect of paclitaxel on the proliferation of B16-LS9-luc<sup>+</sup> cells in vitro. Viable cells were counted after 72 h of incubation with increasing concentrations of the drug. Data are the mean  $\pm$  SEM of three independent experiments. (D) B16-LS9-luc<sup>+</sup> cells were cultured for 24 h in vitro in the absence or in the presence of 0.5  $\mu$ M paclitaxel or with the corresponding volume of DMSO and then grafted in the zebrafish eye. Tumor growth was evaluated at  $t_4$  by measuring the cell luminescence signal in the lysates of the whole embryos. Data are the mean  $\pm$  SEM ( $n = 20$ ). \*  $p < 0.05$  vs. DMSO, Student's  $t$ -test. (E) After injection of B16-LS9-luc<sup>+</sup> cells into the zebrafish eye, embryos were incubated at  $t_0$  with 10  $\mu$ M paclitaxel or with the corresponding volume of DMSO, both dissolved in fish water. Tumor growth was evaluated at  $t_4$  by measuring the cell luminescence signal. Data are the mean  $\pm$  SEM ( $n = 35$ ). (F) After B16-LS9-luc<sup>+</sup> cell grafting into the zebrafish eye, 0.4 pmole/embryo of paclitaxel or of the corresponding volume of DMSO were injected in the same eye. Tumor growth was evaluated at  $t_4$  by measuring the cell luminescence signal. Data are the mean  $\pm$  SEM ( $n = 45$ ). In (D–F), each dot represents one embryo. \*\*\*  $p < 0.0001$  vs. DMSO, Student's  $t$ -test.

In order to assess the response of tumor cells grafted in the embryo eye to anticancer drugs, preliminary experiments were carried out in which B16-LS9-luc<sup>+</sup> cells were treated in vitro for 72 h with increasing concentrations of the microtubule-disrupting agent paclitaxel [38]. As shown in Figure 4C, the compound inhibits the growth of B16-LS9-luc<sup>+</sup> cells with an ID<sub>50</sub> equal to 50 nM. On this basis, three different routes of in vivo administration of the drug were attempted in engrafted zebrafish embryos: (i) 24 h in vitro pretreatment of B16-LS9-luc<sup>+</sup> cells with 0.5 μM paclitaxel, followed by their injection in the zebrafish eye; (ii) injection of B16-LS9-luc<sup>+</sup> cells in the embryo eye, followed by incubation of engrafted embryos with 10 μM paclitaxel dissolved in fish water—an experimental procedure frequently used to test compounds in zebrafish [39]; (iii) engraftment of cells in the zebrafish embryo eye, followed by injection of the drug at 0.4 pmoles/embryo in the same eye. At the end of each protocol, the growth of B16-LS9-luc<sup>+</sup> grafts was assessed by bioluminescence-based quantification of luc<sup>+</sup> tumor cells performed at t<sub>4</sub>.

As anticipated, pretreatment with paclitaxel resulted in a significant inhibition of the growth of the tumor grafts (Figure 4D). No inhibition of the growth of B16-LS9-luc<sup>+</sup> grafts was observed when engrafted embryos were treated with paclitaxel dissolved in the fish water, possibly as a consequence of the limited entry of the drug in the eye compartment (Figure 4E). Interestingly, a significant inhibition of B16-LS9-luc<sup>+</sup> tumor growth occurred when paclitaxel was directly injected in the embryo eye after cell grafting (Figure 4F).

Based on these observations, we decided to extend this experimental model by setting up an orthotopic experimental protocol in which human 92.1-RFP<sup>+</sup>/luc<sup>+</sup> uveal melanoma cells were grafted (100 cells/embryo) in zebrafish embryo eyes at 48 hpf, followed by injection in the same eyes with 0.4 pmoles of different canonical chemotherapeutic drugs (i.e., paclitaxel [38], the histone deacetylase inhibitor panobinostat [40], the mTOR inhibitor everolimus [41], or vehicle). As shown in Figure 5A, all drugs inhibited the growth of uveal melanoma 92.1-RFP<sup>+</sup>/luc<sup>+</sup> cells in vitro, with ID<sub>50</sub> values ranging between 10 nM and 67 nM. Accordingly, treatment of engrafted uveal melanoma cells by eye injection of paclitaxel, panobinostat, or everolimus caused a significant inhibition of tumor growth when assessed by measurement of bioluminescence (Figure 5B). Notably, panobinostat exerts a pro-apoptotic effect on cancer cells, both in vitro and in vivo (Supplementary Materials, Figure S4A,B). Moreover, no significant toxic or pro-apoptotic effect was observed in the zebrafish embryo eye tissue after the injection of the three drugs (Supplementary Materials, Figure S4C).

In addition, light sheet fluorescence microscopy confirmed the efficacy of drug treatment, uveal melanoma cells remaining confined at the bottom of the eye in the proximity of the choroidal vasculature (Figure 5C). These results are in line with previous observations about the efficacy of these drugs on uveal melanoma growth in in vitro and in vivo experimental models [42,43]. Relevant to this point, it must be pointed out that phase 2 clinical trials designed to evaluate the clinical benefits of paclitaxel or everolimus administration showed only a limited efficacy in uveal melanoma metastatic patients [44,45], whereas no data are available about the effect of panobinostat. Further studies will be required to assess the efficacy of histone deacetylase inhibitors in uveal melanoma.

In this paper, we describe the first orthotopic model of uveal melanoma in zebrafish, previous models of uveal melanoma being limited to the injection of cancer cells into the yolk sac of embryos [46–49]. Even though orthotopic models are usually less rapid and more technically challenging with respect to the heterotopic implants, these approaches are more tissue-specific and allow a more realistic recapitulation of the natural microenvironment in which the tumor originated. Altogether, our data extend previous observations about the possibility of engrafting tumor cells, including retinoblastoma and conjunctival melanoma cells, in zebrafish embryo eyes, thus generating orthotopic models of different ocular neoplasms [7–9]. In addition, it should be considered that the eye represents a metastatic site for various tumor types, including cutaneous melanoma, breast, and lung cancer, with choroidal metastases occurring in approximately 8% of human malignancies [50]. Thus, tumor cell grafting in the zebrafish embryo eye may be exploited as a

useful orthotopic model to investigate novel therapeutic approaches not only for primary tumors but for eye metastases as well. Relevant to this point, our work focuses on providing a simple and reliable strategy for the accurate quantification of engrafted tumor cells by exploiting the bioluminescent signal of firefly luciferase-expressing cells. Indeed, the presence of the lens and the cup-like structure of the eye make difficult the acquisition of high-quality fluorescent images and may lead to misleading results. Moreover, the autofluorescent properties of zebrafish embryos and mammalian cells increase the non-specific background and decrease the sensitivity of signal detection. On the other hand, bioluminescence displays a higher detection capacity and allows for greater sensitivity because of the enzymatic nature of the bioluminescent reporter and the absence of the endogenous bioluminescence of cellular components.

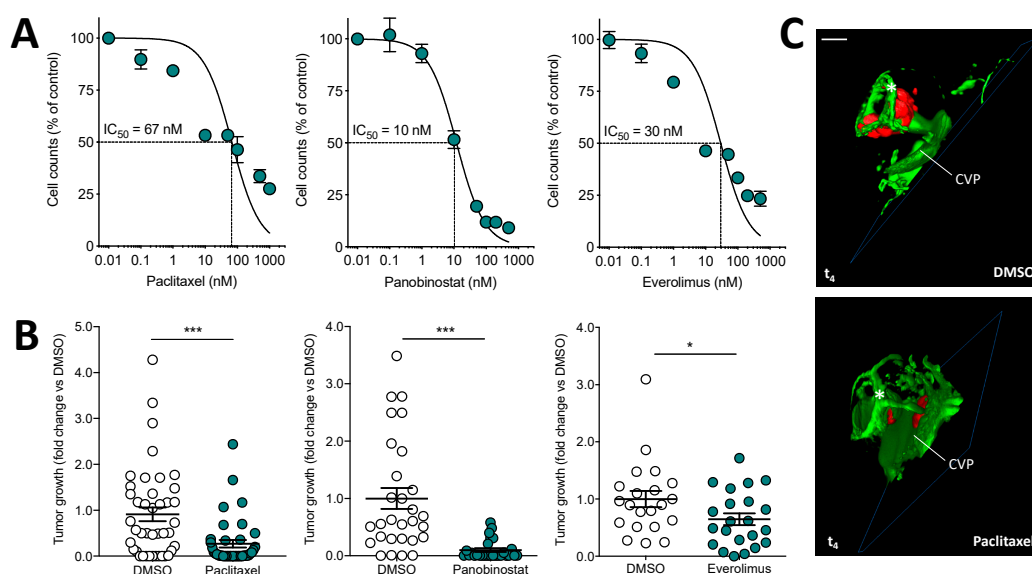


**Figure 5.** Effect of anticancer drugs on the growth of human uveal melanoma 92.1-RFP<sup>+</sup>/luc<sup>+</sup> xenografts. **(A)** Effect of paclitaxel, panobinostat, and everolimus treatments on the proliferation of 92.1-RFP<sup>+</sup>/luc<sup>+</sup> cells in vitro. Viable cells were counted after 48 h of incubation with increasing concentrations of paclitaxel or panobinostat or after 72 h of incubation with everolimus. Data are the mean  $\pm$  SEM of two independent experiments. **(B)** After 92.1-RFP<sup>+</sup>/luc<sup>+</sup> cell grafting into the zebrafish eye, 0.4 pmoles/embryo of paclitaxel, panobinostat, everolimus or the corresponding volume of DMSO were injected in the same eye. Tumor growth was evaluated at  $t_4$  by measuring the cell luminescence signal in the lysates of the whole embryos. Data are the mean  $\pm$  SEM of two independent experiments. Each dot represents one embryo. \*  $p < 0.05$  and \*\*\*  $p < 0.001$  vs. DMSO, Student's *t*-test. **(C)** 3D reconstruction of the eye region of 92.1-RFP<sup>+</sup>/luc<sup>+</sup> xenografts evaluated 4 days post implantation in the absence or in the presence of paclitaxel injection. Scale bar: 50  $\mu$ m. Asterisk indicates the superficial ocular vasculature; CVP, choroidal vascular plexus.

The luminescence-based method herein described allows for a precise quantification without relying on any image analysis software and it provides a simple and quick in vivo evaluation of the efficacy of anticancer drugs after intraocular delivery. In this context, this approach may be exploited for high-throughput analysis and may have relevant implications for the evaluation of new low molecular weight compounds for the treatment of uveal melanoma and other primary ocular neoplasms and metastatic tumors endowed with ocular tropism.

#### 4. Conclusions

In this paper, we described an orthotopic model of uveal melanoma in which tumor cells are grafted in the eye of zebrafish embryos in the proximity of the developing choroidal vasculature. In the following 3–4 days, grafted cells proliferate and move towards the eye surface, thus demonstrating that the zebrafish embryo eye is a permissive environment for the growth of UM cells. In addition, the use of firefly luciferase bioluminescent murine and human tumor cells allowed the assessment of the antitumor activity of candidate drugs when injected into the grafted eyes. In conclusion, we have established a new quantification method based on the ocular implantation of bioluminescent uveal melanoma cells in zebrafish embryos that may represent a useful *in vivo* orthotopic model suitable for the screening of novel drug candidates for uveal melanoma therapy.

**Supplementary Materials:** The following are available online at <https://www.mdpi.com/article/10.3390/biomedicines9121873/s1>, Figure S1: Fluorescence-based quantification of the growth of murine melanoma B16-BL6-DsRed<sup>+</sup> xenografts, Figure S2: Luciferase-based quantification of human melanoma A375M-RFP<sup>+</sup>/Luc<sup>+</sup> xenografts, Figure S3: Luciferase-based quantification of murine melanoma B16-LS9-luc<sup>+</sup> xenografts, Figure S4: Everolimus, paclitaxel, and panobinostat effects on cell apoptosis.

**Author Contributions:** Conceptualization, C.T. and S.R.; methodology, C.T. and S.R.; investigation, C.T., D.C., R.R., A.L., J.G., E.S. and S.R.; formal analysis: C.T. and S.R.; visualization: S.R.; writing—original draft preparation, C.T. and S.R.; writing—review and editing, R.R. and S.R.; supervision, F.S. and S.R.; project administration, S.R.; funding acquisition, R.R. and F.S. All authors have read and agreed to the published version of the manuscript.

**Funding:** This work was supported by Associazione Italiana Ricerca sul Cancro (AIRC) IG grant n° 23151 to R.R.; S.R. was supported by Fondazione Umberto Veronesi and Associazione Garda Vita R. Tosoni fellowships.

**Institutional Review Board Statement:** Not applicable.

**Informed Consent Statement:** Not applicable.

**Data Availability Statement:** Data are contained within the article or the Supplementary Materials.

**Acknowledgments:** The authors wish to thank M. Presta for his valuable suggestions and helpful discussion.

**Conflicts of Interest:** The authors declare no conflict of interest.

#### References

1. Santoriello, C.; Zon, L.I. Hooked! Modeling human disease in zebrafish. *J. Clin. Investig.* **2012**, *122*, 2337–2343. [[CrossRef](#)]
2. Tobia, C.; Gariano, G.; De Sena, G.; Presta, M. Zebrafish embryo as a tool to study tumor/endothelial cell cross-talk. *Biochim. Biophys. Acta* **2013**, *1832*, 1371–1377. [[CrossRef](#)]
3. Rezzola, S.; Paganini, G.; Semeraro, F.; Presta, M.; Tobia, C. Zebrafish (*Danio rerio*) embryo as a platform for the identification of novel angiogenesis inhibitors of retinal vascular diseases. *Biochim. Biophys. Acta* **2016**, *1862*, 1291–1296. [[CrossRef](#)] [[PubMed](#)]
4. Lee, H.-C.; Lin, C.-Y.; Tsai, H.-J. Zebrafish, an *in vivo* platform to screen drugs and proteins for biomedical use. *Pharmaceuticals* **2021**, *14*, 500. [[CrossRef](#)]
5. Barriuso, J.; Nagaraju, R.; Hurlstone, A. Zebrafish: A new companion for translational research in oncology. *Clin. Cancer Res.* **2015**, *21*, 969–975. [[CrossRef](#)]
6. Letrado, P.; De Miguel, I.; Lamberto, I.; Diez-Martínez, R.; Oyarzabal, J. Zebrafish: Speeding up the cancer drug discovery process. *Cancer Res.* **2018**, *78*, 6048–6058. [[CrossRef](#)]
7. Jo, D.H.; Son, D.; Na, Y.; Jang, M.; Choi, J.-H.; Kim, J.H.; Yu, Y.S.; Seok, S.H.; Kim, J.H. Orthotopic transplantation of retinoblastoma cells into vitreous cavity of zebrafish for screening of anticancer drugs. *Mol. Cancer* **2013**, *12*, 71–79. [[CrossRef](#)] [[PubMed](#)]
8. Chen, X.; Wang, J.; Cao, Z.; Hosaka, K.; Jensen, L.; Yang, H.; Sun, Y.; Zhuang, R.; Liu, Y.; Cao, Y. Invasiveness and metastasis of retinoblastoma in an orthotopic zebrafish tumor model. *Sci. Rep.* **2015**, *5*, srep10351. [[CrossRef](#)]
9. Chen, Q.; Ramu, V.; Aydar, Y.; Groenewoud, A.; Zhou, X.-Q.; Jager, M.J.; Cole, H.; Cameron, C.G.; McFarland, S.A.; Bonnet, S.; et al. TLD1433 photosensitizer inhibits conjunctival melanoma cells in zebrafish ectopic and orthotopic tumour models. *Cancers* **2020**, *12*, 587. [[CrossRef](#)] [[PubMed](#)]
10. Zhang, B.; Shimada, Y.; Kuroyanagi, J.; Umemoto, N.; Nishimura, Y.; Tanaka, T. Quantitative phenotyping-based *in vivo* chemical screening in a zebrafish model of leukemia stem cell xenotransplantation. *PLoS ONE* **2014**, *9*, e85439. [[CrossRef](#)]

11. Hill, D.; Chen, L.; Snaar-Jagalska, E.; Chaudhry, B. Embryonic zebrafish xenograft assay of human cancer metastasis. *F1000Research* **2018**, *7*, 1682. [[CrossRef](#)]
12. Jovanovic, P.; Mihajlovic, M.; Djordjevic-Jocic, J.; Vljakovic, S.; Cekic, S.; Stefanovic, V. Ocular melanoma: An overview of the current status. *Int. J. Clin. Exp. Pathol.* **2013**, *6*, 1230–1244. [[PubMed](#)]
13. Yonekawa, Y.; Kim, I.K. Epidemiology and management of uveal melanoma. *Hematol. Oncol. Clin. N. Am.* **2012**, *26*, 1169–1184. [[CrossRef](#)]
14. Mahendraraj, K.; Lau, C.S.; Lee, I.; Chamberlain, R.S. Trends in incidence, survival, and management of uveal melanoma: A population-based study of 7516 patients from the Surveillance, Epidemiology, and End Results database (1973–2012). *Clin. Ophthalmol.* **2016**, *10*, 2113–2119. [[CrossRef](#)]
15. Vivet-Noguer, R.; Tarin, M.; Roman-Roman, S.; Alsafadi, S. Emerging therapeutic opportunities based on current knowledge of uveal melanoma biology. *Cancers* **2019**, *11*, 1019. [[CrossRef](#)]
16. Bedikian, A.Y. Metastatic uveal melanoma therapy. *Int. Ophthalmol. Clin.* **2006**, *46*, 151–166. [[CrossRef](#)]
17. Croce, M.; Ferrini, S.; Pfeffer, U.; Gangemi, R. Targeted therapy of uveal melanoma: Recent failures and new perspectives. *Cancers* **2019**, *11*, 846. [[CrossRef](#)]
18. Diaz, C.E.; Rusciano, D.; Dithmar, S.; Grossniklaus, H.E. B16LS9 melanoma cells spread to the liver from the murine ocular posterior compartment (PC). *Curr. Eye Res.* **1999**, *18*, 125–129. [[CrossRef](#)]
19. Ronca, R.; Giacomini, A.; Di Salle, E.; Coltrini, D.; Pagano, K.; Ragona, L.; Matarazzo, S.; Rezzola, S.; Maiolo, D.; Torella, R.; et al. Long-pentraxin 3 derivative as a small-molecule FGF trap for cancer therapy. *Cancer Cell* **2015**, *28*, 225–239. [[CrossRef](#)] [[PubMed](#)]
20. De Waard-Siebinga, I.; Blom, D.-J.R.; Griffioen, M.; Schrier, P.I.; Hoogendoorn, E.; Beverstock, G.; Danen, E.H.J.; Jager, M.J. Establishment and characterization of an uveal-melanoma cell line. *Int. J. Cancer* **1995**, *62*, 155–161. [[CrossRef](#)] [[PubMed](#)]
21. Rezzola, S.; Guerra, J.; Chandran, A.M.K.; Loda, A.; Cancarini, A.; Sacristani, P.; Semeraro, F.; Presta, M. VEGF-independent activation of Müller cells by the vitreous from proliferative diabetic retinopathy patients. *Int. J. Mol. Sci.* **2021**, *22*, 2179. [[CrossRef](#)]
22. Westerfield, M. *The Zebrafish Book. A Guide for the Laboratory Use of Zebrafish (Danio rerio)*, 4th ed.; University of Oregon Press: Eugene, OR, USA, 2000.
23. Kimmel, C.B.; Ballard, W.W.; Kimmel, S.R.; Ullmann, B.; Schilling, T.F. Stages of embryonic development of the zebrafish. *Dev. Dyn.* **1995**, *203*, 253–310. [[CrossRef](#)]
24. Schindelin, J.; Arganda-Carreras, I.; Frise, E.; Kaynig, V.; Longair, M.; Pietzsch, T.; Preibisch, S.; Rueden, C.; Saalfeld, S.; Schmid, B.; et al. Fiji: An open-source platform for biological-image analysis. *Nat. Methods* **2012**, *9*, 676–682. [[CrossRef](#)]
25. Sabalaukas, N.A.; Foutz, C.A.; Mest, J.R.; Budgeon, L.R.; Sidor, A.T.; Gershenson, J.A.; Joshi, S.B.; Cheng, K.C. High-throughput zebrafish histology. *Methods* **2006**, *39*, 246–254. [[CrossRef](#)] [[PubMed](#)]
26. Malicki, J.; Neuhauss, S.C.; Schier, A.F.; Solnica-Krezel, L.; Stemple, D.L.; Stainier, D.Y.; Abdelilah, S.; Zwartkruis, F.; Rangini, Z.; Driever, W. Mutations affecting development of the zebrafish retina. *Development* **1996**, *123*, 263–273. [[CrossRef](#)]
27. Hashiura, T.; Kimura, E.; Fujisawa, S.; Oikawa, S.; Nonaka, S.; Kurosaka, D.; Hitomi, J. Live imaging of primary ocular vasculature formation in zebrafish. *PLoS ONE* **2017**, *12*, e0176456. [[CrossRef](#)]
28. Singh, A.; Nüsslein-Volhard, C. Zebrafish stripes as a model for vertebrate colour pattern formation. *Curr. Biol.* **2015**, *25*, R81–R92. [[CrossRef](#)]
29. Antinucci, P.; Hindges, R. A crystal-clear zebrafish for in vivo imaging. *Sci. Rep.* **2016**, *6*, 29490. [[CrossRef](#)] [[PubMed](#)]
30. Rusciano, D.; Lorenzoni, P.; Burger, M. Regulation of c-met expression in B16 murine melanoma cells by melanocyte stimulating hormone. *J. Cell Sci.* **1999**, *112 Pt 5*, 623–630. [[CrossRef](#)]
31. Elia, G.; Ren, Y.; Lorenzoni, P.; Zarnegar, R.; Burger, M.M.; Rusciano, D. Mechanisms regulating c-met overexpression in liver-metastatic B16-LS9 melanoma cells. *J. Cell. Biochem.* **2001**, *81*, 477–487. [[CrossRef](#)]
32. Jones, N.M.; Yang, H.; Zhang, Q.; Morales-Tirado, V.M.; Grossniklaus, H.E. Natural killer cells and pigment epithelial-derived factor control the infiltrative and nodular growth of hepatic metastases in an Orthotopic murine model of ocular melanoma. *BMC Cancer* **2019**, *19*, 484. [[CrossRef](#)]
33. Stei, M.M.; Loeffler, K.U.; Holz, F.G.; Herwig-Carl, M. Animal models of uveal melanoma: Methods, applicability, and limitations. *BioMed Res. Int.* **2016**, *2016*, 4521807. [[CrossRef](#)]
34. Yang, W.; Li, H.; Mayhew, E.; Mellon, J.; Chen, P.W.; Niederkorn, J.Y. NKT cell exacerbation of liver metastases arising from melanomas transplanted into either the eyes or spleens of mice. *Investig. Ophthalmol. Vis. Sci.* **2011**, *52*, 3094–3102. [[CrossRef](#)] [[PubMed](#)]
35. Yang, H.; Brackett, C.M.; Morales-Tirado, V.M.; Li, Z.; Zhang, Q.; Wilson, M.W.; Benjamin, C.; Harris, W.; Waller, E.K.; Gudkov, A.; et al. The toll-like receptor 5 agonist entolimod suppresses hepatic metastases in a murine model of ocular melanoma via an NK cell-dependent mechanism. *Oncotarget* **2016**, *7*, 2936–2950. [[CrossRef](#)]
36. Ashur-Fabian, O.; Zloto, O.; Fabian, I.; Tsarfaty, G.; Ellis, M.; Steinberg, D.M.; Hercbergs, A.; Davis, P.J.; Fabian, I.D. Tetrac delayed the onset of ocular melanoma in an orthotopic mouse model. *Front. Endocrinol.* **2018**, *9*, 775. [[CrossRef](#)] [[PubMed](#)]
37. Rezzola, S.; Ronca, R.; Loda, A.; Nawaz, M.I.; Tobia, C.; Paganini, G.; Maccarinelli, F.; Giacomini, A.; Semeraro, F.; Mor, M.; et al. The autocrine FGF/FGFR system in both skin and uveal melanoma: FGF trapping as a possible therapeutic approach. *Cancers* **2019**, *11*, 1305. [[CrossRef](#)] [[PubMed](#)]
38. Owinsky, E.R.K.R.; Onehower, R.O.C.D. Paclitaxel (taxol). *N. Engl. J. Med.* **1995**, *332*, 1004–1014. [[CrossRef](#)]

39. Cassar, S.; Adatto, I.; Freeman, J.L.; Gamse, J.T.; Iturria, I.; Lawrence, C.; Muriana, A.; Peterson, R.T.; Van Cruchten, S.; Zon, L.I. Use of zebrafish in drug discovery toxicology. *Chem. Res. Toxicol.* **2020**, *33*, 95–118. [[CrossRef](#)]
40. Scuto, A.; Kirschbaum, M.; Kowolik, C.; Kretzner, L.; Juhasz, A.; Atadja, P.; Pullarkat, V.; Bhatia, R.; Forman, S.; Yen, Y.; et al. The novel histone deacetylase inhibitor, LBH589, induces expression of DNA damage response genes and apoptosis in Ph- acute lymphoblastic leukemia cells. *Blood* **2008**, *111*, 5093–5100. [[CrossRef](#)]
41. O'Reilly, T.; McSheehy, P.M. Biomarker development for the clinical activity of the mTOR inhibitor everolimus (RAD001): Processes, limitations, and further proposals. *Transl. Oncol.* **2010**, *3*, 65–79. [[CrossRef](#)]
42. Faião-Flores, F.; Emmons, M.F.; Durante, M.A.; Kinose, F.; Saha, B.; Fang, B.; Koomen, J.M.; Chellappan, S.P.; Maria-Engler, S.; Rix, U.; et al. HDAC inhibition enhances the in vivo efficacy of MEK inhibitor therapy in uveal melanoma. *Clin. Cancer Res.* **2019**, *25*, 5686–5701. [[CrossRef](#)] [[PubMed](#)]
43. Amirouchene-Angelozzi, N.; Frisch-Dit-Leitz, E.; Carita, G.; Dahmani, A.; Raymondie, C.; Liot, G.; Gentien, D.; Némati, F.; Decaudin, D.; Roman-Roman, S.; et al. The mTOR inhibitor Everolimus synergizes with the PI3K inhibitor GDC0941 to enhance anti-tumor efficacy in uveal melanoma. *Oncotarget* **2016**, *7*, 23633–23646. [[CrossRef](#)]
44. Shoushtari, A.N.; Ong, L.T.; Schoder, H.; Singh-Kandah, S.; Abbate, K.T.; Postow, M.A.; Callahan, M.K.; Wolchok, J.; Chapman, P.B.; Panageas, K.S.; et al. A phase 2 trial of everolimus and pasireotide long-acting release in patients with metastatic uveal melanoma. *Melanoma Res.* **2016**, *26*, 272–277. [[CrossRef](#)] [[PubMed](#)]
45. Homsy, J.; Bedikian, A.Y.; Papadopoulos, N.E.; Kim, K.B.; Hwu, W.-J.; Mahoney, S.L.; Hwu, P. Phase 2 open-label study of weekly docosahexaenoic acid-paclitaxel in patients with metastatic uveal melanoma. *Melanoma Res.* **2010**, *20*, 507–510. [[CrossRef](#)]
46. Van der Ent, W.; Burrello, C.; Teunisse, A.F.A.S.; Ksander, B.R.; Van Der Velden, P.A.; Jager, M.J.; Jochemsen, A.G.; Snaar-Jagalska, B.E. Modeling of human uveal melanoma in zebrafish xenograft embryos. *Investig. Ophthalmol. Vis. Sci.* **2014**, *55*, 6612–6622. [[CrossRef](#)]
47. Fornabaio, G.; Barnhill, R.L.; Lugassy, C.; Bentolila, L.A.; Cassoux, N.; Roman-Roman, S.; Alsafadi, S.; Del Bene, F. Angiotropism and extravascular migratory metastasis in cutaneous and uveal melanoma progression in a zebrafish model. *Sci. Rep.* **2018**, *8*, 10448. [[CrossRef](#)]
48. Van der Ent, W.; Burrello, C.; De Lange, M.J.; Van Der Velden, P.A.; Jochemsen, A.G.; Jager, M.J.; Snaar-Jagalska, B.E. Embryonic zebrafish: Different phenotypes after injection of human uveal melanoma cells. *Ocul. Oncol. Pathol.* **2015**, *1*, 170–181. [[CrossRef](#)] [[PubMed](#)]
49. Yu, L.; Zhou, D.; Zhang, G.; Ren, Z.; Luo, X.; Liu, P.; Plouffe, S.W.; Meng, Z.; Moroishi, T.; Li, Y.; et al. Co-occurrence of BAP1 and SF3B1 mutations in uveal melanoma induces cellular senescence. *Mol. Oncol.* **2021**. [[CrossRef](#)] [[PubMed](#)]
50. Arepalli, S.; Kaliki, S.; Shields, C.L. Choroidal metastases: Origin, features, and therapy. *Indian J. Ophthalmol.* **2015**, *63*, 122–127. [[CrossRef](#)]





## **Uveal Melanoma Cells Impair the Anti-tumor Activity of Natural Killer Lymphocytes**

**A. Loda**, G. Mutti, M. Rossignoli, F. Semeraro, G. Tabellini, S. Parolini, S. Rezzola.

*Unpublished results.*



## INTRODUCTION

Natural Killer (NK) cells are a highly specialized population belonging to the innate immune response system. In humans, two major subgroups of NK cells have been described.  $CD56^{\text{bright}}/CD16^{-/\text{low}}$  NK cells are involved in regulating adaptive immunity through the production of cytokines and chemokines, while  $CD56^{\text{dim}}/CD16^{\text{high}}$  NK cells are directly responsible for eliminating damaged, infected, or malignant target cells [114]. Moreover, a peculiar subset of poorly cytotoxic, pro-angiogenic NK cells has been identified in the decidual uterine region.  $CD56^{\text{bright}}/CD16^{-}$ ,  $CD9^{+}$ ,  $CD49a^{+}$  decidual NK cells (dNK) have nurturing functions, supporting embryo implant and fetal development [115].

The biological activity of NK cells is finely regulated by the interplay between activating and inhibitory surface receptors. Activating signals, mediated by natural cytotoxicity receptors, such as NKp46 and NKp30, as well as CD16, NKG2D, and DNAM1, are necessary to exert cytotoxic functions against damaged, infected, or malignant cells. On the other hand, inhibitory receptors such as long cytoplasmatic domain killer-cell immunoglobulin-like receptors (KIRs) and NKG2A, are important for preventing the unwanted attack of self, healthy cells [116].

NK cells play a pivotal role in protecting against cancer growth and metastatic dissemination [117, 118]. However, tumors may develop different immune-escape strategies, including the reprogramming of cytotoxic NK cells to a decidual-like phenotype (dNK-like) (**Figure 6**) [118-120]. In addition to their subdued cytotoxic activity, dNK-like cells produce various pro-angiogenic mediators, such as vascular endothelial growth factor (VEGF), placental growth factor (PlGF), angiopoietin 1 (ANG-1), and ANG-2, and they promote tissue remodeling through the expression of metalloproteases [121, 122]. To date, the presence of dNK-like has been reported in various tumor types, including non-small lung cancer, colorectal cancer, prostate cancer, and high-grade serous ovarian cancer [120, 122-124]. Moreover, increasing evidence suggests that dNK-like cells are present also in the peripheral blood of patients and that they could be exploitable as tumor biomarkers [122, 125].

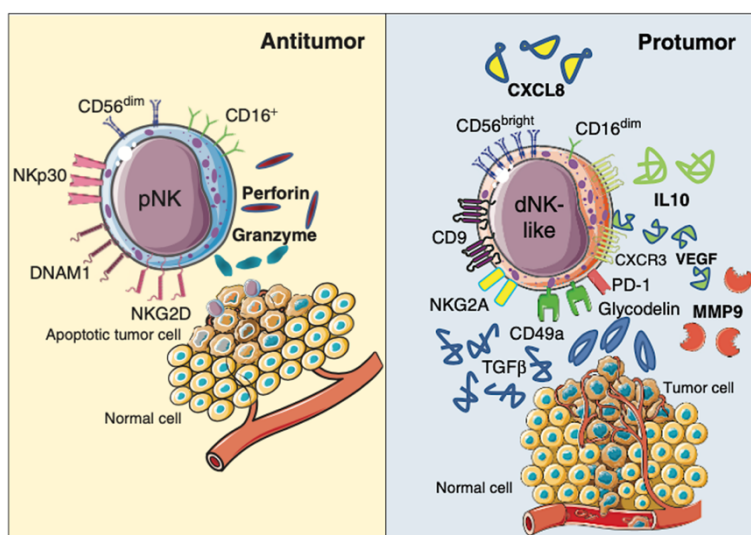


**Figure 6. Different states of NK lymphocytes polarization.**  $CD56^{\text{dim}}/CD16^{+}$  cytotoxic NK lymphocytes (left panel) release lytic enzymes to eliminate malignant cells, while  $CD56^{\text{bright}}/CD16^{\text{dim}}/CD9^{+}/CD49a^{+}$  dNK-like cells produce pro-angiogenic factors that sustain tumor progression. Adapted from [121].

---

Currently, it has been demonstrated that polarization of NK cells towards a dNK-like phenotype may be due to immunosuppressive factors in the tumor microenvironment, with studies pointing to TGF $\beta$  as a main actor in this process [119, 126]. TGF $\beta$  is known to exert a pro-oncogenic role in advanced tumors, where it sustains tumor growth, epithelial-to-mesenchymal transition, angiogenesis, and evasion of immune surveillance [127]. Due to its involvement in tumor progression, targeting TGF $\beta$  represents an interesting therapeutic strategy and several inhibitory approaches have been developed. Among them, the neutralizing antibody fresolimumab has obtained positive results in clinical trials for various tumor types, including renal carcinoma, metastatic breast cancer, and cutaneous melanoma [128].

To date, knowledge on the interplay between NK cells and UM is very limited [129]. Even though decidua-like polarization of NK cells in UM has not been previously described, the production of TGF $\beta$  has been reported in tumor samples from patients [130]. In addition, even though the liver is the organ with the highest concentration of NK cells, it represents the preferential site of UM metastasization. Therefore, we hypothesize that the acquisition of a pro-tumor, decidua-like phenotype by NK lymphocytes may be a critical step in the growth of UM primary tumors as well as in the establishment of a permissive microenvironment that allows for the formation of metastatic lesions.

---

## MATERIALS AND METHODS

### 1. Cell cultures

Human UM cell lines 92.1, Mel285, and Mel270 were obtained from M. Jager (Leiden University, The Netherlands) and cultured in RPMI 1640 medium supplemented with 100 U/mL penicillin, 100 µg/ml streptomycin, and 10% fetal bovine serum (FBS) or 20% FBS for 92.1 and Mel285 or Mel270 UM cells, respectively.

For conditioned media (CM) collection, Mel285, 92.1, and Mel270 cells were seeded at  $2 \times 10^4$  cells/cm<sup>2</sup> in complete medium. After 24 h, medium was replaced with RPMI 0% FBS and cells were cultured for 48 h. Then, CM were harvested, filtered (0.45 µm) and concentrated 10 times.

Peripheral blood mononuclear cells (PBMCs) were isolated from blood of healthy donors (HDs) by density gradient centrifugation over Ficoll-Hypaque 1070 and cultured in RPMI 1640 medium supplemented with 100 U/mL penicillin, 100 µg/ml streptomycin, 10 µg/ml ciproxin and with 10% FBS.

### 2. Semi-quantitative PCR analysis

92.1, Mel270, and Mel285 cells were harvested, and total RNA was extracted using Trizol Reagent. Contaminating DNA was eliminated using DNase before performing retrotranscription. For each sample, 2 µg of RNA were retrotranscribed using MMLV reverse transcriptase. cDNA was then amplified, and the PCR products were electrophoresed on a 2% agarose gel.

### 3. NK lymphocyte polarization

PBMCs isolated from healthy donors were plated at  $2 \times 10^6$  cells/cm<sup>2</sup> in 24-well plates and polarized with 100 U/ml interleukin-2 (IL2), either alone or in the presence of 10 ng/ml TGFβ or 1:2 dilution (*vol:vol*) of CM. PBMC received treatments at day 0 and at 48 h. FACS analysis was performed following 72 h of treatment.

### 4. Phenotype characterization of NKs

The effect of UM-derived CM on NK lymphocytes was evaluated by flow cytometry. A total of  $4 \times 10^6$  PBMCs were stained with anti-human primary monoclonal antibodies as it follows: FITC-conjugated anti-CD3, PC5-conjugated anti-CD56, FITC-conjugated anti-CD14, FITC-conjugated anti-CD20 (Beckman Coulter), PE-conjugated anti-CD9 (Miltenyi Biotec), PE-conjugated anti-CD49a (Miltenyi Biotec), anti-NKG2D, anti-NKp30, anti-NKp46, anti-DNAM (developed in our lab). When required, cells were also incubated with PE-conjugated secondary antibodies for 30 minutes.

For the analysis of intracellular lytic enzymes, PBMCs were first labeled with FITC-conjugated anti-CD3, PC5 conjugated anti-CD56, FITC-conjugated anti-CD14, and FITC-conjugated anti-CD20 (Beckman Coulter). Then, cells were fixed and permeabilized using Cytofix/Cytoperm solution (BD Biosciences) for 20 minutes at 4°C. Next, cells were incubated with saponin (0.9% NaCl, 1% FBS, 0.1% saponin) and PE-conjugated anti-perforin and anti-granzyme B monoclonal antibodies (developed in our lab) for 30 minutes. Protein expression was analyzed on total CD3<sup>+</sup>/CD56<sup>+</sup> NK cells.

### 5. Cytofluorimetric analysis of degranulation activity

After 72 h of polarization, the ability of NK lymphocytes to degranulate against K562 cell line was assessed by analyzing the expression of CD107a. PBMCs and K562 cells were co-cultured at a 1:3 ratio, in the presence of PE-conjugated anti-CD107a (BD Biosciences) and Golgi Stop (Monesin, BD

Biosciences) for 4 h. CD107a expression, as a readout of degranulation activities, was detected on CD3<sup>-</sup>/CD56<sup>+</sup> total NK cells by flow cytometry.

## RESULTS

### 1. TGF $\beta$ overexpression correlates with a decrease of survival in UM patients

TGF $\beta$  has been demonstrated to impair human NK cells in *in vitro* models, shifting their differentiation towards a decidual-like phenotype [131]; additionally, TGF $\beta$  exerts a pro-oncogenic role, and it takes part in modulating the tumor microenvironment [128, 132]. To better understand the involvement of TGF $\beta$  in UM, we have assessed the expression of TGF $\beta$  isoforms by performing a bioinformatic analysis on the publicly available The Cancer Genome Atlas (TCGA) UM Firehose Legacy dataset ([https://www.cbioportal.org/study/summary?426id=uvn\\_tcga](https://www.cbioportal.org/study/summary?426id=uvn_tcga)). Our analysis reveals the overexpression of members of the TGF $\beta$  family in approximately 20% of patients (**Figure 1A**); moreover, TGF $\beta$  overexpression is linked to a worse prognosis in terms of disease-free survival (**Figure 1B**). On this premise, we have assessed the expression of TGF $\beta$  in our human UM cell lines by semi-quantitative PCR. As shown in **Figure 1C**, high expression of TGF $\beta$ 1 was detected across all lines, with a strong expression of TGF $\beta$ 2 as well in Mel285 cells.

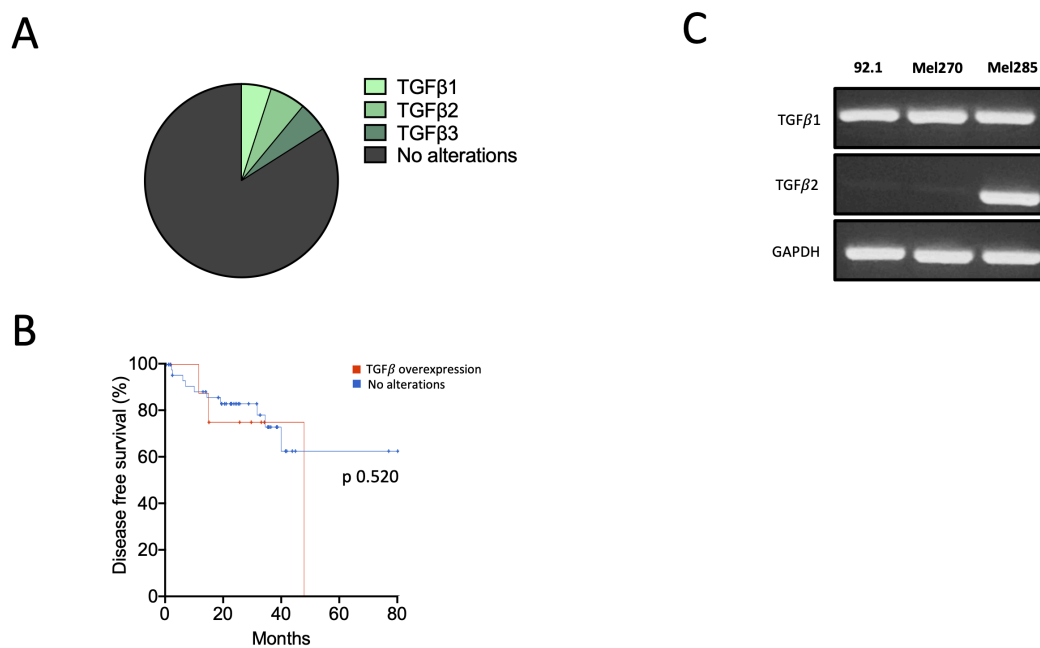


**Figure 1. Analysis of TGF $\beta$  expression in UM tumor samples and cell lines. A)** Analysis of TGF $\beta$  overexpression in 80 UM patients from TCGA UM Firehose Legacy dataset. **B)** Disease-free survival in UM patients overexpressing TGF $\beta$ . **C)** Expression of TGF $\beta$  1 and TGF $\beta$  2 in 92.1, Mel270 and Mel285 UM cell lines, as assessed by semi-quantitative PCR.



## 2. UM cells significantly induces a decidual-like phenotype in NK lymphocytes

Next, we analyzed whether the conditioned media derived from UM cells could affect NK polarization. To this purpose, PBMCs from healthy donors were stimulated for 72 h with the activating cytokine interleukin-2 (IL2), in the presence of either 10 ng/ml TGF $\beta$  or 1:2 (vol:vol) of the conditioned medium (CM) obtained from Mel285, 92.1 or Mel270 UM cells. Then, NK phenotype was assessed by flow cytometry. Our results demonstrate the downregulation of the activating receptors NKp30, NKG2D, and DNAM in the presence of UM-derived CM (**Figure 2A**), whereas markers of decidual-like polarization (*i.e.*, CD9 and CD49) were upregulated (**Figure 2B**); the effect of UM-derived CM was comparable to that exerted by TGF $\beta$ .

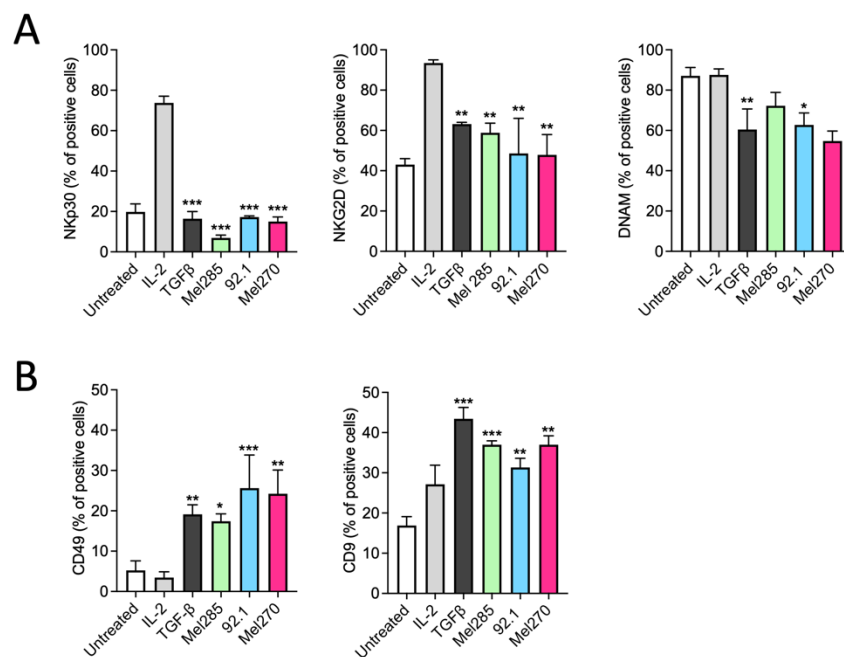


**Figure 2. UM cells induce a decidual-like phenotype in NK lymphocytes.** PBMCs were isolated from healthy donors and cultured for 72 hours with interleukin 2 (IL-2) in the absence or in the presence of 10 ng/ml TGF $\beta$  or 1:2 (vol:vol) of the conditioned medium (CM) obtained by Mel285, 92.1 or Mel270 UM cells. The expression of the activating receptors NKp30, NKG2D, and DNAM (**A**), as well as decidual-like markers CD49 and CD9 (**B**) was assessed by flow cytometry. \*  $p < 0.05$ ; \*\* $p < 0.01$ ; \*\*\* $p < 0.001$  vs IL-2-treated NK cells (ANOVA) (**A**) or vs untreated NK cells (**B**).

### 3. UM Cells Impair the Cytotoxic Activity of NK Lymphocytes

Finally, we evaluated whether UM-derived CM could impair NK cytotoxic activity. As shown in **Figure 3A**, treatment with either TGF $\beta$  or Mel285-derived CM reduces the production of lytic enzymes perforin and granzyme B. Moreover, degranulation efficiency against the human erythroleukemia K562 cell line, a target particularly susceptible to NK cell lysis, is significantly inhibited, as demonstrated by the low surface expression of CD107a (**Figure 3B**).

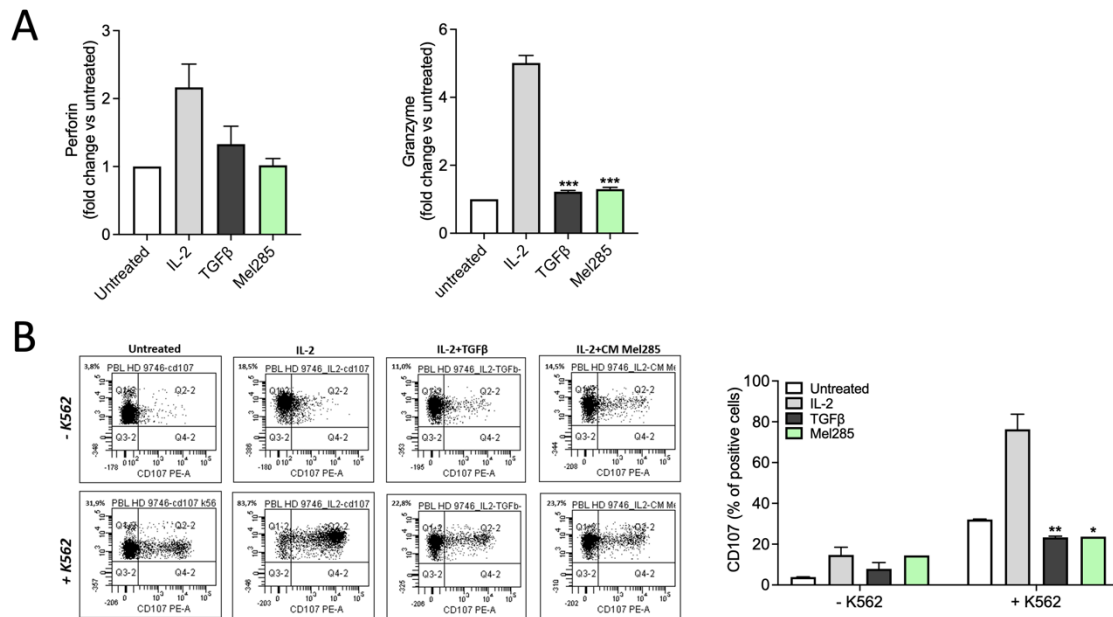


**Figure 3. UM-derived CM inhibits the cytotoxic activity of NK cells.** PBMCs were isolated from healthy donors and cultured for 72 hours with IL-2 in the absence or in the presence of 10 ng/ml TGF $\beta$  or 1:2 (vol:vol) of Mel285 cell CM. **A)** Expression of granzyme B and perforin was assessed by flow cytometry. **B)** NK degranulation against K562 target cells was assessed by analyzing membrane expression of CD107a by flow cytometry. \*  $p < 0.05$ , \*\* $p < 0.01$  and \*\*\* $p < 0.001$  vs IL-2-treated NK cells (ANOVA).

---

## CONCLUSIONS

The immune system plays a critical role in cancer growth, dissemination, and response to therapies. Among alterations affecting innate immune cells, NK lymphocytes may lose their cytotoxic activity and acquire a pro-oncogenic/pro-angiogenic decidual-like phenotype, which actively sustains tumor progression [121].

Our preliminary results indicate that the CM derived from UM cells can reprogram NK lymphocytes, upregulating the expression of decidual-like markers while downregulating activating receptors. In addition, UM-CM reduces NK cytotoxic activity. Together, these data point to the capability of UM cells to modulate the immunologic response of NK lymphocytes. In this context, we showed that UM cells express high levels of the immunosuppressive cytokine TGF $\beta$ , which has been identified as the major regulator of decidual-like NK polarization. Accordingly, UM patients overexpressing TGF $\beta$  have a worse prognosis in terms of disease-free survival. These results set the basis for further analyses aimed at defining the impact of UM-derived TGF $\beta$  on NK reprogramming and hint at TGF $\beta$  as a potential target for the treatment of primary and metastatic UM.

---

## DISCUSSION

Uveal melanoma (UM) is a very aggressive tumor. Due to lack of effective pharmacological therapies, patients affected by metastatic disease have a very poor prognosis, spanning from 3 to 12 months after diagnosis. Therefore, novel therapeutic strategies are eagerly required. In this frame, our research activities have been aimed at gaining a better understanding on the mechanism that regulate tumor progression, in order to identify new potential targets. On one hand, we have assessed the efficacy of hampering the tumor component by inhibiting the Fibroblast Growth Factor (FGF)/FGF Receptor (FGFR) signaling pathway; on the other, we are investigating the immunomodulation strategies exploited by UM to escape Natural Killer (NK) lymphocyte control.

The presence of an autocrine FGF/FGFR activation loop in UM has been previously demonstrated [91, 133, 134]. In this frame, our work has further characterized the effect of FGF/FGFR signaling blockade on UM, highlighting the efficacy of the pan FGF-trap NSC12 in reducing cell proliferation, migration, and survival of UM cell lines [103]. In addition, we have shown the overexpression of FGFRs or FGFs in approximately 60% and 21% of UM patients, which is associated to a worse prognosis [92, 103, 134]. However, the role of FGF-mediated signaling is not limited to tumor regulation and progression. In fact, it has also been linked to the maintenance of cancer stem-like cells (CSCs), a subpopulation of tumor cells crucially involved in tumorigenesis, metastatic dissemination, therapy resistance, and recurrence. On this premise, we have demonstrated for the first time that the inhibition of the FGF/FGFR system is an exploitable strategy to target CSCs in UM. Our results indicate an impairment in the stem-like component, both *in vitro* and *in vivo*, due to the enhanced sensitivity of CSCs to FGF-deprivation following treatment with NSC12. Of note, we have found a strong association between FGFs/FGFRs and stemness in the clinical setting, which has been linked to a poorer prognosis in patients. Altogether, our results demonstrate that targeting the FGF/FGFR system could represent an exploitable strategy to strike both differentiated and stem-like cells and pave the way for the development of novel pharmacological therapies. In this context, given that reliable experimental models of the disease are essential for *in vivo* drug screening, we have recently established the first orthotopic model of UM in zebrafish.

The zebrafish embryo is an extremely useful tool for modeling human cancers and for performing large-scale screening of new drugs, due to ease of manipulation, optical transparency, and relatively low costs of maintenance. In our model, 92.1 UM cells were engrafted at 48 hours post fertilization in close proximity to the developing choroidal vasculature of zebrafish embryos. In the following days, grafted cells proliferate and migrate towards the eye surface, confirming that the zebrafish eye is a permissive environment for tumor growth. Additionally, we have set up a reliable and accurate method for assessing xenograft tumor growth, which overcomes the limitations of fluorescence quantification by exploiting the bioluminescent signal of tumor cells transduced with luciferase. Our model was exploited to demonstrate the efficacy of chemotherapeutic drugs paclitaxel, everolimus, and panobinostat in inhibiting *in vivo* tumor growth.

Recently, the advent of immune-based strategies has significantly improved the management of many tumor types, including cutaneous melanoma; however, clinical studies have demonstrated that similar approaches are ineffective in UM [135]. While the exact mechanisms of immune escape exploited by UM are still unclear, modulation of tumor microenvironment could be involved in the inactivation of immune cells, favoring tumor progression and metastatic dissemination. In this frame, NK lymphocytes

are important regulators of cancer immunosurveillance and their activity is finely controlled by the expression of specific activating and inhibitory receptors that allow them to discriminate and eliminate malignant cells [136]. However, the presence of a pro-tumor/pro-angiogenic subpopulation of decidual-like NK lymphocytes has been identified in many types of tumors. On this premise, we have investigated whether decidual-like polarization of NK lymphocytes could be involved in UM, as a process sustaining tumor progression as well as the establishment of metastatic lesions. Our data demonstrate that the CM from UM cells can reprogram NK lymphocytes to a decidual-like state, characterized by a reduced cytotoxic activity. In this context, the expression of the immunosuppressive cytokine TGF $\beta$  by UM cell lines supports the hypothesis that soluble factors within the tumor microenvironment could actively create permissive conditions for UM growth and dissemination through immune modulation. Our results set the basis for further analysis aimed at assessing the impact of UM-derived TGF $\beta$  on NK reprogramming; moreover, they hint at TGF $\beta$  as a potential target for the treatment of primary and metastatic UM.

To date, the pharmacological treatment of metastatic UM remains a major challenge. In this regard, during my PhD I was involved in characterizing alternative approaches to strike tumor cells as well as the stromal compartment. While further studies are needed, our findings take us one step closer to developing new therapeutic strategies to significantly improve patients' survival.

---

## BIBLIOGRAPHY

1. Kivelä, T., *Incidence, prevalence and epidemiology of ocular melanoma*. 2014: Future Medicine.
2. Woodman, S.E., *Metastatic uveal melanoma: biology and emerging treatments*. *Cancer J*, 2012. **18**(2): p. 148-52.
3. Cholkar, K., et al., *Eye: anatomy, physiology and barriers to drug delivery*. 2013.
4. Mafee, M.F., et al., *Anatomy and pathology of the eye: role of MR imaging and CT*. *Magn Reson Imaging Clin N Am*, 2006. **14**(2): p. 249-70.
5. Malhotra, A., et al., *Ocular anatomy and cross-sectional imaging of the eye*. *Semin Ultrasound CT MR*, 2011. **32**(1): p. 2-13.
6. Sandford-Smith, J., *Eye Diseases in Hot Climates*. 1990, Butterworth-Heinemann.
7. Branisteanu, D.C., et al., *Uveal melanoma diagnosis and current treatment options (Review)*. *Exp Ther Med*, 2021. **22**(6): p. 1428.
8. Chattopadhyay, C., et al., *Uveal melanoma: From diagnosis to treatment and the science in between*. *Cancer*, 2016. **122**(15): p. 2299-312.
9. Shoushtari, A.N. and R.D. Carvajal, *GNAQ and GNA11 mutations in uveal melanoma*. *Melanoma Res*, 2014. **24**(6): p. 525-34.
10. Pašalić, D., et al., *Genetic and Epigenetic Features of Uveal Melanoma-An Overview and Clinical Implications*. *Int J Mol Sci*, 2023. **24**(16).
11. Furney, S.J., et al., *SF3B1 mutations are associated with alternative splicing in uveal melanoma*. *Cancer Discov*, 2013. **3**(10): p. 1122-1129.
12. Bakhoun, M.F., et al., *BAP1 methylation: a prognostic marker of uveal melanoma metastasis*. *NPJ Precis Oncol*, 2021. **5**(1): p. 89.
13. Harbour, J.W., *A prognostic test to predict the risk of metastasis in uveal melanoma based on a 15-gene expression profile*. *Methods Mol Biol*, 2014. **1102**: p. 427-40.
14. Scheffler, A.C., et al., *Relationship between clinical features, GEP class, and PRAME expression in uveal melanoma*. *Graefes Arch Clin Exp Ophthalmol*, 2019. **257**(7): p. 1541-1545.
15. Brewington, B.Y., et al., *Brachytherapy for patients with uveal melanoma: historical perspectives and future treatment directions*. *Clin Ophthalmol*, 2018. **12**: p. 925-934.
16. Chojniak, M.M., et al., *Primary transpupillary thermotherapy for small choroidal melanoma*. *Graefes Arch Clin Exp Ophthalmol*, 2011. **249**(12): p. 1859-65.
17. Bai, H., J.J. Bosch, and L.M. Heindl, *Current management of uveal melanoma: A review*. *Clin Exp Ophthalmol*, 2023. **51**(5): p. 484-494.
18. Wespiser, M., E. Neidhardt, and S. Negrier, *Uveal melanoma: In the era of new treatments*. *Cancer Treat Rev*, 2023. **119**: p. 102599.
19. Croce, M., et al., *Targeted Therapy of Uveal Melanoma: Recent Failures and New Perspectives*. *Cancers (Basel)*, 2019. **11**(6).
20. Yang, J., et al., *Treatment of uveal melanoma: where are we now?* *Ther Adv Med Oncol*, 2018. **10**: p. 1758834018757175.
21. Durante, M.A., et al., *Single-cell analysis reveals new evolutionary complexity in uveal melanoma*. *Nat Commun*, 2020. **11**(1): p. 496.

22. Howlett, S., et al., *Tebentafusp: a first-in-class treatment for metastatic uveal melanoma*. Ther Adv Med Oncol, 2023. **15**: p. 17588359231160140.
23. Montazeri, K., V. Pattanayak, and R.J. Sullivan, *Tebentafusp in the Treatment of Metastatic Uveal Melanoma: Patient Selection and Special Considerations*. Drug Des Devel Ther, 2023. **17**: p. 333-339.
24. Qiu, H., et al., *Cancer stem cells: a potential target for cancer therapy*. Cell Mol Life Sci, 2015. **72**(18): p. 3411-24.
25. Yadav, A.K. and N.S. Desai, *Cancer Stem Cells: Acquisition, Characteristics, Therapeutic Implications, Targeting Strategies and Future Prospects*. Stem Cell Rev Rep, 2019. **15**(3): p. 331-355.
26. Eun, K., S.W. Ham, and H. Kim, *Cancer stem cell heterogeneity: origin and new perspectives on CSC targeting*. BMB Rep, 2017. **50**(3): p. 117-125.
27. Battle, E. and H. Clevers, *Cancer stem cells revisited*. Nat Med, 2017. **23**(10): p. 1124-1134.
28. Prieto-Vila, M., et al., *Drug Resistance Driven by Cancer Stem Cells and Their Niche*. Int J Mol Sci, 2017. **18**(12).
29. Bonnet, D. and J.E. Dick, *Human acute myeloid leukemia is organized as a hierarchy that originates from a primitive hematopoietic cell*. Nat Med, 1997. **3**(7): p. 730-7.
30. Alamgeer, M., et al., *Cancer stem cells in lung cancer: Evidence and controversies*. Respirology, 2013. **18**(5): p. 757-64.
31. Yamashita, T. and X.W. Wang, *Cancer stem cells in the development of liver cancer*. J Clin Invest, 2013. **123**(5): p. 1911-8.
32. Al-Hajj, M., et al., *Prospective identification of tumorigenic breast cancer cells*. Proc Natl Acad Sci U S A, 2003. **100**(7): p. 3983-8.
33. Takaishi, S., et al., *Identification of gastric cancer stem cells using the cell surface marker CD44*. Stem Cells, 2009. **27**(5): p. 1006-20.
34. Li, C., et al., *Identification of pancreatic cancer stem cells*. Cancer Res, 2007. **67**(3): p. 1030-7.
35. Yang, Y.M. and J.W. Chang, *Bladder cancer initiating cells (BCICs) are among EMA-CD44v6+ subset: novel methods for isolating undetermined cancer stem (initiating) cells*. Cancer Invest, 2008. **26**(7): p. 725-33.
36. Vaiopoulos, A.G., et al., *Colorectal cancer stem cells*. Stem Cells, 2012. **30**(3): p. 363-71.
37. Schatton, T., et al., *Identification of cells initiating human melanomas*. Nature, 2008. **451**(7176): p. 345-9.
38. Kalirai, H., B.E. Damato, and S.E. Coupland, *Uveal melanoma cell lines contain stem-like cells that self-renew, produce differentiated progeny, and survive chemotherapy*. Invest Ophthalmol Vis Sci, 2011. **52**(11): p. 8458-66.
39. Walcher, L., et al., *Cancer Stem Cells-Origins and Biomarkers: Perspectives for Targeted Personalized Therapies*. Front Immunol, 2020. **11**: p. 1280.
40. Gopalan, V., F. Islam, and A.K. Lam, *Surface Markers for the Identification of Cancer Stem Cells*. Methods Mol Biol, 2018. **1692**: p. 17-29.
41. Toledo-Guzmán, M.E., et al., *ALDH as a Stem Cell Marker in Solid Tumors*. Curr Stem Cell Res Ther, 2019. **14**(5): p. 375-388.

42. Ishiguro, T., et al., *Tumor-derived spheroids: Relevance to cancer stem cells and clinical applications*. *Cancer Sci*, 2017. **108**(3): p. 283-289.
43. Huang, T., et al., *Stem cell programs in cancer initiation, progression, and therapy resistance*. *Theranostics*, 2020. **10**(19): p. 8721-8743.
44. Cochrane, C.R., et al., *Hedgehog Signaling in the Maintenance of Cancer Stem Cells*. *Cancers (Basel)*, 2015. **7**(3): p. 1554-85.
45. Meisel, C.T., C. Porcheri, and T.A. Mitsiadis, *Cancer Stem Cells, Quo Vadis? The Notch Signaling Pathway in Tumor Initiation and Progression*. *Cells*, 2020. **9**(8).
46. Mohiuddin, I.S., S.J. Wei, and M.H. Kang, *Role of OCT4 in cancer stem-like cells and chemotherapy resistance*. *Biochim Biophys Acta Mol Basis Dis*, 2020. **1866**(4): p. 165432.
47. Vasefifar, P., et al., *Nanog, as a key cancer stem cell marker in tumor progression*. *Gene*, 2022. **827**: p. 146448.
48. Steinbichler, T.B., et al., *Cancer stem cells and their unique role in metastatic spread*. *Semin Cancer Biol*, 2020. **60**: p. 148-156.
49. Puisieux, A., T. Brabletz, and J. Caramel, *Oncogenic roles of EMT-inducing transcription factors*. *Nat Cell Biol*, 2014. **16**(6): p. 488-94.
50. Shibue, T. and R.A. Weinberg, *EMT, CSCs, and drug resistance: the mechanistic link and clinical implications*. *Nat Rev Clin Oncol*, 2017. **14**(10): p. 611-629.
51. Barbato, L., et al., *Cancer Stem Cells and Targeting Strategies*. *Cells*, 2019. **8**(8).
52. Maugeri-Saccà, M., M. Bartucci, and R. De Maria, *DNA damage repair pathways in cancer stem cells*. *Mol Cancer Ther*, 2012. **11**(8): p. 1627-36.
53. Tomita, H., et al., *Aldehyde dehydrogenase 1A1 in stem cells and cancer*. *Oncotarget*, 2016. **7**(10): p. 11018-32.
54. Dean, M., *ABC transporters, drug resistance, and cancer stem cells*. *J Mammary Gland Biol Neoplasia*, 2009. **14**(1): p. 3-9.
55. Takebe, N., et al., *Targeting Notch, Hedgehog, and Wnt pathways in cancer stem cells: clinical update*. *Nat Rev Clin Oncol*, 2015. **12**(8): p. 445-64.
56. Yang, L., et al., *Targeting cancer stem cell pathways for cancer therapy*. *Signal Transduct Target Ther*, 2020. **5**(1): p. 8.
57. Saygin, C., et al., *Targeting Cancer Stemness in the Clinic: From Hype to Hope*. *Cell Stem Cell*, 2019. **24**(1): p. 25-40.
58. Dragu, D.L., et al., *Therapies targeting cancer stem cells: Current trends and future challenges*. *World J Stem Cells*, 2015. **7**(9): p. 1185-201.
59. Huang, B., X. Yan, and Y. Li, *Cancer Stem Cell for Tumor Therapy*. *Cancers (Basel)*, 2021. **13**(19).
60. Sun, H.R., et al., *Therapeutic Strategies Targeting Cancer Stem Cells and Their Microenvironment*. *Front Oncol*, 2019. **9**: p. 1104.
61. Thill, M., et al., *Expression of CD133 and other putative stem cell markers in uveal melanoma*. *Melanoma Res*, 2011. **21**(5): p. 405-16.
62. Djirackor, L., et al., *CD166high Uveal Melanoma Cells Represent a Subpopulation With Enhanced Migratory Capacity*. *Invest Ophthalmol Vis Sci*, 2019. **60**(7): p. 2696-2704.
63. Tuccitto, A., et al., *Melanoma Stem Cell Sphere Formation Assay*. *Bio Protoc*, 2017. **7**(8): p. e2233.



64. Duan, J.J., et al., *ALDEFLUOR activity, ALDH isoforms, and their clinical significance in cancers*. J Enzyme Inhib Med Chem, 2023. **38**(1): p. 2166035.
65. Jin, B., et al., *Verification of EZH2 as a druggable target in metastatic uveal melanoma*. Mol Cancer, 2020. **19**(1): p. 52.
66. Moschos, M.M., et al., *The Role of Histone Deacetylase Inhibitors in Uveal Melanoma: Current Evidence*. Anticancer Res, 2018. **38**(7): p. 3817-3824.
67. Wang, Y., et al., *In vitro and in vivo anti-uveal melanoma activity of JSL-1, a novel HDAC inhibitor*. Cancer Lett, 2017. **400**: p. 47-60.
68. Zhang, B., J. Zhang, and J. Pan, *Pristimerin effectively inhibits the malignant phenotypes of uveal melanoma cells by targeting NF- $\kappa$ B pathway*. Int J Oncol, 2017. **51**(3): p. 887-898.
69. Zhou, J., et al., *The antihelminthic drug niclosamide effectively inhibits the malignant phenotypes of uveal melanoma*. Theranostics, 2017. **7**(6): p. 1447-1462.
70. Naujokat, C. and R. Steinhart, *Salinomycin as a drug for targeting human cancer stem cells*. J Biomed Biotechnol, 2012. **2012**: p. 950658.
71. Liu, L., et al., *Salinomycin suppresses cancer cell stemness and attenuates TGF- $\beta$ -induced epithelial-mesenchymal transition of renal cell carcinoma cells*. Chem Biol Interact, 2018. **296**: p. 145-153.
72. Lee, H.G., et al., *Salinomycin reduces stemness and induces apoptosis on human ovarian cancer stem cell*. J Gynecol Oncol, 2017. **28**(2): p. e14.
73. Zhang, J., et al., *Transcriptional inhibition by CDK7/9 inhibitor SNS-032 abrogates oncogene addiction and reduces liver metastasis in uveal melanoma*. Mol Cancer, 2019. **18**(1): p. 140.
74. Kirschmann, D.A., et al., *Molecular pathways: vasculogenic mimicry in tumor cells: diagnostic and therapeutic implications*. Clin Cancer Res, 2012. **18**(10): p. 2726-32.
75. Peris-Torres, C., et al., *Extracellular Protease ADAMTS1 Is Required at Early Stages of Human Uveal Melanoma Development by Inducing Stemness and Endothelial-Like Features on Tumor Cells*. Cancers (Basel), 2020. **12**(4).
76. Xie, Y., et al., *FGF/FGFR signaling in health and disease*. Signal Transduct Target Ther, 2020. **5**(1): p. 181.
77. Ornitz, D.M. and N. Itoh, *The Fibroblast Growth Factor signaling pathway*. Wiley Interdiscip Rev Dev Biol, 2015. **4**(3): p. 215-66.
78. Itoh, N. and D.M. Ornitz, *Fibroblast growth factors: from molecular evolution to roles in development, metabolism and disease*. J Biochem, 2011. **149**(2): p. 121-30.
79. Giacomini, A., et al., *The FGF/FGFR system in the physiopathology of the prostate gland*. Physiol Rev, 2021. **101**(2): p. 569-610.
80. Santolla, M.F. and M. Maggiolini, *The FGF/FGFR System in Breast Cancer: Oncogenic Features and Therapeutic Perspectives*. Cancers (Basel), 2020. **12**(10).
81. Zhang, J., et al., *Targeting the Oncogenic FGF-FGFR Axis in Gastric Carcinogenesis*. Cells, 2019. **8**(6).
82. Ascione, C.M., et al., *Role of FGFR3 in bladder cancer: Treatment landscape and future challenges*. Cancer Treat Rev, 2023. **115**: p. 102530.
83. Cappellen, D., et al., *Frequent activating mutations of FGFR3 in human bladder and cervix carcinomas*. Nat Genet, 1999. **23**(1): p. 18-20.

84. Biello, F., et al., *Fibroblast Growth Factor Receptor (FGFR): A New Target for Non-small Cell Lung Cancer Therapy*. *Anticancer Agents Med Chem*, 2016. **16**(9): p. 1142-54.
85. Yagasaki, F., et al., *Fusion of ETV6 to fibroblast growth factor receptor 3 in peripheral T-cell lymphoma with a t(4;12)(p16;p13) chromosomal translocation*. *Cancer Res*, 2001. **61**(23): p. 8371-4.
86. Chesi, M., et al., *Frequent translocation t(4;14)(p16.3;q32.3) in multiple myeloma is associated with increased expression and activating mutations of fibroblast growth factor receptor 3*. *Nat Genet*, 1997. **16**(3): p. 260-4.
87. Krook, M.A., et al., *Fibroblast growth factor receptors in cancer: genetic alterations, diagnostics, therapeutic targets and mechanisms of resistance*. *Br J Cancer*, 2021. **124**(5): p. 880-892.
88. Presta, M., et al., *Fibroblast growth factors (FGFs) in cancer: FGF traps as a new therapeutic approach*. *Pharmacol Ther*, 2017. **179**: p. 171-187.
89. Touat, M., et al., *Targeting FGFR Signaling in Cancer*. *Clin Cancer Res*, 2015. **21**(12): p. 2684-94.
90. Zhou, Y., et al., *FGF/FGFR signaling pathway involved resistance in various cancer types*. *J Cancer*, 2020. **11**(8): p. 2000-2007.
91. Lefèvre, G., et al., *Activation of the FGF2/FGFR1 autocrine loop for cell proliferation and survival in uveal melanoma cells*. *Invest Ophthalmol Vis Sci*, 2009. **50**(3): p. 1047-57.
92. Loda, A., et al., *Exploring the FGF/FGFR System in Ocular Tumors: New Insights and Perspectives*. *Int J Mol Sci*, 2022. **23**(7).
93. Giacomini, A., et al., *Blocking the FGF/FGFR system as a "two-compartment" antiangiogenic/antitumor approach in cancer therapy*. *Pharmacol Res*, 2016. **107**: p. 172-185.
94. Walden, D., C. Eslinger, and T. Bekaii-Saab, *Pemigatinib for adults with previously treated, locally advanced or metastatic cholangiocarcinoma with FGFR2 fusions/rearrangements*. *Therap Adv Gastroenterol*, 2022. **15**: p. 17562848221115317.
95. Loriot, Y., et al., *Erdafitinib in Locally Advanced or Metastatic Urothelial Carcinoma*. *N Engl J Med*, 2019. **381**(4): p. 338-348.
96. Freyer, C.W., et al., *Pemigatinib for the treatment of myeloid/lymphoid neoplasms with*. *Expert Rev Anticancer Ther*, 2023. **23**(4): p. 351-359.
97. Ronca, R., et al., *Long-Pentraxin 3 Derivative as a Small-Molecule FGF Trap for Cancer Therapy*. *Cancer Cell*, 2015. **28**(2): p. 225-39.
98. Castelli, R., et al., *Synthesis, Structural Elucidation, and Biological Evaluation of NSC12, an Orally Available Fibroblast Growth Factor (FGF) Ligand Trap for the Treatment of FGF-Dependent Lung Tumors*. *J Med Chem*, 2016. **59**(10): p. 4651-63.
99. Castelli, R., et al., *Chemical modification of NSC12 leads to a specific FGF-trap with antitumor activity in multiple myeloma*. *Eur J Med Chem*, 2021. **221**: p. 113529.
100. Ronca, R., et al., *FGF Trapping Inhibits Multiple Myeloma Growth through c-Myc Degradation-Induced Mitochondrial Oxidative Stress*. *Cancer Res*, 2020. **80**(11): p. 2340-2354.

101. Ronca, R., et al., *Fibroblast growth factor modulates mast cell recruitment in a murine model of prostate cancer*. *Oncotarget*, 2017. **8**(47): p. 82583-82592.
102. Rodrigues, P.F., et al., *Long Pentraxin 3-Mediated Fibroblast Growth Factor Trapping Impairs Fibrosarcoma Growth*. *Front Oncol*, 2018. **8**: p. 472.
103. Rezzola, S., et al., *The Autocrine FGF/FGFR System in both Skin and Uveal Melanoma: FGF Trapping as a Possible Therapeutic Approach*. *Cancers (Basel)*, 2019. **11**(9).
104. Dvorak, P., D. Dvorakova, and A. Hampl, *Fibroblast growth factor signaling in embryonic and cancer stem cells*. *FEBS Lett*, 2006. **580**(12): p. 2869-74.
105. Xu, C., et al., *Basic fibroblast growth factor supports undifferentiated human embryonic stem cell growth without conditioned medium*. *Stem Cells*, 2005. **23**(3): p. 315-23.
106. Haghighi, F., et al., *bFGF-mediated pluripotency maintenance in human induced pluripotent stem cells is associated with NRAS-MAPK signaling*. *Cell Commun Signal*, 2018. **16**(1): p. 96.
107. Lai, S.W., et al., *The therapeutic targeting of the FGFR1/Src/NF- $\kappa$ B signaling axis inhibits pancreatic ductal adenocarcinoma stemness and oncogenicity*. *Clin Exp Metastasis*, 2018. **35**(7): p. 663-677.
108. Quan, M.Y., et al., *An FGFR/AKT/SOX2 Signaling Axis Controls Pancreatic Cancer Stemness*. *Front Cell Dev Biol*, 2020. **8**: p. 287.
109. Maehara, O., et al., *Fibroblast growth factor-2-mediated FGFR/Erk signaling supports maintenance of cancer stem-like cells in esophageal squamous cell carcinoma*. *Carcinogenesis*, 2017. **38**(11): p. 1073-1083.
110. Aytatli, A., et al., *AZD4547 targets the FGFR/Akt/SOX2 axis to overcome paclitaxel resistance in head and neck cancer*. *Cell Oncol (Dordr)*, 2022. **45**(1): p. 41-56.
111. McDermott, S.C., et al., *FGFR signaling regulates resistance of head and neck cancer stem cells to cisplatin*. *Oncotarget*, 2018. **9**(38): p. 25148-25165.
112. Tovar, V., et al., *Tumour initiating cells and IGF/FGF signalling contribute to sorafenib resistance in hepatocellular carcinoma*. *Gut*, 2017. **66**(3): p. 530-540.
113. Fessler, E., T. Borovski, and J.P. Medema, *Endothelial cells induce cancer stem cell features in differentiated glioblastoma cells via bFGF*. *Mol Cancer*, 2015. **14**: p. 157.
114. Wu, S.Y., et al., *Natural killer cells in cancer biology and therapy*. *Mol Cancer*, 2020. **19**(1): p. 120.
115. Hanna, J., et al., *Decidual NK cells regulate key developmental processes at the human fetal-maternal interface*. *Nat Med*, 2006. **12**(9): p. 1065-74.
116. Sivori, S., et al., *Human NK cells: surface receptors, inhibitory checkpoints, and translational applications*. *Cell Mol Immunol*, 2019. **16**(5): p. 430-441.
117. Greppi, M., et al., *Strengthening the AntiTumor NK Cell Function for the Treatment of Ovarian Cancer*. *Int J Mol Sci*, 2019. **20**(4).
118. Patrizi, O., et al., *Natural killer cell impairment in ovarian clear cell carcinoma*. *J Leukoc Biol*, 2020. **108**(4): p. 1425-1434.
119. Santoni, A., et al., *Natural killer (NK) cells from killers to regulators: distinct features between peripheral blood and decidual NK cells*. *Am J Reprod Immunol*, 2007. **58**(3): p. 280-8.

120. Bruno, A., et al., *The proangiogenic phenotype of natural killer cells in patients with non-small cell lung cancer*. *Neoplasia*, 2013. **15**(2): p. 133-42.
121. Albin, A. and D.M. Noonan, *Decidual-Like NK Cell Polarization: From Cancer Killing to Cancer Nurturing*. *Cancer Discov*, 2021. **11**(1): p. 28-33.
122. Bruno, A., et al., *Angiogenin and the MMP9-TIMP2 axis are up-regulated in proangiogenic, decidual NK-like cells from patients with colorectal cancer*. *FASEB J*, 2018. **32**(10): p. 5365-5377.
123. Gallazzi, M., et al., *Prostate Cancer Peripheral Blood NK Cells Show Enhanced CD9, CD49a, CXCR4, CXCL8, MMP-9 Production and Secrete Monocyte-Recruiting and Polarizing Factors*. *Front Immunol*, 2020. **11**: p. 586126.
124. Gonzalez, V.D., et al., *High-grade serous ovarian tumor cells modulate NK cell function to create an immune-tolerant microenvironment*. *Cell Rep*, 2021. **36**(9): p. 109632.
125. Bosi, A., et al., *Natural Killer Cells from Malignant Pleural Effusion Are Endowed with a Decidual-Like Proangiogenic Polarization*. *J Immunol Res*, 2018. **2018**: p. 2438598.
126. Albin, A., et al., *TIMP1 and TIMP2 Downregulate TGF $\beta$  Induced Decidual-like Phenotype in Natural Killer Cells*. *Cancers (Basel)*, 2021. **13**(19).
127. Battle, E. and J. Massagué, *Transforming Growth Factor- $\beta$  Signaling in Immunity and Cancer*. *Immunity*, 2019. **50**(4): p. 924-940.
128. Turati, M., et al., *TGF- $\beta$  mediated drug resistance in solid cancer*. *Cytokine Growth Factor Rev*, 2023.
129. Oliva, M., A.J. Rullan, and J.M. Piulats, *Uveal melanoma as a target for immunotherapy*. *Ann Transl Med*, 2016. **4**(9): p. 172.
130. Esser, P., S. Grisanti, and K. Bartz-Schmidt, *TGF-beta in uveal melanoma*. *Microsc Res Tech*, 2001. **52**(4): p. 396-400.
131. Keskin, D.B., et al., *TGFbeta promotes conversion of CD16+ peripheral blood NK cells into CD16- NK cells with similarities to decidual NK cells*. *Proc Natl Acad Sci U S A*, 2007. **104**(9): p. 3378-83.
132. Yang, L., Y. Pang, and H.L. Moses, *TGF-beta and immune cells: an important regulatory axis in the tumor microenvironment and progression*. *Trends Immunol*, 2010. **31**(6): p. 220-7.
133. Chua, V., et al., *Stromal fibroblast growth factor 2 reduces the efficacy of bromodomain inhibitors in uveal melanoma*. *EMBO Mol Med*, 2019. **11**(2).
134. Wang, Y., et al., *FGF2 promotes metastasis of uveal melanoma cells via store-operated calcium entry*. *Onco Targets Ther*, 2017. **10**: p. 5317-5328.
135. Fu, Y., W. Xiao, and Y. Mao, *Recent Advances and Challenges in Uveal Melanoma Immunotherapy*. *Cancers (Basel)*, 2022. **14**(13).
136. Hodgins, J.J., et al., *Killers 2.0: NK cell therapies at the forefront of cancer control*. *J Clin Invest*, 2019. **129**(9): p. 3499-3510.



## ADDENDUM

During my PhD, I also co-authored the following papers:

**Angiogenesis-Inflammation Cross Talk in Diabetic Retinopathy: Novel Insights From the Chick Embryo Chorioallantoic Membrane/Human Vitreous Platform.**

S. Rezzola, **A. Loda**, M. Corsini, F. Semeraro, T. Annese, M. Presta, D. Ribatti.

Front Immunol. 2020 Sep 29;11:581288. doi: 10.3389/fimmu.2020.581288. PMID: 33117388; PMCID: PMC7552803.

**VEGF-Independent Activation of Müller Cells by the Vitreous from Proliferative Diabetic Retinopathy Patients.**

S. Rezzola, J. Guerra, AM. Krishna Chandran, **A. Loda**, A. Cancarini, P. Sacristani, F. Semeraro, M. Presta.

Int J Mol Sci. 2021 Feb 22;22(4):2179. doi: 10.3390/ijms22042179. PMID: 33671690; PMCID: PMC7926720.

**Diabetic Retinopathy: Soluble and Imaging Ocular Biomarkers.**

M. Ferrara, **A. Loda**, G. Coco, P. Grassi, S. Cestaro, S. Rezzola, V. Romano, F. Semeraro.

J Clin Med. 2023 Jan 24;12(3):912. doi: 10.3390/jcm12030912. PMID: 36769560; PMCID: PMC9917666.

These publications are reported in the following pages.



**Angiogenesis-Inflammation Cross Talk in Diabetic Retinopathy: Novel Insights from the Chick Embryo Chorioallantoic Membrane/Human Vitreous Platform**

S. Rezzola, **A. Loda**, M. Corsini, F. Semeraro, T. Annese, M. Presta, D. Ribatti.

Front Immunol. 2020 Sep 29;11:581288. doi: 10.3389/fimmu.2020.581288. PMID: 33117388; PMCID: PMC7552803.







# Angiogenesis-Inflammation Cross Talk in Diabetic Retinopathy: Novel Insights From the Chick Embryo Chorioallantoic Membrane/Human Vitreous Platform

Sara Rezzola<sup>1</sup>, Alessandra Loda<sup>1</sup>, Michela Corsini<sup>1</sup>, Francesco Semeraro<sup>2</sup>, Tiziana Annese<sup>3</sup>, Marco Presta<sup>1,4\*</sup> and Domenico Ribatti<sup>5\*</sup>

<sup>1</sup> Department of Molecular and Translational Medicine, School of Medicine, University of Brescia, Brescia, Italy, <sup>2</sup> Eye Clinic, Department of Neurological and Vision Sciences, University of Brescia, Brescia, Italy, <sup>3</sup> Department of Basic Medical Sciences, Neurosciences, and Sensory Organs, University of Bari Medical School, Bari, Italy, <sup>4</sup> Italian Consortium for Biotechnology (CIB), Unit of Brescia, Brescia, Italy

## OPEN ACCESS

### Edited by:

Edoardo Midena,  
University of Padua, Italy

### Reviewed by:

Antonella Naldini,  
University of Siena, Italy  
Gareth S. D. Purvis,  
University of Oxford, United Kingdom

### \*Correspondence:

Domenico Ribatti  
domenico.ribatti@uniba.it  
Marco Presta  
marco.presta@unibs.it

### Specialty section:

This article was submitted to  
Inflammation,  
a section of the journal  
Frontiers in Immunology

Received: 08 July 2020

Accepted: 27 August 2020

Published: 29 September 2020

### Citation:

Rezzola S, Loda A, Corsini M, Semeraro F, Annese T, Presta M and Ribatti D (2020) Angiogenesis-Inflammation Cross Talk in Diabetic Retinopathy: Novel Insights From the Chick Embryo Chorioallantoic Membrane/Human Vitreous Platform. *Front. Immunol.* 11:581288. doi: 10.3389/fimmu.2020.581288

Pathological angiogenesis of the retina is a key component of irreversible causes of blindness, as observed in proliferative diabetic retinopathy (PDR). The pathogenesis of PDR is complex and involves vascular, inflammatory, and neuronal mechanisms. Several structural and molecular alterations associated to PDR are related to the presence of inflammation that appears to play a non-redundant role in the neovascular response that characterizes the retina of PDR patients. Vascular endothelial growth factor (VEGF) blockers have evolved over time for the treatment of retinal neovascularization. However, several limitations to anti-VEGF interventions exist. Indeed, the production of other angiogenic factors and pro-inflammatory mediators may nullify and/or cause resistance to anti-VEGF therapies. Thus, appropriate experimental models are crucial for dissecting the mechanisms leading to retinal neovascularization and for the discovery of more efficacious anti-angiogenic/anti-inflammatory therapies for PDR patients. This review focuses on the tight cross talk between angiogenesis and inflammation during PDR and describe how the chick embryo chorioallantoic membrane (CAM) assay may represent a cost-effective and rapid *in vivo* tool for the study of the relationship between neovascular and inflammatory responses elicited by the vitreous humor of PDR patients and for the screening of novel therapeutic agents.

**Keywords:** angiogenesis, inflammation, vitreous, chick embryo CAM, diabetic retinopathy

## INTRODUCTION

Retinal and choroidal neovascularization are the leading causes of visual impairment in various ocular pathologies, including retinal vein occlusion, age-related macular-degeneration, retinopathy of prematurity and diabetic retinopathy (DR).

DR is one of the main complications of diabetes mellitus and it represents the major cause of vision loss in the working-age population (1). At present, 463 million adults are estimated to be living with diabetes worldwide, a number projected to rise to 700 million by 2045 (2). Currently, DR affects more than 93 million people in the world with an overall prevalence close to 35% of the diabetic population (3). In the earlier stages, the disease manifests as

non-proliferative microaneurysms; then, it progresses to proliferative diabetic retinopathy (PDR). Hallmarks of PDR are the presence of hard and soft exudates, neovascularization and hemorrhages. The retinal microvasculature is progressively damaged by the disease, resulting in various events such as retinal ischemia, upregulation of hypoxia inducible factor-1 (HIF-1), and vascular endothelial growth factor (VEGF) secretion, possibly progressing to PDR, which is diagnosed according to the presence of vascular lesions (e.g., preretinal or vitreous hemorrhages or neovascularization) (4).

Inflammation and angiogenesis are two of the main factors that contribute to PDR. During the disease, inflammation and neovascularization establish a strict cross talk, with inflammation promoting neovascularization and *vice versa* [see (5–8) and references therein]. Interestingly, clinical evidence shows a lower occurrence of DR in diabetic patients treated with salicylates for rheumatoid arthritis (9). Accordingly, anti-inflammatory drugs could be beneficial for managing retinal neovascularization. Indeed, the progression of pathological neovascularization and of diabetic macular edema may be reduced by the administration of corticosteroids (e.g., triamcinolone acetonide) via intravitreal injection. Even though, corticosteroids could be effective in improving or at least stabilizing visual acuity, these results are often temporary and administration of corticosteroids may be associated with adverse effects, such as increased intraocular pressure and cataract formation (10–12).

Laser photocoagulation is a widely used technique for treating retinal neovascularization, allowing long-term regression. However, the identification of VEGF as a key mediator in the pathogenesis of DR, able to promote both angiogenesis and vascular permeability, led to the establishment of anti-VEGF agents as an alternative line of treatment (4). Clinical and experimental evidence suggests that intraocular levels of VEGF are increased during retinal ischemia, resulting in the breakdown of the blood-retina barrier, enhanced vascular permeability, and neovascularization (13).

A recent meta-analysis of aggregate data has indicated that anti-VEGF pharmacotherapy is associated with superior visual acuity outcomes and less PDR-related complications when compared to retinal laser photocoagulation (14). However, limitations do exist in the use of anti-VEGF agents. Indeed, due to their brief duration of action, anti-VEGF drugs need to be frequently administered *via* intravitreal injection, possibly resulting in adverse side effects (i.e., endophthalmitis and ocular inflammation). Furthermore, a large percentage of patients do not respond to anti-VEGF drugs or exhibit a poor response. Supposedly, this limited efficacy may depend on the activation of other pathways promoting ocular angiogenesis as a consequence of the local production of various pro-angiogenic and pro-inflammatory factors [reviewed in (15–17)].

Therefore, a better knowledge of the pathogenesis of DR is required, in order to clarify the relationship between inflammation and angiogenesis during the disease progression. Indeed, a better understanding of their role in the disease could allow for the identification of novel anti-inflammatory approaches targeting retinal angiogenesis. In this frame, the implementation of new methods that could allow the discovery

of novel strategies targeting molecular pathways involved in ocular neovascularization is essential. To achieve this aim, many pharmacological studies have been carried out in various *in vitro* and *ex vivo* assays, suitable for the screening of small anti-angiogenic compounds (16, 18). In addition, mouse models have been established in order to investigate retinal angiogenesis (19, 20). However, the use of these models is hindered by various limitations (21).

The chick embryo chorioallantoic membrane (CAM) has been proposed as a valid alternative animal model for the investigation of the mechanisms underlying physiological and pathological angiogenesis (22). This review highlights the use of the CAM as a model system for the study of the cross talk between angiogenesis and inflammation in PDR and for the screening of anti-angiogenic/anti-inflammatory molecules to be employed for the treatment of angiogenesis-dependent eye diseases.

## ANGIOGENESIS AND INFLAMMATION IN DIABETIC RETINOPATHY

Angiogenesis is a complex multi-step process. Various events are necessary for angiogenesis to occur, including the interaction between cell surface receptors, soluble factors, and extracellular matrix components. Several cell types are also required, with endothelial cells playing a major role (23).

The formation of neovessels has been thoroughly investigated and described in several insightful reviews (24–28). Briefly, hypoxia promotes the release of angiogenic factors, such as VEGF, responsible for inducing the detachment of pericytes from the vessel wall, which weakens the interactions among endothelial cells and increases vascular permeability (23). Moreover, pro-angiogenic molecules directly increase vascular permeability by disrupting adherens junctions and by inducing the phosphorylation of vascular endothelial-cadherin, thus allowing serum proteins extravasation from the vascular lumen (29). Pro-angiogenic mediators stimulate the activation of quiescent endothelial cells, which alter their morphology and acquire a “pro-angiogenic phenotype.” Once activated, endothelial cells proliferate and migrate into the stroma, following a chemotactic gradient provided by the angiogenic stimulus (30). Finally, the neovessels complete their maturation process by the deposition of a basal membrane and the recruitment of pericytes/smooth muscle cells. After all these steps have been accomplished, the production of pro-angiogenic mediators decreases, the neovessels are remodeled by the blood flow itself, and endothelial cells return to their quiescent condition (31).

During diabetes, hyperglycemia acts on retinal endothelium, promoting the activation of interconnected biochemical pathways, including the polyol (sorbitol-aldose reductase) (32) and hexosamine (33) pathways, enhanced production of advanced glycation end products (34) and reactive oxygen species (ROS) (35), and activation of protein kinase C (36, 37), poly(ADP-ribose) polymerase (38), and of the renin-angiotensin system (39). All of these events contribute to increasing oxidative stress, which, in turn, triggers neovascularization, inflammation,

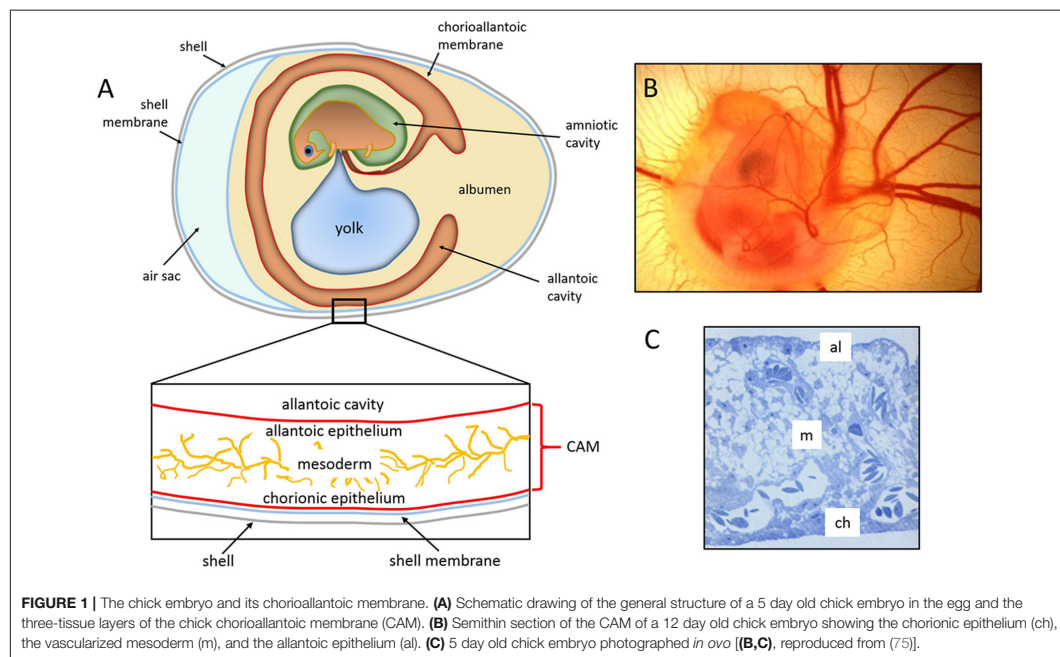


**FIGURE 1 |** The chick embryo and its chorioallantoic membrane. **(A)** Schematic drawing of the general structure of a 5 day old chick embryo in the egg and the three-tissue layers of the chick chorioallantoic membrane (CAM). **(B)** Semithin section of the CAM of a 12 day old chick embryo showing the chorionic epithelium (ch), the vascularized mesoderm (m), and the allantoic epithelium (al). **(C)** 5 day old chick embryo photographed *in ovo* [(B,C), reproduced from (75)].

and early neurodegeneration. Moreover, hyperglycemia affects retinal mitochondria, which become dysfunctional. Consequently, the production of ROS is increased, damaging DNA, promoting the release of cytochrome C, and resulting in endothelial cell apoptosis (40). Another important feature of the vascular dysfunction that occurs during DR is the loss of retinal pericytes, which further destabilizes endothelial cells and alters perfusion (41). The tight interaction between pericytes and endothelium is disrupted by the progressive thickening of the basement membrane that, together with systemic and local hypertension, promotes pericyte apoptosis.

These hyperglycemia-induced alterations are considered one of the primary events in the pathogenesis of DR and they are followed by other dysfunctions, such as retinal hyperpermeability, thickening of the basal endothelial membrane, and activation of a strong inflammatory response.

Another hallmark of DR is the presence of micro-occlusions in the retinal microvasculature (42). Endothelial cells upregulate the expression of the intracellular adhesion molecule 1 (ICAM-1), which is responsible for mediating the adhesion of leukocytes to the endothelium (43). The constriction of major arteries and arterioles leads to areas of decreased perfusion associated with an upregulation of HIF-1, which levels are elevated in the vitreous of PDR patients (44, 45). HIF-1 upregulates several growth factors, cytokines, and chemokines, leading to retinal neovascularization (46). These HIF-1-regulated factors include various pro-angiogenic molecules, such as VEGF, erythropoietin,

fibroblast growth factor 2 (FGF2), insulin-like growth factor-1, stromal cell-derived factor-1, platelet-derived growth factor, tumor necrosis factor  $\alpha$  (TNF $\alpha$ ) and interleukins (ILs) (17, 47–49). In addition, many anti-angiogenic mediators are downregulated, including angiostatin and pigment epithelium-derived factor and decreased levels of these molecules have been reported in the vitreous of diabetic patients (50).

A tight cross talk between inflammation and angiogenesis takes place in several physiological and pathological conditions (51, 52). Inflammatory cells are responsible for the production of various molecules, including growth factors, cytokines, and proteases. All of these mediators contribute to neovessel formation (53). Moreover, activated endothelial cells express pro-inflammatory molecules that mediate the recruitment and the activation of white blood cells (54, 55). Several signaling pathways are shared by neovascularization and inflammation processes (56). Indeed, various chemokines might exert a double function by promoting leukocyte adhesion to the endothelium and stimulating endothelial cell proliferation (57). In addition, several pro-inflammatory cytokines, including IL6, IL1 $\alpha$ , IL1 $\beta$ , osteopontin, high mobility group box-1, and TNF $\alpha$ , may directly activate angiogenesis by acting on endothelial cells. These same cytokines also promote angiogenesis indirectly by activating the production of more pro-angiogenic factors by leukocytes and endothelium (58–60). Conversely, endothelial cells stimulated by the pro-angiogenic factors VEGF and angiopoietin-1 increase the expression of cell adhesion molecules, as well as the production

of inflammatory factors (61, 62). A further example of the cross talk that occurs between angiogenesis and inflammation is provided by the capacity of pro-inflammatory stimuli to induce the upregulation of *HIF-1 $\alpha$*  gene expression *via* the activation of the canonical nuclear factor  $\kappa$ B (NF- $\kappa$ B) pathway, a key regulator of innate immune, inflammatory and angiogenic responses (63). In addition, oxygen-sensing hydroxylases may confer hypoxic sensitivity to both HIF and NF- $\kappa$ B pathways concurrently (64). Thus, a tight interaction exists between HIF and NF- $\kappa$ B signaling that leads to the production of inflammatory and angiogenic mediators under hypoxic conditions, including VEGF (65).

Inflammation is a crucial event for the development of DR. It is especially relevant during the initial stages of the disease, when inflammation activates transcriptional factors and induces the increased expression of both pro-inflammatory and pro-angiogenic mediators (66, 67). Retinal inflammation is closely associated with neovascularization. Indeed, during inflammation, retinal microglia become activated and release cytokines and pro-angiogenic mediators (68) responsible for the maintenance of chronic inflammation in the retina (7, 69). Prolonged inflammation is extremely detrimental and it contributes to damaging retinal vasculature, promoting the formation of neovessels as well as the development of macular edema (7, 70). Moreover, inflammation may be involved in retinal neurodegeneration, which is frequently observed in DR patients (7, 71). New insights into the exact role of inflammation in the pathogenesis of DR may allow for the identification of new molecular pathways and for the discovery of novel therapeutic targets. The association of anti-angiogenic and anti-inflammatory drugs may therefore be beneficial for treating DR (71–73).

## THE CHICK EMBRYO CHORIOALLANTOIC MEMBRANE

The chick embryo CAM is a vascular membrane formed by the fusion of the mesodermal layers, the allantois, and the chorion that appears at day 3–4 of incubation. It consists of three layers, ectoderm (originating from the chorion and attached to the shell membrane), mesoderm (represented by the fusion of the somatic mesoderm from the chorion and the splanchnic mesoderm from the allantois), and endoderm (originating from the allantois and facing up the allantoic cavity) (74). The middle mesodermal layer is enriched in stromal components and blood vessels connected with the embryonic circulation by allantoic arteries and veins (Figure 1).

By 16 days of incubation, the CAM has grown so large that it completely covers most of the yolk sac and becomes adjacent to the shell membrane. The surface area of the CAM, which measures about 6 cm<sup>2</sup> on day 6, increases to 65 cm<sup>2</sup> by day 14 (76). The large surface extension and its position confer to the CAM a respiratory function through the pores in the eggshell (74).

As shown by Schlatter et al. (77), the CAM vasculature develops by both sprouting and intussusceptive angiogenesis in a three-phase process. In the first phase, multiple capillary sprouts

invade the mesenchyme, fuse, and form the primary capillary plexus. During the intermediate phase, tissue pillars, expression of intussusceptive angiogenesis, replace capillary sprouts. In the third phase, the growing pillars increase in size to form intercapillary meshes [see (77, 78) for light microscopy and microvascular corrosion cast images of the three-phase process of the vascular development of the CAM].

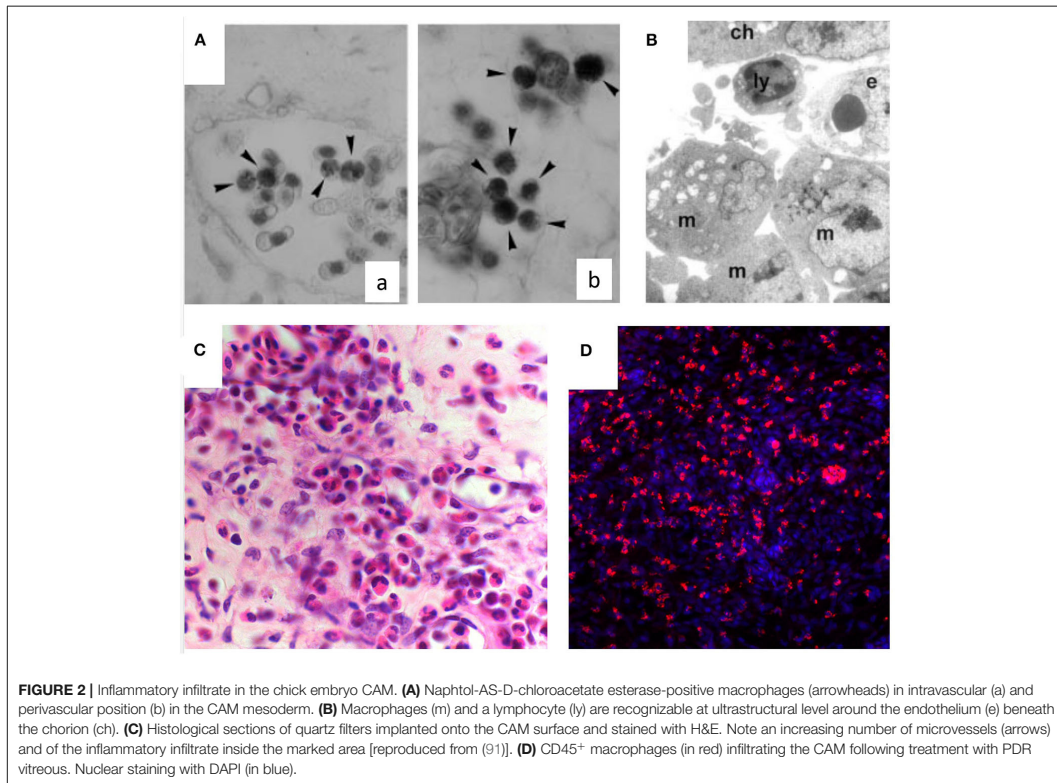
In the early phase, the blood vessels are immature as they are not covered by smooth muscle cells and the basal lamina is incomplete. This initial structure allows the blood vessels to spread into the mesoderm, where they rapidly expand until day 8 to create a capillary plexus. The capillary plexus becomes close to the overlying chorionic epithelial cells, where it mediates gas exchange with the outer environment by receiving oxygen and eliminating carbon dioxide. Blood vessel proliferation continues until day 11. Then, it declines rapidly until day 18 when the vasculature attains its final arrangement up to hatching (79).

## The Chick Embryo Chorioallantoic Membrane for *in vivo* Studies on Angiogenesis

The CAM is a favored system for the *in vivo* study of physiological and pathological angiogenesis. Its extensive vascularization and easy accessibility make the CAM assay a simple experimental platform to investigate the efficacy and mechanisms of action of pro- and anti-angiogenic molecules. The assay is performed by grafting the materials to be tested onto developing CAM through a window cut in the eggshell. The embryogenesis starts as soon as the fertilized eggs are placed horizontally in an incubator at 37°C. The physiological environment for the CAM is guaranteed by working at controlled temperature and humidity. On day 3, after removing of approximately 5 ml of albumen, a window is opened in the shell to detach the CAM from the shell itself and to make the vascular surface accessible. This technique has the advantage of high viability in long-term incubation assays and allows the use of the embryos until just before hatching (at day 21), its disadvantages being represented by a limited area for manipulation and observation (22).

To avoid the disadvantage of the limited area of work, it is possible to transfer the embryo with its extraembryonic membranes into a Petri dish on day 3–4 of incubation. This experimental setting favors CAM development at the top of the Petri dish as a flat membrane on which multiple tests can be grafted (80). In addition, this *ex ovo* system is more suitable for live imaging than *in ovo* techniques and it allows the quantification of the response over a full area of the CAM by testing simultaneously a large number of samples. However, long-term viability is often shorter than *in ovo*, and more care is needed to avoid embryo dehydration. Usually, 50% of the *ex ovo* cultures is lost in the first 3 days after opening, due to the frequent rupture of the yolk membrane or to the sliding of the CAM at the bottom of the dish (80).

Several protocols have been developed for the release of molecules to be tested in the CAM assay. Macromolecules and low molecular weight compounds are placed onto the CAM using



silostatic or silicon rings, methylcellulose disks, filters, plastic rings, or sponges. Sponges can be made in collagen or gelatin and are suitable also for testing the effects of cell xenografts (81). As compared to the direct delivery on the CAM of pure pro- or anti-angiogenic factors, the use of sponges loaded with a small number of cells allows the slow and continuous delivery of cell-secreted factors, thus mimicking a more “physiological” mode of interaction with the CAM vasculature.

Usually, an angiogenic response occurs 72–96 h after stimulation. The pro-angiogenic activity of a compound results in an increased blood vessel density around the implant, with newly formed blood vessels arranged in a radial pattern like the spokes of a wheel. On the contrary, when a compound with an anti-angiogenic activity is tested, the blood vessels become less numerous around the implant, and occasionally they disappear.

Different semi-quantitative and quantitative morphological and molecular methods have been developed to evaluate pro- or anti-angiogenic responses in the CAM assay at macroscopic and microscopic levels. Quantification of the CAM vasculature can be performed with the use of extensive vessel-counting

methods based on visual examination and manual vessel counts or global measurements of the spatial pattern and distribution by algorithms. At the end of the assay, the membranes can be processed for in-depth analysis by immunohistochemistry preceded by paraffin embedding, or for ultrastructure analysis by electron microscopy.

Moreover, fresh CAM samples can be processed for molecular studies, including the determination of DNA amount, selected protein and collagen content (by Western blotting or spectrophotometric based-methods), and gene expression analysis by quantitative RT-PCR.

### The Chick Embryo Chorioallantoic Membrane for *in vivo* Studies on Inflammation

The immune system of the chick begins to develop during the embryonic life (82). Classically, innate responses are essential in the earliest phases of microbial invasion, until adaptive responses (B and T cell-mediated) become active to clear the infection. The chick immune system consists of B and T cells that control

humoral and cell-mediated immunity, respectively. The B cells differentiate in the bursa of Fabricius, whereas T cells differentiate in the thymus (83, 84). The presence of T cells can be first detected at day 11 and of B cells at day 12 (85), and by day 18 chick embryos become immunocompetent (86, 87).

The first line of defense against bacterial pathogens in the chick embryo is represented by heterophils (88). These rounded cells release microbicidal agents, including ROS, proteolytic enzymes, and microbicidal peptides from their cytoplasmic granules. Heterophils present two types of granules. The primary granules are fusiform, display a central body that may be proteinaceous, and appear brick-red in color after Romanowsky stains. The secondary granules are rounded, less abundant, and smaller compared to the primary ones. Unlike mammalian neutrophils, chick heterophils are devoid of myeloperoxidase (88).

The chick embryo yolk sac produces the first generation of macrophages. Chick embryonic macrophages, identified at embryonic day 12–16 in the spleen and liver, recognize and phagocytize microbial antigens (89). In chickens, T-cell membrane protein 4 (TIM4) is a receptor expressed primarily by macrophages, binds to phosphatidylserine, and most likely participates in the recognition and clearance of apoptotic cells (89). Hu and colleagues applied anti-chicken TIM4 monoclonal antibodies in combination with colony stimulating factor 1 receptor reporter transgenes to dissect the function of TIM4 in the chick (90). They demonstrated that TIM4 was present on the large majority of macrophages during development *in ovo* and to be expressed also by other cells with phagocytic activity, such as dendritic cells, after hatching (90).

An inflammatory response may be induced in the CAM assay through different stimuli. Inflammatory cells, first heterophils and then monocyte/macrophages, infiltrate the CAM mesenchyme (Figure 2). These cells can deliver several pro- and anti-inflammatory factors and cytokines, as well as important modifiers of the extracellular matrix [i.e., matrix metalloproteinases (MMPs)]. Chick heterophils express MMP-9 (53), while monocyte/macrophages deliver MMP-13 to facilitate angiogenesis in a coordinated fashion (92).

A systematic study on the interplay between angiogenesis and inflammation, using different carrier materials placed on the CAM (e.g., glass fiber filters, viscose and gelatin sponges, agarose and polyacrylamide gels) have shown that the vascular reaction is also due, at least in part, to an inflammatory reaction induced by the presence of such foreign materials (93). The reactions induced by these materials were compared with those induced by natural egg materials (white eggshell membrane, coagulated albumen, and yolk). In all the cases, the CAM reacted with the proliferation of ectodermal cells, fibroblasts, and blood vessels, resulting in a highly capillarized granulation tissue. Accordingly, the CAM has been used as an *in vivo* model to study wound repair (94). This model consistently reproduces all the phases observed in adult wound healing, including re-epithelization, angiogenesis, inflammation, and fibronectin deposition, resulting in scar formation (94). Histological examination of the CAM during wound healing demonstrated

hyperplasia of the chorionic epithelium in the area involved in the repair process, and inflammatory infiltrates consisting mainly of monocytes/macrophages positive to chloroacetate esterase (Figure 2A). The CAM has been used also as a model for the evaluation of inflammatory effects by tissue tolerable plasma for the determination of the optimum parameters for treatment of chronic wounds. The response patterns, represented by granuloma development (with associated angiogenesis), hemorrhages, coagulation, and contracture, were alleviated when hydrocortisone was added immediately after plasma treatment (95). Hyaluronic acid/bone substitute complexes implanted on the CAM induce instead osteoblastic differentiation and angiogenesis, but not inflammation, while a massive inflammatory infiltrate was detected around the implant of hyaluronic acid and saline samples (96).

The presence of a mononuclear cell infiltrate has been observed also in osteopontin (OPN)-treated CAMs and responsible, at least in part, for the neovascular response triggered by this cytokine (60). Mononuclear cells were frequently found to encircle microvessels located at the boundary between the OPN-loaded sponges and the surrounding CAM mesenchyme, and the presence of mononuclear cells and lymphocytes has also been demonstrated at the ultrastructural level (60). Similarly, Andrés and colleagues demonstrated that FGF2-loaded alginate beads trigger a robust angiogenic response when implanted on the CAM surface (97). In parallel, the presence of an inflammatory cell infiltrate in the stroma among the newly formed blood vessels was revealed by May Grünwald-Giemsa staining of the treated membranes. Furthermore, to prove the non-redundant role of the inflammatory cells/mediators in FGF2-dependent neovascularization, the experiments were repeated in the presence of hydrocortisone and ketoprofen drugs. The results showed that both drugs were able to inhibit the angiogenic response triggered by FGF2 (97). In this frame, Sung et al. examined the *in vivo* effects of the sequential delivery of dexamethasone followed by VEGF on the immune response and vascular network formation in the CAM assay. Cross-section images of control CAMs showed very few inflammatory cells, mostly macrophages and heterophils. In contrast, an abundant presence of inflammatory cells, fibroblast encapsulation, and swelling (edema) were found in the tissue surrounding the VEGF implant that were inhibited by dexamethasone (98).

Together, these data indicate that the chick embryo CAM represents a platform suitable for the study of the cross talk between angiogenesis and inflammation.

## THE CHICK EMBRYO CHORIOALLANTOIC MEMBRANE FOR DIABETIC RETINOPATHY STUDIES

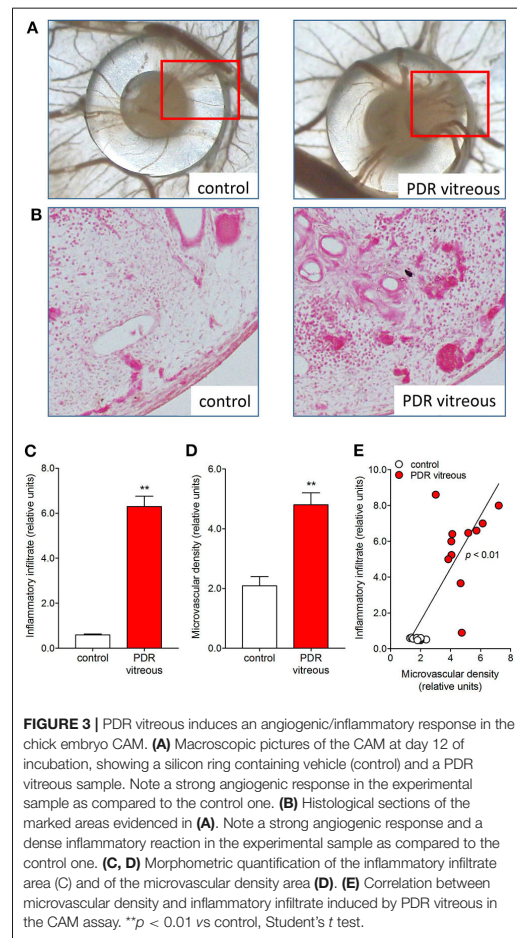
The use of the chick embryo CAM for the study of retinal vascular pathologies dates back to the early '80s. Glaser and colleagues utilized the CAM to investigate the vasoproliferative activities of several mammalian tissue extracts (i.e., liver, cardiac skeletal muscle, and retina). They observed a potent vasoproliferative

response when pellets containing retinal extracts were applied on the top of the CAM, while other adult tissues resulted ineffective (99). With a similar approach, Okamoto and colleagues demonstrated that extracts derived from rabbit retina, iris-ciliary body, and optic nerve exerted an angiogenic activity on CAM, with retinal extracts inducing the strongest effect (100). On these bases, the CAM assay was applied for testing angiogenic factors extracted from both cat and bovine retinas (101), and Prost compared the angiogenic activity of the detached retina with that of the normal attached retina, demonstrating that the detached retina exhibits a stronger angiogenic activity (102). The first experimental evidence that the CAM assay could provide useful information for the study of DR was obtained by Hill and colleagues. In this study, the vitreous humor from PDR patients promoted the proliferation of CAM blood vessels, while vitreous from non-diabetic patients was ineffective (103). Thereafter, Taylor et al. isolated an endothelial cell-stimulating angiogenic factor from the human vitreous and demonstrated its pro-angiogenic activity in the CAM assay (104). In addition to neovascular studies, the CAM has been used as a substrate for maintaining mammalian retinal explants in culture (105) and as a model for testing novel surgical procedures for cutting and coagulating the retinal vasculature (106). More recently, the CAM has represented a platform to evaluate the pro-angiogenic/pro-inflammatory activity of the humor vitreous obtained from PDR patients.

### The Chick Embryo Chorioallantoic Membrane and PDR Vitreous Humor

Vitreous humor obtained via *pars plana* vitrectomy from PDR patients has been shown to exert significant biological responses when delivered *in vitro* and *in vivo* to different cell types in various pre-clinical experimental models [reviewed in (107)]. Thus, the study of the biological activity of PDR vitreous may provide further insights into the relationship between inflammation and angiogenesis. It has been demonstrated that PDR vitreous contains high levels of both pro-inflammatory and pro-angiogenic factors (17, 108). As a consequence, the biological activity exerted by PDR vitreous in *in vitro* and *in vivo* models depends on the balance between all the mediators that have accumulated in the ocular fluid during the progression of the disease and that are present at time of harvesting. Moreover, PDR vitreous can be employed in several experimental models in order to screen and characterize drugs with potential pharmacological applications.

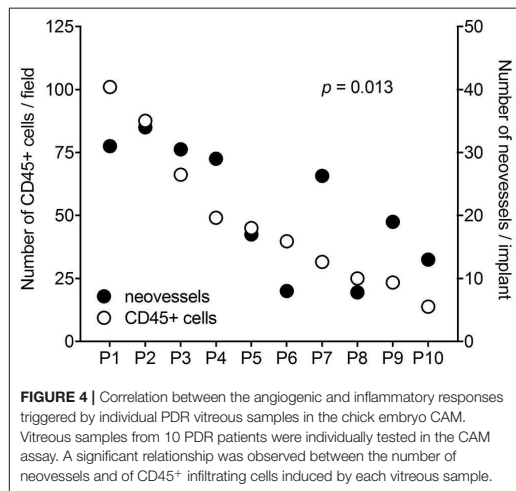
In this frame, we have shown that PDR vitreous induces a pro-angiogenic response in endothelial cells whereas vitreous fluid obtained from macular hole patients was ineffective (109–114). Indeed, PDR vitreous fluid activates *in vitro* all the steps of the angiogenic process, including endothelial cell proliferation, motility, sprouting, and tube formation. At the same time, PDR vitreous induces a pro-inflammatory activation of endothelial cells



characterized by the nuclear translocation of the pro-inflammatory transcription factors NF- $\kappa$ B and CREB, ROS production, disruption of endothelial intercellular junctions, upregulation of the cell adhesion receptors vascular cell adhesion protein 1 and ICAM-1 and consequent increase of leukocyte adhesion.

In keeping with these *in vitro* data, the chick embryo CAM assay provided useful *in vivo* information about the pro-angiogenic/pro-inflammatory activity of PDR vitreous. Alginate beads loaded with 2.0  $\mu$ l/pellet of a pool of vitreous samples obtained from PDR patients were engrafted onto the surface of the chick embryo CAM at 11 days of development. After 72 h, several neovessels moving toward the graft were detected. Moreover, the beads containing PDR vitreous attracted a significant population of mononuclear cells, which was absent in controls (115). Significantly, the number of neovessels

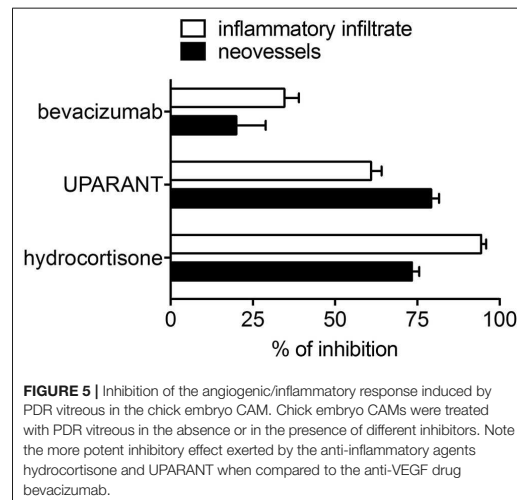




was correlated with the extent of the inflammatory infiltrate (Figure 3).

It is worth noticing that a high variability in the angiogenic and inflammatory responses was observed when vitreous samples obtained from 10 patients with PDR were individually applied to the top of the CAM (115). This may be the consequence of the individual medical case history and clinical features of PDR patients, resulting in a significant qualitative and quantitative heterogeneity in the composition of pro-inflammatory/pro-angiogenic mediators present in the vitreous fluid at the last stages of the disease. Nevertheless, also in this case a significant correlation was observed between the number of infiltrating CD45<sup>+</sup> cells and the number of new blood vessels elicited by PDR vitreous samples in the CAM assay (Figure 4). Since the more angiogenic samples were able to trigger a more significant inflammatory response, these data support the notion that angiogenesis and inflammation are closely related processes during PDR. Accordingly, treatment with hydrocortisone was able to reduce drastically the angiogenic response and the recruitment of inflammatory cells induced by PDR vitreous in the CAM assay. Thus, inflammation appears to play a significant role in the angiogenic activity exerted by PDR vitreous.

*N*-formyl peptide receptors (FPRs) belong to a class of pattern recognition receptors that are involved in controlling inflammation, angiogenesis, tissue repair, and innate immune responses (116). The tetrapeptide Ac-L-Arg-Aib-L-Arg-L-Co(Me)Phe-NH<sub>2</sub> (UPARANT) blocks urokinase-type plasminogen activator receptor (uPAR)-dependent cell signaling by interfering with the complex cross-talk among FPRs, uPAR, and integrins. Accordingly, UPARANT competes with *N*-formyl peptides for the binding to FPRs and inhibits VEGF-driven angiogenesis by preventing FPR activation (117). Recent studies have shown that UPARANT exerts an anti-angiogenic and anti-inflammatory activity when tested in animal



models of oxygen-induced retinopathy by inhibiting ocular neovascularization and by lowering the levels of inflammatory molecules (115). Accordingly, UPARANT successfully inhibited the formation of novel blood vessels promoted by 16 out of 20 individual samples of PDR vitreous in the CAM assay. Again, its anti-angiogenic effect was linearly correlated with a reduced inflammatory infiltrate, suggesting that FPR activation may play a non-redundant role in promoting neovascularization during PDR (115).

Three FPRs have been identified in humans (FPR1–FPR3), characterized by different ligand properties, biological function and cellular distribution (118). Among them, FPR3 appears to mediate pro-angiogenic responses in human endothelial cells (119). It must be pointed out that the murine genome contains eight FPR-related sequences (120) whereas the presence of FPR gene ortholog(s) in birds is more uncertain. Indeed, a cell surface protein immunoreactive with a specific anti-human FPR1 antibody is detectable in chick embryo neurons and glial cells and BLAST search has identified numerous putative *N*-formyl peptide receptors in the avian genome. However, experimental evidences suggest that these receptors might be identified with members of the chemokine receptor CXCR4 subfamily able to act as *N*-formyl peptide binders (121). Thus, caution should be taken before extrapolating the results obtained in animal models, including the CAM, about the possible impact of FPRs on the angiogenic process in humans.

Notably, unlike the anti-inflammatory agents hydrocortisone and UPARANT, the anti-VEGF drug bevacizumab induces only a moderate inhibition of neovascularization and inflammatory cell recruitment promoted in the CAM assay by PDR vitreous-loaded beads [see Figure 5 and (115)]. The limited efficacy of bevacizumab may depend on the presence of several other pro-inflammatory and/or pro-angiogenic cytokines and growth factors in addition to VEGF, which contribute to

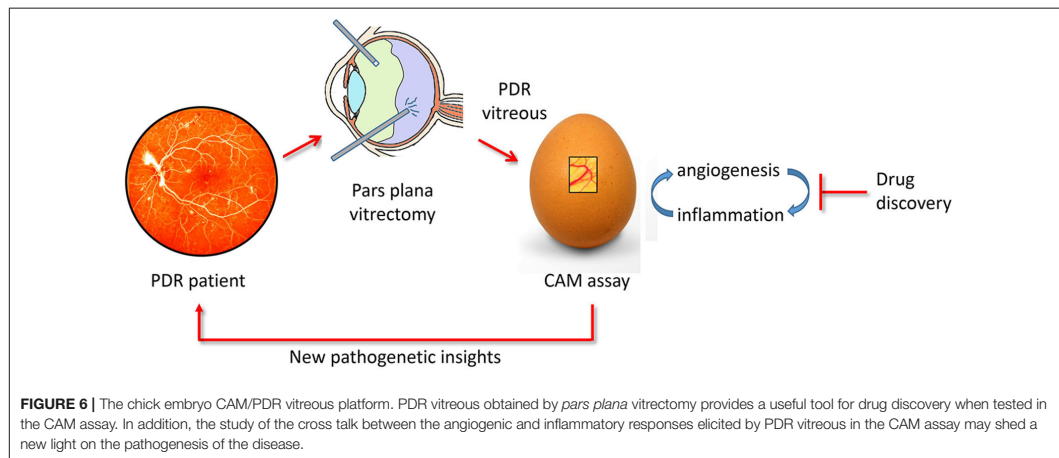


**FIGURE 6 |** The chick embryo CAM/PDR vitreous platform. PDR vitreous obtained by *pars plana* vitrectomy provides a useful tool for drug discovery when tested in the CAM assay. In addition, the study of the cross talk between the angiogenic and inflammatory responses elicited by PDR vitreous in the CAM assay may shed a new light on the pathogenesis of the disease.

the biological activity of PDR vitreous. In keeping with this hypothesis, the biotechnological heparin-like molecule K5-N,OS(H), endowed with the capacity to bind several heparin-binding inflammatory and/or angiogenic mediators present in PDR vitreous, have shown a potency much stronger than bevacizumab in inhibiting the angiogenic response elicited by PDR vitreous (109).

Taken together, these data suggest that the pro-angiogenic and pro-inflammatory activity of PDR vitreous may depend on the synergistic action of multiple molecules, supporting the belief that inflammation and angiogenesis may be strictly correlated, with inflammation being a relevant factor in the formation of novel retinal blood vessels during PDR.

## CONCLUDING REMARKS

The chick embryo CAM assay presents numerous advantages, such as its low cost, reproducibility and reliability, and simplicity in execution. Furthermore, in most countries the use of chick embryo until day 17 of development is not subjected to regulatory rules in order to obtain ethics committee approval for animal experimentation.

As described in this review, recent experimental evidence has shown that the vitreous obtained from PDR patients elicits angiogenic and inflammatory responses when delivered on the top of the CAM. Notably, despite the fact the PDR vitreous samples are collected after *pars plana* vitrectomy at the end stage of the disease, when no other therapeutic interventions are available, individual samples are characterized by a highly variable biological effect when tested in the CAM assay. Such variability has been observed also in *in vitro* experiments when the same samples were tested on cultured endothelial cells. These data indicate that such variability does not represent a drawback of the CAM assay but it rather reflects an individual heterogeneity among PDR patients, possibly related

to differences in their medical case history and clinical features that result in a different angiogenic/inflammatory profile. Nevertheless, despite this heterogeneity, a significant direct correlation has been observed between the extent of neovascular and inflammatory responses elicited by PDR vitreous samples in the CAM assay, strengthening the concept that a tight correlation indeed exists between angiogenesis and inflammation in PDR. This concept is supported by the observations that different anti-inflammatory agents hamper the angiogenic activity exerted by PDR vitreous, as well as by recombinant growth factors/cytokines.

The clinical observation that anti-VEGF therapies may show only a limited effect in PDR patients calls for new pharmacologic interventions. New insights into the impact of inflammation in the pathogenesis of PDR may allow the discovery of novel therapeutic targets. The association of anti-angiogenic and anti-inflammatory drugs may therefore be beneficial for treating PDR. In this frame, the CAM assay may represent a suitable platform for a rapid *in vivo* screening of novel drug candidates.

A critical limitation in the use of the CAM for *in vivo* studies may be the lack of avian-specific reagents, as well as the presence of species-specific differences and the insufficient genomic information. However, the usage of retroviral, adenoviral, and lentiviral vectors has been applied to the infection of the CAM, making them express a long-lasting viral transgene. This technique has been employed for studying dominant-negative gene products, as well as for evaluating the effects of intracellular or membrane-bound proteins. In addition, the achievement of the chick embryo genome sequencing (122) should support the synthesis of a broad panel of antibodies with high specificity for chick cells and stroma components.

In conclusion, the CAM assay may represent a cost-effective and rapid tool for the study of the relationship between

neovascular and inflammatory responses elicited in PDR and for the screening of novel therapeutic agents (Figure 6).

## AUTHOR CONTRIBUTIONS

MP revised and redacted the final version. All authors contributed to the writing of the manuscript.

## REFERENCES

- Congdon N, O'Colmain B, Klaver CC, Klein R, Munoz B, Friedman DS, et al. Causes and prevalence of visual impairment among adults in the United States. *Arch Ophthalmol.* (2004) 122:477–85. doi: 10.1001/archophth.122.4.477
- International Diabetes Federation. *Diabetes Atlas*. 9 ed. (2019). Available online at: <http://www.diabetesatlas.org/>.
- Yau JW, Rogers SL, Kawasaki R, Lamoureux EL, Kowalski JW, Bek T, et al. Global prevalence and major risk factors of diabetic retinopathy. *Diabetes Care.* (2012) 35:556–64. doi: 10.2337/dc11-1909
- Bandello F, Lattanzio R, Zucchiatti I, Del Turco C. Pathophysiology and treatment of diabetic retinopathy. *Acta Diabetol.* (2013) 50:1–20. doi: 10.1007/s00592-012-0449-3
- Semeraro F, Cancarini A, dell'Omo R, Rezzola S, Romano MR, Costagliola C. Diabetic retinopathy: vascular and inflammatory disease. *J Diabetes Res.* (2015) 2015:582060. doi: 10.1155/2015/582060
- Stitt AW, Curtis TM, Chen M, Medina RJ, McKay GJ, Jenkins A, et al. The progress in understanding and treatment of diabetic retinopathy. *Prog Retin Eye Res.* (2016) 51:156–86. doi: 10.1016/j.preteyeres.2015.08.001
- Tang J, Kern TS. Inflammation in diabetic retinopathy. *Prog Retin Eye Res.* (2011) 30:343–58. doi: 10.1016/j.preteyeres.2011.05.002
- Semeraro F, Morescalchi F, Cancarini A, Russo A, Rezzola S, Costagliola C. Diabetic retinopathy, a vascular and inflammatory disease: therapeutic implications. *Diabetes Metab.* (2019) 45:517–27. doi: 10.1016/j.diabet.2019.04.002
- Powell ED, Field RA. Diabetic retinopathy and rheumatoid arthritis. *Lancet.* (1964) 2:17–8. doi: 10.1016/S0140-6736(64)90008-X
- Abu El-Asrar AM. Evolving strategies in the management of diabetic retinopathy. *Middle East Afr J Ophthalmol.* (2013) 20:273–82. doi: 10.4103/0974-9233.119993
- Ahmadi H, Feghhi M, Tabatabaei H, Shoeibi N, Ramezani A, Mohebbi MR. Triamcinolone acetonide in silicone-filled eyes as adjunctive treatment for proliferative vitreoretinopathy: a randomized clinical trial. *Ophthalmology.* (2008) 115:1938–43. doi: 10.1016/j.ophtha.2008.05.016
- Diabetic Retinopathy Clinical Research N. A randomized trial comparing intravitreal triamcinolone acetonide and focal/grid photocoagulation for diabetic macular edema. *Ophthalmology.* (2008) 115:1447–9. doi: 10.1016/j.ophtha.2008.06.015
- Miller JW, Le Couter J, Strauss EC, Ferrara N. Vascular endothelial growth factor a in intraocular vascular disease. *Ophthalmology.* (2013) 120:106–14. doi: 10.1016/j.ophtha.2012.07.038
- Gao S, Lin Z, Shen X. Anti-vascular endothelial growth factor therapy as an alternative or adjunct to pan-retinal photocoagulation in treating proliferative diabetic retinopathy: meta-analysis of randomized trials. *Front Pharmacol.* (2020) 11:849. doi: 10.3389/fphar.2020.00849
- Kwong TQ, Mohamed M. Anti-vascular endothelial growth factor therapies in ophthalmology: current use, controversies and the future. *Br J Clin Pharmacol.* (2014) 78:699–706. doi: 10.1111/bcp.12371
- Rezzola S, Belleri M, Gariano G, Ribatti D, Costagliola C, Semeraro F, et al. *In vitro* and *ex vivo* retina angiogenesis assays. *Angiogenesis.* (2014) 17:429–42. doi: 10.1007/s10456-013-9398-x
- Wang S, Park JK, Duh EJ. Novel targets against retinal angiogenesis in diabetic retinopathy. *Curr Diab Rep.* (2012) 12:355–63. doi: 10.1007/s11892-012-0289-0
- Rezzola S, Paganini G, Semeraro F, Presta M, Tobia C. Zebrafish (Danio rerio) embryo as a platform for the identification of novel angiogenesis inhibitors of retinal vascular diseases. *Biochim Biophys Acta.* (2016) 1862:1291–6. doi: 10.1016/j.bbdis.2016.04.009
- Stahl A, Connor KM, Sapieha P, Chen J, Dennison RJ, Krah NM, et al. The mouse retina as an angiogenesis model. *Invest Ophthalmol Vis Sci.* (2010) 51:2813–26. doi: 10.1167/iovs.10-5176
- Cai X, Sezate SA, McGinnis JF. Neovascularization: ocular diseases, animal models and therapies. *Adv Exp Med Biol.* (2012) 723:245–52. doi: 10.1007/978-1-4614-0631-0\_32
- Wells DJ. Animal welfare and the 3Rs in European biomedical research. *Ann N Y Acad Sci.* (2011) 1245:14–6. doi: 10.1111/j.1749-6632.2011.06335.x
- Ribatti D. The chick embryo chorioallantoic membrane (CAM). A multifaceted experimental model. *Mech Dev.* (2016) 141:70–7. doi: 10.1016/j.mod.2016.05.003
- Carmeliet P. Mechanisms of angiogenesis and arteriogenesis. *Nat Med.* (2000) 6:389–95. doi: 10.1038/74651
- Ribatti D, Crivellato E. "Sprouting angiogenesis", a reappraisal. *Dev Biol.* (2012) 372:157–65. doi: 10.1016/j.ydbio.2012.09.018
- Papetti M, Herman IM. Mechanisms of normal and tumor-derived angiogenesis. *Am J Physiol Cell Physiol.* (2002) 282:C947–70. doi: 10.1152/ajpcell.00389.2001
- Hoying JB, Utzinger U, Weiss JA. Formation of microvascular networks: role of stromal interactions directing angiogenic growth. *Microcirculation.* (2014) 21:278–89. doi: 10.1111/micc.12115
- Eelen G, de Zeeuw P, Treps L, Harjes U, Wong BW, Carmeliet P. Endothelial cell metabolism. *Physiol Rev.* (2018) 98:3–58. doi: 10.1152/physrev.00001.2017
- Ronca R, Benkheil M, Mitola S, Struyf S, Liekens S. Tumor angiogenesis revisited: regulators and clinical implications. *Med Res Rev.* (2017) 37:1231–74. doi: 10.1002/med.21452
- Wallez Y, Vilgrain I, Huber P. Angiogenesis: the VE-cadherin switch. *Trends Cardiovasc Med.* (2006) 16:55–9. doi: 10.1016/j.tcm.2005.11.008
- Potente M, Gerhardt H, Carmeliet P. Basic and therapeutic aspects of angiogenesis. *Cell.* (2011) 146:873–87. doi: 10.1016/j.cell.2011.08.039
- Jain RK. Molecular regulation of vessel maturation. *Nat Med.* (2003) 9:685–93. doi: 10.1038/nm0603-685
- Lorenzi M. The polyol pathway as a mechanism for diabetic retinopathy: attractive, elusive, and resilient. *Exp Diabetes Res.* (2007) 2007:61038. doi: 10.1155/2007/61038
- Du XL, Edelstein D, Rossetti L, Fantus IG, Goldberg H, Ziyadeh F, et al. Hyperglycemia-induced mitochondrial superoxide overproduction activates the hexosamine pathway and induces plasminogen activator inhibitor-1 expression by increasing Sp1 glycosylation. *Proc Natl Acad Sci USA.* (2000) 97:12222–6. doi: 10.1073/pnas.97.22.12222
- Xu J, Chen LJ, Yu J, Wang HJ, Zhang F, Liu Q, et al. Involvement of advanced glycation end products in the pathogenesis of diabetic retinopathy. *Cell Physiol Biochem.* (2018) 48:705–17. doi: 10.1159/000491897
- Santiago AR, Boia R, Aires ID, Ambrósio AF, Fernandes R. Sweet stress: coping with vascular dysfunction in diabetic retinopathy. *Front Physiol.* (2018) 9:820. doi: 10.3389/fphys.2018.00820
- Koya D, King GL. Protein kinase C activation and the development of diabetic complications. *Diabetes.* (1998) 47:859–66. doi: 10.2337/diabetes.47.6.859

## FUNDING

This work was supported in part by Fondazione Diabete Ricerca to SR and by Associazione Italiana per la Ricerca sul Cancro (IG 2019 no. 23116) to MP. SR was supported by Fondazione Umberto Veronesi fellowship and by Associazione Garda Vita (Prof. R. Tosoni fellowship).

37. Geraldes P, King GL. Activation of protein kinase C isoforms and its impact on diabetic complications. *Circ Res.* (2010) 106:1319–31. doi: 10.1161/CIRCRESAHA.110.217117
38. Zheng L, Szabó C, Kern TS. Poly(ADP-ribose) polymerase is involved in the development of diabetic retinopathy via regulation of nuclear factor-kappaB. *Diabetes.* (2004) 53:2960–7. doi: 10.2337/diabetes.53.11.2960
39. Satofuka S, Ichihara A, Nagai N, Noda K, Ozawa Y, Fukamizu A, et al. (Pro)renin receptor-mediated signal transduction and tissue renin-angiotensin system contribute to diabetes-induced retinal inflammation. *Diabetes.* (2009) 58:1625–33. doi: 10.2337/db08-0254
40. Sone H, Kawakami Y, Okuda Y, Kondo S, Hanatani M, Suzuki H, et al. Vascular endothelial growth factor is induced by long-term high glucose concentration and up-regulated by acute glucose deprivation in cultured bovine retinal pigmented epithelial cells. *Biochem Biophys Res Commun.* (1996) 221:193–8. doi: 10.1006/bbrc.1996.0568
41. Durham JT, Herman IM. Microvascular modifications in diabetic retinopathy. *Curr Diab Rep.* (2011) 11:253–64. doi: 10.1007/s11892-011-0204-0
42. Barot M, Gokulgandhi MR, Patel S, Mitra AK. Microvascular complications and diabetic retinopathy: recent advances and future implications. *Fut Med Chem.* (2013) 5:301–14. doi: 10.4155/fmc.12.206
43. Vermees L, Steinmetz ET, Zeyen LJ, van der Veen EA. Rheological properties of white blood cells are changed in diabetic patients with microvascular complications. *Diabetologia.* (1987) 30:434–6. doi: 10.1007/BF00292548
44. Loukovaara S, Koivunen P, Ingles M, Escobar J, Vento M, Andersson S. Elevated protein carbonyl and HIF-1alpha levels in eyes with proliferative diabetic retinopathy. *Acta Ophthalmol.* (2014) 92:323–7. doi: 10.1111/aos.12186
45. Vadlapatla RK, Vadlapudi AD, Mitra AK. Hypoxia-inducible factor-1 (HIF-1): a potential target for intervention in ocular neovascular diseases. *Curr Drug Targets.* (2013) 14:919–35. doi: 10.2174/13894501113149990015
46. Wilkinson CP, Ferris FL, 3rd, Klein RE, Lee PP, Agardh CD, Davis M, et al. Proposed international clinical diabetic retinopathy and diabetic macular edema disease severity scales. *Ophthalmology.* (2003) 110:1677–82. doi: 10.1016/S0161-6420(03)00475-5
47. Gariano RF, Gardner TW. Retinal angiogenesis in development and disease. *Nature.* (2005) 438:960–6. doi: 10.1038/nature04482
48. Sherris D. Ocular drug development—future directions. *Angiogenesis.* (2007) 10:71–6. doi: 10.1007/s10456-007-9068-y
49. Rezzola S, Nawaz MI, Cancarini A, Semeraro F, Presta M. Vascular endothelial growth factor in the vitreous of proliferative diabetic retinopathy patients: chasing a hiding prey? *Diabetes Care.* (2019) 42:e105–6. doi: 10.2337/dc18-2527
50. Spranger J, Osterhoff M, Reimann M, Mohlig M, Ristow M, Francis MK, et al. Loss of the antiangiogenic pigment epithelium-derived factor in patients with angiogenic eye disease. *Diabetes.* (2001) 50:2641–5. doi: 10.2337/diabetes.50.12.2641
51. Jackson JR, Seed MP, Kircher CH, Willoughby DA, Winkler JD. The codependence of angiogenesis and chronic inflammation. *Faseb J.* (1997) 11:457–65. doi: 10.1096/fasebj.11.6.9194526
52. Carmeliet P, Jain RK. Angiogenesis in cancer and other diseases. *Nature.* (2000) 407:249–57. doi: 10.1038/35025220
53. Zijlstra A, Seandel M, Kupriyanova TA, Partridge JJ, Madsen MA, Hahn-Dantona EA, et al. Proangiogenic role of neutrophil-like inflammatory heterophils during neovascularization induced by growth factors and human tumor cells. *Blood.* (2006) 107:317–27. doi: 10.1182/blood-2005-04-1458
54. Pober JS, Sessa WC. Evolving functions of endothelial cells in inflammation. *Nat Rev Immunol.* (2007) 7:803–15. doi: 10.1038/nri2171
55. Danese S, Dejana E, Fiocchi C. Immune regulation by microvascular endothelial cells: directing innate and adaptive immunity, coagulation, and inflammation. *J Immunol.* (2007) 178:6017–22. doi: 10.4049/jimmunol.178.10.6017
56. Williams CS, Mann M, DuBois RN. The role of cyclooxygenases in inflammation, cancer, and development. *Oncogene.* (1999) 18:7908–16. doi: 10.1038/sj.onc.1203286
57. Romagnani P, Lasagni L, Annunziato F, Serio M, Romagnani S. CXC chemokines: the regulatory link between inflammation and angiogenesis. *Trends Immunol.* (2004) 25:201–9. doi: 10.1016/j.it.2004.02.006
58. Voronov E, Shouval DS, Krelin Y, Cagnano E, Benharroch D, Iwakura Y, et al. IL-1 is required for tumor invasiveness and angiogenesis. *Proc Natl Acad Sci USA.* (2003) 100:2645–50. doi: 10.1073/pnas.0437939100
59. Naldini A, Leali D, Pucci A, Morena E, Carraro F, Nico B, et al. Cutting Edge: IL-1beta mediates the proangiogenic activity of osteopontin-activated human monocytes. *J Immunol.* (2006) 177:4267–70. doi: 10.4049/jimmunol.177.7.4267
60. Leali D, Dell'Era P, Stabile H, Sennino B, Chambers AF, Naldini A, et al. Osteopontin (Eta-1) and fibroblast growth factor-2 cross-talk in angiogenesis. *J Immunol.* (2003) 171:1085–93. doi: 10.4049/jimmunol.171.2.1085
61. Aplin AC, Gelati M, Fogel E, Carnevale E, Nicosia RF. Angiopoietin-1 and vascular endothelial growth factor induce expression of inflammatory cytokines before angiogenesis. *Physiol Genomics.* (2006) 27:20–8. doi: 10.1152/physiolgenomics.00048.2006
62. Angelo LS, Kurzrock R. Vascular endothelial growth factor and its relationship to inflammatory mediators. *Clin Cancer Res.* (2007) 13:2825–30. doi: 10.1158/1078-0432.CCR-06-2416
63. Rius J, Guma M, Schachtrup C, Akassoglou K, Zinkernagel AS, Nizet V, et al. NF-kappaB links innate immunity to the hypoxic response through transcriptional regulation of HIF-1alpha. *Nature.* (2008) 453:807–11. doi: 10.1038/nature06905
64. Taylor CT, Cummins EP. The role of NF-kappaB in hypoxia-induced gene expression. *Ann N Y Acad Sci.* (2009) 1177:178–84. doi: 10.1111/j.1749-6632.2009.05024.x
65. Fitzpatrick SF, Tambuwala MM, Bruning U, Schaible B, Scholz CC, Byrne A, et al. An intact canonical NF-kappaB pathway is required for inflammatory gene expression in response to hypoxia. *J Immunol.* (2011) 186:1091–6. doi: 10.4049/jimmunol.1002256
66. Goldberg RB. Cytokine and cytokine-like inflammation markers, endothelial dysfunction, and imbalanced coagulation in development of diabetes and its complications. *J Clin Endocrinol Metab.* (2009) 94:3171–82. doi: 10.1210/jc.2008-2534
67. dell'Omo R, Semeraro F, Bamonte G, Cifariello F, Romano MR, Costagliola C. Vitreous mediators in retinal hypoxic diseases. *Mediators Inflamm.* (2013) 2013:935301. doi: 10.1155/2013/935301
68. Abcouwer SF. Angiogenic factors and cytokines in diabetic retinopathy. *J Clin Cell Immunol.* (2013) 1–12. doi: 10.4172/2155-9899
69. Antonetti DA, Klein R, Gardner TW. Diabetic retinopathy. *N Engl J Med.* (2012) 366:1227–39. doi: 10.1056/NEJMra1005073
70. Kern TS. Contributions of inflammatory processes to the development of the early stages of diabetic retinopathy. *Exp Diabetes Res.* (2007) 2007:95103. doi: 10.1155/2007/95103
71. Zhang W, Liu H, Rojas M, Caldwell RW, Caldwell RB. Anti-inflammatory therapy for diabetic retinopathy. *Immunotherapy.* (2011) 3:609–28. doi: 10.2217/imt.11.24
72. Danis RP, Ciulla TA, Criswell M, Pratt L. Anti-angiogenic therapy of proliferative diabetic retinopathy. *Expert Opin Pharmacother.* (2001) 2:395–407. doi: 10.1517/14656566.2.3.395
73. Nawaz MI, Abouammoh M, Khan HA, Alhomidia AS, Alfaran MF, Ola MS. Novel drugs and their targets in the potential treatment of diabetic retinopathy. *Med Sci Monitor.* (2013) 19:300–8. doi: 10.12659/MSM.883895
74. Romanoff AL. *The Avian Embryo: Structural and Functional Development.* New York, NY: Mac Millan (1960).
75. Ribatti D. The chick embryo chorioallantoic membrane as a model for tumor biology. *Exp Cell Res.* (2014) 328:314–24. doi: 10.1016/j.yexcr.2014.06.010
76. DeFouw DO, Rizzo VJ, Steinfeld R, Feinberg RN. Mapping of the microcirculation in the chick chorioallantoic membrane during normal angiogenesis. *Microvasc Res.* (1989) 38:136–47. doi: 10.1016/0026-2862(89)90022-8
77. Schlatter P, König MF, Karlsson LM, Burri PH. Quantitative study of intussusceptive capillary growth in the chorioallantoic membrane (CAM) of the chicken embryo. *Microvasc Res.* (1997) 54:65–73. doi: 10.1006/mvres.1997.2022

78. Dimitropoulou C, Malkusch W, Fait E, Maragoudakis ME, Konerding MA. The vascular architecture of the chick chorioallantoic membrane: sequential quantitative evaluation using corrosion casting. *Angiogenesis*. (1998) 2:255–63. doi: 10.1023/A:1009210918738
79. Ausprunk DH, Knighton DR, Folkman J. Differentiation of vascular endothelium in the chick chorioallantois: a structural and autoradiographic study. *Dev Biol*. (1974) 38:237–48. doi: 10.1016/0012-1606(74)90004-9
80. Auerbach R, Kubai L, Knighton D, Folkman J. A simple procedure for the long-term cultivation of chicken embryos. *Dev Biol*. (1974) 41:391–4. doi: 10.1016/0012-1606(74)90316-9
81. Ribatti D, Nico B, Vacca A, Presta M. The gelatin sponge-chorioallantoic membrane assay. *Nat Protoc*. (2006) 1:85–91. doi: 10.1038/nprot.2006.13
82. Mast J, Goddeeris BM. Development of immunocompetence of broiler chickens. *Vet Immunol Immunopathol*. (1999) 70:245–56. doi: 10.1016/S0165-2427(99)00079-3
83. Davison TF. The immunologists' debt to the chicken. *Br Poult Sci*. (2003) 44:6–21. doi: 10.1080/0007166031000085364
84. Funk PE, Thompson CB. Current concepts in chicken B cell development. *Curr Top Microbiol Immunol*. (1996) 212:17–28. doi: 10.1007/978-3-642-80057-3\_3
85. Janse EM, Jeurissen SH. Ontogeny and function of two non-lymphoid cell populations in the chicken embryo. *Immunobiology*. (1991) 182:472–81. doi: 10.1016/S0171-2985(11)80211-1
86. Jankovic BD, Isakovic K, Lukic ML, Vujanovic NL, Petrovic S, Markovic BM. Immunological capacity of the chicken embryo. I. Relationship between the maturation of lymphoid tissues and the occurrence of cell-mediated immunity in the developing chicken embryo. *Immunology*. (1975) 29:497–508.
87. Weber WT, Mausner R. Migration patterns of avian embryonic bone marrow cells and their differentiation to functional T and B cells. *Adv Exp Med Biol*. (1977) 88:47–59. doi: 10.1007/978-1-4613-4169-7\_5
88. Genovese KJ, He H, Swaggerty CL, Kogut MH. The avian heterophil. *Dev Comp Immunol*. (2013) 41:334–40. doi: 10.1016/j.dci.2013.03.021
89. Jeurissen SH, Janse EM. Distribution and function of non-lymphoid cells in liver and spleen of embryonic and adult chickens. *Prog Clin Biol Res*. (1989) 307:149–57.
90. Hu T, Wu Z, Bush SJ, Freem L, Vervelde L, Summers KM, et al. Characterization of subpopulations of chicken mononuclear phagocytes that express TIM4 and CSF1R. *J Immunol*. (2019) 202:1186–99. doi: 10.4049/jimmunol.1800504
91. Catino S, Tutino M, Ruggieri S, Marinaccio C, Giua R, de Gennaro G, et al. Angiogenic activity *in vivo* of the particulate matter (PM10). *Ecotoxicol Environ Saf*. (2017) 140:156–61. doi: 10.1016/j.ecoenv.2017.02.036
92. Zijlstra A, Aimes RT, Zhu D, Regazzoni K, Kupriyanova T, Seandel M, et al. Collagenolysis-dependent angiogenesis mediated by matrix metalloproteinase-13 (collagenase-3). *J Biol Chem*. (2004) 279:27633–45. doi: 10.1074/jbc.M313617200
93. Jakob W, Jentzsch KD, Mauersberger B, Heder G. The chick embryo chorioallantoic membrane as a bioassay for angiogenesis factors: reactions induced by carrier materials. *Exp Pathol*. (1978) 15:241–9. doi: 10.1016/S0014-4908(78)80064-7
94. Ribatti D, Nico B, Vacca A, Roncali L, Presta M. Endogenous and exogenous fibroblast growth factor-2 modulate wound healing in the chick embryo chorioallantoic membrane. *Angiogenesis*. (1999) 3:89–95. doi: 10.1023/A:1009049932252
95. Bender C, Partecke LI, Kindel E, Döring F, Lademann J, Heidecke CD, et al. The modified HET-CAM as a model for the assessment of the inflammatory response to tissue tolerable plasma. *Toxicol In Vitro*. (2011) 25:530–7. doi: 10.1016/j.tiv.2010.11.012
96. Cirligeriu L, Cimpeanu AM, Calniceanu H, Vladau M, Sarb S, Raica M, et al. Hyaluronic acid/bone substitute complex implanted on chick embryo chorioallantoic membrane induces osteoblastic differentiation and angiogenesis, but not inflammation. *Int J Mol Sci*. (2018) 19:4119. doi: 10.3390/ijms19124119
97. Andrés G, Leali D, Mitola S, Coltrini D, Camozzi M, Corsini M, et al. A pro-inflammatory signature mediates FGF2-induced angiogenesis. *J Cell Mol Med*. (2009) 13:2083–108. doi: 10.1111/j.1582-4934.2008.00415.x
98. Sung J, Barone PW, Kong H, Strano MS. Sequential delivery of dexamethasone and VEGF to control local tissue response for carbon nanotube fluorescence based micro-capillary implantable sensors. *Biomaterials*. (2009) 30:622–31. doi: 10.1016/j.biomaterials.2008.09.052
99. Glaser BM, D'Amore PA, Michels RG, Patz A, Fenselau A. Demonstration of vasoproliferative activity from mammalian retina. *J Cell Biol*. (1980) 84:298–304. doi: 10.1083/jcb.84.2.298
100. Okamoto T, Oikawa S, Toyota T, Goto Y. Angiogenesis factors in ocular tissues of normal rabbits on chorioallantoic membrane assay. *Tohoku J Exp Med*. (1988) 154:63–70. doi: 10.1620/tjem.154.63
101. Kissun RD, Hill CR, Garner A, Phillips P, Kumar S, Weiss JB. A low-molecular-weight angiogenic factor in cat retina. *Br J Ophthalmol*. (1982) 66:165–9. doi: 10.1136/bjo.66.3.165
102. Prost M. Experimental studies on the angiogenic activity of the detached retina. *Graefes Arch Clin Exp Ophthalmol*. (1990) 228:83–5. doi: 10.1007/BF02764297
103. Hill CR, Kissun RD, Weiss JB, Garner A. Angiogenic factor in vitreous from diabetic retinopathy. *Experientia*. (1983) 39:583–5. doi: 10.1007/BF01971107
104. Taylor CM, Kissun RD, Schor AM, McLeod D, Garner A, Weiss JB. Endothelial cell-stimulating angiogenic factor in vitreous from extraretinal neovascularizations. *Invest Ophthalmol Vis Sci*. (1989) 30:2174–8.
105. Huxlin KR, Sefton AJ, Furby J. Explanation of fetal murine retinae to the chorioallantoic membrane of the chicken embryo. *J Neurosci Methods*. (1992) 41:53–64. doi: 10.1016/0165-0270(92)90123-U
106. Leng T, Miller JM, Bilbao KV, Palanker DV, Huie P, Blumenkranz MS. The chick chorioallantoic membrane as a model tissue for surgical retinal research and simulation. *Retina*. (2004) 24:427–34. doi: 10.1097/00006982-200406000-00014
107. Nawaz IM, Rezzola S, Cancarini A, Russo A, Costagliola C, Semeraro F, et al. Human vitreous in proliferative diabetic retinopathy: characterization and translational implications. *Prog Retin Eye Res*. (2019) 72:100756. doi: 10.1016/j.preteyeres.2019.03.002
108. Dai Y, Wu Z, Wang F, Zhang Z, Yu M. Identification of chemokines and growth factors in proliferative diabetic retinopathy vitreous. *Biomed Res Int*. (2014) 2014:486386. doi: 10.1155/2014/486386
109. Rezzola S, Dal Monte M, Belleri M, Bugatti A, Chioldelli P, Corsini M, et al. Therapeutic potential of anti-angiogenic multitarget N,O-sulfated *E. coli* K5 polysaccharide in diabetic retinopathy. *Diabetes*. (2015) 64:2581–92. doi: 10.2337/db14-1378
110. Dal Monte M, Rezzola S, Cammalleri M, Belleri M, Locri F, Morbidelli L, et al. Antiangiogenic effectiveness of the urokinase receptor-derived peptide UPARANT in a model of oxygen-induced retinopathy. *Invest Ophthalmol Vis Sci*. (2015) 56:2392–407. doi: 10.1167/iovs.14-16323
111. Aiello LP, Avery RL, Arrigg PG, Keyt BA, Jampel HD, Shah ST, et al. Vascular endothelial growth factor in ocular fluid of patients with diabetic retinopathy and other retinal disorders. *N Engl J Med*. (1994) 331:1480–7. doi: 10.1056/NEJM199412013312203
112. Takagi H, Watanabe D, Suzuma K, Kurimoto M, Suzuma I, Ohashi H, et al. Novel role of erythropoietin in proliferative diabetic retinopathy. *Diabetes Res Clin Pract*. (2007) 77(Suppl. 1):S62–4. doi: 10.1016/j.diabres.2007.01.035
113. Murugeswari P, Shukla D, Kim R, Namperumalsamy P, Stitt AW, Muthukkaruppan V. Angiogenic potential of vitreous from proliferative diabetic retinopathy and eales' disease patients. *PLoS ONE*. (2014) 9:e107551. doi: 10.1371/journal.pone.0107551
114. Rezzola S, Nawaz IM, Cancarini A, Ravelli C, Calza S, Semeraro F, et al. 3D endothelial cell spheroid/human vitreous humor assay for the characterization of anti-angiogenic inhibitors for the treatment of proliferative diabetic retinopathy. *Angiogenesis*. (2017) 20:629–40. doi: 10.1007/s10456-017-9575-4
115. Rezzola S, Corsini M, Chioldelli P, Cancarini A, Nawaz IM, Coltrini D, et al. Inflammation and N-formyl peptide receptors mediate the angiogenic activity of human vitreous humour in proliferative diabetic retinopathy. *Diabetologia*. (2017) 60:719–28. doi: 10.1007/s00125-016-4204-0
116. Preveze N, Liotti F, Marone G, Melillo RM, de Paulis A. Formyl peptide receptors at the interface of inflammation, angiogenesis and tumor growth. *Pharmacol Res*. (2015) 102:184–91. doi: 10.1016/j.phrs.2015.09.017

117. Carriero MV, Bifulco K, Minopoli M, Lista L, Maglio O, Mele L, et al. UPARANT: a urokinase receptor-derived peptide inhibitor of VEGF-driven angiogenesis with enhanced stability and *in vitro* and *in vivo* potency. *Mol Cancer Ther.* (2014) 13:1092–104. doi: 10.1158/1535-7163.MCT-13-0949
118. Ye RD, Boulay F, Wang JM, Dahlgren C, Gerard C, Parmentier M, et al. International union of basic and clinical pharmacology. LXXIII. Nomenclature for the formyl peptide receptor (FPR) family. *Pharmacol Rev.* (2009) 61:119–61. doi: 10.1124/pr.109.001578
119. Nawaz IM, Chiodelli P, Rezzola S, Paganini G, Corsini M, Lodola A, et al. N-tert-butylloxycarbonyl-Phe-Leu-Phe-Leu-Phe (BOC2) inhibits the angiogenic activity of heparin-binding growth factors. *Angiogenesis.* (2018) 21:47–59. doi: 10.1007/s10456-017-9581-6
120. Winther M, Dahlgren C, Forsman H. Formyl peptide receptors in mice and men: similarities and differences in recognition of conventional ligands and modulating lipopeptides. *Basic Clin Pharmacol Toxicol.* (2018) 122:191–8. doi: 10.1111/bcpt.12903
121. Panaro MA, Cianciulli A, Lisi S, Sisto M, Acquafredda A, Mitolo V. Formyl peptide receptor expression in birds. *Immunopharmacol Immunotoxicol.* (2007) 29:1–16. doi: 10.1080/08923970701277569
122. International Chicken Genome Sequencing Consortium. Sequence and comparative analysis of the chicken genome provide unique perspectives on vertebrate evolution. *Nature.* (2004) 432:695–716. doi: 10.1038/nature03154

**Conflict of Interest:** The authors declare that the research was conducted in the absence of any commercial or financial relationships that could be construed as a potential conflict of interest.

Copyright © 2020 Rezzola, Loda, Corsini, Semeraro, Annesse, Presta and Ribatti. This is an open-access article distributed under the terms of the Creative Commons Attribution License (CC BY). The use, distribution or reproduction in other forums is permitted, provided the original author(s) and the copyright owner(s) are credited and that the original publication in this journal is cited, in accordance with accepted academic practice. No use, distribution or reproduction is permitted which does not comply with these terms.



**VEGF-Independent Activation of Müller Cells by the Vitreous from Proliferative Diabetic Retinopathy Patients**

S. Rezzola, J. Guerra, AM. Krishna Chandran, A. Loda, A. Cancarini, P. Sacristani, F. Semeraro, M. Presta.

Int J Mol Sci. 2021 Feb 22;22(4):2179. doi: 10.3390/ijms22042179. PMID: 33671690; PMCID: PMC7926720.







## Article

# VEGF-Independent Activation of Müller Cells by the Vitreous from Proliferative Diabetic Retinopathy Patients

Sara Rezzola <sup>1,\*</sup>, Jessica Guerra <sup>1</sup>, Adwaid Manu Krishna Chandran <sup>1</sup>, Alessandra Loda <sup>1</sup>, Anna Cancarini <sup>2</sup>, Piergiuseppe Sacristani <sup>2</sup>, Francesco Semeraro <sup>2</sup> and Marco Presta <sup>1,3,\*</sup><sup>1</sup> Department of Molecular and Translational Medicine, School of Medicine, University of Brescia, 25123 Brescia, Italy; j.guerra@unibs.it (J.G.); adwaid.krishna@unibs.it (A.M.K.C.); a.loda025@unibs.it (A.L.)<sup>2</sup> Eye Clinic, Department of Neurological and Vision Sciences, University of Brescia, 25123 Brescia, Italy; acancarini@gmail.com (A.C.); piergiuseppe.sacristani@gmail.com (P.S.); francesco.semeraro@unibs.it (F.S.)<sup>3</sup> Italian Consortium for Biotechnology (CIB), Unit of Brescia, 25123 Brescia, Italy

\* Correspondence: sara.rezzola@unibs.it (S.R.); marco.presta@unibs.it (M.P.); Tel.: +39-030-3717311



**Citation:** Rezzola, S.; Guerra, J.; Krishna Chandran, A.M.; Loda, A.; Cancarini, A.; Sacristani, P.; Semeraro, F.; Presta, M. VEGF-Independent Activation of Müller Cells by the Vitreous from Proliferative Diabetic Retinopathy Patients. *Int. J. Mol. Sci.* **2021**, *22*, 2179. <https://doi.org/10.3390/ijms22042179>

Academic Editor: Young Sook Kim

Received: 7 January 2021

Accepted: 19 February 2021

Published: 22 February 2021

**Publisher's Note:** MDPI stays neutral with regard to jurisdictional claims in published maps and institutional affiliations.



**Copyright:** © 2021 by the authors. Licensee MDPI, Basel, Switzerland. This article is an open access article distributed under the terms and conditions of the Creative Commons Attribution (CC BY) license (<https://creativecommons.org/licenses/by/4.0/>).

**Abstract:** Proliferative diabetic retinopathy (PDR), a major complication of diabetes mellitus, results from an inflammation-sustained interplay among endothelial cells, neurons, and glia. Even though anti-vascular endothelial growth factor (VEGF) interventions represent the therapeutic option for PDR, they are only partially efficacious. In PDR, Müller cells undergo reactive gliosis, produce inflammatory cytokines/chemokines, and contribute to scar formation and retinal neovascularization. However, the impact of anti-VEGF interventions on Müller cell activation has not been fully elucidated. Here, we show that treatment of MIO-M1 Müller cells with vitreous obtained from PDR patients stimulates cell proliferation and motility, and activates various intracellular signaling pathways. This leads to cytokine/chemokine upregulation, a response that was not mimicked by treatment with recombinant VEGF nor inhibited by the anti-VEGF drug ranibizumab. In contrast, fibroblast growth factor-2 (FGF2) induced a significant overexpression of various cytokines/chemokines in MIO-M1 cells. In addition, the FGF receptor tyrosine kinase inhibitor BGJ398, the pan-FGF trap NSC12, the heparin-binding protein antagonist N-tert-butylloxycarbonyl-Phe-Leu-Phe-Leu-Phe Boc2, and the anti-inflammatory hydrocortisone all inhibited Müller cell activation mediated by PDR vitreous. These findings point to a role for various modulators beside VEGF in Müller cell activation and pave the way to the search for novel therapeutic strategies in PDR.

**Keywords:** diabetic retinopathy; inflammation; Müller cells; VEGF; vitreous humor

## 1. Introduction

Proliferative diabetic retinopathy (PDR) is an ocular microvascular complication of diabetes [1]. Currently, it affects more than 93 million people in the world, and it represents the leading cause of acquired blindness in the working age population of industrialized regions [1]. PDR is considered as a multifactorial disease, albeit its pathogenesis is not yet fully understood. Indeed, numerous factors contribute to PDR development, including hyperglycemia, oxidative stress, inflammation, and hypoxia, leading to the damage of the vasculature, as well as of neurons and glial cells in the retina [2,3]. Anti-vascular endothelial growth factor (VEGF) drugs represent the pharmacologic option for PDR treatment to this day [4]. Even though anti-VEGF interventions have shown better outcomes than alternative treatments, limitations to anti-VEGF therapies do exist, including poor response in a significant percentage of patients [5–7]. Indeed, VEGF-driven pathways are only part of the complex machinery regulating angiogenesis and inflammation in the eye and the production of other factors may cause resistance to anti-VEGF therapies and limit their efficacy [8]. This creates an unmet need for a better understanding of the pathogenesis of PDR in order to develop more efficacious therapeutic strategies.

Müller cells represent the main glial population of the retina and provide structural support to the neuroretina, radially stretching across its entire thickness. They are the anatomical link between blood vessels and vitreous body, creating a micro-unit involved in the exchange of nourishing molecules and oxygen and in the maintenance of retinal homeostasis [9,10]. During PDR, high blood glucose levels may induce retinal dysfunctions caused by increased levels of oxidative stress, which triggers early neurodegeneration, activation of inflammatory responses, and abnormal neovessel formation [3]. Because of the pathological changes that occur in the retina during PDR, activated Müller cells may undergo reactive gliosis, a non-specific reactive response of glial cells to damage characterized by uncontrolled proliferation, migration, and increased expression of gliosis markers [11,12]. Moreover, Müller cells may undertake a fibrotic trans-differentiation, contributing to the formation of a fibrovascular epiretinal membrane (ERM), which can exert tractional forces on the retinal surface, thus causing retinal detachment [13,14]. In addition, activated Müller cells produce several cytokines and chemokines, contributing to the maintenance of the inflammatory environment, alteration of the blood–retinal barrier (BRB) integrity, and neovascularization [12,15,16].

The vitreous humor undergoes structural and molecular alterations during chronic diabetic conditions that may significantly impact the progression of PDR [3]. Thus, the vitreous obtained via pars plana vitrectomy from patients with PDR can represent a sort of receptacle where pro-angiogenic and proinflammatory mediators with pathological effects on retinal cells accumulate [3,17]. By mimicking the microenvironment facing the diabetic retina, PDR vitreous may therefore represent a valuable tool for a better understanding of the pathogenesis of PDR. Indeed, it has been demonstrated that PDR vitreous induces potent angiogenic and inflammatory responses in endothelial cells [3,18], suitable for the identification of novel pharmacological targets and the evaluation of the efficacy of new drug candidates [3,17–23].

Here, vitreous fluid obtained from PDR patients was used as a tool to investigate the activation that occurs in Müller cells during PDR. The results show that PDR vitreous induces the acquisition of an activated phenotype in Müller cells, characterized by an increase of cell proliferation and migration, intracellular signaling activation, and proinflammatory cytokine/chemokine expression. Surprisingly, we found that the acquisition of this phenotype is not related to VEGF stimulation, whereas treatment of Müller cells with basic fibroblast growth factor (FGF2), a prototypic member of the FGF family [24], induces a significant increase of the expression of various cytokines/chemokines in MIO-M1 cells. Accordingly, the anti-VEGF drug ranibizumab does not affect Müller cell activation mediated by PDR vitreous whereas treatment with the FGF receptor (FGFR) tyrosine kinase inhibitor BGJ398 [25], the pan-FGF trap NSC12 [26], the multi-target heparin-binding protein antagonist N-tert-butylloxycarbonyl-Phe-Leu-Phe-Leu-Phe Boc2 [20], or the anti-inflammatory drug hydrocortisone inhibits, at least in part, the activity of PDR vitreous samples. Together, these data point to a role for various mediators beside VEGF in the response elicited by PDR vitreous in Müller cells.

## 2. Results

### 2.1. MIO-M1 Müller Cells Are Activated by PDR Vitreous

In order to investigate the capacity of PDR vitreous to induce Müller cell activation, MIO-M1 cells were treated with vitreous samples, each pooled from 5–6 diabetic patients. As shown in Figure 1A,B, PDR vitreous stimulates MIO-M1 cell proliferation in a dose- and time-dependent manner. Moreover, it modulates Müller cell motility when assessed in an in vitro wound healing assay (Figure 1C). No significant stimulation of cell proliferation and motility was instead observed when Müller cells were treated with a pool of vitreous samples obtained from patients affected by rhegmatogenous retinal detachment (Figure S1). It must be pointed out that MIO-M1 cells were maintained in culture medium containing 25 mM glucose in these and all the following experiments, thus mimicking more closely a “diabetic-like” microenvironment when cells were treated with PDR vitreous.

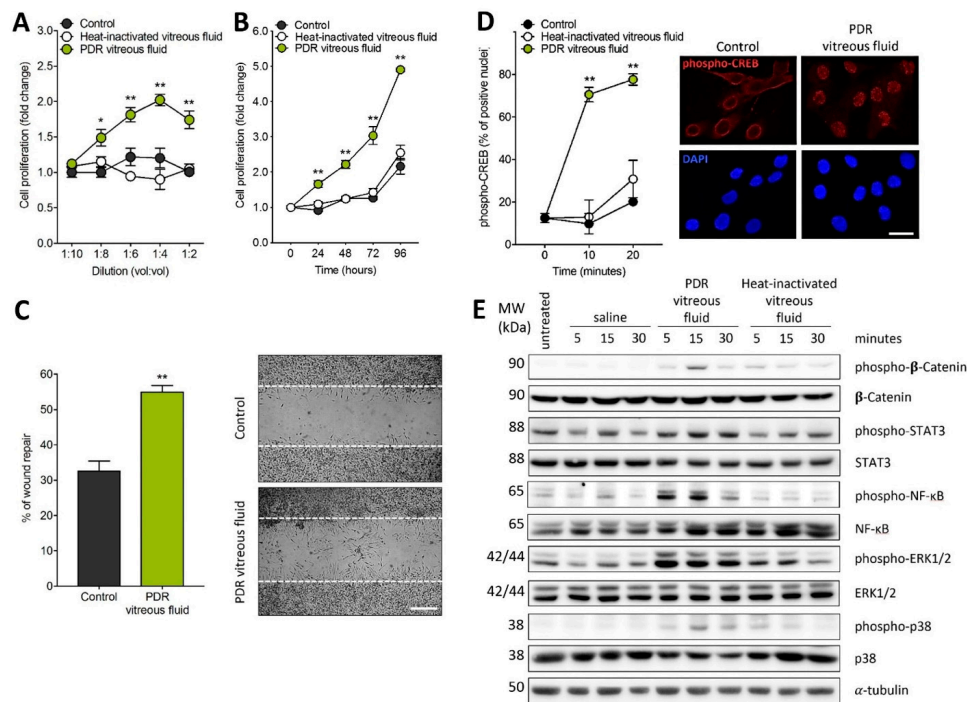


**Figure 1.** Müller cell activation by proliferative diabetic retinopathy (PDR) vitreous. (**A,B**) MIO-M1 cells were treated with increasing amounts of PDR or heat-inactivated vitreous samples (vol:vol dilution in cell culture medium) and counted 72 h thereafter (**A**) or were incubated with 1:4 vitreous dilution and counted at different time points (**B**). Cell proliferation was expressed as fold change in respect to the control. Data are the mean  $\pm$  SD of 5 independent experiments. \*  $p < 0.05$  and \*\*  $p < 0.01$  vs. control or heat-inactivated vitreous fluid, one-way ANOVA. (**C**) Wounded MIO-M1 cells were treated with PDR vitreous fluid. After 24 h, MIO-M1 cells invading the wounded area were quantified by computerized analysis of the digitalized images. Data are the mean  $\pm$  SD of 2 independent experiments (8 microscopic fields per experimental point). \*\*  $p < 0.01$  vs. control, Student's *t* test. Inset: representative images of the repaired area in control cells (upper panel) and PDR vitreous fluid-treated cells (lower panel). Scale bar = 500  $\mu$ m. (**D**) MIO-M1 cells were treated with PDR or heat-inactivated vitreous samples. After 0–20 min, the percentage of phospho-CREB immunoreactive MIO-M1 nuclei were quantified ( $n = 80$  cells per experimental point). \*\*  $p < 0.01$  vs. control or heat-inactivated vitreous, one-way ANOVA. Inset: phospho-CREB immunoreactivity (red) in MIO-M1 cells at 10 min in control (left panels) and after PDR vitreous treatment (right panels); nuclei were stained with DAPI (blue). Data are representative of 2 independent experiments. Scale bar = 25  $\mu$ m. (**E**) Western blot analysis of the phosphorylation of the signaling proteins  $\beta$ -catenin, STAT3, NF- $\kappa$ B, ERK1/2, and p38 in MIO-M1 cells following 0–30 min of stimulation with PDR or heat-inactivated vitreous samples. Data are representative of 2 independent experiments that gave similar results. MW, molecular weight. Densitometric analysis of the Western blot membranes is shown in Figure S2.

In keeping with its capacity to induce Müller cell activation, PDR vitreous induces the rapid nuclear translocation of the proinflammatory transcription factor phospho-cAMP-response element-binding protein (phospho-CREB) (Figure 1D). Accordingly, PDR vitreous rapidly triggers the phosphorylation of a variety of intracellular mediators, including  $\beta$ -catenin, STAT3, ERK1/2, p38, and nuclear factor kappa light chain enhancer of activated B cells (NF- $\kappa$ B) (Figure 1E).

In accordance with its capacity to trigger  $\beta$ -catenin and NF- $\kappa$ B activation, treatment with PDR vitreous induces the overexpression of the inflammasome nucleotide-binding oligomerization domain (NOD), leucine-rich repeat (LRR)-containing proteins 3 (*NLRP3*)

gene. In parallel, activated MIO-M1 cells upregulate the expression of the inflammatory mediators interleukin  $1\beta$  ( $IL1\beta$ ),  $IL6$ ,  $IL8$ , interferon  $\gamma$  ( $INF\gamma$ ), monocyte chemoattractant protein 1 ( $MCP1$ ), tumor necrosis factor  $\alpha$  ( $TNF\alpha$ ), and  $VEGF-A$  (Figure 2). No modulation was instead observed for  $NLRP1$ ,  $NLRP6$ ,  $CASPASE1$ , apoptosis-associated speck like protein ( $ASC$ ), and  $IL18$  genes, or for  $IL4$ ,  $IL17$ , and transforming growth factor  $\beta$  ( $TGF\beta$ ) (data not shown). In all the assays, negligible activity was exerted by heat-inactivated vitreous, pointing to a proteinaceous nature of the vitreal mediators responsible for the biological activity exerted by PDR vitreous on MIO-M1 cells. However, it is interesting to note that heat-inactivated vitreous retains a significant, even though limited, capacity to stimulate the expression of  $NLRP3$ ,  $IL8$ , and  $VEGF-A$  in Müller cells (Figure 2), possibly due to the presence in PDR vitreous of non-proteinaceous components, including bioactive lipids or heat-stable cytokines like  $TGF\beta$  [3]. Further studies will be required to clarify this point.

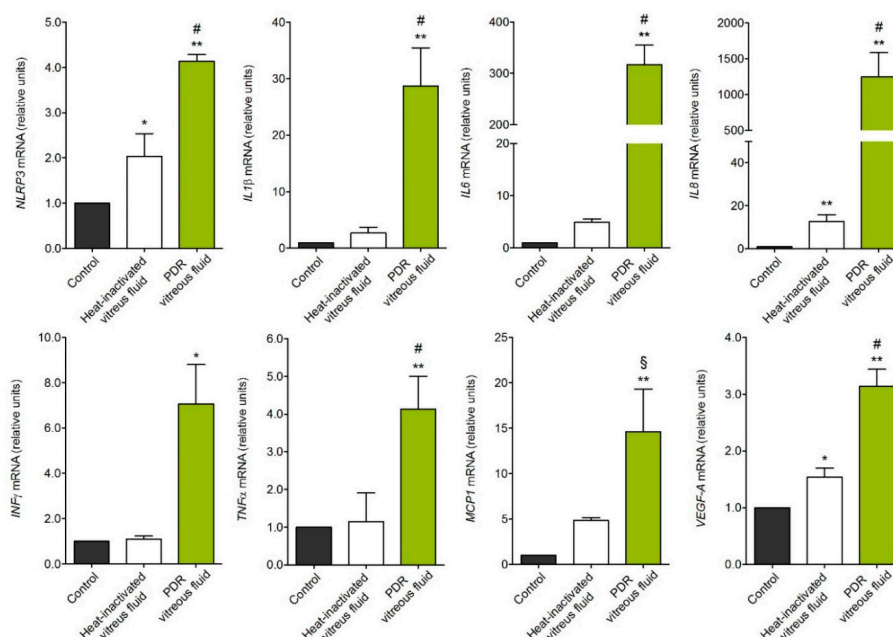


**Figure 2.** Gene expression analysis of PDR vitreous-activated Müller cells. qPCR analysis of MIO-M1 cells treated with PDR or heat-inactivated vitreous samples.  $NLRP3$ ,  $IL1\beta$ ,  $IL6$ ,  $IL8$ ,  $INF\gamma$ ,  $MCP1$ , and  $VEGF-A$  expression levels were assessed 4 h after treatment, whereas  $TNF\alpha$  expression was evaluated at 8 h. Data are representative of 3 independent experiments in triplicate that gave similar results and are expressed as relative units in respect to control. \*  $p < 0.05$  and \*\*  $p < 0.01$  vs. control; §  $p < 0.05$  and #  $p < 0.01$  vs. heat-inactivated vitreous, one-way ANOVA.

## 2.2. PDR Vitreous-Induced Activation of Müller Cells Is Independent from VEGF

The major therapeutic target in PDR is represented by VEGF, which is thought to play a pivotal role in retinal inflammation, vascular leakage, and neovascularization [3]. To evaluate the effect of VEGF stimulation on Müller cells, MIO-M1 cells were treated with recombinant VEGF-A. As shown in Figure 3, VEGF treatment does not modulate the expression of the analyzed proinflammatory genes. These results prompted us to evaluate the effect of the anti-VEGF drug ranibizumab on PDR vitreous-mediated activation of Müller cells. To obtain a complete inhibition of the activity of VEGF, ranibizumab was administered to MIO-M1 cells at a concentration equal to  $10\ \mu\text{M}$ , consistent with the dose

currently used in clinical practice [27]. In keeping with the results obtained following treatment with recombinant VEGF-A, ranibizumab exerted only a negligible inhibitory effect on the activation of MIO-M1 cells induced by PDR vitreous (Figure 3).

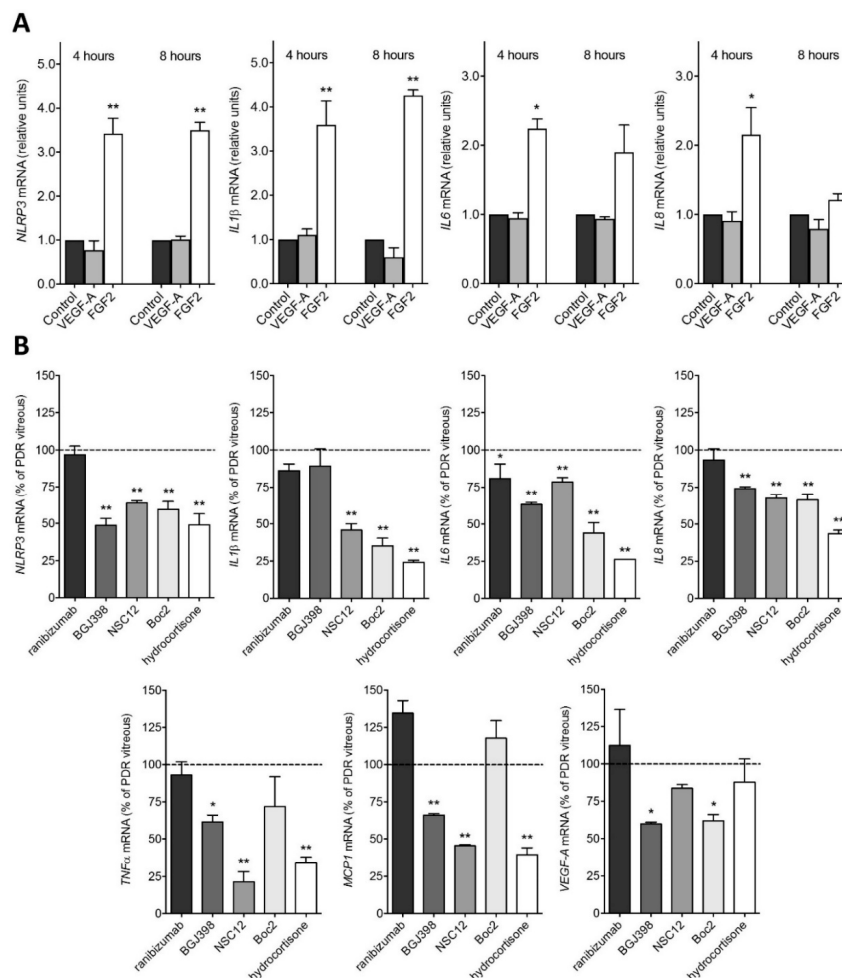


**Figure 3.** Inhibition of PDR vitreous-induced activation of MIO-M1 cells. **(A)** qPCR analysis of *NLRP3*, *IL1β*, *IL6*, and *IL8* expression in MIO-M1 cells treated with recombinant human VEGF-A or FGF2 for 4 and 8 h. Data are representative of 2 independent experiments in triplicate that gave similar results and are expressed as relative units in respect to control. \*  $p < 0.05$  and \*\*  $p < 0.01$  vs. control or VEGF-A, one-way ANOVA. **(B)** qPCR analysis of *NLRP3*, *IL1β*, *IL6*, *IL8*, *TNFα*, *MCP1*, and *VEGF-A* expression in MIO-M1 cells treated with PDR vitreous for 4 h in the absence or in the presence of 10  $\mu$ M ranibizumab, 100 nM BGJ398, 10  $\mu$ M NSC12, 60  $\mu$ M Boc2, or 10  $\mu$ M hydrocortisone. Data are representative of 2 independent experiments in triplicate that gave similar results and are expressed as % in respect to PDR vitreous stimulation. \*  $p < 0.05$  and \*\*  $p < 0.01$  vs. PDR vitreous, one-way ANOVA.

Based on these observations, we investigated the expression and activation of VEGFRs in MIO-M1 cells. As shown in Figure 4A, MIO-M1 cells express *VEGFR2* transcripts at levels similar to those detected in human umbilical vein endothelial cells (HUVECs) whereas they fail to express significant levels of *VEGFR1* and *VEGFR3*. However, Western blot analysis of

the cell extracts demonstrate that VEGFR2 protein is present at negligible levels in MIO-M1 cells when compared to HUVECs (Figure 4C). Accordingly, VEGF treatment induces a rapid VEGFR2 phosphorylation and ERK1/2 activation in HUVECs, but not in MIO-M1 cells (Figure 4B,C). Together, these data confirm that MIO-M1 cells are irresponsive to VEGF stimulation in our experimental conditions.

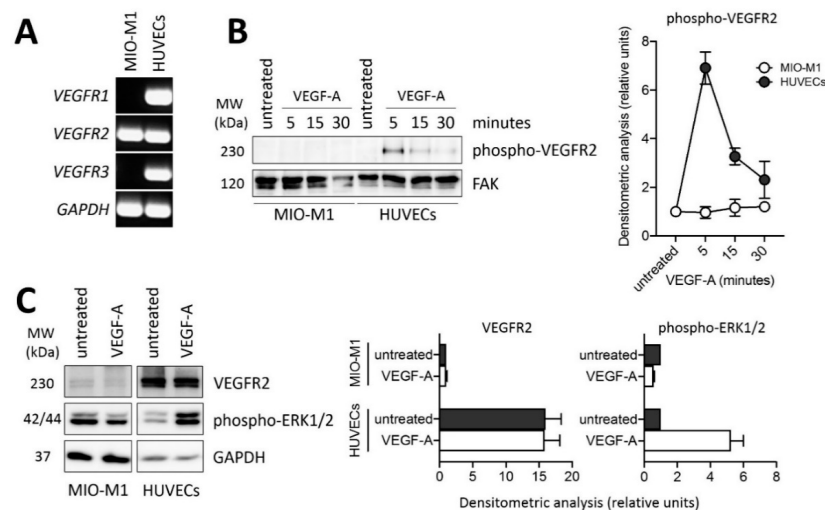


**Figure 4.** VEGFR2 expression and lack of response in MIO-M1 cells. (A) Semi-quantitative RT-PCR analysis of *VEGFR1*, *VEGFR2*, and *VEGFR3* expression in MIO-M1 cells and in human umbilical vein endothelial cells (HUVECs). Data are representative of 2 independent experiments that gave similar results. (B) Western blot analysis of VEGFR2 phosphorylation following 0–30 min of stimulation with 30 ng/mL VEGF-A in MIO-M1 cells and HUVECs. Densitometric analysis is shown in the right panel. Data are the mean  $\pm$  SD of 2 independent experiments. (C) Western blot analysis of VEGFR2 protein levels and ERK1/2 phosphorylation following 10 min of stimulation with 30 ng/mL VEGF-A in MIO-M1 cells and HUVECs. Densitometric analysis is shown in the right and far right panel, respectively. Data are the mean  $\pm$  SD of 2 independent experiments. MW, molecular weight.

FGF2 is the prototypic member of the heparin-binding FGF family [24]. Previous observations showed that FGF2 may induce proliferation and gliotic responses in Müller cells [28]. Accordingly, in contrast with recombinant VEGF-A, recombinant FGF2 induces the overexpression of *NLRP3*, *IL1 $\beta$* , *IL6*, and *IL8* in MIO-M1 cells, even though to a limited extent when compared to the effect exerted by PDR vitreous (Figure 3). In keeping with these findings, the ATP-competitive tyrosine kinase FGF receptor (FGFR) inhibitor BGJ398 [25] exerts a significant, though partial, inhibition of the overexpression of the proinflammatory genes upregulated by PDR vitreous when administered to MIO-M1 cells at 100 nM, a concentration selective for FGFR1-3 and ineffective for VEGF receptor-2 and various other tyrosine kinase receptors [25] (Figure 3). Similar results were obtained by treating MIO-M1 cells with PDR vitreous in the presence of NSC12, a small FGF-trap molecule which is able to bind and inhibit the activity of all the members of the FGF family [26] (Figure 3). Together, these data raise the hypothesis that stimulation of the FGF/FGFR system triggered by FGF2 and/or by other members of the FGF family may contribute, at least in part, to the activation of Müller cells by PDR vitreous.

Recent observations from our laboratory have shown that the peptide N-tert-butyloxy carbonyl-Phe-Leu-Phe-Leu-Phe (Boc2), widely used as a pan-formyl peptide receptor (FPR) antagonist [29], hampers the angio-inflammatory responses mediated by PDR vitreous on endothelial cells [18]. This FPR-independent effect is due to the capacity of Boc2 to inhibit the binding of a variety of heparin-binding cytokines/growth factors to heparin (including

the heparin-binding VEGF-A<sub>165</sub> isoform, FGF2, connective tissue growth factor, stromal cell-derived factor-1, placenta-derived growth factor-2, high mobility group box-1, platelet-derived growth factor-BB (PDGF-BB), and hepatocyte growth factor), thus preventing their interaction with cell surface heparan-sulphate proteoglycans and cognate receptors [20]. On this basis, in order to assess the effect exerted by a multi-target growth factor/cytokine inhibitor on the activation triggered by PDR vitreous on Müller cells, MIO-M1 cells were incubated with PDR vitreous samples in the absence or in the presence of Boc2. As shown in Figure 3, Boc2 inhibits the upregulation of *NLRP3*, *IL1 $\beta$* , *IL6*, *IL8*, and *VEGF-A* expression induced by PDR vitreous, whereas it has no effect on the modulation of *TNF $\alpha$*  and *MCP1*.

Various proinflammatory cytokines/chemokines have been detected in PDR vitreous (see [3] and references therein) that are endowed with the capacity to activate Müller cells [30–32]. Glucocorticoid receptor signaling exerts an anti-inflammatory action in Müller cells via the modulation of the activity of various transcription factors, including STAT3 and NF- $\kappa$ B (reviewed in [33]). Accordingly, the anti-inflammatory steroid drug hydrocortisone prevented to a significant extent the upregulation of *NLRP3*, *IL1 $\beta$* , *IL6*, *IL8*, and *VEGF-A* that occurs in MIO-M1 cells treated with PDR vitreous (Figure 3). Altogether, these observations point to a role for various vitreal modulators beside VEGF in Müller cell activation during PDR.

### 3. Discussion

The role of retinal glial cells in the pathogenesis of PDR has been thoroughly described [11,12]. In the early stages of DR, Müller cells become hyperactive and start to produce and release angiogenic and neurotrophic factors in order to protect the retina from the insult consequent to the high glucose conditions. However, this response may establish over time an inflammatory milieu that further triggers Müller cell activation and neovascular events typical of the later stages of PDR [11–16]. In this frame, the understanding of the reactive responses of Müller cells and of their protective/detrimental effects in PDR is of pivotal importance to bring new therapeutic strategies to patients.

Here, PDR vitreous humor obtained from diabetic patients after pars plana vitrectomy was used as a tool to explore the activation that occurs in Müller cells during PDR. Previous observations have shown that high glucose concentrations may cause the upregulation of various cytokines in Müller cells [31,34–36]. In our work, all experiments were performed with MIO-M1 cells maintained in culture medium containing 25 mM glucose, thus mimicking more closely a “diabetic-like” microenvironment when cells were treated with PDR vitreous. The results show that PDR vitreous stimulates MIO-M1 cell proliferation and motility, hallmarks of the gliotic response that characterizes Müller cells [11] and may contribute to ERM formation in PDR patients [37]. No significant stimulation was instead exerted by the vitreous obtained from patients affected by rhegmatogenous retinal detachment, pointing to a specificity of the effect. Accordingly, vitreous samples collected from patients undergoing vitrectomy for diabetic and non-diabetic retinal disorders have shown a different ability to drive the contractile activity of Müller cells, PDR vitreous samples being the most effective (reviewed in [37]). Further studies will be required to assess whether the activation observed in MIO-M1 cells following treatment with PDR vitreous can be induced, and to which extent, by vitreous samples obtained from patients affected by other retinal disorders in which Müller cells may exert a pathogenic role, including macular hole and idiopathic ERM [37–39]. Relevant to this point, preliminary observations on a limited set of samples indicate that vitreous from PDR patients with ERM may exert a more potent mitogenic response in MIO-M1 cells when compared to samples from PDR patients without ERM, with no significant difference in their capacity to exert a mitogenic stimulus in these cells (data not shown). Analysis of a large cohort of patients will be required to confirm these findings.

Phospho-CREB accumulates in the nucleus of Müller cells in response to acute retinal damage, where it participates in glia de-differentiation, proliferation, and modulation of gene expression [40,41]. Consistent with this observation, treatment with PDR vitreous



causes the rapid nuclear translocation of phospho-CREB in MIO-M1 cells. In addition, PDR vitreous induces the phosphorylation of the intracellular mediators  $\beta$ -catenin, STAT3, p38, ERK1/2, and NF- $\kappa$ B, and upregulates the expression of various proinflammatory cytokines/chemokines, including *IL1 $\beta$* , *IL6*, *IL8*, *INF $\gamma$* , *TNF $\alpha$* , *MCP1*, and *VEGF-A*. This goes in parallel with the upregulation of *NLRP3*, a key component of the NLRP3 inflammasome [42]. These data extend previous observations about the uncontrolled release of IL1 $\beta$ , IL6, and MCP1 by microglial and macroglial cells in diabetic and Akimba animal models [11,43–45] and the putative role of NLRP3 inflammasome in PDR [44,46,47].

The activity of the NLRP3 inflammasome is mediated at the transcriptional level (priming) by NF- $\kappa$ B activation and at the post-transcriptional level (activation) by a variety of stimuli (reviewed in [48]). Previous observations have shown that tyrosine kinase signaling might exert both stimulatory and inhibitory effects on the activation of the NLRP3 inflammasome [48,49]. Accordingly, our data demonstrate that FGF2 induces NLRP3 upregulation in Müller cells that express high levels of *FGFR1* and *FGFR2* mRNAs and low levels of *FGFR3* transcript under our experimental conditions (Figure S3B). In addition, the selective FGFR tyrosine kinase inhibitor BGJ398 [25] and the pan-FGF trap NSC12 [26] inhibit *NLRP3* upregulation triggered by PDR vitreous in these cells. A similar inhibitory effect was observed following incubation of PDR vitreous-treated MIO-M1 cells with the pan-heparin-binding protein inhibitor Boc2 or with hydrocortisone. In contrast with FGF2, VEGF does not affect *NLRP3* expression in MIO-M1 cells and the anti-VEGF drug ranibizumab does not prevent the upregulation of *NLRP3* in PDR vitreous-treated MIO-M1 cells. These data point to a role for the FGF/FGFR system and possibly for other mediators, but not VEGF, in NLRP3 inflammasome activation in Müller cells during PDR.

As observed for *NLRP3* expression, our data demonstrate that VEGF-A is unable to induce the upregulation of various proinflammatory cytokines/chemokines in MIO-M1 cells. Accordingly, the anti-VEGF drug ranibizumab does not affect the capacity of PDR vitreous to trigger an inflammatory response in Müller cells when administered at 10  $\mu$ M, the intravitreal concentration commonly used in the clinical practice [27]. It is worth noticing that similar results were obtained also on endothelial cells, where anti-VEGF drugs showed a limited capacity to hamper the pro-angiogenic/proinflammatory responses induced by PDR vitreous in these cells [18,21]. It must be pointed out that the vitreous samples utilized for our experiments were collected only from PDR patients that received the last drug injection at least 15 days before vitrectomy. Given the intravitreal half-life of anti-VEGF drugs (approx. 5–7 days [50]), the residual levels of the drug in these samples do not affect the activity nor the response of PDR vitreous to anti-VEGF interventions when tested on endothelial cells [19].

No matter the presence of VEGF in PDR vitreous, our results indicate that VEGFR2 protein is present at negligible levels in MIO-M1 cells under our experimental conditions, no VEGFR2 phosphorylation and ERK1/2 activation being observed following VEGF treatment. This occurs despite the levels of *VEGFR2* transcripts being similar to those detected in HUVECs, a prototypic cell type responsive to the VEGF/VEGFR2 axis. This apparent discrepancy may be due to an inefficient translation or instability of the *VEGFR2* transcripts or to an increase in VEGFR2 protein degradation by the ubiquitin/proteasome pathway in MIO-M1 cells when compared to HUVECs. Previous observations had shown the presence of the VEGFR2 protein in Müller cells of rat and murine retina, VEGF neutralization or *Vegfr2* disruption under diabetic conditions leading to Müller cell apoptosis in the two animal models, respectively [51,52]. On the other hand, treatment of MIO-M1 cells with anti-VEGF agents have led to contrasting results with modest or no effect on cell viability/apoptosis [53,54]. Further experiments are required to fully elucidate the role of the VEGF/VEGFR2 system in Müller cells.

A variety of pro-angiogenic/proinflammatory mediators beside VEGF accumulate in the vitreous of PDR patients during disease progression (see [3] and references therein). FGF2 has been detected in ERM [55–57] and pro-inflammatory mediators can induce FGF2 expression in Müller cells [58,59]. Conversely, FGF2 may trigger proliferation and gliotic

responses in these cells [28]. Here, we extend these findings by showing that recombinant FGF2 induces the upregulation of proinflammatory genes in MIO-M1 cells. In keeping with this observation, the FGFR tyrosine kinase inhibitor BGJ398 and the pan-FGF trap NSC12 partially inhibit the activation of MIO-M1 cells by PDR vitreous, thus suggesting that the deregulation of the FGF/FGFR system may play a role in Müller cell activation during PDR. FGF2 is the prototypic member of the canonical FGF family that includes the FGF subfamilies FGF1/2/5, FGF3/4/6, FGF7/10/22, FGF8/17/18, and FGF9/16/20 [60] which are able to induce angiogenic, fibrogenic, and inflammatory responses under various pathological conditions [61]. Together, our data indicate that one or more members of the FGF family are present in PDR vitreous and may contribute to its capacity to trigger a proinflammatory response in MIO-M1 cells. Previous observations have shown the capacity of the FGF/FGFR system to activate the canonical WNT/ $\beta$ -catenin pathway via ERK-MAP kinase signaling [62]. In turn,  $\beta$ -catenin may promote NLRP3 inflammasome activation [63]. Further studies will be required to identify the bioactive vitreal member(s) of the FGF family present in PDR vitreous and to fully dissect the FGF/FGFR-dependent signaling leading to the activation of a putative  $\beta$ -catenin/NF- $\kappa$ B/NLRP3 inflammasome pathway in Müller cells.

Finally, the capacity of the multi-target heparin-binding protein antagonist Boc2 and of the anti-inflammatory agent hydrocortisone to inhibit MIO-M1 cell activation triggered by PDR vitreous indicates that other yet unidentified heparin-binding growth factors and inflammatory cytokines may contribute to Müller cell activation. For instance, TGF $\beta$ -1 induces glial-to-mesenchymal transition in Müller cells [64], PDGF acts as an autocrine modulator for Müller cells [65,66], and insulin-like growth factor-1 can induce Müller cell proliferation and contractility [65,67,68]. In addition, Müller cells may proliferate in response to the pro-inflammatory cytokine TNF $\alpha$  [32], and IL1 $\beta$  stimulation mediates the upregulation of CCL2, CXCL1, CXCL10, and IL8 chemokines [30,69], as well as the overexpression of IL6 in MIO-M1 cells [31].

Clinical observations demonstrate that anti-VEGF approaches are only partially efficacious for the treatment of PDR patients [5–7]. Based on the evidence that anti-VEGF drugs show only a limited effect on the activity exerted by PDR vitreous on Müller cells and endothelial cells [18,21], our results indicate that the characterization of novel drug candidates with different mechanisms of action may contribute, in association with anti-VEGF interventions, to the development of more efficacious therapeutic approaches in PDR.

#### 4. Materials and Methods

##### 4.1. Reagents

Dulbecco's modified Eagle medium (DMEM) medium, M199 medium, fetal calf serum (FCS), and SYBR Green PCR master mix were from GIBCO Life Technologies (Grand Island, NY, USA). Endothelial cell growth factor, porcine heparin, penicillin, streptomycin, Triton-X100, Brij, sodium orthovanadate, protease inhibitor cocktail, 4',6-diamidino-2-phenylindole (DAPI), hydrocortisone, and anti- $\alpha$ -tubulin antibody were from Sigma-Aldrich (St. Louis, MO, USA). Bradford reagent, enhanced chemiluminescence reagent, and iTaq Universal Syber Green Supermix were from Bio-Rad Laboratories (Hercules, CA, USA). PVP-free polycarbonate filters were obtained from Costar (Cambridge, MA, USA). TRIzol Reagent, Moloney murine leukemia virus (MMLV) reverse transcriptase, anti-phospho-VEGFR2 (pTyr1175), and anti-focal adhesion kinase (FAK) antibodies were from Invitrogen (Carlsbad, CA, USA). ReliaPrep<sup>TM</sup> RNA Miniprep System was from Promega (Madison, WI, USA). Anti-phospho-NF- $\kappa$ B (pSer311), anti-NF- $\kappa$ B, anti-phospho-STAT3 (pSer727), anti-STAT3, anti-GAPDH, anti-mouse-horseradish peroxidase (HRP), and anti-rabbit-HRP antibodies were from Santa Cruz Biotechnologies (Santa Cruz, CA, USA). Anti-phospho-CREB (pSer133), anti-phospho- $\beta$ -catenin (pSer552), anti- $\beta$ -catenin, anti-phospho-ERK1/2 (pThr202/Tyr204), anti-ERK1/2, anti-phospho-p38 (pThr180/pTyr182), anti-p38, and anti-VEGFR2 antibodies were from Cell Signaling Technology (Beverly, MA, USA). Chicken anti-rabbit Alexa Fluor 594 antibody was from Molecular Probes (Eugene,

OR, USA). Boc2 was from Phoenix Europe GmbH (Karlsruhe, Germany). Ranibizumab (Lucentis©) was from Novartis (Horsham, UK). BGJ398 was from Selleckchem (Houston, TX, USA). Recombinant human FGF2 was from TecnoGen (Caserta, Italy). Recombinant human VEGF-A (VEGF-A<sub>165</sub> isoform) was kindly provided by Dr. K. Ballmer-Hofer (PSI, Villigen, Switzerland). Human dermal fibroblast cDNA was kindly provided by Dr. M. Ritelli (University of Brescia, Brescia, Italy). NSC12 was kindly provided by Dr. M. Mor (University of Parma, Parma, Italy).

#### 4.2. Human Vitreous Fluid Samples

PDR patients (Table 1) underwent *pars plana* vitrectomy at the Clinics of Ophthalmology (University of Brescia) during the period November 2018–August 2020. Samples were stored at  $-80^{\circ}\text{C}$ . All assays were performed on vitreous samples pooled at random from 5–6 patients. Heat-inactivated vitreous samples were prepared by incubating vitreous pools for 20 min at  $95^{\circ}\text{C}$ . Pools of vitreous samples obtained from patients affected by rhegmatogenous retinal detachment were used as control.

**Table 1.** PDR patients. Data are n unless indicated otherwise and are expressed as mean  $\pm$  SD.

Patients/Eyes	39/42
<b>Clinical features</b>	
Gender (male/female)	28/11
Age (years)	65 $\pm$ 10
Type 1/type 2 diabetes	4/35
Duration of diabetes (years)	21 $\pm$ 6
Oral hypoglycemic drug treatment	10/39
Insulin treatment	10/39
Oral hypoglycemic drug + insulin treatment	19/39
Glycaemia (mg/dL)	161 $\pm$ 56
HbA1c (%)	7.9 $\pm$ 1.1
Neuropathy	6/39
Nephropathy	13/39
Cardiopathy	15/39
Hypertension	37/39
Dyslipidemia	23/39
Triglycerides (mg/dL)	120 $\pm$ 54
Cholesterol (mg/dL)	153 $\pm$ 44
Creatinine (mg/dL)	1.4 $\pm$ 0.7
Hemoglobin (g/dL)	13.1 $\pm$ 1.6
<b>Ophthalmic features</b>	
PDR	42/42
PDR with vitreous hemorrhage	19/42
PDR with macular edema	19/42
PDR with ERM	31/38
<b>Ocular therapies</b>	
Intravitreal injection of anti-VEGF blocker	29/42
Panretinal laser photocoagulation	32/42

**Abbreviations:** ERM: epiretinal membranes; PDR: proliferative diabetic retinopathy; VEGF: vascular endothelial growth factor.

#### 4.3. Cell Cultures

The human Müller cell line Moorfields/Institute of Ophthalmology-Müller 1 (MIO-M1) was obtained from the UCL Institute of Ophthalmology, London, UK [70]. MIO-M1 cells were immediately amplified and stock aliquots were frozen in liquid nitrogen. After thawing, cells were used for no more than 4–5 passages. MIO-M1 cells were grown in DMEM with 4.5 g/L glucose plus 10% FCS and 1.0 mM glutamine. Cells were maintained in a humidified 5% CO<sub>2</sub> incubator at 37 °C, with medium replaced every 2–3 days until cells reached confluency. Cells were tested regularly for *Mycoplasma* negativity. When compared to human dermal fibroblasts by quantitative PCR (qPCR) analysis, these cells express high levels of the Müller cell markers *vimentin* (VIM) and *retinaldehyde binding protein 1* (RLBP1), encoding for cellular retinaldehyde binding protein CRALBP and negligible levels of the *actin α 2* (ACTA2) and *S100 calcium-binding protein A4* (S100A4) fibroblast markers, encoding for α-smooth muscle actin (α-SMA) and fibroblast-specific protein 1 (S100), respectively (Figure S3A). HUVECs were isolated from human umbilical cords and grown in M199 medium supplemented with 20% FCS, endothelial cell growth factor (100 µg/mL), and porcine heparin (50 µg/mL) as previously described [71].

#### 4.4. MIO-M1 Proliferation Assay

MIO-M1 cells were seeded at 5000 cells/cm<sup>2</sup> in DMEM plus 2.0% FCS. After 3 days, cells were treated with increasing amounts of saline or vitreous diluted in culture medium. After 24, 48, 72, or 96 h, cells were detached with trypsin, suspended in 200 µL of PBS plus 5.0% FCS, and counted with a MACSQuant cytofluorimeter (Milteny Biotec).

#### 4.5. MIO-M1 Wound Healing Assay

MIO-M1 cells were seeded at 100,000 cells/cm<sup>2</sup> in DMEM plus 2.0% FCS. After 3 days, MIO-M1 cell monolayers were scratched with a 200 µL tip to obtain a 2-mm-thick denuded area and cultured in the presence of saline or PDR vitreous diluted 1:4 with culture medium. After 24 h, wounded monolayers were photographed, and the percentage of repaired area was quantified with Fiji software [72].

#### 4.6. Western Blot Analysis

MIO-M1 cells were seeded at 50,000 cells/cm<sup>2</sup> in DMEM plus 2.0% FCS. After 3 days of starvation, cells were treated for 0–30 min with saline, 30 ng/mL VEGF or vitreous fluid diluted 1:4 with culture medium. After treatment, cells were lysed in 50 mM Tris-HCl 150 mM NaCl buffer (pH 7.4) containing 1.0% Triton-X100, 0.1% Brij, 1.0 mM sodium orthovanadate, and protease inhibitor cocktail. Aliquots of each sample containing equal amount of proteins (15–30 µg) were subjected to SDS-PAGE. Gels were transblotted onto a PVDF membrane and blots were blocked with 1.0% BSA for 1 h at room temperature. Western blotting analysis was performed with anti-phospho-β-catenin, anti-β-catenin, anti-phospho-ERK1/2, anti-ERK1/2, anti-phospho-NF-κB, anti-NF-κB, anti-phospho-p38, anti-p38, anti-phospho-STAT3, anti-STAT3, anti-phospho-VEGFR2, anti-VEGFR2, anti-α-tubulin, anti-FAK, or anti-GAPDH antibodies (1:1000). After treating the membranes with appropriate secondary HRP-labeled secondary antibody (1:5000), blots were developed with enhanced chemiluminescence reagent. Images were acquired using a ChemiDoc Touch instrument and band intensity was evaluated with Image Lab 3.0 software (Bio-Rad Laboratories). When specified, MIO-M1 cells were compared to HUVECs for VEGFR2 expression and activation as previously described [73].

#### 4.7. RT-PCR Analyses

Semi-quantitative RT-PCR was used to analyze FGFR1-4 and VEGFR1-3 expression in MIO-M1 cells. To this aim, total RNA was isolated from MIO-M1 cells after 3 days of starvation in DMEM plus 2.0% FCS using TRIzol® Reagent according to manufacturers' instruction. A total of 2.0 µg of total RNA was retro-transcribed with MMLV reverse transcriptase using random hexaprimers in a final 20 µL volume. Then, 1/10th of the

reaction was analyzed by semi-quantitative RT-PCR using the primers listed in Table 2. The PCR products were electrophoresed on a 1.5% agarose gel and visualized by ethidium bromide staining. When specified, MIO-M1 cells were compared to HUVECs for VEGFR expression.

**Table 2.** Oligonucleotide primers used for RT-PCR analysis.

Gene	Forward	Reverse
ACTA2	5'-AATGGCTCTGGGCTCTGTAA-3'	5'-TTTTGCTCTGTGCTTCGTCA-3'
FGFR1	5'-GGGCTGGAATACTGCTACAA-3'	5'-GCCAAAGTCTGCTATCTTCATC-3'
FGFR2	5'-GGATAACAACACGCCTCTCT-3'	5'-GCCAAAGCAACCTTC-3'
FGFR3	5'-TGGTGTCTGTGCCTACC-3'	5'-CCGTGGTCTGTCTTGT-3'
FGFR4	5'-AACCGCATTGGAGGCATT-3'	5'-TCTACCAGGCAGGTGTATGT-3'
GAPDH	5'-GAAGGTCCGAGTCAACGGATT-3'	5'-TGACGGTGCCATGGAATTTG-3'
IL1 $\beta$	5'-GTGGCAATGAGGATGACTTG-3'	5'-GTGGTGGTCGGAGATTCGTA-3'
IL6	5'-TGTGTGGGTCTGTTGTAGGG-3'	5'-CCCGTCAATATCTAGGAAAA-3'
IL8	5'-TGTGTGGGTCTGTTGTAGGG-3'	5'-CCCGTCAATATCTAGGAAAA-3'
INF $\gamma$	5'-GCAGGTCATTAGATGTAGCGG-3'	5'-CCACACTCTTTGGATGCTCTGG-3'
MCP1	5'-CTCAGCCAGATGCAATCAA-3'	5'-CACTTCTGCTGGGGTCA-3'
NLRP3	5'-GGACTGAAGCACCTGTTGTGCA-3'	5'-TCCTGAGTCTCCCAAGGCATTC-3'
RLBP1	5'-GCTGCTGGAGAATGAGGAAA-3'	5'-TGGTGGATGAAGTGGATGG-3'
S100A4	5'-CCTGGATGTGATGGTGTCC-3'	5'-TCGTTGTCCCTGTGTGT-3'
TNF $\alpha$	5'-TGCTTGTTCCTCAGCCTCTT-3'	5'-GCTTGTCACTCGGGGTTTC-3'
VEGF-A	5'-AATCGAGACCCTGGTGGAC-3'	5'-GGTGAGGTTTGATCCGCATA-3'
VEGFR1	5'-AGCAGTCCACCACTTTAGA-3'	5'-GAACCTTCCACAGAGCCCTT-3'
VEGFR2	5'-GGAAATGACACTGGAGCCTA-3'	5'-TTTAAAATGGACCCGAGACA-3'
VEGFR3	5'-CAACGACCTACAAAGGCTCT-3'	5'-GTAACACCTGGCCTCCTC-3'
VIM	5'-CGCCAGATGCGTGAATG-3'	5'-ACCAGAGGGAGTGAATCCAGA-3'

**Abbreviations.** ACTA2: actin  $\alpha$  2; FGFR: fibroblast growth factor receptor; GAPDH: glyceraldehyde-3-phosphate dehydrogenase; IL: interleukin; INF $\gamma$ : interferon  $\gamma$ ; MCP1: monocyte chemoattractant protein 1; NLRP3: nucleotide-binding oligomerization domain (NOD), leucine-rich repeat (LRR)-containing proteins 3; RLBP1: retinaldehyde-binding protein 1; S100A4: S100 calcium-binding protein A4; TNF $\alpha$ : tumor necrosis factor  $\alpha$ ; VEGF-A: vascular endothelial growth factor-A; VEGFR: vascular endothelial growth factor receptor; VIM: vimentin.

For qPCR analysis, MIO-M1 cells were seeded at 50,000 cells/cm<sup>2</sup> in DMEM plus 2.0% FCS. After 3 days of starvation, cells were treated for 4 h or 8 h with 30 ng/mL VEGF-A, 30 ng/mL FGF2, saline, or vitreous diluted 1:4 with culture medium in the absence or in the presence of 10  $\mu$ M ranibizumab, 100 nM BGJ398, 10  $\mu$ M NSC12, 60  $\mu$ M Boc2, or 10  $\mu$ M hydrocortisone. Total RNA was isolated using TRIzol<sup>®</sup> Reagent and ReliaPrep<sup>™</sup> RNA Miniprep System according to manufacturers' instructions. Then, 2.0  $\mu$ g of total RNA was retrotranscribed and 1/10th of the retrotranscribed cDNA was used for qPCR that was performed with the ViiA 7 Real-Time PCR System (ThermoFisher) using iTaq Universal Syber Green Supermix according to the manufacturer's instructions. Samples were analyzed in triplicate using the oligonucleotide primers listed in Table 2 and data were normalized to the levels of GAPDH expression.

#### 4.8. MIO-M1 Immunofluorescence Analysis

A total of 50,000 cells/cm<sup>2</sup> was seeded on  $\mu$ -slide 8-well chambers (Ibidi) in DMEM plus 2.0% FCS. After 3 days of starvation, cells were treated for 0–30 min with saline or vitreous diluted 1:4 with culture medium, fixed in cold methanol, permeabilized with 0.2% Triton-X100, and saturated with 3.0% BSA in PBS (blocking solution). Then, cells were incubated overnight at 4  $^{\circ}$ C with anti-phospho-CREB antibody (1:800 in blocking solution) and for 1 more hour at room temperature with an anti-rabbit Alexa Fluor 594 secondary antibody (1:500 in blocking solution). Nuclei were counterstained with DAPI and cells were photographed using a Zeiss Axiovert 200M epifluorescence microscope equipped with Apotome and a Plan-Apochromat  $\times$ 63/1.4 NA oil objective.

#### 4.9. Statistical Analysis

Data are expressed as mean  $\pm$  SD. Statistical significance was evaluated with the GraphPad Prism 7 software (San Diego, CA, USA) using Student's *t* test or one-way ANOVA followed by Bonferroni multiple comparison post-test to test the probability of significant differences between 2 or more groups of samples, respectively. Differences were considered significant when *p* value < 0.05.

**Supplementary Materials:** The following is available online at <https://www.mdpi.com/1422-0067/22/4/2179/s1>. Figure S1: Retinal detachment vitreous fluid does not activate MIO-M1 Müller cells; Figure S2: Müller cell signaling activated by PDR vitreous; Figure S3: Molecular characterization of MIO-M1 Müller cells.

**Author Contributions:** Conceptualization, S.R. and M.P.; investigation, S.R., J.G., A.M.K.C., A.L.; resources, A.C., P.S., F.S.; data curation, S.R. and M.P.; validation, S.R. and M.P.; writing—original draft preparation, S.R. and M.P.; writing—review and editing, S.R., F.S., M.P.; visualization, S.R.; supervision, M.P.; project administration, M.P.; funding acquisition, S.R., F.S., M.P. All authors have read and agreed to the published version of the manuscript.

**Funding:** This research was funded by Fondazione Diabete Ricerca to S.R. and by Associazione Italiana per la Ricerca sul Cancro, grant number IG 2019 n° 23116 to M.P. SR was supported by Fondazione Umberto Veronesi and by Associazione Garda Vita (R. Tosoni) fellowships.

**Institutional Review Board Statement:** The study was conducted according to the guidelines of the Declaration of Helsinki, and approved by the Institutional Review of Spedali Civili di Brescia (protocol code NP1276, 6 February 2013).

**Informed Consent Statement:** Informed consent was obtained from all subjects involved in the study.

**Data Availability Statement:** The data that support the findings of this study are available from the corresponding authors upon reasonable request.

**Acknowledgments:** The authors wish to thank D. Bosisio (University of Brescia, Brescia, Italy) for helpful suggestions and criticisms.

**Conflicts of Interest:** The authors declare no conflict of interest.

#### Abbreviations

ACTA2	actin $\alpha$ 2
ERM	epiretinal membrane
FGF2	basic fibroblast growth factor
FGFR	fibroblast growth factor receptor
GAPDH	glyceraldehyde-3-phosphate dehydrogenase
HUVECs	human umbilical vein endothelial cells
IL	interleukin
INF $\gamma$	interferon $\gamma$
MCP1	monocyte chemoattractant protein 1
NLRP3	nucleotide-binding oligomerization domain (NOD), leucine-rich repeat (LRR)-containing proteins 3
PDGF	platelet derived growth factor
PDR	proliferative diabetic retinopathy
RLBP1	retinaldehyde binding protein 1
S100A4	S100 calcium-binding protein A4
TNF $\alpha$	tumor necrosis factor $\alpha$
VEGF-A	vascular endothelial growth factor-A
VEGFR	vascular endothelial growth factor receptor
VIM	vimentin

## References

- International Diabetes Federation Diabetes Atlas (9th ed.). Available online: <http://www.diabetesatlas.org/> (accessed on 28 December 2020).
- Al-Kharashi, A.S. Role of oxidative stress, inflammation, hypoxia and angiogenesis in the development of diabetic retinopathy. *Saudi J. Ophthalmol.* **2018**, *32*, 318–323. [[CrossRef](#)] [[PubMed](#)]
- Nawaz, I.M.; Rezzola, S.; Cancarini, A.; Russo, A.; Costagliola, C.; Semeraro, F.; Presta, M. Human vitreous in proliferative diabetic retinopathy: Characterization and translational implications. *Prog. Retin. Eye Res.* **2019**, *72*, 100756. [[CrossRef](#)]
- Osaadon, P.; Fagan, X.J.; Lifshitz, T.; Levy, J. A review of anti-VEGF agents for proliferative diabetic retinopathy. *Eye (Lond)* **2014**, *28*, 510–520. [[CrossRef](#)] [[PubMed](#)]
- Zhao, Y.; Singh, R.P. The role of anti-vascular endothelial growth factor (anti-VEGF) in the management of proliferative diabetic retinopathy. *Drugs Context.* **2018**, *7*, 212532. [[CrossRef](#)]
- Tan, G.S.; Cheung, N.; Simo, R.; Cheung, G.C.; Wong, T.Y. Diabetic macular oedema. *Lancet Diabetes Endocrinol.* **2017**, *5*, 143–155. [[CrossRef](#)]
- Brown, D.M.; Nguyen, Q.D.; Marcus, D.M.; Boyer, D.S.; Patel, S.; Feiner, L.; Schlottmann, P.G.; Rundle, A.C.; Zhang, J.; Rubio, R.G.; et al. Long-term outcomes of ranibizumab therapy for diabetic macular edema: The 36-month results from two phase III trials: RISE and RIDE. *Ophthalmology* **2013**, *120*, 2013–2022. [[CrossRef](#)] [[PubMed](#)]
- Semeraro, F.; Morescalchi, F.; Cancarini, A.; Russo, A.; Rezzola, S.; Costagliola, C. Diabetic retinopathy, a vascular and inflammatory disease: Therapeutic implications. *Diabetes Metab.* **2019**, *45*, 517–527. [[CrossRef](#)]
- Le, Y.Z. VEGF production and signaling in Müller glia are critical to modulating vascular function and neuronal integrity in diabetic retinopathy and hypoxic retinal vascular diseases. *Vision Res.* **2017**, *139*, 108–114. [[CrossRef](#)]
- Reichenbach, A.; Bringmann, A. New functions of Müller cells. *Glia* **2013**, *61*, 651–678. [[CrossRef](#)]
- Bringmann, A.; Iandiev, I.; Pannicke, T.; Wurm, A.; Hollborn, M.; Wiedemann, P.; Osborne, N.N.; Reichenbach, A. Cellular signaling and factors involved in Müller cell gliosis: Neuroprotective and detrimental effects. *Prog. Retin. Eye Res.* **2009**, *28*, 423–451. [[CrossRef](#)] [[PubMed](#)]
- Bringmann, A.; Pannicke, T.; Grosche, J.; Francke, M.; Wiedemann, P.; Skatchkov, S.N.; Osborne, N.N.; Reichenbach, A. Müller cells in the healthy and diseased retina. *Prog. Retin. Eye Res.* **2006**, *25*, 397–424. [[CrossRef](#)]
- Oberstein, S.Y.; Byun, J.; Herrera, D.; Chapin, E.A.; Fisher, S.K.; Lewis, G.P. Cell proliferation in human epiretinal membranes: Characterization of cell types and correlation with disease condition and duration. *Mol. Vis.* **2011**, *17*, 1794–1805.
- Roy, S.; Amin, S.; Roy, S. Retinal fibrosis in diabetic retinopathy. *Exp. Eye Res.* **2016**, *142*, 71–75. [[CrossRef](#)] [[PubMed](#)]
- Rodrigues, M.; Xin, X.; Jee, K.; Babapoor-Farrokhran, S.; Kashiwabuchi, F.; Ma, T.; Bhutto, I.; Hassan, S.J.; Daoud, Y.; Baranano, D.; et al. VEGF secreted by hypoxic Müller cells induces MMP-2 expression and activity in endothelial cells to promote retinal neovascularization in proliferative diabetic retinopathy. *Diabetes* **2013**, *62*, 3863–3873. [[CrossRef](#)]
- Portillo, J.C.; Lopez Corcino, Y.; Miao, Y.; Tang, J.; Sheibani, N.; Kern, T.S.; DUBYAK, G.R.; Subauste, C.S. CD40 in Retinal Müller Cells Induces P2X7-Dependent Cytokine Expression in Macrophages/Microglia in Diabetic Mice and Development of Early Experimental Diabetic Retinopathy. *Diabetes* **2017**, *66*, 483–493. [[CrossRef](#)]
- Rezzola, S.; Nawaz, M.I.; Cancarini, A.; Semeraro, F.; Presta, M. Vascular Endothelial Growth Factor in the Vitreous of Proliferative Diabetic Retinopathy Patients: Chasing a Hiding Prey? *Diabetes Care* **2019**, *42*, e105–e106. [[CrossRef](#)]
- Rezzola, S.; Corsini, M.; Chiodelli, P.; Cancarini, A.; Nawaz, I.M.; Coltrini, D.; Mitola, S.; Ronca, R.; Belleri, M.; Lista, L.; et al. Inflammation and N-formyl peptide receptors mediate the angiogenic activity of human vitreous humour in proliferative diabetic retinopathy. *Diabetologia* **2017**, *60*, 719–728. [[CrossRef](#)] [[PubMed](#)]
- Rezzola, S.; Nawaz, I.M.; Cancarini, A.; Ravelli, C.; Calza, S.; Semeraro, F.; Presta, M. 3D endothelial cell spheroid/human vitreous humor assay for the characterization of anti-angiogenic inhibitors for the treatment of proliferative diabetic retinopathy. *Angiogenesis* **2017**, *20*, 629–640. [[CrossRef](#)]
- Nawaz, I.M.; Chiodelli, P.; Rezzola, S.; Paganini, G.; Corsini, M.; Lodola, A.; Lodola, A.; Di Ianni, A.; Mor, M.; Presta, M. N-tert-butylloxycarbonyl-Phe-Leu-Phe-Leu-Phe (BOC2) inhibits the angiogenic activity of heparin-binding growth factors. *Angiogenesis* **2018**, *21*, 47–59. [[CrossRef](#)]
- Rezzola, S.; Dal Monte, M.; Belleri, M.; Bugatti, A.; Chiodelli, P.; Corsini, M.; Cammalleri, M.; Cancarini, A.; Morbidelli, L.; Oreste, P.; et al. Therapeutic Potential of Anti-Angiogenic Multitarget, N,O-Sulfated E. Coli K5 Polysaccharide in Diabetic Retinopathy. *Diabetes* **2015**, *64*, 2581–2592. [[CrossRef](#)]
- Rezzola, S.; Loda, A.; Corsini, M.; Semeraro, F.; Annese, T.; Presta, M.; Ribatti, D. Angiogenesis-Inflammation Cross Talk in Diabetic Retinopathy: Novel Insights from the Chick Embryo Chorioallantoic Membrane/Human Vitreous Platform. *Front. Immunol.* **2020**, *11*, 581288. [[CrossRef](#)]
- Dal Monte, M.; Rezzola, S.; Cammalleri, M.; Belleri, M.; Locri, F.; Morbidelli, L.; Corsini, M.; Paganini, G.; Semeraro, F.; Cancarini, A.; et al. Antiangiogenic Effectiveness of the Urokinase Receptor-Derived Peptide UPARANT in a Model of Oxygen-Induced Retinopathy. *Investig. Ophthalmol. Vis. Sci.* **2015**, *56*, 2392–2407. [[CrossRef](#)]
- Presta, M.; Dell’Era, P.; Mitola, S.; Moroni, E.; Ronca, R.; Rusnati, M. Fibroblast growth factor/fibroblast growth factor receptor system in angiogenesis. *Cytokine Growth Factor Rev.* **2005**, *16*, 159–178. [[CrossRef](#)]

25. Guagnano, V.; Furet, P.; Spanka, C.; Bordas, V.; Le Douget, M.; Stamm, C.; Brueggen, J.; Jensen, M.R.; Schnell, C.; Schmid, H.; et al. Discovery of 3-(2,6-dichloro-3,5-dimethoxy-phenyl)-1-[6-[4-(4-ethyl-piperazin-1-yl)-phenylamino]-pyrimidin-4-yl]-1-methyl-urea (NVP-BGJ398), a potent and selective inhibitor of the fibroblast growth factor receptor family of receptor tyrosine kinase. *J. Med. Chem.* **2011**, *54*, 7066–7083. [[CrossRef](#)] [[PubMed](#)]
26. Ronca, R.; Giacomini, A.; Di Salle, E.; Coltrini, D.; Pagano, K.; Ragona, L.; Matarazzo, S.; Rezzola, S.; Maiolo, D.; Torrella, R.; et al. Long-Pentraxin 3 Derivative as a Small-Molecule FGF Trap for Cancer Therapy. *Cancer Cell* **2015**, *28*, 225–239. [[CrossRef](#)] [[PubMed](#)]
27. Bressler, S.B.; Liu, D.; Glassman, A.R.; Blodi, B.A.; Castellarin, A.A.; Jampol, L.M.; Kaufman, P.L.; Melia, M.; Singh, H.; Wells, J.A.; et al. Change in Diabetic Retinopathy Through 2 Years: Secondary Analysis of a Randomized Clinical Trial Comparing Aflibercept, Bevacizumab, and Ranibizumab. *JAMA Ophthalmol.* **2017**, *135*, 558–568. [[CrossRef](#)] [[PubMed](#)]
28. Hollborn, M.; Jahn, K.; Limb, G.A.; Kohen, L.; Wiedemann, P.; Bringmann, A. Characterization of the basic fibroblast growth factor-evoked proliferation of the human Muller cell line, MIO-M1. *Graefes Arch. Clin. Exp. Ophthalmol.* **2004**, *242*, 414–422. [[CrossRef](#)]
29. Toniolo, C.; Bonora, G.M.; Showell, H.; Freer, R.J.; Becker, E.L. Structural requirements for formyl homooligopeptide chemoattractants. *Biochemistry* **1984**, *23*, 698–704. [[CrossRef](#)]
30. Liu, X.; Ye, F.; Xiong, H.; Hu, D.; Limb, G.A.; Xie, T.; Peng, L.; Yang, W.; Sun, Y.; Zhou, M.; et al. IL-1beta Upregulates IL-8 Production in Human Muller Cells Through Activation of the p38 MAPK and ERK1/2 Signaling Pathways. *Inflammation* **2014**, *37*, 1486–1495. [[CrossRef](#)]
31. Liu, X.; Ye, F.; Xiong, H.; Hu, D.N.; Limb, G.A.; Xie, T.; Peng, L.; Zhang, P.; Wei, Y.; Zhang, W.; et al. IL-1beta induces IL-6 production in retinal Muller cells predominantly through the activation of p38 MAPK/NF-kappaB signaling pathway. *Exp. Cell Res.* **2015**, *331*, 223–231. [[CrossRef](#)]
32. Nelson, C.M.; Ackerman, K.M.; O'Hayer, P.; Bailey, T.J.; Gorsuch, R.A.; Hyde, D.R. Tumor necrosis factor-alpha is produced by dying retinal neurons and is required for Muller glia proliferation during zebrafish retinal regeneration. *J. Neurosci.* **2013**, *33*, 6524–6539. [[CrossRef](#)] [[PubMed](#)]
33. Ghaseminejad, F.; Kaplan, L.; Pfaller, A.M.; Hauck, S.M.; Grosche, A. The role of Muller cell glucocorticoid signaling in diabetic retinopathy. *Graefes Arch. Clin. Exp. Ophthalmol.* **2020**, *258*, 221–230. [[CrossRef](#)] [[PubMed](#)]
34. Zong, H.; Ward, M.; Madden, A.; Yong, P.H.; Limb, G.A.; Curtis, T.M.; Stitt, A.W. Hyperglycaemia-induced pro-inflammatory responses by retinal Muller glia are regulated by the receptor for advanced glycation end-products (RAGE). *Diabetologia* **2010**, *53*, 2656–2666. [[CrossRef](#)]
35. Mu, H.; Zhang, X.M.; Liu, J.J.; Dong, L.; Feng, Z.L. Effect of high glucose concentration on VEGF and PEDF expression in cultured retinal Muller cells. *Mol. Biol. Rep.* **2009**, *36*, 2147–2151. [[CrossRef](#)]
36. Wang, J.; Xu, X.; Elliott, M.H.; Zhu, M.; Le, Y.Z. Muller cell-derived VEGF is essential for diabetes-induced retinal inflammation and vascular leakage. *Diabetes* **2010**, *59*, 2297–2305. [[CrossRef](#)] [[PubMed](#)]
37. Guidry, C. The role of Muller cells in fibrocontractive retinal disorders. *Prog. Retin. Eye Res.* **2005**, *24*, 75–86. [[CrossRef](#)] [[PubMed](#)]
38. Chen, Q.; Liu, Z.X. Idiopathic Macular Hole: A Comprehensive Review of Its Pathogenesis and of Advanced Studies on Metamorphopsia. *J. Ophthalmol.* **2019**, *2019*, 7294952. [[CrossRef](#)] [[PubMed](#)]
39. Bu, S.C.; Kuijer, R.; van der Worp, R.J.; Postma, G.; Renardel de Lavalette, V.W.; Li, X.R.; Hooymans, J.M.M.; Los, L.I. Immunohistochemical Evaluation of Idiopathic Epiretinal Membranes and In Vitro Studies on the Effect of TGF-beta on Muller Cells. *Investig. Ophthalmol. Vis. Sci.* **2015**, *56*, 6506–6514. [[CrossRef](#)] [[PubMed](#)]
40. Mayr, B.; Montminy, M. Transcriptional regulation by the phosphorylation-dependent factor CREB. *Nat. Rev. Mol. Cell Biol.* **2001**, *2*, 599–609. [[CrossRef](#)]
41. Fischer, A.J.; Scott, M.A.; Tuten, W. Mitogen-activated protein kinase-signaling stimulates Muller glia to proliferate in acutely damaged chicken retina. *Glia* **2009**, *57*, 166–181. [[CrossRef](#)]
42. Swanson, K.V.; Deng, M.; Ting, J.P. The NLRP3 inflammasome: Molecular activation and regulation to therapeutics. *Nat. Rev. Immunol.* **2019**, *19*, 477–489. [[CrossRef](#)] [[PubMed](#)]
43. Liu, Y.; Biarnes Costa, M.; Gerhardinger, C. IL-1beta is upregulated in the diabetic retina and retinal vessels: Cell-specific effect of high glucose and IL-1beta autostimulation. *PLoS ONE* **2012**, *7*, e36949. [[CrossRef](#)]
44. Chaurasia, S.S.; Lim, R.R.; Parikh, B.H.; Wey, Y.S.; Tun, B.B.; Wong, T.Y.; Luu, C.D.; Agrawal, R.; Ghosh, A.; Mortellaro, A.; et al. The NLRP3 Inflammasome May Contribute to Pathologic Neovascularization in the Advanced Stages of Diabetic Retinopathy. *Sci Rep.* **2018**, *8*, 2847. [[CrossRef](#)] [[PubMed](#)]
45. Yang, L.P.; Sun, H.L.; Wu, L.M.; Guo, X.J.; Dou, H.L.; Tso, M.O.; Zhao, L.; Li, S. Baicalein reduces inflammatory process in a rodent model of diabetic retinopathy. *Investig. Ophthalmol. Vis. Sci.* **2009**, *50*, 2319–2327. [[CrossRef](#)]
46. Loukovaara, S.; Piippo, N.; Kinnunen, K.; Hytti, M.; Kaarniranta, K.; Kauppinen, A. NLRP3 inflammasome activation is associated with proliferative diabetic retinopathy. *Acta Ophthalmol.* **2017**, *95*, 803–808. [[CrossRef](#)] [[PubMed](#)]
47. Chen, H.; Zhang, X.; Liao, N.; Mi, L.; Peng, Y.; Liu, B.; Zhang, S.; Wen, F. Enhanced Expression of NLRP3 Inflammasome-Related Inflammation in Diabetic Retinopathy. *Investig. Ophthalmol. Vis. Sci.* **2018**, *59*, 978–985. [[CrossRef](#)]
48. He, Y.; Hara, H.; Nunez, G. Mechanism and Regulation of NLRP3 Inflammasome Activation. *Trends Biochem. Sci.* **2016**, *41*, 1012–1021. [[CrossRef](#)] [[PubMed](#)]



49. Chung, I.C.; Yuan, S.N.; OuYang, C.N.; Lin, H.C.; Huang, K.Y.; Chen, Y.J.; Chung, A.K.; Chu, C.L.; Ojcius, D.M.; Chang, Y.S.; et al. Src-family kinase-Cbl axis negatively regulates NLRP3 inflammasome activation. *Cell Death Dis.* **2018**, *9*, 1109. [[CrossRef](#)] [[PubMed](#)]
50. Fogli, S.; Del Re, M.; Rofi, E.; Posarelli, C.; Figus, M.; Danesi, R. Clinical pharmacology of intravitreal anti-VEGF drugs. *Eye (Lond)* **2018**, *32*, 1010–1020. [[CrossRef](#)] [[PubMed](#)]
51. Fu, S.; Dong, S.; Zhu, M.; Sherry, D.M.; Wang, C.; You, Z.; Haigh, J.J.; Le, Y.Z. Muller Glia Are a Major Cellular Source of Survival Signals for Retinal Neurons in Diabetes. *Diabetes* **2015**, *64*, 3554–3563. [[CrossRef](#)]
52. Saint-Geniez, M.; Maharaj, A.S.; Walshe, T.E.; Tucker, B.A.; Sekiyama, E.; Kurihara, T.; Darland, D.C.; Young, M.J.; D'Amore, P.A. Endogenous VEGF is required for visual function: Evidence for a survival role on muller cells and photoreceptors. *PLoS ONE* **2008**, *3*, e3554. [[CrossRef](#)] [[PubMed](#)]
53. Caceres-Del-Carpio, J.; Moustafa, M.T.; Toledo-Corral, J.; Hamid, M.A.; Atilano, S.R.; Schneider, K.; Fukuhara, P.S.; Donato Costa, R.; Norman, J.L.; Malik, D.; et al. In vitro response and gene expression of human retinal Muller cells treated with different anti-VEGF drugs. *Exp. Eye Res.* **2020**, *191*, 107903. [[CrossRef](#)] [[PubMed](#)]
54. Matsuda, M.; Krempel, P.G.; Marquezini, M.V.; Sholl-Franco, A.; Lameu, A.; Monteiro, M.L.R.; de Oliveira Miguel, N.C. Cellular stress response in human Muller cells (MIO-M1) after bevacizumab treatment. *Exp. Eye Res.* **2017**, *160*, 1–10. [[CrossRef](#)]
55. Hueber, A.; Wiedemann, P.; Esser, P.; Heimann, K. Basic fibroblast growth factor mRNA, bFGF peptide and FGF receptor in epiretinal membranes of intraocular proliferative disorders (PVR and PDR). *Int. Ophthalmol.* **1996**, *20*, 345–350. [[CrossRef](#)]
56. Liang, X.; Li, C.; Li, Y.; Huang, J.; Tang, S.; Gao, R.; Li, S. Platelet-derived growth factor and basic fibroblast growth factor immunolocalized in proliferative retinal diseases. *Chin. Med. J.* **2000**, *113*, 144–147.
57. Coltrini, D.; Belleri, M.; Gambicorti, E.; Romano, D.; Morescalchi, F.; Krishna Chandran, A.M.; Calza, S.; Semeraro, F.; Presta, M. Gene expression analysis identifies two distinct molecular clusters of idiopathic epiretinal membranes. *Biochim. Biophys. Acta Mol. Basis Dis.* **2020**, *1866*, 165938. [[CrossRef](#)]
58. Yoshida, S.; Yoshida, A.; Ishibashi, T. Induction of IL-8, MCP-1, and bFGF by TNF-alpha in retinal glial cells: Implications for retinal neovascularization during post-ischemic inflammation. *Graefes Arch. Clin. Exp. Ophthalmol.* **2004**, *242*, 409–413. [[CrossRef](#)] [[PubMed](#)]
59. Cheng, T.; Cao, W.; Wen, R.; Steinberg, R.H.; LaVail, M.M. Prostaglandin E2 induces vascular endothelial growth factor and basic fibroblast growth factor mRNA expression in cultured rat Muller cells. *Investig. Ophthalmol. Vis. Sci.* **1998**, *39*, 581–591.
60. Itoh, N.; Ornitz, D.M. Functional evolutionary history of the mouse Fgf gene family. *Developmental. Dyn.* **2008**, *237*, 18–27. [[CrossRef](#)]
61. Beenken, A.; Mohammadi, M. The FGF family: Biology, pathophysiology and therapy. *Nat. Rev. Drug Discov.* **2009**, *8*, 235–253. [[CrossRef](#)] [[PubMed](#)]
62. Krejci, P.; Aklian, A.; Kaucka, M.; Sevcikova, E.; Prochazkova, J.; Masek, J.K.; Mikolka, P.; Pospisilova, T.; Spoustova, T.; Weis, M.; et al. Receptor tyrosine kinases activate canonical WNT/beta-catenin signaling via MAP kinase/LRP6 pathway and direct beta-catenin phosphorylation. *PLoS ONE* **2012**, *7*, e35826. [[CrossRef](#)] [[PubMed](#)]
63. Huang, L.; Luo, R.; Li, J.; Wang, D.; Zhang, Y.; Liu, L.; Zhang, N.; Xu, X.; Lu, B.; Zhano, K. beta-catenin promotes NLRP3 inflammasome activation via increasing the association between NLRP3 and ASC. *Mol. Immunol.* **2020**, *121*, 186–194. [[CrossRef](#)] [[PubMed](#)]
64. Kanda, A.; Noda, K.; Hirose, I.; Ishida, S. TGF-beta-SNAIL axis induces Muller glial-mesenchymal transition in the pathogenesis of idiopathic epiretinal membrane. *Sci. Rep.* **2019**, *9*, 673. [[CrossRef](#)]
65. Guidry, C.; Bradley, K.M.; King, J.L. Tractional force generation by human muller cells: Growth factor responsiveness and integrin receptor involvement. *Investig. Ophthalmol. Vis. Sci.* **2003**, *44*, 1355–1363. [[CrossRef](#)] [[PubMed](#)]
66. Bringmann, A.; Wiedemann, P. Involvement of Muller glial cells in epiretinal membrane formation. *Graefes Arch. Clin. Exp. Ophthalmol.* **2009**, *247*, 865–883. [[CrossRef](#)]
67. Guidry, C.; Feist, R.; Morris, R.; Hardwick, C.W. Changes in IGF activities in human diabetic vitreous. *Diabetes* **2004**, *53*, 2428–2435. [[CrossRef](#)]
68. Romaniuk, D.; Kimsa, M.W.; Strzalka-Mrozik, B.; Kimsa, M.C.; Kabiesz, A.; Romaniuk, W.; Mazurek, U. Gene expression of IGF1, IGF1R, and IGFBP3 in epiretinal membranes of patients with proliferative diabetic retinopathy: Preliminary study. *Mediat. Inflamm.* **2013**, *2013*, 986217. [[CrossRef](#)] [[PubMed](#)]
69. Natoli, R.; Fernando, N.; Madigan, M.; Chu-Tan, J.A.; Valter, K.; Provis, J.; Rutar, M. Microglia-derived IL-1beta promotes chemokine expression by Muller cells and RPE in focal retinal degeneration. *Mol. Neurodegener.* **2017**, *12*, 31. [[CrossRef](#)] [[PubMed](#)]
70. Limb, G.A.; Salt, T.E.; Munro, P.M.; Moss, S.E.; Khaw, P.T. In vitro characterization of a spontaneously immortalized human Muller cell line (MIO-M1). *Investig. Ophthalmol. Vis. Sci.* **2002**, *43*, 864–869.
71. Ravelli, C.; Grillo, E.; Corsini, M.; Coltrini, D.; Presta, M.; Mitola, S. beta3 Integrin Promotes Long-Lasting Activation and Polarization of Vascular Endothelial Growth Factor Receptor 2 by Immobilized Ligand. *Arter. Thromb. Vasc. Biol.* **2015**, *35*, 2161–2171. [[CrossRef](#)]
72. Schindelin, J.; Arganda-Carreras, I.; Frise, E.; Kaynig, V.; Longair, M.; Pietzsch, T.; Preibisch, S.; Rueden, C.; Saalfeld, S.; Schimdt, B.; et al. Fiji: An open-source platform for biological-image analysis. *Nat. Methods* **2012**, *9*, 676–682. [[CrossRef](#)]
73. Rezzola, S.; Di Somma, M.; Corsini, M.; Leali, D.; Ravelli, C.; Polli, V.A.B.; Grillo, E.; Presta, M.; Mitola, S. VEGFR2 activation mediates the pro-angiogenic activity of BMP4. *Angiogenesis* **2019**, *22*, 521–533. [[CrossRef](#)]

**Diabetic Retinopathy: Soluble and Imaging Ocular Biomarkers.**

M. Ferrara, **A. Loda**, G. Coco, P. Grassi, S. Cestaro, S. Rezzola, V. Romano, F. Semeraro.

J Clin Med. 2023 Jan 24;12(3):912. doi: 10.3390/jcm12030912. PMID: 36769560; PMCID: PMC9917666.



Review

# Diabetic Retinopathy: Soluble and Imaging Ocular Biomarkers

Mariantonia Ferrara <sup>1</sup>, Alessandra Loda <sup>2</sup>, Giulia Coco <sup>3</sup>, Piergiacomo Grassi <sup>4,5</sup>, Silvia Cestaro <sup>6</sup>, Sara Rezzola <sup>2</sup>, Vito Romano <sup>6,7,\*</sup> and Francesco Semeraro <sup>6,7,\*</sup>

<sup>1</sup> Manchester Royal Eye Hospital, Oxford Road, Manchester M13 9WL, UK

<sup>2</sup> Department of Molecular and Translational Medicine, University of Brescia, Viale Europa 11, 25123 Brescia, Italy

<sup>3</sup> Department of Clinical Science and Translational Medicine, University of Rome Tor Vergata, 00133 Rome, Italy

<sup>4</sup> Northern Care Alliance NHS Foundation Trust, Whitehall St, Rochdale OL12 0NB, UK

<sup>5</sup> School of Medical Sciences, Faculty of Biology, Medicine and Health, The University of Manchester, Oxford Road, Manchester M13 9PL, UK

<sup>6</sup> Eye Clinic, Department of Medical and Surgical Specialties, Radiological Sciences, and Public Health, University of Brescia, 25121 Brescia, Italy

<sup>7</sup> ASST Civil Hospital of Brescia, 25123 Brescia, Italy

\* Correspondence: vito.romano@gmail.com (V.R.); francesco.semeraro@unibs.it (F.S.)

**Abstract:** Diabetic retinopathy (DR), the most common microvascular complication of diabetes mellitus, represents the leading cause of acquired blindness in the working-age population. Due to the potential absence of symptoms in the early stages of the disease, the identification of clinical biomarkers can have a crucial role in the early diagnosis of DR as well as for the detection of prognostic factors. In particular, imaging techniques are fundamental tools for screening, diagnosis, classification, monitoring, treatment planning and prognostic assessment in DR. In this context, the identification of ocular and systemic biomarkers is crucial to facilitate the risk stratification of diabetic patients; moreover, reliable biomarkers could provide prognostic information on disease progression as well as assist in predicting a patient's response to therapy. In this context, this review aimed to provide an updated and comprehensive overview of the soluble and anatomical biomarkers associated with DR.

**Keywords:** corneal endothelial cell count; confocal microscopy; diabetic retinopathy; fluorescein angiography; ocular biomarkers diabetic retinopathy; optical coherence tomography; optical coherence tomography angiography; serum biomarkers diabetic retinopathy; ultra-widefield fundus photography



**Citation:** Ferrara, M.; Loda, A.; Coco, G.; Grassi, P.; Cestaro, S.; Rezzola, S.; Romano, V.; Semeraro, F. Diabetic Retinopathy: Soluble and Imaging Ocular Biomarkers. *J. Clin. Med.* **2023**, *12*, 912. <https://doi.org/10.3390/jcm12030912>

Academic Editor: Michele Lanza

Received: 31 December 2022

Revised: 18 January 2023

Accepted: 22 January 2023

Published: 24 January 2023



**Copyright:** © 2023 by the authors. Licensee MDPI, Basel, Switzerland. This article is an open access article distributed under the terms and conditions of the Creative Commons Attribution (CC BY) license (<https://creativecommons.org/licenses/by/4.0/>).

## 1. Introduction

Diabetic retinopathy (DR) is the most common microvascular complication of diabetes mellitus (DM), and it represents the leading cause of acquired blindness in the working-age population in developed countries [1]. The disease is characterized by an initial, non-proliferative stage (NPDR) that manifests with increased vascular permeability due to damage to the retinal microvasculature, and, consequently, vascular leakage, lipidic exudates, areas of ischemia, and microaneurysms [2,3]. NPDR can progress into proliferative DR (PDR), which is characterized by a marked neovascularization and by the formation of fragile new blood vessels through the retina and into the vitreous humor. If untreated, DR can lead to vitreous hemorrhage, diabetic macular edema (DME), tractional detachment of the retina, and, eventually, blindness [2,4]. Patients with DR can be asymptomatic until advanced stages of the disease; thus, regular eye screenings play a crucial role in order to timely identify pathologic signs. Imaging techniques are fundamental tools in ophthalmology and their role for screening, diagnosis, classification, monitoring, treatment planning and prognostic assessment in several common ophthalmic diseases, including DR, is constantly expanding [5–12]. Importantly, the high resolution and sensitivity of these techniques can lead to detect microstructural subclinical changes,

potentially improving the effectiveness of population-screening programs and facilitating an early diagnosis. Furthermore, newly identified biomarkers could also provide new insights into the pathogenesis of DR.

In this context, the identification of ocular and systemic biomarkers is crucial to facilitate the early diagnosis and to guide the risk stratification of diabetic patients; moreover, reliable biomarkers could provide prognostic information on disease progression as well as assist in predicting a patient's response to therapy. This review aimed to provide a comprehensive overview of the soluble and anatomical biomarkers associated with diabetic retinopathy.

## 2. Methods

We performed a comprehensive literature review regarding ocular and serum biomarkers of diabetic retinopathy using PubMed, Cochrane and the Embase database up to October 2022, with no limit associated with the year of publication. The keywords used for this search were: corneal endothelial cell count; confocal microscopy; diabetic retinopathy; fluorescein angiography; ocular biomarkers diabetic retinopathy; optical coherence tomography; optical coherence tomography angiography; serum biomarkers diabetic retinopathy; ultra-widefield fundus photography. We included clinical studies with both prospective or retrospective design, whereas editorials, case reports, observations, expert opinions, letters to the editor and non-inherent studies were excluded.

## 3. Brief Overview on the Pathogenesis of Diabetic Retinopathy

Diabetic retinopathy is a multifactorial disease and several factors contribute to its onset, including hyperglycemia, hypoxia, inflammation, and oxidative stress. For a long time, DR has been considered as a vascular disorder due to the extensive involvement of vascular alterations in the pathogenesis of the disease; however, several studies have demonstrated that endothelial dysfunction and microangiopathy are only one aspect of a more widespread retinal dysfunction, affecting also glial and neuronal cells [13–15]. Indeed, long-term hyperglycemia activates numerous metabolic pathways involved in the production of reactive oxygen species (ROS) and pro-inflammatory mediators, which are in turn associated to leukostasis, disruption of cell–cell junctions, loss of endothelial cells and pericytes, and breakdown of the blood–retinal barrier BRB, resulting in vascular dysfunction, neurodegeneration and microglia activation [16]. In addition, hyperglycemia promotes the dysfunction and loss of the endothelial glycocalyx contributing to the increase in vascular permeability, capillary occlusion and leukostasis, and, thus potentially to atherothrombotic processes and DR progression [17,18]. The concomitant complement hyperactivation and the accumulation of immune cells and pro-inflammatory molecules into the retina due to the BRB breakdown contribute to DR progression further promoting retinal neurovascular damage and local chronic low-grade inflammation [19]. As the severity of the disease progresses, capillary non-perfusion leads to retinal ischemia, increasingly affecting larger areas of the retina [20]; as a consequence, the balance between pro-angiogenic and anti-angiogenic mediators is shifted, resulting in neovascularization [4,21].

## 4. Angiogenic and Inflammatory Mediators in Diabetic Retinopathy

Several studies investigated the presence of exploitable biomarkers by analyzing different biological fluids obtained from patients, such as vitreous humor, aqueous humor, and blood (Figure 1).

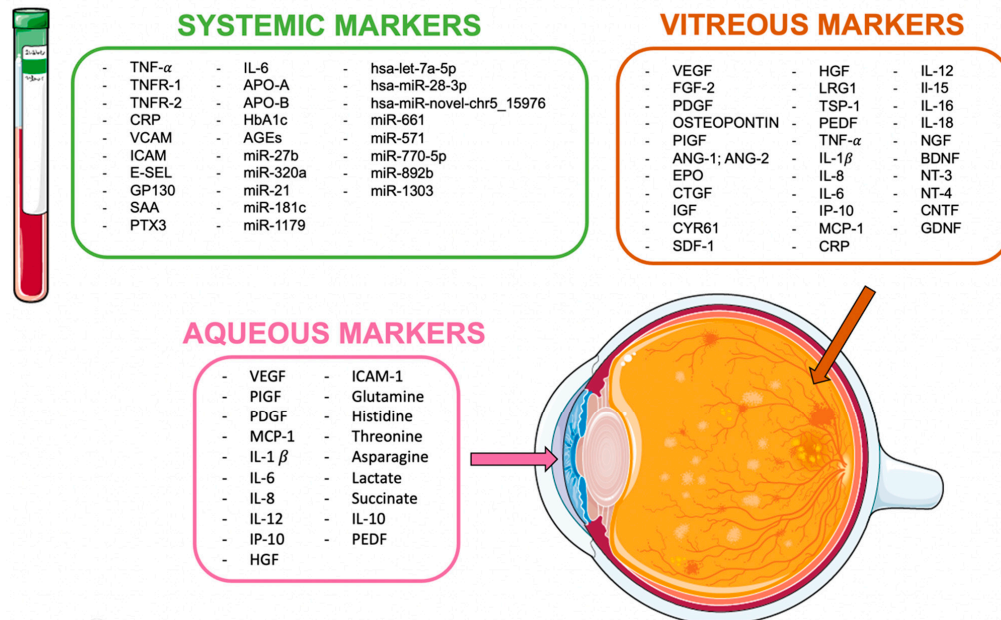


Figure 1. Soluble biomarkers in diabetic retinopathy.

#### 4.1. Vitreous Humor Biomarkers

Due to its proximity to the retina, the vitreous is deeply affected by the pathological events that occur during DR progression, and it undergoes structural and molecular alterations, which are reflected by a marked change of its proteomic profile [22]. A recent extensive analysis on 138 vitreous samples from eyes with DR identified over 1350 distinct proteins, with 230 proteins being more abundant in patients with PDR compared to NPDR, including angiogenic factors and inflammatory mediators, complement and coagulation cascade proteins, protease inhibitors, apolipoproteins, immunoglobulins, proteins involved in ROS production, and cell adhesion molecules [23].

In the diabetic retina, the balance between pro-angiogenic and anti-angiogenic mediators is shifted toward the establishment of a more pro-angiogenic microenvironment. Consistently, in diabetic vitreous, several pro-angiogenic mediators are upregulated, whereas some anti-angiogenic mediators are downregulated (Table 1) [24–39]. Consistently with the extensive role of inflammation in DR, several pro-inflammatory cytokines and chemokines are commonly found to be upregulated in the vitreous of patients with PDR (Table 1) [2,40–43]. Interestingly, increased levels of interleukin (IL) 1b, IL-18, and IL-6, as well as vascular endothelial growth factor (VEGF), have been shown to correlate with disease severity [43,44]. It is worth mentioning that patients with NPDR had significantly higher vitreous concentrations of neurotrophins when compared to patients with PDR, supposedly due to an increased production of neurotrophins by retinal glial cells, as an attempt to rescue neuronal cells during the early stages of DR [45,46]. Finally, the vitreous obtained from patients with PDR exerts a significant biological activity in several *in vitro* and *in vivo* experimental models, and it reflects the biological variability that occurs in patients as a consequence of different clinical parameters [47–49]; thus, the diabetic vitreous might be employed to guide drug discovery as well as to facilitate the selection of more personalized pharmacological treatments better suited to the clinical features of each patient.

**Table 1.** Angiogenic and inflammatory mediators in diabetic retinopathy.

Molecules	Vitreous	Aqueous
Upregulated pro-angiogenic mediators	VEGF, FGF-2, Ang-1, Ang-2, PDGF, EPO, osteopontin, PIGF, CTGF, IGF, CYR61, SDF-1, HGF, LRG1	VEGF, PIGF, PDGF, HGF
Downregulated anti-angiogenic mediators	PEDF, TSP-1	PEDF
Upregulated pro-inflammatory mediators	TNF- $\alpha$ , IL-1 $\alpha$ , IL-8, IL-6, IP-10, MCP-1, CRP, IL-12, IL-15, IL-16, IL-18	MCP-1, IL-1b, IL-6, IL-8, IL-12, IP-10
Other molecules—upregulated		glutamine, histidine, threonine, asparagine, PTX3
Other molecules—downregulated	NGF, BDNF, NT-3, NT-4, CNTF, GDNF	lactate, succinate, IL-10

Ang-1, angiopoietin-1; Ang-2, angiopoietin-2; BDNF, brain-derived neurotrophic factor; CNTF, ciliary neurotrophic factor; CRP, c-reactive protein; CTGF, connective tissue growth factor; CYR61, cysteine-rich 61; EPO, erythropoietin; FGF-2, fibroblast growth factor 2; GDNF, glial cell-derived neurotrophic factor; HGF, hepatocyte growth factor; ICAM-1, intracellular adhesion molecule type 1; IGF, insulin-like growth factor; IL, interleukin; IP-10, interferon- $\alpha$ -inducible protein-10; LRG1, leucine-rich  $\alpha$ -2-glycoprotein; MCP-1, monocyte chemoattractant protein-1; NGF, nerve growth factor; NT, neurotrophin; PDGF, platelet-derived growth factor; PEDF, pigment epithelium-derived factor; PIGF, placental growth factor; SDF-1, stromal cell-derived factor 1; TNF- $\alpha$ , tumor necrosis factor- $\alpha$ ; TSP-1, thrombospondin 1; VEGF, vascular endothelial growth factor.

#### 4.2. Aqueous Humor Biomarkers

Aqueous humor might represent a useful tool to better characterize the ocular angio-inflammatory profile of diabetic patients and to monitor their response to therapy as proteins released from the diabetic retina diffuse from the vitreous humor into the aqueous [50]. In addition, the analysis of the aqueous is favored by the relative ease and safety of sample withdraw compared to vitreous [51].

Despite its high turnover rate, several pro-inflammatory and pro-angiogenic mediators have been found upregulated in the aqueous humor of patients affected by DR (Table 1) [52–59]. On the other hand, significantly lower levels of the anti-inflammatory cytokine IL-10 and of the anti-angiogenic factor pigment epithelium-derived factor (PEDF) have been associated with increased severity of DR and higher risk of developing DME [53–62]. In this context, the presence of DR seems also to be associated to higher levels of the long pentraxin 3, supporting the role of this protein in the local inflammatory reaction to hyperglycemia [60].

The metabolomic profile of aqueous humor revealed increased levels of the glucogenic amino acids glutamine, histidine, threonine, and asparagine in patients with DR compared to diabetic patients without DR [61]. This was paralleled by reduced levels of lactate and succinate, which was probably due to the mitochondrial damage that occurs in the diabetic retina [61].

The relative concentration of different aqueous biomarkers has been exploited to investigate and/or to compare the therapeutic effect of different drugs through measurement before and after a certain treatment. For instance, it has been reported that intravitreal triamcinolone acetonide resulted in a significative reduction in several angio-inflammatory mediators (i.e., IL-6, IP-10, MCP-1, PDGF-AA, and VEGF), whereas intravitreal bevacizumab led to reduced levels only of VEGF [54]. In addition, a progressive decrease in VEGF, placental growth factor (PIGF), and tumor necrosis factor (TNF)  $\alpha$  levels has been demonstrated following panretinal photocoagulation (PRP), supporting the effectiveness of targeting hypoxic retinal areas for reducing the angio-inflammatory microenvironment of DR [54].

#### 4.3. Serum and Plasma Biomarkers

A variety of mediators has been associated to the onset of microvascular complications in diabetic patients, including high concentrations of soluble VCAM, ICAM, E-selectin, glycoprotein 130, serum amyloid A, pentraxin 3, and IL6 [63–66]. In addition, high levels of TNF- $\alpha$ , as well as of soluble TNF receptors 1 and 2 (TNFR-1 and TNFR-2, respectively), have been found in serum of patients with DR, and they have been associated with disease progression and with an increased risk of developing PDR and DME; interestingly, while soluble receptors are usually regarded as TNF-antagonists, in this context, they represent a reservoir of circulating TNF- $\alpha$  [65,67]. Furthermore, high serum levels of CRP have been identified as predictive of developing retinal hard exudates and DME [68]. Moreover, an in-depth analysis of serum metabolic markers suggested that increased levels of apolipoprotein B (APO-B) and decreased levels of apolipoprotein A (APO-A) correlate to DR severity, whereas a high APO-B/APO-A ratio is positively associated to increased risk of developing DME [69]. Conversely, even though serum levels of VEGF are increased in patients with DR, they are not predictive of eye disease progression; however, the evidence that circulating levels of VEGF are significantly reduced in DR patients after intravitreal administration of the anti-VEGF aflibercept suggests a potential utility of dosing VEGF in plasma to monitor response to therapy [65].

Despite the identification of the above-mentioned biological mediators, the only validated biomarker for the prediction of DR onset and progression is glycated hemoglobin (HbA1c), confirming that a good glycemic control is effective in reducing the risk of DR and its complications [70]. Accordingly, higher baseline levels of advanced glycation-end products (AGEs) are significantly associated to increased risk of disease progression [71].

Recently, noncoding RNAs have emerged as a promising biomarker for the early diagnosis and monitoring of various diseases [72]. MicroRNAs (miRNAs) are highly conserved 19–25 nucleotide noncoding RNAs that regulate gene expression by blocking the translation of messenger RNAs [73]. When released into the circulation, miRNAs are very stable and they have a long lifespan, which makes them suitable for investigation [74]. miRNAs have been also implicated in the microvascular complications of diabetes, promoting inflammation and endothelial dysfunction [75]. Circulating miR-27b and miR-320a have been associated with increased risk of DR, probably exerting a pro-angiogenic function [75]. Moreover, increased levels of miR-21, miR-181c, and miR-1179 have been found in patients with PDR compared to NPDR; supposedly, they provide a distinct fingerprint for PDR with a moderate efficacy in discriminating between NPDR and more advanced disease [73]. Additionally, a panel of three circulating miRNAs, which includes hsa-let-7a-5p, hsa-miR-28-3p, and hsa-miR-novel-chr5\_15976, has been reported as successful in discriminating between diabetic patients with or without DR as well as in distinguishing between early and severe DR [76]. Finally, high levels of miR-661, miR-571, miR-770-5p, miR-892b, and miR-1303 in diabetic patients have been associated with increased risk of microvascular complications [77].

#### 5. Corneal Biomarkers

Anterior segment sequelae of DM are not as well defined as DR. However, up to 2/3 of patients can develop diabetic keratopathy [78,79]. Despite its limited and occasionally controversial nature, the available evidence suggests that corneal structural and biomechanical changes in diabetic eyes may be potential biomarkers in the early diagnosis of DM and its complications [80].

In general, all corneal layers may be affected by morphological and functional changes in diabetic eyes, and a variety of alterations have been described [81]. Indeed, the metabolic stress induced by chronic hyperglycemia activates several pathological pathways, resulting in endothelium damage, corneal edema, endothelial cells loss, progressive deprivation in corneal nerve fiber mass with consequent increased epithelial fragility, reduced epithelial cell density and corneal susceptibility to persistent epithelial defects, recurrent corneal ulcerations and infections [82–84]. In addition, due to the inability of the corneal endothe-



lium to regenerate in response to the endothelial cell loss, compensatory morphological changes of the endothelial cells can be observed, such as increased cellular pleomorphism, polymegathism and decrease in the percentage of hexagonal cells (Hex) [83].

In this light, corneal parameters related to endothelial dysfunction and corneal neuropathy have been investigated as surrogate markers for DM. This section will focus on the main DM-associated corneal changes and, in particular, on the findings that each imaging technique allows us to analyze.

### 5.1. Corneal Thickness

Diabetes-related alterations in central corneal thickness (CCT) may be due to the endothelial damage and the subsequent unbalanced corneal hydration and corneal edema [83,85]. The studies analyzing CCT in diabetic and non-diabetic eyes are resumed in Table 2.

#### 5.1.1. Anterior Segment OCT

Studies with AS-OCT described an increased CCT in diabetic patients compared to controls (Table 2) [86–88]. It is worth noting that CCT measurements using AS-OCT may be higher than those obtained with slit-scanning topography and ultrasonic pachymetry [88].

Yusufoğlu et al. [87] showed an average percentage increase in CCT of about 2% in patients with DM compared to healthy controls and a reduction in the central corneal epithelial thickness (CCET) in diabetic patients with DR compared to those without DR (Table 2). In particular, CCET may decrease due to dry eye [89], impaired epithelial homeostasis associated with corneal neuropathy, and/or the effect of retinal photocoagulation [90].

Central corneal thickness may not correlate with the duration of DM and the presence of DR as suggested by the evidence of increased CCT regardless of the DR stage in two recent cross-sectional studies (Table 2) [86,88]. Interestingly, an analysis with AS-OCT of 100 diabetic eyes showed that the mean anterior chamber width (ACW) was narrower in eyes with NPDR than those with no DR [86], suggesting that ACW may be an adjunctive marker of DR. The increased oxidative stress and/or the reduced antioxidant capacities of diabetic eyes may lead to lens thickening, reduction in the anterior chamber volume and narrowing of the angle [91,92]. Based on ACW findings, in the absence of DR, diabetes itself might not be considered as a risk factor for primary angle closure glaucoma.

#### 5.1.2. Ultrasound Pachymetry

Cross-sectional studies, in which ultrasound pachymetry was used to assess CCT, confirmed the significant increase in CCT in diabetic eyes compared to controls regardless of the DR severity (Table 2) [93,94]. CCT may correlate positively with levels of serum glucose and HbA1c [95], and DM duration and increased CCT is controversial (Table 2) [91,92,94].

#### 5.1.3. Specular Microscopy

The studies analyzing CCT with specular microscopy provided conflicting results on the effect of the duration of DM, HbA1c levels and severity of DR on CCT in diabetic patients (Table 2) [79,83,92–102]. In particular, with regard to HbA1c, on the one hand, the 3-month timeframe reflected by HbA1c might be too short to correlate with long-standing corneal alterations [103]; on the other hand, CCT can increase during acute hyperglycemia, and Hb1Ac is not a good marker of short-term blood glucose fluctuation [104].

**Table 2.** Principal studies comparing central corneal thickness (CCT) in diabetic and non-diabetic patients.

Authors, Years	Study Design	Imaging Method	Eyes (n)		CCT (µm)		Conclusions
			DM	Controls	DM	Controls	
Suraida et al., 2018 [86]	CS	AS-OCT	DM = 100 NoDR = 50 NPDR = 50	50	524.60 ± 28.74 529.26 ± 33.88	493.12 ± 67.08	Diabetic patients appear to have significantly thicker CCT regardless of the retinopathy status ( $p < 0.001$ )
Yusufoglu et al., 2022 [87]	P, CS	AS-OCT	72	72	544.33 ± 31.20	533.77 ± 24.45	The CCT was statistically significantly thicker in diabetic patients than in the controls ( $p = 0.025$ )
		AS-OCT	NoDR = 49 NPDR = 30 PDR = 17		521.71 ± 27.58 528.20 ± 29.16 516.94 ± 34.25		
Canan et al., 2020 [88]	P, CS	SST	NoDR = 49 NPDR = 30 PDR = 17		568.10 ± 32.5 567.57 ± 35.49 554.47 ± 25.95		No correlation between CCT and the severity of retinopathy ( $p > 0.05$ ) Better correlation for OCT and UP.
		UP	NoDR = 49 NPDR = 30 PDR = 17		551.1 ± 29.64 556.07 ± 31.18 544.18 ± 36.33		
Lee et al., 2006 [93]	CS	UP	200 ≤10y = 111 >10y = 89	100	588.2 ± 2.7 582.2 ± 3.7 595.9 ± 4.2	567.8 ± 3.8	Diabetic patients show significantly higher CCT differences compared to controls ( $p < 0.05$ ) DM of over 10 years' duration showed thicker corneas ( $p < 0.05$ ) The CCT of diabetic patients is thicker when compared with non-diabetic patients ( $p = 0.001$ ) Differences between DM subgroups are not statistically significant ( $p = 0.056$ )
Özdamar et al., 2010 [92]	CS	UP	DM = 100 NoDR = 29 NPDR = 48 PDR = 23	145	564 ± 30 565 ± 32 558 ± 31 582 ± 23	538 ± 35	Thicker corneas in patients with DM ( $p < 0.001$ ) CCT is significantly higher in diabetic patients ( $p < 0.05$ ) No significant difference in CCT between diabetic and control groups ( $p = 0.301$ ) CCT is not increased in type II DM ( $p = 0.90$ )
Su et al., 2008 [94]	CS	UP	748	2491	547.2 ± 1.2	539.3 ± 0.7	CCT is increased in children and adolescents with DM ( $p < 0.0001$ ) Diabetic patients show a significant increase in CCT ( $p < 0.05$ )
Galgauskas et al., 2016 [97]	P, CS	NCSM	123	120	566.7 ± 35.7	550.0 ± 56.4	
El-Agamy et al., 2020 [98]	P, CS	NCSM	DM 2 = 57	45	545.61 ± 30.39	539.42 ± 29.22	No significant increase in CCT in diabetic patients ( $p = 0.923$ and $p = 0.511$ with Pentacam and Corvis, respectively)
Inoue et al., 2002 [100]	CS	UP	DM 2 = 99	97	538 ± 36	537 ± 38	No significant increase in CCT in diabetic patients ( $p = 0.923$ and $p = 0.511$ with Pentacam and Corvis, respectively)
Urban et al., 2013 [101]	CS	NCSM	DM 1 = 123	124	550 ± 30	530 ± 33	
Storr-Paulsen et al., 2014 [102]	P, CS	NCSM	107	128	546 ± 7	538 ± 5	
Ramm et al., 2020 [105]	P, CS	Pentacam Corvis ST	59	57	552.6 ± 33.2 553.4 ± 35	552 ± 36.6 558 ± 38.6	

AS-OCT: anterior segment optical coherence tomography; CS: cross-sectional; DM: diabetes mellitus; DR: diabetic retinopathy; NCSM, noncontact specular microscope; NPDR: non-proliferative diabetic retinopathy; P: prospective; PDR: proliferative diabetic retinopathy; SM: specular microscope; SST: slit-scanning topographer; UP: ultrasonic pachymeter.

#### 5.1.4. Dynamic Sheimpflug Analyzer Corvis ST (CST) and Pentacam

The comparison of diabetic versus healthy eyes in terms of spatial corneal thickness distribution showed that the values of pachy slope (indicator of the corneal thickness change from the apex to the periphery), thinnest corneal thickness (TCT) and peripheral pachymetry were significantly greater in the former, with no correlation with HbA1c value or DM duration [105]. Conversely, no CCT increase was reported [105].

### 5.2. Epithelial Cell Density

A lower basal epithelial cell density has been described in diabetic eyes, but the overall epithelial cell density may not significantly differ compared to that in healthy eyes [106–108]. This findings in diabetic eyes may be due an increased turnover rate of basal epithelial cells and the subsequent increased maturation and differentiation of superficial cells, compensating for the reduced basal epithelial cells density [109].

### 5.3. Endothelial Cell Density (ECD)

#### 5.3.1. Specular Microscopy

The vast majority of studies that investigated ECD through specular microscopy found this parameter to be lower in diabetic patients than healthy controls, with a reported reduction rate ranging from 3 to 5.3% (Table 3) [83,98,100,101,110–114]. No significant difference has been documented in a minority of studies [102,115,116], which is potentially due to the different glycemic status and different severity of the patients included (Table 3). Indeed, poor glycemic control, high HbA1c and longer duration of DM in diabetic patients may influence negatively ECD and cells morphology [109]. However, the evidence on the impact of DM duration, Hb1Ac levels and severity of DR is still controversial [83,98,113]. Finally, Módis et al. suggested a role of DM type on ECD reduction, as they reported a lower ECD in type I DM patients but no significant difference between type II DM patients and healthy controls [111].

#### 5.3.2. In Vivo Corneal Confocal Microscopy (CCM)

Consistently with the proved equivalency of CCM and specular microscopy proved in ECD measurements [117,118], the significant reduction in ECD in diabetic eyes compared with healthy controls has been confirmed by most of the studies conducted using CCM (Table 3) [106,107,119].

**Table 3.** Studies comparing endothelial cell density in diabetic and non-diabetic patients.

Authors, Years	Study Design	Imaging Method	Eyes (n)		ECD Cell/mm <sup>2</sup>		Conclusions
			DM	Controls	DM	Controls	
Choo et al., 2010 [83]	CS	NCSM	DM 2 = 100	100	2541.6 ± 516.4	2660.1 ± 515.5	ECD in DM2 group was significantly lower than in the control group ( <i>p</i> < 0.05)
El-Agamy et al., 2020 [98]	CS	NCSM	DM 2 = 57	45	2491.98 ± 261.08	2629.68 ± 293.45	ECD was significantly lower in the diabetic cornea than in the control group ( <i>p</i> = 0.014)
Inoue et al., 2002 [100]	CS	SM	DM 2 = 99	97	2493 ± 330	2599 ± 278	ECD was significantly lower in the diabetic cornea than in the control group ( <i>p</i> = 0.016)
Urban et al., 2013 [101]	CS	NCSM	DM 1 = 123	124	2435.55 ± 443.43	2970.75 ± 270.1	ECD was significantly lower in patients with diabetes than in the control group ( <i>p</i> = 0.0001)
Jha et al., 2022 [110]	CS	NCSM	DM 2 = 592	596	2484.5 ± 299.5	2555.9 ± 258.2	ECD was significantly lower in the diabetic cornea than in the control group ( <i>p</i> = 0.017)
Módis et al., 2010 [111]	CS	NCSM	DM 1 = 41 DM 2 = 59	N/A	2428 ± 219 2495 ± 191	N/A	ECD was significantly lower in the diabetic cornea than in the control group ( <i>p</i> = 0.02). No significant differences between DM2 and controls
Sudhir et al., 2012 [112]	CS, P	NCSM	1191	120	2550.96 ± 326.17	2634.44 ± 256.0	ECD was significantly lower in the diabetic cornea than in the control group ( <i>p</i> = 0.001).
Islam et al., 2017 [113]	CS	NCSM	149	149	2494.47 ± 394.10	2574.46 ± 279.97	ECD was significantly lower in the diabetic cornea than in the control group ( <i>p</i> = 0.04).
Storr-Paulsen et al., 2014 [102]	CS, P	NCSM	DM 2 = 107	128	2578 ± 77	2605 ± 66	No differences in ECD between well-controlled diabetic subjects and non-diabetic subjects ( <i>p</i> = 0.60)
Quadrado et al., 2006 [106]	CS, P	CCM	15	15	2660 ± 364	2690 ± 302	ECD in diabetic patients is not significantly different from healthy controls ( <i>p</i> = 0.5)
Szalai et al., 2016 [107]	CS	CCM	No DR = 10 DR = 18	17	3250.36 ± 421.5 2639.17 ± 227.5	3497.62 ± 519.8	ECD was significantly lower in patients with DM without and with retinopathy compared to control subjects ( <i>p</i> = 0.001)
Shenoy et al., 2009 [119]	Cohort study	CCM	110	110	2342 ± 392	2517 ± 647	ECD was significantly lower in the diabetic cornea than in the control group

CCM: corneal confocal microscopy; CS: cross-sectional; DM: diabetes mellitus; DR: diabetic retinopathy; NCSM, noncontact specular microscope; NPDR: non-proliferative diabetic retinopathy; P: prospective; PDR: proliferative diabetic retinopathy; SM: specular microscope.

#### 5.4. Coefficient of Variation in Cell Size (CV)

Coefficient of variation in cell size has been more commonly found to be greater in patient with diabetes compared with healthy controls [83,98,100,110,114,116,120], with the exception of a few studies that did not find any significant difference [112,113]. As for ECD, there is no agreement on the potential correlation between CV and duration of DM, HbA1c levels, or DR severity [93,98,120]. In particular, no statistically significant correlation between any of the above-mentioned parameters and CV was reported by El-Agamy et al. [98]. In contrast, Lee et al. noted that CV was higher in patients with longer DM duration (more versus less than 10 years) [93]. Additionally, Taşlı et al. reported that CV correlated positively with HbA1c levels as well as the presence and progression of DR [120].

#### 5.5. Percentage of Hexagonal Cells

The reduction in Hex is an established DM-related alteration [83,110,116,120], even if the difference with healthy eye has not always been found to be significant [98,100,113]. This may correlate negatively with DR presence and stage [110,120].

#### 5.6. Diabetic Corneal Neuropathy

Diabetic corneal neuropathy is the ocular manifestation of the diabetic peripheral neuropathy (DPN), a long-term complication of DM, consisting of a length-dependent axonopathy that affects approximately 50% of diabetic patients [121]. So far, the diagnosis of DPN is clinical [122], and most of the methods currently used to define its severity only evaluate large nerve fiber function [123]. However, modifications in small nerve fibers are potentially a more sensitive marker of DPN, as these are involved earlier in the course of the disease [124,125]. In addition, the current gold standard to detect small nerve fibers, skin biopsy, is an invasive and non-repeatable procedure, which is not applicable to routine clinical practice [126]. Conversely, the analysis of corneal nerves thought in vivo CCM, a real-time and non-invasive imaging method, has the potential to offer a crucial opportunity to identify early nerves damage in diabetic patients [127,128]. Indeed, the cornea is the most densely innervated structure in the human body, and DM-induced metabolic stress leads to damage in corneal small nerve fibers in the early stages of DM [129].

#### In Vivo Corneal Confocal Microscopy

The parameters most frequently evaluated as possible biomarkers of DPN are corneal nerve fiber density (CNFD, the total number of main nerve fibers in a CCM image, expressed in fibers/mm<sup>2</sup>); corneal nerve branch density (CNBD, the number of branches connected to main nerve fibers, expressed in branches/mm<sup>2</sup>); corneal nerve fiber length (CNFL, the total length of all nerve fibers and branches per image, expressed in mm/mm<sup>2</sup>), and tortuosity of the main nerve fibers [130]. In particular, CNFD, CNFL and CNBD were reported to be significantly reduced in both type 1 and type 2 DM [107,131,132], and CNFL may be the parameter most strongly related to the severity of small nerve fiber neuropathy [133,134].

Diabetic corneal neuropathy may correlate with DPN [131,135,136], as supported by the demonstration of significant changes in CNFD, CNFL and CNBD in diabetic patients with the worsening of DPN [137,138]. In addition, recently, the rapid corneal fiber loss (RCNFL) defined by values exceeding the 5th percentile of 6% corneal fiber loss, has been proposed as new marker of DPN development as associated with progression of the impairment of large nerve fiber, even in absence of HbA1c changes [139]. Importantly, the demonstration of the same trend of progressive reduction in nerve fiber density, nerve branch density and nerve fiber length at intraepidermal and corneal level with increasing severity of DPN supported the comparable diagnostic value of CCM and skin biopsy [140–142].

With regard to the potential correlation between DR and corneal nerve fiber changes, the evidence is still controversial. Corneal sub-basal nerve plexus alterations may be more severe in eyes with DR than in those without DR as well as correlate with DR stage [131]. In addition, corneal and intraepidermal nerve fiber loss was found to be more pronounced in advanced stages of DR [143]. Argon laser photocoagulation may contribute to the

worsening of the corneal nerve damage [90]. The neuronal damage of both cornea and retina may occur in early stages of DR [144–146], specifically in terms of CNFL [144]. This underlines the importance of the examination of the corneal sub-basal nerve plexus when clinical signs of DR are absent. Furthermore, the higher concentration of antigen-presenting cells, including Langerhans cells and dendritic cells, in the cornea of diabetic eyes compared to healthy controls, negatively correlated with corneal nerve fiber density, may support a role of the inflammation in the development of diabetic corneal neuropathy [147].

Alterations in corneal nerve fiber may also correlate with complications of DM other than DR. For instance, a history of clinically known nephropathy has been found to be significantly associated with reduced CNFD, CNFL and CNB [130,148].

Finally, the significant improvement of CNFL 1 year after simultaneous pancreas and kidney transplantation in patients with DM type 1 may suggest that in vivo CCM may represent a precious tool also for the monitoring of diabetic therapy effectiveness [149,150].

## 6. Retinal Biomarkers

DR has been traditionally classified on the basis of specific retinal findings detectable on fundus examination, color fundus photography and fluorescein angiography, such as microaneurysms, dot and blot hemorrhages, venous beading, intraretinal microvascular anomalies (IRMA), vitreous/preretinal hemorrhage and neovascular [151].

### 6.1. Diabetic Macular Oedema

#### 6.1.1. OCT

The OCT plays an invaluable role in the assessment and management of DME, which is the main cause of moderate vision loss in patients affected by DR [152]. Multiple retinal OCT-biomarkers have been identified so far:

- Intraretinal cystoid spaces: The persistence of intraretinal cystoid spaces can result in permanent photoreceptor damage and visual impairment. Some findings of intraretinal cysts, including the location, size and presence of bridging hyperreflective material, have been associated with functional prognosis in diabetic eyes [153]. In particular, intraretinal cysts larger than 200  $\mu\text{m}$  in the outer nuclear layer (ONL) have been associated with the disruption of IS/OS junction, reduced retinal sensitivity on microperimetry, poor visual prognosis and greater extent of macular ischemia [154–156]. The size of the cysts may also have a predictive value in case of pars plana vitrectomy (PPV) and internal limiting membrane (LM) peeling for chronic DME, as the presence of intraretinal cysts larger than 390  $\mu\text{m}$  has been associated with the postoperative development of subfoveal atrophy [157].
- Increased retinal thickness: Although increased retinal thickness (RT) is strictly associated with the presence of subretinal and/or intraretinal fluid, these findings appeared to be not correlated with visual acuity and visual outcomes in eyes with DME [154].
- Hyperreflective retinal foci (HRF) is defined as intraretinal dots located in both inner and outer retina, with reflectivity similar to that of retinal nerve fiber layer, diameter  $<30 \mu\text{m}$  and no back-shadowing. These lesions may represent extravasated lipoproteins [158] or activated microglial cells [159] and are widely considered biomarkers of retinal inflammation [160]. It has been suggested as a better response to intravitreal dexamethasone implant compared to anti-VEGFs, but there is also a higher rate of recurrence in eyes with a higher number of HRF [161,162].
- Hard exudates: Differently from HRF, hard exudates are characterized by size  $>30 \mu\text{m}$ , back-shadowing, reflectivity similar to the RPE–Bruch’s membrane complex and location within the outer retinal layers. Conversely, hyperreflective dots with the same characteristics but located in the inner retina have been described as microaneurysms [163]. It has been suggested that hard exudates may be used as markers for treatment response in DME [164] and may be associated with better response to dexamethasone implant compared to intravitreal anti-VEGF agents [165].

- Disorganization of retinal inner layers: The presence of disorganization of retinal inner layers (DRIL) is evaluated in an area of 1 mm diameter centered on the foveal center. This finding has been associated with retinal dysfunction, even in case of early neuroretinal impairment [166]. An extent of DRIL of more than 50% of this area has been proposed as a negative prognostic factor for visual outcomes in eyes with DME before and/or after treatment [167]. In addition, DRIL may be associated with the presence of diabetic maculopathy regardless of the presence of DME, being correlated with the size of FAZ, the area of capillary non-perfusion, increased foveal thickness, the presence of EZ/ELM disruption and the severity of DR [168–170]. A negative correlation between RNFL thickness and DRIL has also been reported [171].
- Hyperreflective bridging retinal processes: It has been suggested that these processes between the cystic cavities represent neuronal tissue bridging between outer and inner retina [153]. Bridging retinal processes may be associated with better visual outcomes after anti-VEGF injections in eyes with DME [172], whereas eyes with no bridging retinal processes may be more likely to develop foveal atrophy post-treatment [173].
- Subfoveal neurosensory detachment (SND): The potential influence of SND on visual outcomes after intravitreal anti-VEGF agents for DME remains controversial [174–177]. This finding has been described in up to 30% of eyes with DME and may be correlated with the disruption of the external limiting membrane (ELM) that allow fluid and protein to migrate from the retina to the subretinal space [178]. In addition, the presence of SND may correlate with a greater amount of HF and a reduced retinal sensitivity [178]. Based on the detection of higher levels of IL-6 in eyes with SND, the latter has been proposed as a sign of retinal inflammation, and good response following dexamethasone implant has been reported [179,180]. A better response to aflibercept injection has also been reported in eyes with SND compared with those without SND [181].
- Alteration in outer retinal layers: The length of the photoreceptor outer segment may be reduced in patients with DR with or without DME compared to healthy eyes and may be a good indicator of visual acuity in eyes with DME [182,183]. As in other macular pathologies, the presence of preserved outer retinal layers, in particular an external limiting membrane (ELM) and ellipsoid (EZ) band appears to be associated with better visual outcomes in eyes with DME [179].

#### 6.1.2. Fluorescein Angiography (FA)

Fluorescein angiography has been traditionally used for the staging and management planning in DR and represents still a crucial diagnostic technique for the detection of leakage [184]. Diabetic maculopathy has been traditionally divided in focal, diffuse and ischemic based on the fluorangiographic appearance of the macula [185]. The former is characterized by focal leakage from microaneurysms surrounded by hard exudates; diffuse maculopathy manifests as a diffuse leakage involving the posterior pole in the early phase of FA. Finally, the latter refers to the presence of macular ischemia, which is characterized by an increase in the foveal avascular zone (FAZ) [186]. It is worth noting that FAZ is known to be enlarged and irregular in eyes with DR due to the occlusion of perifoveal capillaries regardless of the presence of ischemic maculopathy [187].

#### 6.1.3. OCT-Angiography (OCTA)

OCTA may be more sensitive to the detection of capillary non-perfusion areas compared to FA thanks to the absence of areas obscured by fluorescein leakage [188]. An enlargement of FAZ and, more specifically of the deep capillary plexus (DCP), has been reported in diabetic eyes, regardless of the presence of DR [189]. In addition, both superficial capillary plexus (SCP) and DCP appeared to be significantly reduced on fractal analysis and in terms of vessel density (VD) in patients with DM compared to healthy controls [190,191]. However, the reduction in VD of SCP and DCP may be more marked in eyes with DR compared to those without DR [192,193] as well as in eyes with DME compared

to those without DME [194] and correlate with the degree of DR [192,193]. The reduction in VD in the DCP may also be associated with worse visual acuity and the progression of NPDR [195]. The analysis of the changes in both SCP and DCP has been performed before and after macular surgery in diabetic eyes, confirming that the DCP may be more sensible to vascular and iatrogenic damage [196,197]. In addition of the reduced VD, the non-perfusion area (NPA) may increase as the severity of DR increases [198]. Finally, an enlargement of FAZ may be associated with the presence of DRIL [199].

Recently, the perfused capillary density (PCD) has been suggested as a biomarker for DR as reported to be reduced in eyes with DR compared with those without DR, and this reduction may be more marked in eyes with PDR compared to eyes with NPDR [200].

### 6.2. Peripheral Retinal Ischemia

Ultra-widefield fluorescein angiography (UWFA) represents the standard imaging method used to evaluate the vascular changes in retinal periphery in diabetic eyes. The wider field detectable with UWF photography and FA can be particularly useful in the assessment of DR, as peripheral retinal findings may correlate with a higher risk of DR progression [184,201].

Retinal ischemic areas, characterized by the absence of visible retinal vasculature, can be delimited by tortuous, dilated, shunt vessels. The extent of peripheral retinal ischemia may correlate with DME [202,203]. The ischemia index has been defined as the percentage of the extent of ischemic areas of ischemia out of the total retinal area and has been suggested as biomarker of DR activity [204–206].

Recently, the retinal vascular bed area (RVBA), measured as the automatic sum of the real size (in mm<sup>2</sup>) of all the pixels, has been proposed as a new biomarker for the efficiency of retinal vascular changes following anti-VEGF injection [207]. In particular, a reduction on RVBA may be present in eyes with PDR and significant ischemia after anti-VEGF treatment [207].

### 6.3. IRMA and Neovessels

The differential diagnosis between IRMA and retinal neovascularization is crucial to distinguish between NPDR and PDR and, thus, for the patient management and prognosis.

FA represents the mainstay to detect neovessels and, in particular, for the differential diagnosis between neovessels and IRMA. Indeed, the former are characterized by an early and intense focal leakage, whereas the latter do not show leakage on FA. However, recent studies supported the role of OCTA for the detection of neovessels and their changes following treatment [208].

## 7. Conclusions

Over the last decades, the developments in ocular imaging allowed us to assess the structure of several ocular tissue at a near-histological level at high resolution and in a non-invasive manner. The management of DR has significantly benefited from the identification of objective, quantifiable signs, used as biomarkers, of greater relevance in clinical practice and research for diagnosis, prognosis and treatment planning. In addition, the association between some of these biomarkers with early or even subclinical stages of the disease, has the potential to result in a significant contribution in the screening protocols and, thus, prevention of the development and progression of DR and the optimization of visual outcomes. Along with the ocular imaging biomarkers, biomarkers detectable in the serum/plasma and ocular fluid are playing a crucial role not only for the diagnosis and prognosis of DM and DR but also for the insights provided in the understanding of DR pathogenesis.

Despite the promising applications in clinical practice and research, the acquisition technique as well as the operator-dependent evaluation can still represent a limitation for some imaging methodologies; in this regard, the development of automated analysis and

deep learning algorithms capable of a fast, reproducible and accurate image segmentation can overcome these limitations.

**Author Contributions:** Conceptualization, F.S., V.R. and M.F.; methodology, V.R. and M.F.; writing—original draft preparation, M.F., G.C., S.C., A.L. and P.G.; writing—review and editing, F.S., V.R. and S.R. All authors have read and agreed to the published version of the manuscript.

**Funding:** S.R. was supported by Fondazione Cariplo (Grant ID. 2021-1563).

**Institutional Review Board Statement:** Not applicable.

**Informed Consent Statement:** Not applicable.

**Data Availability Statement:** Not applicable.

**Conflicts of Interest:** The authors declare no conflict of interest.

## References

- International Diabetes Federation. Diabetes Atlas. 10th ed. Available online: <http://www.diabetesatlas.org/> (accessed on 11 October 2022).
- Tang, J.; Kern, T.S. Inflammation in Diabetic Retinopathy. *Prog. Retin. Eye Res.* **2011**, *30*, 343–358. [\[CrossRef\]](#)
- Singh, R.P.; Elman, M.J.; Singh, S.K.; Fung, A.E.; Stoilov, I. Advances in the Treatment of Diabetic Retinopathy. *J. Diabetes Complicat.* **2019**, *33*, 107417. [\[CrossRef\]](#)
- Al-Kharashi, A.S. Role of Oxidative Stress, Inflammation, Hypoxia and Angiogenesis in the Development of Diabetic Retinopathy. *Saudi J. Ophthalmol.* **2018**, *32*, 318–323. [\[CrossRef\]](#)
- Ferrara, M.; Zheng, Y.; Romano, V. Editorial: Imaging in Ophthalmology. *J. Clin. Med.* **2022**, *11*, 5433. [\[CrossRef\]](#)
- Ferrara, M.; Coco, G.; Sorrentino, T.; Jasani, K.M.; Moussa, G.; Morescalchi, F.; Dhawahir-Scala, F.; Semeraro, F.; Steel, D.H.W.; Romano, V.; et al. Retinal and Corneal Changes Associated with Intraocular Silicone Oil Tamponade. *J. Clin. Med.* **2022**, *11*, 5234. [\[CrossRef\]](#)
- Romano, V.; Steger, B.; Ahmad, M.; Coco, G.; Pagano, L.; Ahmad, S.; Zhao, Y.; Zheng, Y.; Kaye, S.B. Imaging of Vascular Abnormalities in Ocular Surface Disease. *Surv. Ophthalmol.* **2022**, *67*, 31–51. [\[CrossRef\]](#)
- Palme, C.; Ahmad, S.; Romano, V.; Seifarth, C.; Williams, B.; Parekh, M.; Kaye, S.B.; Steger, B. En-Face Analysis of the Human Limbal Lymphatic Vasculature. *Exp. Eye Res.* **2020**, *201*, 108278. [\[CrossRef\]](#)
- Hanson, R.L.W.; Airoyd, A.; Sivaprasad, S.; Gale, R.P. Optical Coherence Tomography Imaging Biomarkers Associated with Neovascular Age-Related Macular Degeneration: A Systematic Review. *Eye* **2022**. [\[CrossRef\]](#)
- Murtaza, F.; Goud, R.; Belhouari, S.; Eng, K.T.; Mandelcorn, E.D.; da Costa, B.R.; Miranda, R.N.; Felfeli, T. Prognostic Features of Preoperative Optical Coherence Tomography in Retinal Detachments: A Systematic Review and Meta-Analysis. *Ophthalmol. Retina* **2022**, *in press*. [\[CrossRef\]](#)
- Petropoulos, I.N.; Bitirgen, G.; Ferdousi, M.; Kalteniece, A.; Azmi, S.; D'Onofrio, L.; Lim, S.H.; Ponirakis, G.; Khan, A.; Gad, H.; et al. Corneal Confocal Microscopy to Image Small Nerve Fiber Degeneration: Ophthalmology Meets Neurology. *Front. Pain Res.* **2021**, *2*, 725363. [\[CrossRef\]](#)
- Romano, M.R.; Ilardi, G.; Ferrara, M.; Cennamo, G.; Parolini, B.; Mariotti, C.; Staibano, S.; Cennamo, G. Macular Peeling-Induced Retinal Damage: Clinical and Histopathological Evaluation after Using Different Dyes. *Graefes Arch. Clin. Exp. Ophthalmol.* **2018**, *256*, 1573–1580. [\[CrossRef\]](#)
- Barber, A.J.; Baccouche, B. Neurodegeneration in Diabetic Retinopathy: Potential for Novel Therapies. *Vis. Res.* **2017**, *139*, 82–92. [\[CrossRef\]](#)
- Rezzola, S.; Guerra, J.; Krishna Chandran, A.M.; Loda, A.; Cancarini, A.; Sacristani, P.; Semeraro, F.; Presta, M. VEGF-Independent Activation of Müller Cells by the Vitreous from Proliferative Diabetic Retinopathy Patients. *Int. J. Mol. Sci.* **2021**, *22*, 2179. [\[CrossRef\]](#)
- Stitt, A.W.; Curtis, T.M.; Chen, M.; Medina, R.J.; McKay, G.J.; Jenkins, A.; Gardiner, T.A.; Lyons, T.J.; Hammes, H.-P.; Simó, R.; et al. The Progress in Understanding and Treatment of Diabetic Retinopathy. *Prog. Retin. Eye Res.* **2016**, *51*, 156–186. [\[CrossRef\]](#)
- Semeraro, F.; Morescalchi, F.; Cancarini, A.; Russo, A.; Rezzola, S.; Costagliola, C. Diabetic Retinopathy, a Vascular and Inflammatory Disease: Therapeutic Implications. *Diabetes Metab.* **2019**, *45*, 517–527. [\[CrossRef\]](#)
- Kaur, G.; Rogers, J.; Rashdan, N.A.; Cruz-Topete, D.; Pattillo, C.B.; Hartson, S.D.; Harris, N.R. Hyperglycemia-Induced Effects on Glycocalyx Components in the Retina. *Exp. Eye Res.* **2021**, *213*, 108846. [\[CrossRef\]](#)
- Noble, M.I.M.; Drake-Holland, A.J.; Vink, H. Hypothesis: Arterial Glycocalyx Dysfunction Is the First Step in the Atherothrombotic Process. *QJM* **2008**, *101*, 513–518. [\[CrossRef\]](#)
- Kinuthia, U.M.; Wolf, A.; Langmann, T. Microglia and Inflammatory Responses in Diabetic Retinopathy. *Front. Immunol.* **2020**, *11*, 564077. [\[CrossRef\]](#)
- Lechner, J.; O'Leary, O.E.; Stitt, A.W. The Pathology Associated with Diabetic Retinopathy. *Vis. Res.* **2017**, *139*, 7–14. [\[CrossRef\]](#)



21. Liu, S.; Romano, V.; Steger, B.; Kaye, S.B.; Hamill, K.J.; Willoughby, C.E. Gene-Based Antiangiogenic Applications for Corneal Neovascularization. *Surv. Ophthalmol.* **2018**, *63*, 193–213. [[CrossRef](#)]
22. Nawaz, I.M.; Rezzola, S.; Cancarini, A.; Russo, A.; Costagliola, C.; Semeraro, F.; Presta, M. Human Vitreous in Proliferative Diabetic Retinopathy: Characterization and Translational Implications. *Prog. Retin. Eye Res.* **2019**, *72*, 100756. [[CrossRef](#)]
23. Loukovaara, S.; Nurkkala, H.; Tamene, F.; Gucciardo, E.; Liu, X.; Repo, P.; Lehti, K.; Varjosalo, M. Quantitative Proteomics Analysis of Vitreous Humor from Diabetic Retinopathy Patients. *J. Proteome Res.* **2015**, *14*, 5131–5143. [[CrossRef](#)]
24. Semeraro, F.; Cancarini, A.; Morescalchi, F.; Romano, M.R.; dell’Omo, R.; Ruggeri, G.; Agnifili, L.; Costagliola, C. Serum and Intraocular Concentrations of Erythropoietin and Vascular Endothelial Growth Factor in Patients with Type 2 Diabetes and Proliferative Retinopathy. *Diabetes Metab.* **2014**, *40*, 445–451. [[CrossRef](#)]
25. Rezzola, S.; Nawaz, M.I.; Cancarini, A.; Semeraro, F.; Presta, M. Vascular Endothelial Growth Factor in the Vitreous of Proliferative Diabetic Retinopathy Patients: Chasing a Hiding Prey? *Diabetes Care* **2019**, *42*, e105–e106. [[CrossRef](#)]
26. Boulton, M.; Gregor, Z.; McLeod, D.; Charteris, D.; Jarvis-Evans, J.; Moriarty, P.; Khaliq, A.; Foreman, D.; Allamby, D.; Bardsley, B. Intravitreal Growth Factors in Proliferative Diabetic Retinopathy: Correlation with Neovascular Activity and Glycaemic Management. *Br. J. Ophthalmol.* **1997**, *81*, 228–233. [[CrossRef](#)]
27. Praidou, A.; Klangas, I.; Papakonstantinou, E.; Androudi, S.; Georgiadis, N.; Karakiulakis, G.; Dimitrakos, S. Vitreous and Serum Levels of Platelet-Derived Growth Factor and Their Correlation in Patients with Proliferative Diabetic Retinopathy. *Curr. Eye Res.* **2009**, *34*, 152–161. [[CrossRef](#)]
28. Abu El-Asrar, A.M.; Imtiaz Nawaz, M.; Kangave, D.; Siddiquei, M.M.; Geboes, K. Osteopontin and Other Regulators of Angiogenesis and Fibrogenesis in the Vitreous from Patients with Proliferative Vitreoretinal Disorders. *Mediat. Inflamm.* **2012**, *2012*, 1–8. [[CrossRef](#)]
29. Mitamura, Y.; Tashimo, A.; Nakamura, Y.; Tagawa, H.; Ohtsuka, K.; Mizue, Y.; Nishihira, J. Vitreous Levels of Placenta Growth Factor and Vascular Endothelial Growth Factor in Patients With Proliferative Diabetic Retinopathy. *Diabetes Care* **2002**, *25*, 2352. [[CrossRef](#)]
30. Patel, J.I. Angiopoietin Concentrations in Diabetic Retinopathy. *Br. J. Ophthalmol.* **2005**, *89*, 480–483. [[CrossRef](#)]
31. Loukovaara, S.; Robciuc, A.; Holopainen, J.M.; Lehti, K.; Pessi, T.; Liinamaa, J.; Kukkonen, K.-T.; Jauhainen, M.; Koli, K.; Keski-Oja, J.; et al. Ang-2 Upregulation Correlates with Increased Levels of MMP-9, VEGF, EPO and TGFβ1 in Diabetic Eyes Undergoing Vitrectomy. *Acta Ophthalmol.* **2013**, *91*, 531–539. [[CrossRef](#)]
32. Hinton, D.R.; Spee, C.; He, S.; Weitz, S.; Usinger, W.; LaBree, L.; Oliver, N.; Lim, J.I. Accumulation of NH2-Terminal Fragment of Connective Tissue Growth Factor in the Vitreous of Patients With Proliferative Diabetic Retinopathy. *Diabetes Care* **2004**, *27*, 758–764. [[CrossRef](#)]
33. Grant, M.; Russell, B.; Fitzgerald, C.; Merimee, T.J. Insulin-Like Growth Factors in Vitreous: Studies in Control and Diabetic Subjects with Neovascularization. *Diabetes* **1986**, *35*, 416–420. [[CrossRef](#)]
34. You, J.J.; Yang, C.M.; Chen, M.S.; Yang, C.-H. Elevation of Angiogenic Factor Cysteine-Rich 61 Levels in Vitreous of Patients with Proliferative Diabetic Retinopathy. *Retina* **2012**, *32*, 103–111. [[CrossRef](#)]
35. Butler, J.M.; Guthrie, S.M.; Koc, M.; Afzal, A.; Caballero, S.; Brooks, H.L.; Mames, R.N.; Segal, M.S.; Grant, M.B.; Scott, E.W. SDF-1 Is Both Necessary and Sufficient to Promote Proliferative Retinopathy. *J. Clin. Investig.* **2005**, *115*, 86–93. [[CrossRef](#)]
36. Canton, A. Hepatocyte Growth Factor in Vitreous and Serum from Patients with Proliferative Diabetic Retinopathy. *Br. J. Ophthalmol.* **2000**, *84*, 732–735. [[CrossRef](#)]
37. Chen, C.; Chen, X.; Huang, H.; Han, C.; Qu, Y.; Jin, H.; Niu, T.; Zhang, Y.; Liu, K.; Xu, X. Elevated Plasma and Vitreous Levels of Leucine-rich-α2-glycoprotein Are Associated with Diabetic Retinopathy Progression. *Acta Ophthalmol.* **2019**, *97*, 260–264. [[CrossRef](#)]
38. Wang, S. Modulation of Thrombospondin 1 and Pigment Epithelium-Derived Factor Levels in Vitreous Fluid of Patients with Diabetes. *Arch. Ophthalmol.* **2009**, *127*, 507. [[CrossRef](#)]
39. Spranger, J.; Osterhoff, M.; Reimann, M.; Möhlig, M.; Ristow, M.; Francis, M.K.; Cristofalo, V.; Hammes, H.-P.; Smith, G.; Boulton, M.; et al. Loss of the Antiangiogenic Pigment Epithelium-Derived Factor in Patients With Angiogenic Eye Disease. *Diabetes* **2001**, *50*, 2641–2645. [[CrossRef](#)]
40. Loporchio, D.F.; Tam, E.K.; Cho, J.; Chung, J.; Jun, G.R.; Xia, W.; Fiorello, M.G.; Siegel, N.H.; Ness, S.; Stein, T.D.; et al. Cytokine Levels in Human Vitreous in Proliferative Diabetic Retinopathy. *Cells* **2021**, *10*, 1069. [[CrossRef](#)]
41. Wu, F.; Phone, A.; Lamy, R.; Ma, D.; Laotaweerungawat, S.; Chen, Y.; Zhao, T.; Ma, W.; Zhang, F.; Psaras, C.; et al. Correlation of Aqueous, Vitreous, and Plasma Cytokine Levels in Patients With Proliferative Diabetic Retinopathy. *Investig. Ophthalmol. Vis. Sci.* **2020**, *61*, 26. [[CrossRef](#)]
42. Pessoa, B.; Heitor, J.; Coelho, C.; Leander, M.; Menéres, P.; Figueira, J.; Meireles, A.; Beirão, M. Systemic and Vitreous Biomarkers—New Insights in Diabetic Retinopathy. *Graefes Arch. Clin. Exp. Ophthalmol.* **2022**, *260*, 2449–2460. [[CrossRef](#)] [[PubMed](#)]
43. Chen, H.; Zhang, X.; Liao, N.; Mi, L.; Peng, Y.; Liu, B.; Zhang, S.; Wen, F. Enhanced Expression of NLRP3 Inflammasome-Related Inflammation in Diabetic Retinopathy. *Investig. Ophthalmol. Vis. Sci.* **2018**, *59*, 978. [[CrossRef](#)] [[PubMed](#)]
44. Funatsu, H.; Yamashita, H.; Noma, H.; Mimura, T.; Nakamura, S.; Sakata, K.; Hori, S. Aqueous Humor Levels of Cytokines Are Related to Vitreous Levels and Progression of Diabetic Retinopathy in Diabetic Patients. *Graefes Arch. Clin. Exp. Ophthalmol.* **2005**, *243*, 3–8. [[CrossRef](#)] [[PubMed](#)]
45. Rübsam, A.; Parikh, S.; Fort, P. Role of Inflammation in Diabetic Retinopathy. *Int. J. Mol. Sci.* **2018**, *19*, 942. [[CrossRef](#)]

46. Boss, J.D.; Singh, P.K.; Pandya, H.K.; Tosi, J.; Kim, C.; Tewari, A.; Juzych, M.S.; Abrams, G.W.; Kumar, A. Assessment of Neurotrophins and Inflammatory Mediators in Vitreous of Patients With Diabetic Retinopathy. *Investig. Ophthalmol. Vis. Sci.* **2017**, *58*, 5594. [[CrossRef](#)] [[PubMed](#)]
47. Rezzola, S.; Nawaz, I.M.; Cancarini, A.; Ravelli, C.; Calza, S.; Semeraro, F.; Presta, M. 3D Endothelial Cell Spheroid/Human Vitreous Humor Assay for the Characterization of Anti-Angiogenic Inhibitors for the Treatment of Proliferative Diabetic Retinopathy. *Angiogenesis* **2017**, *20*, 629–640. [[CrossRef](#)] [[PubMed](#)]
48. Rezzola, S.; Loda, A.; Corsini, M.; Semeraro, F.; Annese, T.; Presta, M.; Ribatti, D. Angiogenesis-Inflammation Cross Talk in Diabetic Retinopathy: Novel Insights From the Chick Embryo Chorioallantoic Membrane/Human Vitreous Platform. *Front. Immunol.* **2020**, *11*, 581288. [[CrossRef](#)]
49. Rezzola, S.; Corsini, M.; Chiodelli, P.; Cancarini, A.; Nawaz, I.M.; Coltrini, D.; Mitola, S.; Ronca, R.; Belleri, M.; Lista, L.; et al. Inflammation and N-Formyl Peptide Receptors Mediate the Angiogenic Activity of Human Vitreous Humour in Proliferative Diabetic Retinopathy. *Diabetologia* **2017**, *60*, 719–728. [[CrossRef](#)]
50. Chen, H.; Qiu, B.; Gao, G.; Chen, Y.; Min, H.; Wu, Z. Proteomic Changes of Aqueous Humor in Proliferative Diabetic Retinopathy Patients Treated with Different Intravitreal Anti-VEGF Agents. *Exp. Eye Res.* **2022**, *216*, 108942. [[CrossRef](#)]
51. Trivedi, D.; Denniston, A.K.; Murray, P.I. Safety Profile of Anterior Chamber Paracentesis Performed at the Slit Lamp. *Clin. Exp. Ophthalmol.* **2011**, *39*, 725–728. [[CrossRef](#)]
52. Funatsu, H.; Yamashita, H.; Noma, H.; Mimura, T.; Yamashita, T.; Hori, S. Increased Levels of Vascular Endothelial Growth Factor and Interleukin-6 in the Aqueous Humor of Diabetics with Macular Edema. *Am. J. Ophthalmol.* **2002**, *133*, 70–77. [[CrossRef](#)] [[PubMed](#)]
53. Dong, N.; Xu, B.; Wang, B.; Chu, L. Study of 27 Aqueous Humor Cytokines in Patients with Type 2 Diabetes with or without Retinopathy. *Mol. Vis.* **2013**, *19*, 1734–1746. [[PubMed](#)]
54. Kwon, J.; Oh, J. Aqueous Humor Analyses in Patients with Diabetic Retinopathy Who Had Undergone Panretinal Photocoagulation. *J. Diabetes Res.* **2022**, *2022*, 1–7. [[CrossRef](#)] [[PubMed](#)]
55. Noma, H.; Mimura, T.; Yasuda, K.; Motohashi, R.; Kotake, O.; Shimura, M. Aqueous Humor Levels of Soluble Vascular Endothelial Growth Factor Receptor and Inflammatory Factors in Diabetic Macular Edema. *Ophthalmologica* **2017**, *238*, 81–88. [[CrossRef](#)]
56. Sohn, H.J.; Han, D.H.; Kim, I.T.; Oh, I.K.; Kim, K.H.; Lee, D.Y.; Nam, D.H. Changes in Aqueous Concentrations of Various Cytokines After Intravitreal Triamcinolone Versus Bevacizumab for Diabetic Macular Edema. *Am. J. Ophthalmol.* **2011**, *152*, 686–694. [[CrossRef](#)] [[PubMed](#)]
57. Gverović Antunica, A.; Karaman, K.; Znaor, L.; Sapunar, A.; Buško, V.; Puzović, V. IL-12 Concentrations in the Aqueous Humor and Serum of Diabetic Retinopathy Patients. *Graefes Arch. Clin. Exp. Ophthalmol.* **2012**, *250*, 815–821. [[CrossRef](#)]
58. Chen, H.; Zhang, X.; Liao, N.; Wen, F. Assessment of Biomarkers Using Multiplex Assays in Aqueous Humor of Patients with Diabetic Retinopathy. *BMC Ophthalmol.* **2017**, *17*, 176. [[CrossRef](#)]
59. Costagliola, C.; Daniele, A.; dell’Omo, R.; Romano, M.R.; Aceto, F.; Agnifili, L.; Semeraro, F.; Porcellini, A. Aqueous Humor Levels of Vascular Endothelial Growth Factor and Adiponectin in Patients with Type 2 Diabetes before and after Intravitreal Bevacizumab Injection. *Exp. Eye Res.* **2013**, *110*, 50–54. [[CrossRef](#)]
60. Stravalaci, M.; Ferrara, M.; Pathak, V.; Davi, F.; Bottazzi, B.; Mantovani, A.; Medina, R.J.; Romano, M.R.; Inforzato, A. The Long Pentraxin PTX3 as a New Biomarker and Pharmacological Target in Age-Related Macular Degeneration and Diabetic Retinopathy. *Front. Pharm.* **2022**, *12*, 811344. [[CrossRef](#)]
61. Jin, H.; Zhu, B.; Liu, X.; Jin, J.; Zou, H. Metabolic Characterization of Diabetic Retinopathy: An 1H-NMR-Based Metabolomic Approach Using Human Aqueous Humor. *J. Pharm. Biomed. Anal.* **2019**, *174*, 414–421. [[CrossRef](#)]
62. Boehm, B.O.; Lang, G.; Volpert, O.; Jehle, P.M.; Kurkhaus, A.; Rosinger, S.; Lang, G.K.; Bouck, N. Low Content of the Natural Ocular Anti-Angiogenic Agent Pigment Epithelium-Derived Factor (PEDF) in Aqueous Humor Predicts Progression of Diabetic Retinopathy. *Diabetologia* **2003**, *46*, 394–400. [[CrossRef](#)]
63. Gouliopoulos, N.S.; Kalogeropoulos, C.; Lavaris, A.; Rouvas, A.; Asproudis, I.; Garmpi, A.; Damaskos, C.; Garmpis, N.; Kostakis, A.; Moschos, M.M. Association of Serum Inflammatory Markers and Diabetic Retinopathy: A Review of Literature. *Eur. Rev. Med. Pharmacol. Sci.* **2018**, *22*, 7113–7128. [[CrossRef](#)] [[PubMed](#)]
64. Soedamah-Muthu, S.S.; Chaturvedi, N.; Schalkwijk, C.G.; Stehouwer, C.D.A.; Ebeling, P.; Fuller, J.H. Soluble Vascular Cell Adhesion Molecule-1 and Soluble E-Selectin Are Associated with Micro- and Macrovascular Complications in Type 1 Diabetic Patients. *J. Diabetes Complicat.* **2006**, *20*, 188–195. [[CrossRef](#)] [[PubMed](#)]
65. Sharma, S.; Purohit, S.; Sharma, A.; Hopkins, D.; Steed, L.; Bode, B.; Anderson, S.W.; Caldwell, R.; She, J.-X. Elevated Serum Levels of Soluble TNF Receptors and Adhesion Molecules Are Associated with Diabetic Retinopathy in Patients with Type-1 Diabetes. *Mediat. Inflamm.* **2015**, *2015*, 1–8. [[CrossRef](#)] [[PubMed](#)]
66. Zhou, W.; Hu, W. Serum and Vitreous Pentraxin 3 Concentrations in Patients with Diabetic Retinopathy. *Genet. Test. Mol. Biomark.* **2016**, *20*, 149–153. [[CrossRef](#)]
67. Gustavsson, C.; Agardh, E.; Bengtsson, B.; Agardh, C.-D. TNF- $\alpha$  Is an Independent Serum Marker for Proliferative Retinopathy in Type 1 Diabetic Patients. *J. Diabetes Complicat.* **2008**, *22*, 309–316. [[CrossRef](#)] [[PubMed](#)]
68. Muni, R.H.; Kohly, R.P.; Lee, E.Q.; Manson, J.E.; Semba, R.D.; Schaumberg, D.A. Prospective Study of Inflammatory Biomarkers and Risk of Diabetic Retinopathy in the Diabetes Control and Complications Trial. *JAMA Ophthalmol.* **2013**, *131*, 514. [[CrossRef](#)] [[PubMed](#)]

69. Crosby-Nwaobi, R.; Chatziralli, I.; Sergentanis, T.; Dew, T.; Forbes, A.; Sivaprasad, S. Cross Talk between Lipid Metabolism and Inflammatory Markers in Patients with Diabetic Retinopathy. *J. Diabetes Res.* **2015**, *2015*, 1–9. [[CrossRef](#)]
70. Progression of Retinopathy with Intensive versus Conventional Treatment in the Diabetes Control and Complications Trial. *Ophthalmology* **1995**, *102*, 647–661. [[CrossRef](#)]
71. Ono, Y.; Aoki, S.; Ohnishi, K.; Yasuda, T.; Kawano, K.; Tsukada, Y. Increased Serum Levels of Advanced Glycation End-Products and Diabetic Complications. *Diabetes Res. Clin. Pract.* **1998**, *41*, 131–137. [[CrossRef](#)]
72. Shaker, O.G.; Abdelaleem, O.O.; Mahmoud, R.H.; Abdelghaffar, N.K.; Ahmed, T.I.; Said, O.M.; Zaki, O.M. Diagnostic and Prognostic Role of Serum MiR-20b, MiR-17-3p, HOTAIR, and MALAT1 in Diabetic Retinopathy. *IUBMB Life* **2019**, *71*, 310–320. [[CrossRef](#)] [[PubMed](#)]
73. Qing, S.; Yuan, S.; Yun, C.; Hui, H.; Mao, P.; Wen, F.; Ding, Y.; Liu, Q. Serum MiRNA Biomarkers Serve as a Fingerprint for Proliferative Diabetic Retinopathy. *Cell. Physiol. Biochem.* **2014**, *34*, 1733–1740. [[CrossRef](#)] [[PubMed](#)]
74. Joglekar, M.V.; Januszewski, A.S.; Jenkins, A.J.; Hardikar, A.A. Circulating MicroRNA Biomarkers of Diabetic Retinopathy. *Diabetes* **2016**, *65*, 22–24. [[CrossRef](#)] [[PubMed](#)]
75. Zampetaki, A.; Willeit, P.; Burr, S.; Yin, X.; Langley, S.R.; Kiechl, S.; Klein, R.; Rossing, P.; Chaturvedi, N.; Mayr, M. Angiogenic MicroRNAs Linked to Incidence and Progression of Diabetic Retinopathy in Type 1 Diabetes. *Diabetes* **2016**, *65*, 216–227. [[CrossRef](#)] [[PubMed](#)]
76. Liang, Z.; Gao, K.P.; Wang, Y.X.; Liu, Z.C.; Tian, L.; Yang, X.Z.; Ding, J.Y.; Wu, W.T.; Yang, W.H.; Li, Y.L.; et al. RNA Sequencing Identified Specific Circulating MiRNA Biomarkers for Early Detection of Diabetes Retinopathy. *Am. J. Physiol.-Endocrinol. Metab.* **2018**, *315*, E374–E385. [[CrossRef](#)] [[PubMed](#)]
77. Wang, C.; Wan, S.; Yang, T.; Niu, D.; Zhang, A.; Yang, C.; Cai, J.; Wu, J.; Song, J.; Zhang, C.-Y.; et al. Increased Serum MicroRNAs Are Closely Associated with the Presence of Microvascular Complications in Type 2 Diabetes Mellitus. *Sci. Rep.* **2016**, *6*, 20032. [[CrossRef](#)]
78. Abdelkader, H.; Patel, D.V.; McGhee, C.N.; Alany, R.G. New Therapeutic Approaches in the Treatment of Diabetic Keratopathy: A Review. *Clin. Exp. Ophthalmol.* **2011**, *39*, 259–270. [[CrossRef](#)]
79. Vieira-Potter, V.J.; Karamichos, D.; Lee, D.J. Ocular Complications of Diabetes and Therapeutic Approaches. *Biomed. Res. Int.* **2016**, *2016*, 1–14. [[CrossRef](#)]
80. Wang, X.; Xu, G.; Wang, W.; Wang, J.; Chen, L.; He, M.; Chen, Z. Changes in Corneal Biomechanics in Patients with Diabetes Mellitus: A Systematic Review and Meta-Analysis. *Acta Diabetol.* **2020**, *57*, 973–981. [[CrossRef](#)]
81. del Buey, M.A.; Casas, P.; Caramello, C.; López, N.; de la Rica, M.; Subirón, A.B.; Lanchares, E.; Huerva, V.; Grzybowski, A.; Ascaso, F.J. An Update on Corneal Biomechanics and Architecture in Diabetes. *J. Ophthalmol.* **2019**, *2019*, 1–20. [[CrossRef](#)]
82. Yoon, K.-C.; Im, S.-K.; Seo, M.-S. Changes of Tear Film and Ocular Surface in Diabetes Mellitus. *Korean J. Ophthalmol.* **2004**, *18*, 168. [[CrossRef](#)] [[PubMed](#)]
83. Choo, M.; Prakash, K.; Samsudin, A.; Soong, T.; Ramli, N.; Kadir, A. Corneal Changes in Type II Diabetes Mellitus in Malaysia. *Int. J. Ophthalmol.* **2010**, *3*, 234–236. [[CrossRef](#)] [[PubMed](#)]
84. Coco, G.; Hamill, K.J.; Troughton, L.D.; Kaye, S.B.; Romano, V. Risk Factors for Corneal Epithelial Wound Healing: Can Sex Play a Role? *Eur. J. Ophthalmol.* **2022**, *32*, 2676–2682. [[CrossRef](#)] [[PubMed](#)]
85. Kim, J.; Kim, C.-S.; Sohn, E.; Jeong, I.-H.; Kim, H.; Kim, J.S. Involvement of Advanced Glycation End Products, Oxidative Stress and Nuclear Factor-KappaB in the Development of Diabetic Keratopathy. *Graefes Arch. Clin. Exp. Ophthalmol.* **2011**, *249*, 529–536. [[CrossRef](#)] [[PubMed](#)]
86. Suraida, A.-R.; Ibrahim, M.; Zunaina, E. Correlation of the Anterior Ocular Segment Biometry with HbA1c Level in Type 2 Diabetes Mellitus Patients. *PLoS ONE* **2018**, *13*, e0191134. [[CrossRef](#)] [[PubMed](#)]
87. Yusufoglu, E.; Güngör Kobat, S.; Keser, S. Evaluation of Central Corneal Epithelial Thickness with Anterior Segment OCT in Patients with Type 2 Diabetes Mellitus. *Int. Ophthalmol.* **2022**. [[CrossRef](#)]
88. Canan, H.; Sahinoglu-Keskek, N.; Altan-Yaycioglu, R. The Relationship of Central Corneal Thickness with the Status of Diabetic Retinopathy. *BMC Ophthalmol.* **2020**, *20*, 220. [[CrossRef](#)]
89. Cui, X.; Hong, J.; Wang, F.; Deng, S.X.; Yang, Y.; Zhu, X.; Wu, D.; Zhao, Y.; Xu, J. Assessment of Corneal Epithelial Thickness in Dry Eye Patients. *Optom. Vis. Sci.* **2014**, *91*, 1446–1454. [[CrossRef](#)]
90. de Cillà, S.; Ranno, S.; Carini, E.; Fogagnolo, P.; Ceresara, G.; Orzalesi, N.; Rossetti, L.M. Corneal Subbasal Nerves Changes in Patients with Diabetic Retinopathy: An In Vivo Confocal Study. *Investig. Ophthalmol. Vis. Sci.* **2009**, *50*, 5155. [[CrossRef](#)]
91. Kulaksızoglu, S.; Karalezli, A. Aqueous Humour and Serum Levels of Nitric Oxide, Malondialdehyde and Total Antioxidant Status in Patients with Type 2 Diabetes with Proliferative Diabetic Retinopathy and Nondiabetic Senile Cataracts. *Can. J. Diabetes* **2016**, *40*, 115–119. [[CrossRef](#)]
92. Chang, D.; Sha, Q.; Zhang, X.; Liu, P.; Rong, S.; Han, T.; Liu, P.; Pan, H. The Evaluation of the Oxidative Stress Parameters in Patients with Primary Angle-Closure Glaucoma. *PLoS ONE* **2011**, *6*, e27218. [[CrossRef](#)]
93. Lee, J.S.; Oum, B.S.; Choi, H.Y.; Lee, J.E.; Cho, B.M. Differences in Corneal Thickness and Corneal Endothelium Related to Duration in Diabetes. *Eye* **2006**, *20*, 315–318. [[CrossRef](#)] [[PubMed](#)]
94. Ozdamar, Y.; Cankaya, B.; Ozalp, S.; Acaroglu, G.; Karakaya, J.; Ozkan, S.S. Is There a Correlation between Diabetes Mellitus and Central Corneal Thickness? *J. Glaucoma* **2010**, *19*, 613–616. [[CrossRef](#)] [[PubMed](#)]

95. Su, D.H.W.; Wong, T.Y.; Wong, W.-L.; Saw, S.-M.; Tan, D.T.H.; Shen, S.Y.; Loon, S.-C.; Foster, P.J.; Aung, T. Diabetes, Hyperglycemia, and Central Corneal Thickness. *Ophthalmology* **2008**, *115*, 964–968. [[CrossRef](#)]
96. Busted, N.; Olsen, T.; Schmitz, O. Clinical Observations on the Corneal Thickness and the Corneal Endothelium in Diabetes Mellitus. *Br. J. Ophthalmol.* **1981**, *65*, 687–690. [[CrossRef](#)]
97. Galgauskas, S.; Laurinavičiūtė, G.; Norvydaitė, D.; Stech, S.; Ašoklis, R. Changes in Choroidal Thickness and Corneal Parameters in Diabetic Eyes. *Eur. J. Ophthalmol.* **2016**, *26*, 163–167. [[CrossRef](#)] [[PubMed](#)]
98. El-Agamy, A.; Alsubaie, S. Corneal Endothelium and Central Corneal Thickness Changes in Type 2 Diabetes Mellitus. *Clin. Ophthalmol.* **2017**, *11*, 481–486. [[CrossRef](#)] [[PubMed](#)]
99. Keoleian, G.M.; Pach, J.M.; Hodge, D.O.; Trocme, S.D.; Bourne, W.M. Structural and Functional Studies of the Corneal Endothelium in Diabetes Mellitus. *Am. J. Ophthalmol.* **1992**, *113*, 64–70. [[CrossRef](#)] [[PubMed](#)]
100. Inoue, K. The Corneal Endothelium and Thickness in Type II Diabetes Mellitus. *Jpn J. Ophthalmol.* **2002**, *46*, 65–69. [[CrossRef](#)]
101. Urban, B.; Raczyńska, D.; Bakunowicz-Łazarczyk, A.; Raczyńska, K.; Krętowska, M. Evaluation of Corneal Endothelium in Children and Adolescents with Type 1 Diabetes Mellitus. *Mediat. Inflamm.* **2013**, *2013*, 1–6. [[CrossRef](#)]
102. Storr-Paulsen, A.; Singh, A.; Jeppesen, H.; Norregaard, J.C.; Thulesen, J. Corneal Endothelial Morphology and Central Thickness in Patients with Type II Diabetes Mellitus. *Acta Ophthalmol.* **2014**, *92*, 158–160. [[CrossRef](#)] [[PubMed](#)]
103. Schnell, O.; Crocker, J.B.; Weng, J. Impact of HbA1c Testing at Point of Care on Diabetes Management. *J. Diabetes Sci. Technol.* **2017**, *11*, 611–617. [[CrossRef](#)]
104. Jeziorny, K.; Niwald, A.; Moll, A.; Piasecka, K.; Pyziak-Skupien, A.; Waszczykowska, A.; Baranska, D.; Malachowska, B.; Szadkowska, A.; Mlynarski, W.; et al. Measurement of Corneal Thickness, Optic Nerve Sheath Diameter and Retinal Nerve Fiber Layer as Potential New Non-Invasive Methods in Assessing a Risk of Cerebral Edema in Type 1 Diabetes in Children. *Acta Diabetol.* **2018**, *55*, 1295–1301. [[CrossRef](#)]
105. Ramm, L.; Spoerl, E.; Pillunat, L.E.; Terai, N. Is the Corneal Thickness Profile Altered in Diabetes Mellitus? *Curr. Eye Res.* **2020**, *45*, 1228–1234. [[CrossRef](#)]
106. Quadrado, M.J.; Popper, M.; Morgado, A.M.; Murta, J.N.; van Best, J.A. Diabetes and Corneal Cell Densities in Humans by In Vivo Confocal Microscopy. *Cornea* **2006**, *25*, 761–768. [[CrossRef](#)]
107. Szalai, E.; Deák, E.; Módis, L.; Németh, G.; Berta, A.; Nagy, A.; Felszeghy, E.; Káposzta, R.; Malik, R.A.; Csutak, A. Early Corneal Cellular and Nerve Fiber Pathology in Young Patients With Type 1 Diabetes Mellitus Identified Using Corneal Confocal Microscopy. *Investig. Ophthalmol. Vis. Sci.* **2016**, *57*, 853. [[CrossRef](#)] [[PubMed](#)]
108. Frueh, B.; Körner, U.; Böhnke, M. Konfokale Mikroskopie Der Hornhaut Bei Patienten Mit Diabetes Mellitus. *Klin. Monbl. Augenheilkd.* **1995**, *206*, 317–319. [[CrossRef](#)] [[PubMed](#)]
109. Vracko, R. Basal Lamina Layering in Diabetes Mellitus. Evidence for Accelerated Rate of Cell Death and Cell Regeneration. *Diabetes* **1974**, *23*, 94–104. [[CrossRef](#)]
110. Jha, A.; Verma, A.; Alagorie, A.R. Association of Severity of Diabetic Retinopathy with Corneal Endothelial and Thickness Changes in Patients with Diabetes Mellitus. *Eye* **2022**, *36*, 1202–1208. [[CrossRef](#)]
111. Módis, L.; Szalai, E.; Kertész, K.; Kemény-Beke, A.; Kettesy, B.; Berta, A. Evaluation of the Corneal Endothelium in Patients with Diabetes Mellitus Type I and II. *Histol. Histopathol.* **2010**, *25*, 1531–1537. [[CrossRef](#)]
112. Sudhir, R.R.; Raman, R.; Sharma, T. Changes in the Corneal Endothelial Cell Density and Morphology in Patients with Type 2 Diabetes Mellitus: A Population-Based Study, Sankara Nethralaya Diabetic Retinopathy and Molecular Genetics Study (SN-DREAMS, Report 23). *Cornea* **2012**, *31*, 1119–1122. [[CrossRef](#)] [[PubMed](#)]
113. Islam, Q.U.; Mehboob, M.A.; Amin, Z.A. Comparison of Corneal Morphological Characteristics between Diabetic and Non Diabetic Population. *Pak. J. Med. Sci.* **2017**, *33*, 1307–1311. [[CrossRef](#)] [[PubMed](#)]
114. Siribunkum, J.; Kosrirukvongs, P.; Singalavanija, A. Corneal Abnormalities in Diabetes. *J. Med. Assoc. Thai.* **2001**, *84*, 1075–1083.
115. Leelawongtawun, W.; Suphachearaphan, W.; Kampitak, K.; Leelawongtawun, R. A Comparative Study of Corneal Endothelial Structure between Diabetes and Non-Diabetes. *J. Med. Assoc. Thai.* **2015**, *98*, 484–488. [[PubMed](#)]
116. Schultz, R.O.; Matsuda, M.; Yee, R.W.; Edelhofer, H.F.; Schultz, K.J. Corneal Endothelial Changes in Type I and Type II Diabetes Mellitus. *Am. J. Ophthalmol.* **1984**, *98*, 401–410. [[CrossRef](#)]
117. Hara, M.; Morishige, N.; Chikama, T.; Nishida, T. Comparison of Confocal Biomicroscopy and Noncontact Specular Microscopy for Evaluation of the Corneal Endothelium. *Cornea* **2003**, *22*, 512–515. [[CrossRef](#)]
118. Klais, C.M.C.; Bühren, J.; Kohnen, T. Comparison of Endothelial Cell Count Using Confocal and Contact Specular Microscopy. *Ophthalmologica* **2003**, *217*, 99–103. [[CrossRef](#)]
119. Shenoy, R.; Khandekar, R.; Bialasiewicz, A.A.; Muniri, A. al Corneal Endothelium in Patients with Diabetes Mellitus: A Historical Cohort Study. *Eur. J. Ophthalmol.* **2009**, *19*, 369–375. [[CrossRef](#)]
120. Taşlı, N.G.; İcel, E.; Karakurt, Y.; Ucak, T.; Ugurlu, A.; Yilmaz, H.; Akbas, E.M. The Findings of Corneal Specular Microscopy in Patients with Type-2 Diabetes Mellitus. *BMC Ophthalmol.* **2020**, *20*, 214. [[CrossRef](#)]
121. Albers, J.W.; Pop-Busui, R. Diabetic Neuropathy: Mechanisms, Emerging Treatments, and Subtypes. *Curr. Neurol. Neurosci. Rep.* **2014**, *14*, 473. [[CrossRef](#)]
122. Boulton, A.J. Diabetic Neuropathy: Classification, Measurement and Treatment. *Curr. Opin. Endocrinol. Diabetes Obes.* **2007**, *14*, 141–145. [[CrossRef](#)] [[PubMed](#)]

123. Selvarajah, D.; Kar, D.; Khunti, K.; Davies, M.J.; Scott, A.R.; Walker, J.; Tesfaye, S. Diabetic Peripheral Neuropathy: Advances in Diagnosis and Strategies for Screening and Early Intervention. *Lancet Diabetes Endocrinol.* **2019**, *7*, 938–948. [[CrossRef](#)] [[PubMed](#)]
124. Malik, R.A.; Veves, A.; Tesfaye, S.; Smith, G.; Cameron, N.; Zochodne, D.; Lauria, G. Small Fibre Neuropathy: Role in the Diagnosis of Diabetic Sensorimotor Polyneuropathy. *Diabetes Metab. Res. Rev.* **2011**, *27*, 678–684. [[CrossRef](#)] [[PubMed](#)]
125. Körei, A.E.; Istenes, I.; Papanas, N.; Kempler, P. Small-Fiber Neuropathy. *Angiology* **2016**, *67*, 49–57. [[CrossRef](#)]
126. Basantsova, N.Y.; Starshinova, A.A.; Dori, A.; Zinchenko, Y.S.; Yablonskiy, P.K.; Shoenfeld, Y. Small-Fiber Neuropathy Definition, Diagnosis, and Treatment. *Neurol. Sci.* **2019**, *40*, 1343–1350. [[CrossRef](#)]
127. Williams, B.M.; Borrioni, D.; Liu, R.; Zhao, Y.; Zhang, J.; Lim, J.; Ma, B.; Romano, V.; Qi, H.; Ferdousi, M.; et al. An Artificial Intelligence-Based Deep Learning Algorithm for the Diagnosis of Diabetic Neuropathy Using Corneal Confocal Microscopy: A Development and Validation Study. *Diabetologia* **2020**, *63*, 419–430. [[CrossRef](#)]
128. dell’Omo, R.; Cifariello, F.; de Turrís, S.; Romano, V.; di Renzo, F.; di Taranto, D.; Coclite, G.; Agnifili, L.; Mastropasqua, L.; Costagliola, C. Confocal Microscopy of Corneal Nerve Plexus as an Early Marker of Eye Involvement in Patients with Type 2 Diabetes. *Diabetes Res. Clin. Pract.* **2018**, *142*, 393–400. [[CrossRef](#)]
129. Zhao, H. Corneal Alteration and Pathogenesis in Diabetes Mellitus. *Int. J. Ophthalmol.* **2019**, *12*, 1939–1950. [[CrossRef](#)]
130. Petropoulos, I.N.; Alam, U.; Fadavi, H.; Asghar, O.; Green, P.; Ponirakis, G.; Marshall, A.; Boulton, A.J.M.; Tavakoli, M.; Malik, R.A. Corneal Nerve Loss Detected With Corneal Confocal Microscopy Is Symmetrical and Related to the Severity of Diabetic Polyneuropathy. *Diabetes Care* **2013**, *36*, 3646–3651. [[CrossRef](#)]
131. Nitoda, E.; Kallinikos, P.; Pallikaris, A.; Moschandrea, J.; Amoiridis, G.; Ganotakis, E.S.; Tsilimbaris, M. Correlation of Diabetic Retinopathy and Corneal Neuropathy Using Confocal Microscopy. *Curr. Eye Res.* **2012**, *37*, 898–906. [[CrossRef](#)]
132. Messmer, E.M.; Schmid-Tannwald, C.; Zapp, D.; Kampik, A. In Vivo Confocal Microscopy of Corneal Small Fiber Damage in Diabetes Mellitus. *Graefes Arch. Clin. Exp. Ophthalmol.* **2010**, *248*, 1307–1312. [[CrossRef](#)]
133. Hertz, P.; Bril, V.; Orszag, A.; Ahmed, A.; Ng, E.; Nwe, P.; Ngo, M.; Perkins, B.A. Reproducibility of in Vivo Corneal Confocal Microscopy as a Novel Screening Test for Early Diabetic Sensorimotor Polyneuropathy. *Diabet. Med.* **2011**, *28*, 1253–1260. [[CrossRef](#)] [[PubMed](#)]
134. Edwards, K.; Pritchard, N.; Vagenas, D.; Russell, A.; Malik, R.A.; Efron, N. Utility of Corneal Confocal Microscopy for Assessing Mild Diabetic Neuropathy: Baseline Findings of the LANDMark Study. *Clin. Exp. Optom.* **2012**, *95*, 348–354. [[CrossRef](#)] [[PubMed](#)]
135. Li, Q.; Zhong, Y.; Zhang, T.; Zhang, R.; Zhang, Q.; Zheng, H.; Ji, L.; Sun, W.; Zhu, X.; Zhang, S.; et al. Quantitative Analysis of Corneal Nerve Fibers in Type 2 Diabetics with and without Diabetic Peripheral Neuropathy: Comparison of Manual and Automated Assessments. *Diabetes Res. Clin. Pract.* **2019**, *151*, 33–38. [[CrossRef](#)] [[PubMed](#)]
136. Chen, X.; Graham, J.; Petropoulos, I.N.; Ponirakis, G.; Asghar, O.; Alam, U.; Marshall, A.; Ferdousi, M.; Azmi, S.; Efron, N.; et al. Corneal Nerve Fractal Dimension: A Novel Corneal Nerve Metric for the Diagnosis of Diabetic Sensorimotor Polyneuropathy. *Invest. Ophthalmol. Vis. Sci.* **2018**, *59*, 1113–1118. [[CrossRef](#)] [[PubMed](#)]
137. Kalteniece, A.; Ferdousi, M.; Azmi, S.; Mubita, W.M.; Marshall, A.; Lauria, G.; Faber, C.G.; Soran, H.; Malik, R.A. Corneal Confocal Microscopy Detects Small Nerve Fibre Damage in Patients with Painful Diabetic Neuropathy. *Sci. Rep.* **2020**, *10*, 3371. [[CrossRef](#)]
138. Dhage, S.; Ferdousi, M.; Adam, S.; Ho, J.H.; Kalteniece, A.; Azmi, S.; Alam, U.; Ponirakis, G.; Petropoulos, I.; Atkinson, A.J.; et al. Corneal Confocal Microscopy Identifies Small Fibre Damage and Progression of Diabetic Neuropathy. *Sci. Rep.* **2021**, *11*, 1859. [[CrossRef](#)]
139. Lewis, E.J.H.; Lovblom, L.E.; Ferdousi, M.; Halpern, E.M.; Jeziorska, M.; Pacaud, D.; Pritchard, N.; Dehghani, C.; Edwards, K.; Srinivasan, S.; et al. Rapid Corneal Nerve Fiber Loss: A Marker of Diabetic Neuropathy Onset and Progression. *Diabetes Care* **2020**, *43*, 1829–1835. [[CrossRef](#)] [[PubMed](#)]
140. Alam, U.; Jeziorska, M.; Petropoulos, I.N.; Asghar, O.; Fadavi, H.; Ponirakis, G.; Marshall, A.; Tavakoli, M.; Boulton, A.J.M.; Efron, N.; et al. Diagnostic Utility of Corneal Confocal Microscopy and Intra-Epidermal Nerve Fibre Density in Diabetic Neuropathy. *PLoS ONE* **2017**, *12*, e0180175. [[CrossRef](#)]
141. Chen, X.; Graham, J.; Dabbah, M.A.; Petropoulos, I.N.; Ponirakis, G.; Asghar, O.; Alam, U.; Marshall, A.; Fadavi, H.; Ferdousi, M.; et al. Small Nerve Fiber Quantification in the Diagnosis of Diabetic Sensorimotor Polyneuropathy: Comparing Corneal Confocal Microscopy With Intraepidermal Nerve Fiber Density. *Diabetes Care* **2015**, *38*, 1138–1144. [[CrossRef](#)]
142. Quattrini, C.; Tavakoli, M.; Jeziorska, M.; Kallinikos, P.; Tesfaye, S.; Finnigan, J.; Marshall, A.; Boulton, A.J.M.; Efron, N.; Malik, R.A. Surrogate Markers of Small Fiber Damage in Human Diabetic Neuropathy. *Diabetes* **2007**, *56*, 2148–2154. [[CrossRef](#)]
143. Hafner, J.; Zadrzail, M.; Grisold, A.; Ricken, G.; Krenn, M.; Kitzmantl, D.; Pollreis, A.; Gleiss, A.; Schmidt-Erfurth, U. Retinal and Corneal Neurodegeneration and Their Association with Systemic Signs of Peripheral Neuropathy in Type 2 Diabetes. *Am. J. Ophthalmol.* **2020**, *209*, 197–205. [[CrossRef](#)] [[PubMed](#)]
144. Srinivasan, S.; Dehghani, C.; Pritchard, N.; Edwards, K.; Russell, A.W.; Malik, R.A.; Efron, N. Corneal and Retinal Neuronal Degeneration in Early Stages of Diabetic Retinopathy. *Investig. Ophthalmol. Vis. Sci.* **2017**, *58*, 6365. [[CrossRef](#)]
145. Petropoulos, I.N.; Green, P.; Chan, A.W.S.; Alam, U.; Fadavi, H.; Marshall, A.; Asghar, O.; Efron, N.; Tavakoli, M.; Malik, R.A. Corneal Confocal Microscopy Detects Neuropathy in Patients with Type 1 Diabetes without Retinopathy or Microalbuminuria. *PLoS ONE* **2015**, *10*, e0123517. [[CrossRef](#)]
146. Ziegler, D.; Papanas, N.; Zhivov, A.; Allgeier, S.; Winter, K.; Ziegler, I.; Brüggemann, J.; Strom, A.; Peschel, S.; Köhler, B.; et al. Early Detection of Nerve Fiber Loss by Corneal Confocal Microscopy and Skin Biopsy in Recently Diagnosed Type 2 Diabetes. *Diabetes* **2014**, *63*, 2454–2463. [[CrossRef](#)]

147. Ferdousi, M.; Romanchuk, K.; Mah, J.K.; Virtanen, H.; Millar, C.; Malik, R.A.; Pacaud, D. Early Corneal Nerve Fibre Damage and Increased Langerhans Cell Density in Children with Type 1 Diabetes Mellitus. *Sci. Rep.* **2019**, *9*, 8758. [[CrossRef](#)]
148. Tummanapalli, S.S.; Issar, T.; Yan, A.; Kwai, N.; Poynten, A.M.; Krishnan, A.V.; Willcox, M.D.P.; Markoulli, M. Corneal Nerve Fiber Loss in Diabetes with Chronic Kidney Disease. *Ocul. Surf.* **2020**, *18*, 178–185. [[CrossRef](#)]
149. Tavakoli, M.; Kallinikos, P.; Iqbal, A.; Herbert, A.; Fadavi, H.; Efron, N.; Boulton, A.J.M.; AMalik, R. Corneal Confocal Microscopy Detects Improvement in Corneal Nerve Morphology with an Improvement in Risk Factors for Diabetic Neuropathy. *Diabet. Med.* **2011**, *28*, 1261–1267. [[CrossRef](#)]
150. Mehra, S.; Tavakoli, M.; Kallinikos, P.A.; Efron, N.; Boulton, A.J.M.; Augustine, T.; Malik, R.A. Corneal Confocal Microscopy Detects Early Nerve Regeneration After Pancreas Transplantation in Patients With Type 1 Diabetes. *Diabetes Care* **2007**, *30*, 2608–2612. [[CrossRef](#)]
151. Wilkinson, C.P.; Ferris III, F.L.; Klein, R.E.; Lee, P.P.; Agardh, C.D.; Davis, M.; Dills, D.; Kampik, A.; Pararajasegaram, R.; Verdaguer, J.T.; et al. Proposed international clinical diabetic retinopathy and diabetic macular edema disease severity scale. *Ophthalmology* **2003**, *110*, 1677–1683. [[CrossRef](#)]
152. Hariprasad, S.M.; Mieler, W.F.; Grassi, M.; Green, J.L.; Jager, R.D.; Miller, L. Vision-Related Quality of Life in Patients with Diabetic Macular Oedema. *Br. J. Ophthalmol.* **2008**, *92*, 89–92. [[CrossRef](#)]
153. Suci, C.-I.; Suci, V.-I.; Nicoara, S.-D. Optical Coherence Tomography (Angiography) Biomarkers in the Assessment and Monitoring of Diabetic Macular Edema. *J. Diabetes Res.* **2020**, *2020*, 1–10. [[CrossRef](#)]
154. Markan, A.; Agarwal, A.; Arora, A.; Bazgain, K.; Rana, V.; Gupta, V. Novel Imaging Biomarkers in Diabetic Retinopathy and Diabetic Macular Edema. *Ther. Adv. Ophthalmol.* **2020**, *12*, 251584142095051. [[CrossRef](#)] [[PubMed](#)]
155. Deák, G.G.; Bolz, M.; Ritter, M.; Prager, S.; Benesch, T.; Schmidt-Erfurth, U. A Systematic Correlation between Morphology and Functional Alterations in Diabetic Macular Edema. *Investig. Ophthalmol. Vis. Sci.* **2010**, *51*, 6710. [[CrossRef](#)] [[PubMed](#)]
156. Murakami, T.; Nishijima, K.; Akagi, T.; Uji, A.; Horii, T.; Ueda-Arakawa, N.; Muraoka, Y.; Yoshimura, N. Optical Coherence Tomographic Reflectivity of Photoreceptors beneath Cystoid Spaces in Diabetic Macular Edema. *Investig. Ophthalmol. Vis. Sci.* **2012**, *53*, 1506. [[CrossRef](#)] [[PubMed](#)]
157. Romano, M.R.; Romano, V.; Vallejo-Garcia, J.L.; Vinciguerra, R.; Romano, M.; Cereda, M.; Angi, M.; Valldeperas, X.; Costagliola, C.; Vinciguerra, P. Macular hypotrophy after internal limiting membrane removal for diabetic macular edema. *Retina* **2014**, *34*, 1182–1189. [[CrossRef](#)]
158. Bolz, M.; Schmidt-Erfurth, U.; Deak, G.; Mylonas, G.; Kriechbaum, K.; Scholda, C. Optical Coherence Tomographic Hyperreflective Foci. *Ophthalmology* **2009**, *116*, 914–920. [[CrossRef](#)]
159. Lee, H.; Jang, H.; Choi, Y.A.; Kim, H.C.; Chung, H. Association between Soluble CD14 in the Aqueous Humor and Hyperreflective Foci on Optical Coherence Tomography in Patients with Diabetic Macular Edema. *Investig. Ophthalmol. Vis. Sci.* **2018**, *59*, 715. [[CrossRef](#)]
160. Midena, E.; Pilotto, E.; Bini, S. Hyperreflective Intraretinal Foci as an OCT Biomarker of Retinal Inflammation in Diabetic Macular Edema. *Investig. Ophthalmol. Vis. Sci.* **2018**, *59*, 5366. [[CrossRef](#)]
161. Hwang, T.S.; Jia, Y.; Gao, S.S.; Bailey, S.T.; Lauer, A.K.; Flaxel, C.J.; Wilson, D.J.; Huang, D. Optical coherence tomography angiography features of diabetic retinopathy. *Retina* **2015**, *35*, 2371–2376. [[CrossRef](#)]
162. Kim, K.T.; Kim, D.Y.; Chae, J.B. Association between Hyperreflective Foci on Spectral-Domain Optical Coherence Tomography and Early Recurrence of Diabetic Macular Edema after Intravitreal Dexamethasone Implantation. *J. Ophthalmol.* **2019**, *2019*, 1–9. [[CrossRef](#)] [[PubMed](#)]
163. Vujosevic, S.; Bini, S.; Torresin, T.; Berton, M.; Midena, G.; Parrozzani, R.; Martini, F.; Pucci, P.; Daniele, A.R.; Cavarzeran, F.; et al. Hyperreflective Retinal Spots in Normal and Diabetic Eyes. *Retina* **2017**, *37*, 1092–1103. [[CrossRef](#)] [[PubMed](#)]
164. Sasaki, M.; Kawasaki, R.; Noonan, J.E.; Wong, T.Y.; Lamoureux, E.; Wang, J.J. Quantitative Measurement of Hard Exudates in Patients With Diabetes and Their Associations With Serum Lipid Levels. *Investig. Ophthalmol. Vis. Sci.* **2013**, *54*, 5544. [[CrossRef](#)]
165. Shin, Y.U.; Hong, E.H.; Lim, H.W.; Kang, M.H.; Seong, M.; Cho, H. Quantitative Evaluation of Hard Exudates in Diabetic Macular Edema after Short-Term Intravitreal Triamcinolone, Dexamethasone Implant or Bevacizumab Injections. *BMC Ophthalmol.* **2017**, *17*, 182. [[CrossRef](#)] [[PubMed](#)]
166. Joltikov, K.A.; Sesi, C.A.; de Castro, V.M.; Davila, J.R.; Anand, R.; Khan, S.M.; Farbman, N.; Jackson, G.R.; Johnson, C.A.; Gardner, T.W. Disorganization of Retinal Inner Layers (DRIL) and Neuroretinal Dysfunction in Early Diabetic Retinopathy. *Investig. Ophthalmol. Vis. Sci.* **2018**, *59*, 5481. [[CrossRef](#)]
167. Sun, J.K.; Lin, M.M.; Lammer, J.; Prager, S.; Sarangi, R.; Silva, P.S.; Aiello, L.P. Disorganization of the Retinal Inner Layers as a Predictor of Visual Acuity in Eyes With Center-Involved Diabetic Macular Edema. *JAMA Ophthalmol.* **2014**, *132*, 1309. [[CrossRef](#)]
168. Nicholson, L.; Ramu, J.; Triantafyllou, I.; Patrao, N.V.; Comyn, O.; Hykin, P.; Sivaprasad, S. Diagnostic Accuracy of Disorganization of the Retinal Inner Layers in Detecting Macular Capillary Non-Perfusion in Diabetic Retinopathy. *Clin. Exp. Ophthalmol.* **2015**, *43*, 735–741. [[CrossRef](#)]
169. Balaratnasingam, C.; Inoue, M.; Ahn, S.; McCann, J.; Dhrami-Gavazi, E.; Yannuzzi, L.A.; Freund, K.B. Visual Acuity Is Correlated with the Area of the Foveal Avascular Zone in Diabetic Retinopathy and Retinal Vein Occlusion. *Ophthalmology* **2016**, *123*, 2352–2367. [[CrossRef](#)]
170. Das, R.; Spence, G.; Hogg, R.E.; Stevenson, M.; Chakravarthy, U. Disorganization of Inner Retina and Outer Retinal Morphology in Diabetic Macular Edema. *JAMA Ophthalmol.* **2018**, *136*, 202. [[CrossRef](#)]

171. Nadri, G.; Saxena, S.; Stefanickova, J.; Ziak, P.; Benacka, J.; Gilhotra, J.S.; Kruzliak, P. Disorganization of Retinal Inner Layers Correlates with Ellipsoid Zone Disruption and Retinal Nerve Fiber Layer Thinning in Diabetic Retinopathy. *J. Diabetes Complicat.* **2019**, *33*, 550–553. [[CrossRef](#)]
172. al Faran, A.; Mousa, A.; al Shamsi, H.; al Gaeed, A.; Ghazi, N.G. Spectral domain optical coherence tomography predictors of visual outcome in diabetic cystoid macular edema after bevacizumab injection. *Retina* **2014**, *34*, 1208–1215. [[CrossRef](#)] [[PubMed](#)]
173. Pelosini, L.; Hull, C.C.; Boyce, J.F.; McHugh, D.; Stanford, M.R.; Marshall, J. Optical Coherence Tomography May Be Used to Predict Visual Acuity in Patients with Macular Edema. *Investig. Ophthalmol. Vis. Sci.* **2011**, *52*, 2741. [[CrossRef](#)]
174. Seo, K.H.; Yu, S.-Y.; Kim, M.; Kwak, H.W. Visual and morphologic outcomes of intravitreal ranibizumab for diabetic macular edema based on optical coherence tomography patterns. *Retina* **2016**, *36*, 588–595. [[CrossRef](#)] [[PubMed](#)]
175. Giocanti-Aurégan, A.; Hrarat, L.; Qu, L.M.; Sarda, V.; Boubaya, M.; Levy, V.; Chaine, G.; Fajnkuchen, F. Functional and Anatomical Outcomes in Patients With Serous Retinal Detachment in Diabetic Macular Edema Treated With Ranibizumab. *Investig. Ophthalmol. Vis. Sci.* **2017**, *58*, 797. [[CrossRef](#)]
176. Gerendas, B.; Simader, C.; Deak, G.G.; Prager, S.G.; Lammer, J.; Waldstein, S.M.; Kundi, M.; Schmidt-Erfurth, U. Morphological Parameters Relevant for Visual and Anatomic Outcomes during Anti-VEGF Therapy of Diabetic Macular Edema in the RESTORE Trial. *Invest. Ophthalmol. Vis. Sci.* **2014**, *55*, 1791.
177. Sophie, R.; Lu, N.; Campochiaro, P.A. Predictors of Functional and Anatomic Outcomes in Patients with Diabetic Macular Edema Treated with Ranibizumab. *Ophthalmology* **2015**, *122*, 1395–1401. [[CrossRef](#)]
178. Vujosevic, S.; Torresin, T.; Berton, M.; Bini, S.; Convento, E.; Midena, E. Diabetic Macular Edema With and Without Subfoveal Neuroretinal Detachment: Two Different Morphologic and Functional Entities. *Am. J. Ophthalmol.* **2017**, *181*, 149–155. [[CrossRef](#)]
179. Zur, D.; Igllicki, M.; Busch, C.; Invernizzi, A.; Mariussi, M.; Loewenstein, A.; Busch, C.; Cebeci, Z.; Chhablani, J.K.; Chaikitmongkol, V.; et al. OCT Biomarkers as Functional Outcome Predictors in Diabetic Macular Edema Treated with Dexamethasone Implant. *Ophthalmology* **2018**, *125*, 267–275. [[CrossRef](#)]
180. Moon, B.G.; Lee, J.Y.; Yu, H.G.; Song, J.H.; Park, Y.-H.; Kim, H.W.; Ji, Y.-S.; Chang, W.; Lee, J.E.; Oh, J.; et al. Efficacy and Safety of a Dexamethasone Implant in Patients with Diabetic Macular Edema at Tertiary Centers in Korea. *J. Ophthalmol.* **2016**, *2016*, 1–9. [[CrossRef](#)]
181. Korobelnik, J.-F.; Lu, C.; Katz, T.A.; Dhoot, D.S.; Loewenstein, A.; Arnold, J.; Staurengi, G. Effect of Baseline Subretinal Fluid on Treatment Outcomes in VIVID-DME and VISTA-DME Studies. *Ophthalmol. Retina* **2019**, *3*, 663–669. [[CrossRef](#)]
182. Forooghian, F.; Stetson, P.F.; Meyer, S.A.; Chew, E.Y.; Wong, W.T.; Cukras, C.; Meyerle, C.B.; Ferris, F.L. Relationship between photoreceptor outer segment length and visual acuity in diabetic macular edema. *Retina* **2010**, *30*, 63–70. [[CrossRef](#)] [[PubMed](#)]
183. Ozkaya, A.; Alkin, Z.; Karakucuk, Y.; Karatas, G.; Fazil, K.; Gurkan Erdogan, M.; Perente, I.; Taskapili, M. Thickness of the Retinal Photoreceptor Outer Segment Layer in Healthy Volunteers and in Patients with Diabetes Mellitus without Retinopathy, Diabetic Retinopathy, or Diabetic Macular Edema. *Saudi J. Ophthalmol.* **2017**, *31*, 69–75. [[CrossRef](#)]
184. Jampol, L.M.; Glassman, A.R.; Sun, J. Evaluation and Care of Patients with Diabetic Retinopathy. *New Engl. J. Med.* **2020**, *382*, 1629–1637. [[CrossRef](#)]
185. Bresnick, G.H. Diabetic Macular Edema. *Ophthalmology* **1986**, *93*, 989–997. [[CrossRef](#)] [[PubMed](#)]
186. Witkin, A.; Salz, D. Imaging in Diabetic Retinopathy. *Middle East Afr. J. Ophthalmol.* **2015**, *22*, 145. [[CrossRef](#)] [[PubMed](#)]
187. Mansour, A.M.; Schachat, A.; Bodiford, G.; Haymond, R. Foveal avascular zone in diabetes mellitus. *Retina* **1993**, *13*, 125–128. [[CrossRef](#)]
188. Couturier, A.; Rey, P.-A.; Erginay, A.; Lavia, C.; Bonnin, S.; Dupas, B.; Gaudric, A.; Tadayoni, R. Widefield OCT-Angiography and Fluorescein Angiography Assessments of Nonperfusion in Diabetic Retinopathy and Edema Treated with Anti-Vascular Endothelial Growth Factor. *Ophthalmology* **2019**, *126*, 1685–1694. [[CrossRef](#)] [[PubMed](#)]
189. Salz, D.A.; de Carlo, T.E.; Adhi, M.; Moul, E.; Choi, W.; Bauml, C.R.; Witkin, A.J.; Duker, J.S.; Fujimoto, J.G.; Waheed, N.K. Select Features of Diabetic Retinopathy on Swept-Source Optical Coherence Tomographic Angiography Compared With Fluorescein Angiography and Normal Eyes. *JAMA Ophthalmol.* **2016**, *134*, 644. [[CrossRef](#)]
190. Zahid, S.; Dolz-Marco, R.; Freund, K.B.; Balaratnasingam, C.; Dansingani, K.; Gilani, F.; Mehta, N.; Young, E.; Klifto, M.R.; Chae, B.; et al. Fractal Dimensional Analysis of Optical Coherence Tomography Angiography in Eyes With Diabetic Retinopathy. *Investig. Ophthalmol. Vis. Sci.* **2016**, *57*, 4940. [[CrossRef](#)] [[PubMed](#)]
191. Carnevali, A.; Sacconi, R.; Corbelli, E.; Tomasso, L.; Querques, L.; Zerbini, G.; Scorcia, V.; Bandello, F.; Querques, G. Optical Coherence Tomography Angiography Analysis of Retinal Vascular Plexuses and Choriocapillaris in Patients with Type 1 Diabetes without Diabetic Retinopathy. *Acta Diabetol.* **2017**, *54*, 695–702. [[CrossRef](#)]
192. Al-Sheikh, M.; Akil, H.; Pfau, M.; Sadda, S.R. Swept-Source OCT Angiography Imaging of the Foveal Avascular Zone and Macular Capillary Network Density in Diabetic Retinopathy. *Investig. Ophthalmol. Vis. Sci.* **2016**, *57*, 3907. [[CrossRef](#)]
193. Tang, F.Y.; Chan, E.O.; Sun, Z.; Wong, R.; Lok, J.; Szeto, S.; Chan, J.C.; Lam, A.; Tham, C.C.; Ng, D.S.; et al. Clinically Relevant Factors Associated with Quantitative Optical Coherence Tomography Angiography Metrics in Deep Capillary Plexus in Patients with Diabetes. *Eye Vis.* **2020**, *7*, 7. [[CrossRef](#)]
194. AttaAllah, H.R.; Mohamed, A.A.M.; Ali, M.A. Macular Vessels Density in Diabetic Retinopathy: Quantitative Assessment Using Optical Coherence Tomography Angiography. *Int. Ophthalmol.* **2019**, *39*, 1845–1859. [[CrossRef](#)]

195. Veiby, N.C.B.B.; Simeunovic, A.; Heier, M.; Brunborg, C.; Saddique, N.; Moe, M.C.; Dahl-Jørgensen, K.; Margeisdottir, H.D.; Petrovski, G. Associations between Macular OCT Angiography and Nonproliferative Diabetic Retinopathy in Young Patients with Type 1 Diabetes Mellitus. *J. Diabetes Res.* **2020**, *2020*, 1–12. [[CrossRef](#)]
196. Romano, M.R.; Ilardi, G.; Ferrara, M.; Cennamo, G.; Allegrini, D.; Pafundi, P.; Costagliola, C.; Staibano, S.; Cennamo, G. Intraretinal Changes in Idiopathic versus Diabetic Epiretinal Membranes after Macular Peeling. *PLoS ONE* **2018**, *13*, e0197065. [[CrossRef](#)]
197. Romano, M.R.; Allegrini, D.; della Guardia, C.; Schiemer, S.; Baronissi, I.; Ferrara, M.; Cennamo, G. Vitreous and Intraretinal Macular Changes in Diabetic Macular Edema with and without Tractional Components. *Graefe's Arch. Clin. Exp. Ophthalmol.* **2019**, *257*, 1–8. [[CrossRef](#)]
198. Garg, I.; Uwakwe, C.; Le, R.; Lu, E.S.; Cui, Y.; Wai, K.M.; Katz, R.; Zhu, Y.; Moon, J.Y.; Li, C.Y.; et al. Nonperfusion Area and Other Vascular Metrics by Wider Field Swept-Source OCT Angiography as Biomarkers of Diabetic Retinopathy Severity. *Ophthalmol. Sci.* **2022**, *2*, 100144. [[CrossRef](#)]
199. Moein, H.-R.; Novais, E.A.; Rebhun, C.B.; Cole, E.D.; Louzada, R.N.; Witkin, A.J.; Bauml, C.R.; Duker, J.S.; Waheed, N.K. Optical coherence tomography angiography to detect macular capillary ischemia in patients with inner retinal changes after resolved diabetic macular edema. *Retina* **2018**, *38*, 2277–2284. [[CrossRef](#)]
200. Rosen, R.B.; Andrade Romo, J.S.; Krawitz, B.D.; Mo, S.; Fawzi, A.A.; Linderman, R.E.; Carroll, J.; Pinhas, A.; Chui, T.Y.P. Earliest Evidence of Preclinical Diabetic Retinopathy Revealed Using Optical Coherence Tomography Angiography Perfused Capillary Density. *Am. J. Ophthalmol.* **2019**, *203*, 103–115. [[CrossRef](#)]
201. Aiello, L.P.; Odia, I.; Glassman, A.R.; Melia, M.; Jampol, L.M.; Bressler, N.M.; Kiss, S.; Silva, P.S.; Wykoff, C.C.; Sun, J.K. Comparison of Early Treatment Diabetic Retinopathy Study Standard 7-Field Imaging With Ultrawide-Field Imaging for Determining Severity of Diabetic Retinopathy. *JAMA Ophthalmol.* **2019**, *137*, 65. [[CrossRef](#)]
202. Wessel, M.M.; Nair, N.; Aaker, G.D.; Ehrlich, J.R.; D'Amico, D.J.; Kiss, S. Peripheral Retinal Ischaemia, as Evaluated by Ultra-Widefield Fluorescein Angiography, Is Associated with Diabetic Macular Oedema. *Br. J. Ophthalmol.* **2012**, *96*, 694–698. [[CrossRef](#)] [[PubMed](#)]
203. Patel, R.D.; Messner, L.V.; Teitelbaum, B.; Michel, K.A.; Hariprasad, S.M. Characterization of Ischemic Index Using Ultra-Widefield Fluorescein Angiography in Patients With Focal and Diffuse Recalcitrant Diabetic Macular Edema. *Am. J. Ophthalmol.* **2013**, *155*, 1038–1044.e2. [[CrossRef](#)]
204. Jiang, A.C.; Sevgi, D.D.; Mugnaini, C.; Whitney, J.; Srivastava, S.K.; Talcott, K.E.; Hu, M.; Reese, J.L.; Ehlers, J.P. Predictive Assessment of Quantitative Ultra-Widefield Angiographic Features for Future Need for Anti-VEGF Therapy in Diabetic Eye Disease. *J. Pers. Med.* **2022**, *12*, 608. [[CrossRef](#)] [[PubMed](#)]
205. Ehlers, J.P.; Jiang, A.C.; Boss, J.D.; Hu, M.; Figueiredo, N.; Babiuch, A.; Talcott, K.; Sharma, S.; Hach, J.; Le, T.; et al. Quantitative Ultra-Widefield Angiography and Diabetic Retinopathy Severity. *Ophthalmology* **2019**, *126*, 1527–1532. [[CrossRef](#)] [[PubMed](#)]
206. Wykoff, C.C.; Nittala, M.G.; Zhou, B.; Fan, W.; Velaga, S.B.; Lampen, S.I.R.; Rusakevich, A.M.; Ehlers, J.P.; Babiuch, A.; Brown, D.M.; et al. Intravitreal Aflibercept for Retinal Nonperfusion in Proliferative Diabetic Retinopathy. *Ophthalmol. Retina* **2019**, *3*, 1076–1086. [[CrossRef](#)]
207. Fan, W.; Nittala, M.G.; Wykoff, C.C.; Brown, D.M.; Uji, A.; Van Hemert, J.; Fleming, A.; Robertson, G.; Sadda, S.R.; Michael, I.P. New Biomarker Quantifying the Effect of Anti-Vegf Therapy in Eyes with Proliferative Diabetic Retinopathy on Ultrawide Field Fluorescein Angiography. *Retina* **2022**, *42*, 426–433. [[CrossRef](#)]
208. Russell, J.F.; Shi, Y.; Hinkle, J.W.; Scott, N.L.; Fan, K.C.; Lyu, C.; Gregori, G.; Rosenfeld, P.J. Longitudinal Wide-Field Swept-Source OCT Angiography of Neovascularization in Proliferative Diabetic Retinopathy after Panretinal Photocoagulation. *Ophthalmol. Retina* **2019**, *3*, 350–361. [[CrossRef](#)] [[PubMed](#)]

**Disclaimer/Publisher's Note:** The statements, opinions and data contained in all publications are solely those of the individual author(s) and contributor(s) and not of MDPI and/or the editor(s). MDPI and/or the editor(s) disclaim responsibility for any injury to people or property resulting from any ideas, methods, instructions or products referred to in the content.